Novel approaches to regenerative medicine of the skin

Construction and comprehensive molecular analysis of collagenous biomaterials *in vitro* and *in vivo*

Gerwen Lammers

Research presented in this thesis was performed at the Department of Biochemistry, Nijmegen Centre for Molecular Life Sciences, Radboud University Nijmegen Medical Centre, and funded by the Dutch Program for Tissue Engineering.

Cover image: www.istockphoto.com, scaffolding by Joe Gough
Lay-out: G. Lammers
Printed by: CPI Wöhrmann, Zutphen, The Netherlands

ISBN: 978-90-8570-765-3

Novel approaches to regenerative medicine of the skin

Construction and comprehensive molecular analysis of collagenous biomaterials *in vitro* and *in vivo*

Een wetenschappelijke proeve op het gebied van de
Medische Wetenschappen

Proefschrift

ter verkrijging van de graad van doctor
aan de Radboud Universiteit Nijmegen
op gezag van de rector magnificus prof. mr. S.C.J.J. Kortmann,
volgens besluit van het college van decanen
in het openbaar te verdedigen op woensdag 18 januari 2012
om 13.30 uur precies

door

Gerwen Lammers

geboren op 25 oktober 1980
te Doetinchem

Promotor:
Prof. dr. R.E. Brock

Copromotoren:
Dr. T.H. van Kuppevelt
Dr. W.F. Daamen

Manuscriptcommissie:
Prof. dr. J.A. Jansen (voorzitter)
Prof. dr. E. Middelkoop, Vrije Universiteit Amsterdam
Dr. P.L.J.M. Zeeuwen

Table of contents

Chapter 1

General introduction
Aims and outline of this thesis

General introduction

The skin is the largest organ of the body and it plays an important role in the regulation of body temperature, the defence against pathogens, and the prevention from dehydration. Morphologically, the skin can be divided in a dermal and an epidermal layer, positioned on top of a subcutaneous fat layer (Fig. 1).

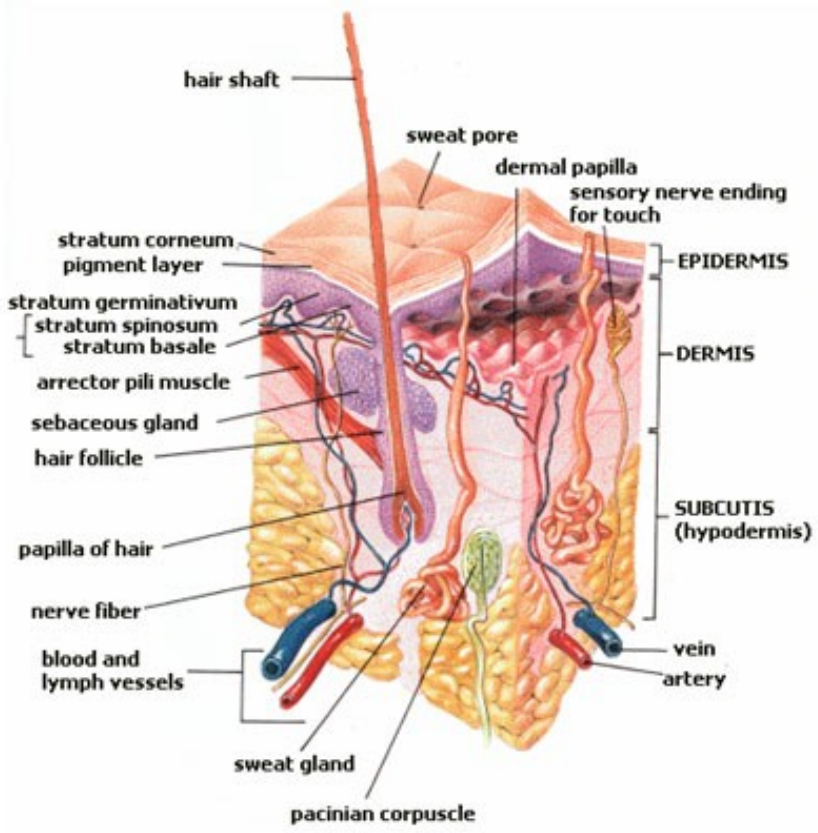

Figure 1. Schematic representation of the human skin. Three different layers are visible: The epidermis (top), dermis (middle) and subcutaneous fat layer (bottom part). Blood and lymph vessels are present throughout the dermis and appendages like a hair follicle, sebaceous and sweat gland are indicated. Reprinted from: http://commons.wikimedia.org/wiki/File:HumanSkinDiagram.jpg.

The dermis consists of soft connective tissue containing fibroblasts as the major cell type. It contains functional structures like hair follicles, sweat glands, sebaceous glands, blood and lymph vessels. The dermal extracellular matrix consists mainly of type I collagen providing the skin its structural strength, elastic fibres providing elasticity, and long, unbranched polysaccharides called glycosaminoglycans, which provide water-binding capacity and play an important role in the binding and modulation of growth factors and other effector molecules [1]. The top of the dermis has a wave-like pattern consisting of dermal papillae.

The epidermis consists of a cell-dense layer of mainly keratinocytes, and these cells produce a basement membrane containing type IV collagen. The basal cells continuously divide and undergo differentiation when moving upwards, thereby outlining the different layers of the epidermis. The top layer, the stratum corneum, consists of dead keratinocytes filled with a highly crosslinked network of structural proteins like keratins that form a physical barrier.

When the skin is damaged, its functions and architecture have to be restored as quickly as possible. Evolutionary, the fastest way to close large full-thickness wounds and burns is by contraction, but this often results in scarring [2]. Scar tissue may differ from normal skin by an aberrant colour, increased thickness, irregular surface area and poor functional quality and this can have functional, cosmetic, and psychological consequences [3]. A novel approach in the reduction of contraction and its negative consequences may be found in the use of tissue engineering/regenerative medicine.

Tissue engineering has been defined as an interdisciplinary field that applies the principles of engineering and the life sciences toward the development of biological substitutes that restore, maintain, or improve tissue function [4]. Different approaches can be used, mostly requiring a natural or synthetic scaffold, often in combination with cells. Our approach is to construct molecularly-defined acellular scaffolds based on natural type I collagen [5,6]. By using natural components, the original extracellular matrix can be mimicked as closely as possible. Biological effector molecules can be incorporated to attract cells from the surrounding tissue to infiltrate the scaffold and to stimulate regeneration of the original tissue. Highly-purified constituents are used to facilitate the investigation of the effect of each individual component on the wound healing process. From a commercial point of view, acellular constructs are preferred, since cellular constructs require additional handling and storage conditions. In addition, the use of cells from the patient will require time, knowledge, and equipment for cell isolation, expansion and/or scaffold seeding.

Growth factors are potent biological signalling molecules that regulate cellular processes like growth, proliferation, and differentiation. Binding of growth factor to specific receptors on the cell membrane of target cells leads to activation of a signalling pathway and finally results in regulation of gene expression. Growth factors play an important role during development, tissue homeostasis and repair. Therefore, specific growth factors can be incorporated in tissue-engineered constructs to guide the cellular regeneration process. Members of the fibroblast growth factor (FGF) family are involved in angiogenesis, wound healing and embryonic development [7], and members of the vascular endothelial growth factor (VEGF) family are involved more specifically in the process of angiogenesis. Like most FGFs, FGF2 (also known as basic FGF) has an effect on a large variety of different cell types and can bind to isoforms of all four FGF tyrosine kinase receptor types (FGFR1-4) [8]. FGF7 (also known as keratinocyte growth factor, KGF) is a special member of the FGF family and acts only on epithelial cells and specifically binds FGFR2b. Members of the VEGF family (VEGF A-VEGFE, and placental growth factor (PIGF)) also signal through tyrosine kinase receptors

[9]. VEGFA, the best studied VEGF, exists in five isoforms which all bind to VEGFR-1 (Flt-1) and VEGFR-2 (KDR/Flk-1) homo- and heterodimers, and the isoform that we used (VEGF-A165) also binds receptors neurophilin 1 and 2. Receptor signalling of most FGFs and most VEGFA isoforms is dependent on simultaneous binding to glycosaminoglycans like heparin and heparan sulfate. We have previously demonstrated that incorporation of heparin, FGF2 and VEGF stimulates blood vessel formation and maturation in an acellular skin construct *in vivo* [10], and since FGF7 can stimulate keratinocytes this can be incorporated in the epidermal part of a construct to guide re-epithelialisation.

A wide range of tissue-engineered skin constructs has been reviewed by others [11-17]. However, despite the multitude of constructs that have already been developed, perfect skin regeneration without complications is for large wounds still science fiction.

Aims and outline of this thesis

This thesis focuses on the development and evaluation of tissue-engineered collagen-based scaffolds for skin regeneration.

Chapter 2 starts with an overview of methods that are currently used in the clinic for the assessment of scar tissue. Subsequently, methods are reviewed that have been used for the evaluation of tissue-engineered skin constructs in animal models. A large variation in evaluation methods between different reports was noticed, and therefore recommendations are given for a more uniform evaluation to enable a more systematic comparison between different studies.

The next chapters deal with different steps in the development of a novel tissue-engineered skin construct.

Glycosaminoglycans like heparin can be incorporated in such a construct, but the presence of the insoluble biomaterial may interfere with the analysis of the exact amount and/or activity of bound glycosaminoglycan. In **chapter 3**, seven different methods are compared that can be used for the determination of scaffold-bound heparin. The (dis)advantages of these methods are discussed and the hexosamine assay is recommended for the determination of the absolute amount of bound heparin.

Chapter 4 describes the development a biomaterial array for the *in vitro* evaluation of the proliferation and differentiation of keratinocytes on collagen membranes that can be used as the epidermal component of a construct. An array of 48 different membranes was prepared and only a few membranes stimulated keratinocyte proliferation. This type of pre-screening facilitates the selection of the proper modifications for a specific application and may reduce the number of animals required for further *in vivo* evaluation studies.

Growth factors are potent biological effector molecules that may also be incorporated in tissue-engineered skin constructs. Regenerating skin requires a vascular network for nourishment of infiltrating cells and removal of waste products, but formation of this network is often a slow process. Vascular endothelial growth factor can stimulate the formation of new blood vessels, and the production and purification of this molecule is described in **chapter 5**.

Based on a rational design, a double-layered collagen-based construct containing elastin, glycosaminoglycans and growth factors was constructed. **Chapter 6** describes the production, implantation and evaluation of this molecularly-defined, acellular skin construct in a rat full-thickness wound model. Compared with a commercially available construct (Integra) and an untreated wound, the double-layered construct showed more cellular influx, less contraction, and an increased formation of blood vessels at early time points, and more newly-formed elastic fibres at a later time point. This indicates that the skin regeneration process can be guided by providing the appropriate extracellular microenvironment.

The last chapters describe novel evaluation tools and techniques to construct innovative scaffolds.

In **chapter 7**, gene expression microarrays are presented as a fast and unbiased tool for the *in vivo* evaluation of tissue-engineered constructs. Gene expression levels were compared between regenerating wounds treated with or without the double-layered skin construct of chapter 6. Lists of up- and downregulated genes were analysed for associated biological processes using gene ontology (GO) terms. The presence/absence of identified processes was confirmed by immunohistochemical staining, demonstrating the power of microarrays as a novel evaluation tool.

Finally, **chapter 8**, shows the feasibility to produce a microstructured collagen membrane that mimics the 3D-architecture of the dermal papillae. Keratinocytes cultured on these membranes were morphologically different and microarray analysis showed that genes involved in proliferation and migration were upregulated when compared to keratinocytes on flat membranes. These microstructured membranes have therefore potential to be used as an epidermal component to stimulate re-epithelialisation and rete ridge formation in an innovative tissue-engineered skin construct.

References

1. Esko JD, Kimata K, Lindahl U. Proteoglycans and Sulfated Glycosaminoglycans. Essentials of Glycobiology, 2nd edition. 2009.
2. Gurtner GC, Werner S, Barrandon Y, Longaker MT. Wound repair and regeneration. Nature 2008;453:314-21.
3. van Zuijlen PP, Angeles AP, Kreis RW, Bos KE, Middelkoop E. Scar assessment tools: implications for current research. Plast Reconstr Surg 2002;109:1108-22.
4. Langer R, Vacanti JP. Tissue engineering. Science 1993;260:920-6.
5. Geutjes PJ, Daamen WF, Buma P, Feitz WF, Faraj KA, Van Kuppevelt TH. From molecules to matrix: construction and evaluation of molecularly defined bioscaffolds. Adv Exp Med Biol 2006;585:279-95.
6. Daamen WF, Faraj KA, Koens MJW, Lammers G, Brouwer KM, Uijtdewilligen PJE, Nillesen STM, Roelofs LA, Nuininga JE, Geutjes PJ, Feitz WFJ, Van Kuppevelt TH. Extracellular-matrix based scaffolds from scratch. Handbook of intelligent scaffold for regenerative medicine. 2011.
7. Alzheimer C, Werner S. Fibroblast Growth Factors. Molecular and Cellular Biology of Neuroprotection in the CNS. 2002.
8. Ornitz DM, Xu J, Colvin JS, McEwen DG, MacArthur CA, Coulier F, *et al.* Receptor specificity of the fibroblast growth factor family. J Biol Chem 1996;271:15292-7.
9. Marti HH. Vascular Endothelial Growth Factor. Molecular and Cellular Biology of Neuroprotection in the CNS. 2002.
10. Nillesen ST, Geutjes PJ, Wismans R, Schalkwijk J, Daamen WF, Van Kuppevelt TH. Increased angiogenesis and blood vessel maturation in acellular collagen-heparin scaffolds containing both FGF2 and VEGF. Biomaterials 2007;28:1123-31.

11. Brusselaers N, Pirayesh A, Hoeksema H, Richters CD, Verbelen J, Beele H, *et al.* Skin replacement in burn wounds. J Trauma 2010;68:490-501.
12. Bottcher-Haberzeth S, Biedermann T, Reichmann E. Tissue engineering of skin. Burns 2010;36:450-60.
13. Lee KH. Tissue-engineered human living skin substitutes: development and clinical application. Yonsei Med J 2000;41:774-9.
14. MacNeil S. Progress and opportunities for tissue-engineered skin. Nature 2007;445:874-80.
15. Metcalfe AD, Ferguson MW. Bioengineering skin using mechanisms of regeneration and repair. Biomaterials 2007;28:5100-13.
16. Metcalfe AD, Ferguson MW. Tissue engineering of replacement skin: the crossroads of biomaterials, wound healing, embryonic development, stem cells and regeneration. J R Soc Interface 2007;4:413-37.
17. Priya SG, Jungvid H, Kumar A. Skin tissue engineering for tissue repair and regeneration. Tissue Eng Part B Rev 2008;14:105-18.

Chapter 2

An overview of methods for the *in vivo* evaluation of tissue-engineered skin constructs

Gerwen Lammers[1]
Pauline D.H.M. Verhaegen[2,3]
Magda M. Ulrich[3,4]
Joost Schalkwijk[5]
Esther Middelkoop[2,4]
Daniela Weiland[1]
Suzan T.M. Nillesen[1]
Toin H. van Kuppevelt[1]
Willeke F. Daamen[1]

[1]Department of Biochemistry, Nijmegen Centre for Molecular Life Sciences, Radboud University Nijmegen Medical Centre, Nijmegen
[2]Association of Dutch Burn Centres, Red Cross Hospital, Beverwijk
[3]Department of Plastic, Reconstructive, and Hand Surgery, Academic Medical Centre, Amsterdam
[4]Department of Plastic, Reconstructive and Hand Surgery, VU Medical Center, Amsterdam
[5]Department of Dermatology, Nijmegen Centre for Molecular Life Sciences, Radboud University Nijmegen Medical Centre, Nijmegen

Tissue Engineering part B – Reviews
2011 volume 17 issue 1 pages 33-55

Abstract

Cutaneous wounding often leads to contraction and scarring, which may result in a range of functional, cosmetic and psychological complications. Tissue-engineered skin substitutes are being developed to enhance restoration of the skin and improve the quality of wound healing. The aim of this review is to provide researchers in the field of tissue engineering an overview of the methods that are currently used to clinically evaluate skin wound healing, and methods that are used to evaluate tissue engineered constructs in animal models.

Clinically, the quality of wound healing is assessed by non-invasive subjective scar assessment scales and objective techniques to measure individual scar features. Alternatively, invasive technologies are used.

In animal models, most tissue-engineered skin constructs studied are at least evaluated macroscopically and by using conventional histology (H&E staining). Planimetry and immunohistochemistry are also often applied. An overview of antibodies used is provided. In addition, some studies used methods to assess gene expression levels and mRNA location, transillumination for blood vessel visualisation, in situ/*in vivo* imaging, electron microscopy, mechanical strength assessment, animal behaviour analysis and microbiological sampling.

A more systematic evaluation of tissue-engineered skin constructs in animal models is recommended to enhance the comparison of different constructs, thereby accelerating the trajectory to application in human patients. This would be further enhanced by the embracement of more clinically relevant objective evaluation methods. In addition, fundamental knowledge on construct-mediated wound healing may be increased by new developments in e.g. gene expression analysis and non-invasive imaging.

Introduction

Cutaneous wound healing is a complex process, often resulting in contraction and scar tissue formation [1]. Scars may lead to an array of functional, cosmetic and psychological implications, and often differ from normal skin by an aberrant colour, increased thickness, irregular surface area and a poor functional quality. Each individual scar feature is important and contributes to the final form and cosmetic acceptability of a scar [2].

Tissue-engineered skin substitutes are being developed to enhance restoration of the skin and improve the quality of wound healing. Different approaches exist to reach this goal, including commercially available constructs, and these have been reviewed extensively [3-10]. Typical approaches use a natural or synthetic scaffold, often in combination with cells. Prior to possible application to humans, constructs are first evaluated in cell culture systems and in animal models.

As will be apparent, a large variability exists in the read-out methods used to evaluate the performance of these constructs in animal models. This variability, combined with the lack of standard protocols, severely hampers the systematic comparison of different studies/constructs.

This review will first provide an overview of standard methods that are currently used in the clinic to evaluate wound healing in patients (without tissue-engineered constructs). Second, methods are listed that are currently used to evaluate the performance of tissue-engineered constructs in animal models, and the strengths and limitations of these methods will be discussed. Finally, recommendations are presented to introduce standardisation in the evaluation of tissue-engineered skin constructs *in vivo* which will allow a more systematic comparison between studies.

Evaluation methods for wound healing in patients

Methods that are currently used for the clinical evaluation of wound healing in patients can be divided in non-invasive and invasive. The non-invasive methods can be further subdivided into subjective (mainly questionnaires) and objective evaluation methods that assess specific scar features.

Non-invasive evaluation methods

Subjective methods

Subjective non-invasive measurement tools predominantly include the scar assessment scales that have been developed to give an easy and quick impression of a scar. They are filled out by an observer (O) and sometimes by the patient (P) as well. In the past decades, several attempts have been made to create an appropriate scale and their origin is mostly found in the assessment of burn scars. A chronologic overview of the different scar assessment scales is given in Table 1.

Table 1. Overview of subjective scar assessment scales.

Scale name	Scar type evaluated	Asses-sor	Reference
Cosmetic Disfigurement Scale	Burns	O	Smith 1988 [11]
Vancouver Scar Scale (VSS)	Burns	O	Sullivan 1990 [12]
VSS with additional tool	Burns	O	Baryza 1995 [13]
Seattle Scale	Burns	O	Yeong 1997 [14]
Manchester Scar Scale	Surgical, hypertro-phic and keloids	O	Beausang 1998 [15]
Hamilton Scale	Burns	O	Crowe 1998 [16]
Modified VSS	Burns and surgical	O	Nedelec 2000 [17]
Patient and Observer Scar Assessment Scale (POSAS)	Burns	O, P	Draaijers 2004 [18]
Matching Assessment of Scars and Photographs	Burns	O	Masters 2005 [19]
Modified POSAS	Burns and surgical	O, P	Van de Kar 2005 [20]
Stony Brook Scale	Surgical	O	Singer 2007 [21]

O=observer, P=patient

Objective methods

Table 2 lists objective evaluation techniques that are currently used in the clinic and for patient studies for the assessment of specific scar features. Each scar feature with its concomitant measurement tools is described separately below.

1. Colour

Scar colour can be determined by measuring the wavelengths of reflected light. Based on this principle, two different methods can be distinguished: tristimulus reflectance colorimetry and narrow-band spectrophotometry. In tristimulus reflectance colorimetry any color is described by three values: L*, the lightness (relative brightness of the color); a*, the amount of green or red (redness); and b*, the amount of yellow or blue (pigmentation). Examples of tristimulus devices are the *Labscan XE* (Hunter Associates Inc., Texas, USA) and the *Minolta Chromameter CR-221-R* and *CR-300* (Minolta Camera Co., Ltd., Osaka, Japan). For narrow-band spectrophotometry, redness and pigmentation is measured in the form of erythema and melanin. This method is based on the differences in light absorption of red and green by haemoglobin and melanin [22-24]. The *DermaSpectrometer* (Cortex Technology, Hadsund, Denmark) and the *Mexameter* (Courage and Khazaka, Cologne, Germany) are examples of narrow-band spectrophotometers.

2. Thickness

When measuring thickness of a scar it is important to distinguish clinical thickness from histological thickness. Clinically, thickness is usually measured by comparing the height of the scar with the normal surrounding skin, whereas the histological thickness may differ because of bulky connective tissue occupying deeper skin layers, especially in immature

scars. Ultrasound measurement devices such as the *Tissue Ultrasound Palpation System (TUPS)* (Biomedical Ultrasonic Solutions, Hong Kong) and the *Dermascan C* (Fig. 1, Cortex Technology, Denmark) are devices frequently used for measuring thickness of normal and scarred skin [25-28]. In addition, the Vivid 900 (Konica-Minolta, Milton Keynes, United Kingdom), a laser scanning technique for volume measurements, can be used for this purpose [29].

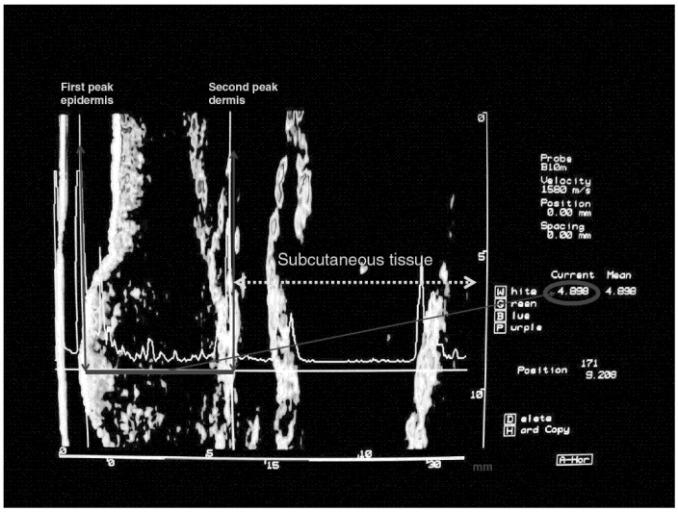

Figure 1. A non-invasive method for the objective evaluation of cutaneous thickness (circled, in mm) using the Dermascan C. An echogenic profile (line) generated by dedicated software can be used to select the set points for thickness calculation, in this case the stratum corneum peak (first peak) and the peak just inside the subcutaneous fat (second peak). Reprinted from Nedelec B *et al.* Quantitative measurement of hypertrophic scar: interrater reliability and concurrent validity. J Burn Care Res 29, 501. Copyright (2008), with permission from Wolters Kluwer Health [28].

3. Relief

Surface irregularities, also referred to as relief, can be measured by various measurement tools. Relief measurement tools should be subdivided in devices which measure small irregularities of normal skin and devices which are more suitable to measure larger irregularities of scars. Devices like the Skin-Visiometer (Courage and Khazaka electronic, Cologne, Germany) for transparency profilometry [30] and the Dermatop system (Breuckmann, Meersburg, Germany) for interference fringe profilometry (interferometry) [31] are able to precisely measure skin microrelief, which can be relevant for the evaluation of therapies for dermatological diseases or the cosmetic industry. Devices that could be more useful for quantifying macrorelief of scars are the TKC 300 Hommeltester (Hommelwerke, Villingen-Schwenningen, Germany) for mechanical profilometry [32], digital image analysis for optical profilometry [33], laser profilometry [34] and Phaseshift Rapid *In vivo* Measurement Of the Skin **(**PRIMOS, GF Messtechnik, Berlin, Germany) [35]. Of all profilometry methods mentioned, PRIMOS is the only validated technique that can directly measure relief and does not require an intermediate silicone replicate of the skin.

4. Mechanical properties

The most important mechanical characteristics to distinguish normal skin from scar tissue are tensile strength, ultimate extension, and stress-strain curves that describe the visco-elastic properties of the tissue [36]. Tools that measure these mechanical qualities are based on different types of load on the skin: suction, pressure, torsion, and tension.

The *Cutometer® Skin Elasticity Meter* [37-41] (Courage and Khazaka Electronic GmbH, Cologne, Germany) is a visco-elasticity measurement tool which works by suction on the skin or scar. Similarly, the *DermaLab®* [42] (Cortex Technology, Hadsund, Denmark), which has replaced the Dermaflex® [43-46], measures the stress that is required to achieve an elevation of the skin of 1.5 mm. The *Cicatrometer* (University of California, San Diego, USA) [47], *Pneumatonometer* (Medtronic Solan, Jacksonville, USA) [48], *Tissue Tonometer* (Flinders University Biomedical Engineering Department, Adelaide, Australia) [49], and *Durometer* (Rex Gauge Company Inc., Glenview, USA) [50-55] are all tonometers. Tonometry is a measurement method which works by exerting pressure on the scar, and was used to quantify firmness and flexibility of skin and scars. The *Dermal Torque Meter* (Dia-stron, Andover, United Kingdom) is a measurement tool that assesses visco-elasticity via torsional force onto the skin [56-58]. This device has also been used on patients with burn scars treated with a tissue-engineered skin construct [59]. Finally, the *Elastometer* (Washington University, St. Louis, USA) [60] and the *Extensometer* (University of Hong Kong, Hong Kong, China) [61] work by measuring skin deformation after tension is exerted in the horizontal plane of the skin, but these measurement tools are not commercially available anymore.

5. Planimetry

One of the most simple methods to evaluate wound healing and the size of a scar is by measuring the length and width with a ruler and, if applicable, its depth by insertion of e.g. a sterile cotton swab in the deepest part of the wound. To determine the wound or scar surface area different measurement methods are available. Scar or wound margins can be traced on e.g. *Transparent Acetate Wound Perimeter Sheets* (Labelon Projection Transparencies, Braintree, United Kingdom) [62-66]. A cut-out of this trace can be used in the *Weighing Method* (Transparency Film, Scotch 3M, St Paul, USA, and Gram-atic® Balance, Metler Instrument Corporation, Highstown, USA) [62]. In *Computer Assisted Planimetry* digitised sheets are analysed [67-70].

In Photogrammetry, a camera is positioned on a standardised distance from the area of interest and the area can be calculated using a calibrated grid [71]. The Measurement of Area and Volume Instrument System (MAVIS) uses coloured stripes to generate a three-dimensional image of the wound area [72]. Stereophotogrammetry is Photogrammetry, which is extended by the use of two cameras to generate a more detailed three-dimensional reconstruction of the area of interest [73].

6. Epidermal barrier

The epidermal barrier function of skin has several characteristics that can be assessed. However, most devices that have been developed for this purpose require further clinimetric evaluation to determine its reliability. Stratum corneum/surface hydration can be measured using techniques like confocal Raman spectroscopy [74] and devices like a nova dermal phase meter (Nova Technology Corporation, Gloucester, MA, USA) [75], and corneometer (Courage and Khazaka Electronic GmbH) [76]. Trans-epidermal water loss (TEWL) can be assessed using e.g. a VapoMeter (Delfin Technologies Ltd, Kuopio,Finland) [77], a DermaLab (Cortex Technologies, Hadsund, Denmark) [77] or Cyberderm evaporimeter (Broomall, PA, USA) [75,76]. Other aspects like the epidermal pH and percutaneous penetration of different substances may also be subject of investigation.

Invasive evaluation methods

Ample research has been performed to unravel the wound healing process on the molecular and cellular level, in order to find clues for the prevention of scar formation. Growth factors and cytokines, for example, play an important role in the precisely orchestrated process of wound healing [1]. A derailed inflammatory reaction leads to excessive scarring, although the exact mechanism is unknown [87]. Scarring is characterized by the deposition of excessive extracellular matrix components, contraction and altered extracellular matrix remodelling. Cells involved in these processes, like (myo)fibroblasts [88], and proteins like matrix metalloproteinases [89] have therefore received much attention. This section discusses the invasive methods that are often required to study the presence and location of specific proteins and cells.

To explore the effects of a specific treatment in time or to identify the sequential events during wound healing on the cellular and molecular level, tissue specimens at different time points in the healing process are required. Since this puts a heavy burden on patients, these methods are mainly confined to animal experiments. When performed in human studies, sampling is mostly limited to the scenario when a scar has to be surgically corrected. Samples obtained by invasive methods are generally analysed using molecular or histological techniques. Usually, this analysis is performed directly, but cells may also be isolated from the samples and cultured first to answer specific research questions.

Molecular biological methods

On the molecular level, mRNA and protein expression are the main subjects of investigation.

Table 2. Overview of objective scar assessment tools.

Scar Feature	Technique name	Tested on	Reference
Colour	**Minolta CR-300 and CR-221-R**	Normal skin, Burn scars	Van den Kerckhove 2001 [78], Draaijers 2004 [79]
	Labscan XE	Normal skin Burn scars	Li-Tsang 2003 [80]
	DermaSpectrometer	Burn scars	Draaijers 2004 [79]
	Mexameter	Normal skin Hypertrophic burn scars	Nedelec 2008 [26]
Thickness	**Tissue Ultrasound Palpation System (TUPS)**	Surgical and burn scars	Lau 2005 [81]
	Vivid 900 (volume)	Keloids (surgical scars)	Taylor 2007 [29]
	Dermascan C	Hypertrophic burn scars	Nedelec 2008 [28]
Relief	**Optical Profilometry**	Normal skin	Corcuff 1982 [33]
	Mechanical Profilometry	Normal skin	Kautzky 1995 [32]
	Laser Profilometry	Normal skin	Saur 1991 [34]
	Transparency Profilometry	Metal plates, Normal skin	De Paepe 2000 [30]
	Interferometry	Normal skin	Lagarde 2001 [31]
	Phaseshift Rapid *In vivo* Measurement Of the Skin (PRIMOS)	Normal skin Burn scars	Bloemen 2010 [35]
Mechanical properties	**Tonometry**	Sclerodermal skin Normal skin Burn scars	Spann 1996 [48], Lye 2006 [49], Corica 2006 [82], Merkel 2008 [53]
	Dermal Torque meter	Burn scars	Murray 1997 [83] Boyce 2000 [59]
	Cutometer	Normal skin (Hypertrophic) burn scars	Draaijers 2004 [38], Nedelec 2008 [26]
	Dermaflex, Dermalab	Normal skin	Pedersen 2003 [42]
Planimetry	**Weighing method**	Wounds	Bohannon 1983 [62]
	Stereophotogrammetry	Wounds	Johnson 1996 [69]
	Photogrammetry (including MAVIS)	Normal skin (artificial drawings) Wounds	Van Zuijlen 2004 [84], Plassmann 1998 [72]
	Computer Assisted Planimetry (Visitrak and Videometry)	Wounds	Gethin 2006 [85], Wunderlich 2000 [86]
	Transparent Acetate Wound Perimeter Tracing	Normal skin (artificial drawings)	Van Zuijlen 2004 [84]
Epidermal barrier	**Surface hydration: Raman spectroscopy, Dermal Phase Meter, Corneometer**	Normal skin	Caspers 2001 [74], Visscher 2001 [75] Eberlein-König 2000 [76]
	Trans-epidermal water loss (TEWL): Vapometer, Dermalab, Evaporimeter	Normal skin, artificial skin	Cohen 2009 [77], Eberlein-König 2000 [76] , Visscher 2001 [75]

1. mRNA expression

The mRNA expression levels of relevant proteins are usually evaluated by two common techniques: microarrays and real time quantitative Reversed Transcription PCR (real-time qRT-PCR). With microarrays, differences in genes expression can be determined between samples. Depending on the method used, the expression profile of the total genome can be studied. Greco *et al.* used this technique to compare skin gene expression levels between patients with burn wounds with normal skin samples [90], and Nassiri *et al.* investigated keloids with arrays specific for genes involved in apoptosis and cytokine signalling [91].

Microarrays are seen as an exploratory method to study differentially expressed genes in different RNA populations. In addition, qRT-PCR is often performed to confirm the differences detected with microarrays [92]. Since, in this method, the expression levels of target genes are expressed relative to reference genes, a validation of these reference genes is important. However, it is often not examined whether the expression level of the reference gene is also influenced by the treatment or different conditions of the tissues under investigation. In addition, while in the microarray field it is widely acknowledged that the mRNA populations to be studied should be of indisputable quality, in qRT-PCR research this is less well recognized and proper quality control experiments are not always performed [93].

RT-qPCR was used to determine gene expression levels in keloids [91,94]. Discrimination between collagen subtypes is often difficult to establish at the protein level because of the lack of specific antibodies. Therefore, changes in collagen synthesis are often assessed by qRT-PCR. Excessive extracellular matrix deposition is not only caused by increased synthesis but also by decreased breakdown due to reduced matrix metalloproteinase activity. The latter may be caused by decreased synthesis and activation of the proteins and increased inhibitors of the enzymes. Van der Slot *et al.* analysed wound-derived fibroblasts for collagen and collagen modifying enzymes with qRT-PCR [95].

Next to the identification of differentially expressed genes with the above mentioned methods, mRNA expression can also be localised using in situ hybridization techniques. Toksoy *et al.* used this technique to visualise the spatiotemporal expression of the chemokine CXCL12 during human wound healing [96].

2. Protein expression

Although analysis of mRNA expression can provide valuable information, it is the resulting protein that plays a role in the wound healing process. Since many factors are involved in translation, it is important to confirm the differences found at the mRNA level at the (active) protein level.

Different assays can be used to assess protein expression. One of these methods is SDS-PAGE, e.g. used to assess collagen production of fibroblasts isolated from scar tissue [97]. In combination with Western blotting, this technique can also be used to differentiate e.g. between inactive and active (phosphorylated) proteins [98]. Enzyme-Linked Immuno Sorbent Assay (ELISA) is frequently used to study the role of cytokines and growth factors in wound healing. Schrementi *et al.* used ELISA to compare the levels of TGF-β in oral and dermal wounds [99].

To analyse the activity of proteolytic enzymes, specific ELISAs were developed as well as the less specific Azocoll assay, or zymography [100]. The Azocoll assay measures azo dye release of impregnated collagen and Zymography is an electrophoretic method in which a substrate (gelatin or casein) is incorporated and can be cleaved in a polyacrylamide gel [101-103]. For several proteases such as cathepsins, trypsin and plasmin, more specific chromogenic synthetic peptide substrates were developed [104], which allows a colorimetric measurement of the specific proteolytic activity.

To study the localisation of enzymatic degradation by matrix metalloproteinases in the tissue *in situ* zymography can be used [105-107]. In this technique cryo-sections are covered with a substrate which is subsequently cleaved by the protease and visualised. The development of substrates labelled with both a fluorescent label and a quencher which quenches the fluorescent dye in the uncleaved substrate greatly enhanced this technique. At the location of proteolytic activity the substrate is cleaved and the fluorescence becomes apparent. This and various other techniques to study proteolytic activity of various enzymes in situ are reviewed by Frederics *et al.* [108].

Cellular viability

The hypertrophic nature of a scar can be assessed by investigation of the balance between cell proliferative capacity and apoptosis of e.g. cells isolated from scar tissue. Techniques include a DNA fragmentation assay using agarose gel electrophoresis, propidium iodide staining for apoptotic cells, and an MTT assay for cell viability [109].

Histopathology and immunohistochemistry

Standard histochemical staining techniques (like haematoxylin-eosin (H&E) staining) on tissue sections can be used to evaluate tissue cellularity, cell morphology, and architectural aspects such as thickness of the epidermis or dermis and orientation of the collagen bundles. Immunohistochemical techniques can visualise the presence and location of specific cell types and proteins. This technique was used to visualise epidermal components in hypertrophic scars [110], angiogenesis in surgical wounds [111], and components of the immune system after thermal injury [112].

One of the most pronounced differences between normal skin and scar tissue is the architecture of the collagen fibres. These differences are already apparent on the standard H&E-stained sections. With the picrosirius red staining individual collagen fibres can be visualised with polarised light. In scar tissue fibre thickness differs from normal skin and fibres are oriented more parallel to each other [113]. Images of these sections can be used for Fourier analysis to quantify collagen bundle orientation and collagen “bundle packing” [114,115]. The Fourier transformation calculates the structure organization in two-dimensional images. The Fourier zeroth order maximum can be used for calculating the orientation of collagen bundles and has been widely applied to determine the orientation of structures in diseased skin and scars [113,115-120]. Secondly, the Fourier first order maximum allows the estimation of the “bundle packing”, which is the distance between the cen-

tres of the collagen bundles. This morphometric method has also been applied in several studies[113,120,121].

Evaluation methods for tissue-engineered skin constructs in animal models

Tissue-engineered skin constructs are being developed with the goal to improve wound healing. Most constructs are first evaluated *in vitro* to assess e.g. their biocompatibility and capacity to induce cell proliferation and/or differentiation. Based on these results, some constructs are further evaluated *in vivo*. For this review, a literature study was performed to list methods that have been used to evaluate tissue-engineered skin constructs (i.e. a natural or synthetic scaffold with or without cells) in full-thickness skin wounds in animal models (summarised in Table 3). Pubmed was searched for original research papers primarily based on the following search terms: “skin wound scaffold”, “biomaterial vivo skin wound”, “tissue engineering skin wound vivo”, and “substitute full-thickness wound”. Studies describing an animal full-thickness wound model in combination with a tissue-engineered skin construct in English were included. Tissue engineering is a highly dynamic field, combining various fields of scientific research, and using a variety of materials and cell sources. Therefore, the authors acknowledge the possibility of not being completely comprehensive, and apologise beforehand when a particular study is missing.

As will be apparent, not all clinical methods as described in section 2 are used to evaluate constructs in animal models. One reason is that animal models are more suitable for invasive evaluation methods. However, this does not explain the remarkable underrepresentation of non-invasive (clinical) measurement methods, the latter is very well possible without omission of the first. Another striking observation is that different types of animal models are being used, ranging from rat and mouse to pig. This may have major impact on the translation of results to the human situation, since wounds in rodents heal primarily by contraction, while pig skin is more comparable to human skin and heals by the formation of granulation tissue. In addition, a large variation in animal strains was noticed and also the size and location of wounds varied between studies (outside the scope of this review and therefore not further discussed in detail). Various wound models have been reviewed by others [122-125].

Table 3. Overview of studies describing the evaluation of tissue-engineered skin constructs in animal models, including the animal species, type of construct, and evaluation methods, sorted on publication year.

A=Macroscopic evaluation, **B**=Planimetry, **C**=Histology, **D**=Immunohistochemistry (see Table 4), **E**=Gene expression, **F**=Transillumination, **G**=*In vivo* imaging, **H**=Electron microscopy, **I**=Mechanical properties, **J**=Epidermal barrier

Reference	Species	Construct	A	B	C	D	E	F	G	H	I	J
Lammers 2010 [126]	Rat	Collagen-GAG + GFs				✓	✓					
Matsumoto 2010 [127]	Rat	Hyaluronic acid-collagen -/+ human FBs	✓		✓	✓						
Steinstraesser 2010 [128]	Pig	Collagen	✓		✓							
Kurpinski 2010 [129]	Rat	PLLA -/+ GAG	✓		✓							
Wang 2010 [130]	Rat	Collagen-GAG + rat FBs	✓	✓	✓							
Klingenberg 2009 [131]	Mouse	Collagen-GAG + human FBs & KCs	✓		✓	✓	✓					
Egana 2009 [132]	Mouse	Collagen-GAG + pancreatic/submandibular gland SCs			✓			✓				
Egana 2009 [133]	Mouse	Collagen-GAG + human MSCs	✓			✓		✓				
Scherer 2009 [134]	Mouse	poly-N-acetyl-glucosamine vs. cellulose	✓	✓	✓	✓	✓					
Kim 2009 [135]	Mouse	PLLA -/+ human EPCs			✓	✓	✓		✓			
Li 2009 [136]	Rat	Polyurethane + PDGF			✓							
Okabayashi 2009 [137]	Pig	Hydroxyapatite-silk fibroin gel		✓	✓							
Masuda 2009 [138]	Mouse	Peptide-conjugated chitosan + human KCs			✓	✓						
Xiao 2009 [139]	Mouse	Porcine DED + porcine vs. human KCs	✓									
Salem 2009 [140]	Mouse	Collagen-elastin + pancreatic SCs	✓		✓	✓		✓				
Bao 2008 [141]	Rabbit	Agar-collagen	✓		✓							
Altman 2009 [142]	Mouse	Silk fibroin-chitosan + ASCs		✓	✓	✓						
Breen 2009 [143]	Rabbit	Fibrin -/+ beta-galactosidase expression vector			✓	✓						
Yang 2009 [144]	Mouse	Human amniotic membrane + human FBs & KCs	✓		✓							
Baynosa 2009 [145]	Rat	Collagen			✓							
Windsor 2009 [146]	Mouse	Collagen + human FBs & KCs	✓	✓	✓	✓						
Zhang 2009 [147]	Mouse	Porcine DED + human FBs	✓	✓	✓	✓						
Schneider 2009 [148]	Rat	Collagen-elastin or collagen-GAG	✓	✓	✓	✓						
Wang 2008 [149]	Mouse	Collagen			✓				✓			
Kalyanaraman 2008 [150]	Mouse	Collagen-GAG + human FBs & KCs	✓	✓	✓							
Bannasch 2008 [151]	Pig	Fibrin + porcine KCs -/+ DED	✓	✓	✓	✓						
Bannasch 2008 [152]	Mouse & Pig	Mouse: DED + human KCs; Pig: Fibrin + porcine FBs -/+ DED	✓	✓	✓	✓						
Powell 2008 [153]	Mouse	Collagen + human FBs & KCs	✓	✓	✓	✓						
Garcia 2008 [154]	Rat	Collagen		✓	✓	✓						
Nillesen 2007 [155]	Rat	Collagen-GAG + GFs	✓	✓	✓	✓						
Falanga 2007 [156]	Mouse	Fibrin + murine BMCSs	✓		✓	✓						
Myers 2007 [157]	Pig	GAG + porcine KCs	✓	✓	✓							
Tanihara 2008 [158]	Rabbit	Collagen			✓							
Ma 2007 [159]	Pig	Collagen-chitosan	✓		✓	✓						
Perng 2008 [160]	Mouse	Gelatin-acrylamide + human BMSCs				✓			✓			
Breen 2008 [161]	Rabbit	Fibrin -/+ eNOS expressing vector		✓		✓						
Richters 2008 [162]	Pig	Human DED	✓	✓	✓	✓						
Lee 2007 [163]	Mouse	GAG, PEG-PLGA-PEG + murine HSCs, MDSCs or MSCs		✓	✓	✓						
Waldeck 2007 [164]	Rat	PEGylated-RGD gelatin & KGF-1		✓	✓							
Lin 2006 [165]	Rat	Collagen -/+ PDGF			✓							
Ng 2006 [166]	Rat	Collagen-GAG or PLGA -/+ human FBs & KCs	✓	✓	✓	✓						

Table 3 (continued)

Reference	Species	Construct	A	B	C	D	E	F	G	H	I	J
Lee 2005 [167]	Mouse	Gelatin -/+ human FBs			✓							
Zweers 2005 [168]	Mouse	Collagen + human FBs & KCs			✓	✓				✓		
Druecke 2004 [169]	Pig	Collagen(-GAG) or PEGT/PBT	✓	✓	✓	✓						
Gu 2004 [170]	Rabbit	Collagen -/+ transfected PDGF			✓	✓	✓					
Price 2004 [171]	Pig	GAG -/+ porcine FBs -/+ porcine KCs	✓		✓	✓	✓					
Llames 2004 [172]	Mouse	Plasma + human FBs & KCs	✓		✓	✓						
Middelkoop 2004 [124]	Pig	Biological and synthetic scaffolds -/+ porcine FBs	✓	✓	✓							
Wang 2004 [173]	Mouse	PEGT/PBT -/+ human FBs	✓	✓	✓	✓						
Breitbart 2003 [174]	Mouse	PGA -/+ murine FBs -/+ transfected PDGF			✓	✓						
Lee 2003 [175]	Mouse	Gelatin-B-glucan -/+ human FBs & KCs			✓							
Grant 2002 [176]	Pig	Collagen-GAG + fibrin & porcine KCs	✓			✓						
Lamme 2002 [177]	Pig	Collagen-elastin hydrosylate + porcine FBs	✓	✓	✓	✓						
Breitbart 2001 [178]	Rabbit	PGA -/+ rabbit FBs -/+ transfected VEGF/PDGF			✓	✓						
Pandit 2000 [179]	Rabbit	Fibrin -/+ FGF-1			✓						✓	
Lamme 2000 [180]	Pig	Collagen-elastin hydrosylate -/+ porcine FBs	✓	✓	✓	✓						
Gorodetsky 1999 [181]	Pig	Fibrin -/+ human FBs -/+ PDGF			✓							
Breitbart 1999 [182]	Rat	PGA -/+ rat FBs -/+ transfected PDGF			✓	✓						
Pandit 1999 [183]	Rabbit	Collagen-/+ TGFβ		✓	✓						✓	
Supp 1999 [184]	Mouse	Collagen-GAG + human FBs & KCs	✓	✓		✓						✓
Pandit 1998 [185]	Rabbit	Collagen -/+ FGF-1			✓						✓	
Fauza 1998 [186]	Sheep	PGA -/+ sheep FBs & KCs	✓		✓							
Pandit 1998 [187]	Rabbit	Fibrin + PEG beads			✓							
Pandit 1998 [188]	Rabbit	Fibrin-PEG beads + FGF-1			✓							
Lamme 1998 [189]	Pig	Collagen-elastin hydrosylate + porcine FBs			✓	✓						
Orgill 1998 [190]	Pig	Collagen-GAG	✓		✓	✓				✓		
Compton 1998 [191]	Pig	Collagen-GAG + porcine KCs	✓		✓	✓						
Butler 1998 [192]	Pig	Collagen-GAG + porcine KCs	✓		✓							
Lamme 1996 [193]	Pig	Collagen-elastin hydrosylate			✓	✓				✓		
Boyce 1996 [194]	Mouse	Collagen-GAG + human FBs & KCs	✓	✓								✓
De Vries 1995 [195]	Pig	Collagen-elastin hydrolysate -/+ FBs or stromal cells		✓	✓	✓						
Hafemann 1994 [196]	Rat	Collagen + rat KCs -/+ fibrin	✓			✓				✓		
Hansbrough 1993 [197]	Mouse	Polyglactin + human FBs & KCs	✓		✓	✓						
De Vries 1993 [198]	Pig	Collagen, polyglactin or PEU	✓	✓	✓	✓						
Yannas 1989 [199]	Guinea pig	Collagen-GAG -/+ guinea pig FBs & KCs	✓	✓						✓		
Doillon 1984 [200]	Guinea pig	Collagen -/+ fibronectin								✓		
Bell 1981 [201]	Rat	Collagen + rat FBs	✓		✓							
Yannas 1981 [202]	Guinea pig	Collagen-GAG -/+ KCs	✓	✓	✓							
Chardack 1962 [203]	Pig	Polyvinyl alcohol	✓		✓							

ASCs=adipose-derived SCs, BMSCs=Bone marrow-derived SCs, DED=de-epidermised dermis, EPCs=endothelial progenitor cells, FBs=fibroblasts, FGF=fibroblast growth factor, GAG=glycosaminoglycan, GF=growth factor, HSCs=hematopoetic SCs, KCs=keratinocytes, KGF=keratinocyte growth factor, MDSCs=muscle-derived SCs, MSCs=mesenchymal stromal/SCs, PBT=polybuthylene therephthalate, PDGF=platelet-derived growth factor, PEG=polyethylene glycol, PEGT=polyethylene oxide therephthalathe, PEU=polyether urethane, PGA=poly glycolic acid, PLGA=poly(lactic-co-glycolic acid), PLLA=poly-L-lactide acid, RGD=arginine-glycine-aspartic acid, SCs=stem cells, TGF=transforming growth factor, VEGF=vascular endothelial growth factor

Macroscopic evaluation

Most of the studies reviewed describe macroscopic aspects of the healing wounds and approximately half of the studies show macroscopic pictures. However, the description is often limited to one or two sentences, predominantly mentioning the take rate of the construct, colour (pigmentation, vascularisation), signs of granulation tissue or epithelialisation and the absence of signs of infection/inflammation or necrosis. Bannasch *et al.* provided a relatively detailed description of the appearance of the healing wounds in time, and specified different areas with e.g. granulation tissue and neo-epithelium [151]. Llames *et al.* mentioned the presence of fine wrinkles and hyperkeratosis, characteristic for the regenerated human skin in their mouse model, and stated that the regenerated skin was easy to lift and move [172], and Hansbrough *et al.* also mentioned graft surface smoothness during the regeneration process [197]. Druecke *et al.* mentioned in their macroscopic evaluation the presence of epidermal flakes/scales, white opaque granules representing hyperkeratinisation. In addition, they used a scale that was also used in other studies to systematically score for wound colour, surface smoothness, and wound suppleness/stiffness [169,177,180,198].

Taken together, most studies provide a macroscopic but unsystematic description of wounds. To improve the comparison between studies, we recommend the use of a standard checklist: a subjective scar assessment tool could be used for this purpose, as described in Table 1. Since an animal 'patient' cannot evaluate its own wounds, scoring can only be performed by the observer. Therefore, the observer part (OSAS) of the clinically emerging POSAS would be suitable, containing a 1-10 scale to score for scar vascularity, pigmentation, thickness, relief, pliability, and surface area [204].

Macroscopic analysis was also used to evaluate wound contraction and reepithelialisation subjectively, but in most cases these were further analysed by planimetry.

Planimetry to measure wound contraction and/or reepithelialisation

Analogous to the clinical evaluation of wound healing, approximately half of the animal studies mentioned wound contraction. However, it is not always stated what was measured exactly (e.g. how wound margins were defined), which makes it unclear whether wound healing (closure) by re-epithelialisation or real contraction is reported. Also the exact method used to measure contraction is not always completely clear [164,166]. A calliper can be used to manually measure wound area [163], but most studies make use of photographs to analyse wound contraction. Occasionally, it is stated that a ruler was included in the photograph [142,147], but in other cases it is not clear how corrections for photographing distance were made. Other studies used transparent papers to trace the wounds edges [153,154,169]. In some cases, the software used to calculate the wound area is specified [134,137,142,146,147,150]. However, differences in software is probably causing the least variation. Most studies do not correct for growth of the animals during the study by e.g. the use of reference spots on the unaffected skin. In pig, this has been achieved by determination of a tattooed wound outline with respect to a larger tattooed grid, unaffected by contraction (Fig. 2) [124,162,177,180,198]. As long as corrections for animal growth and e.g. photo-

graphing distance and wound surface convex are made, the method employed for area calculation is of less importance when contraction has to be compared between different studies.

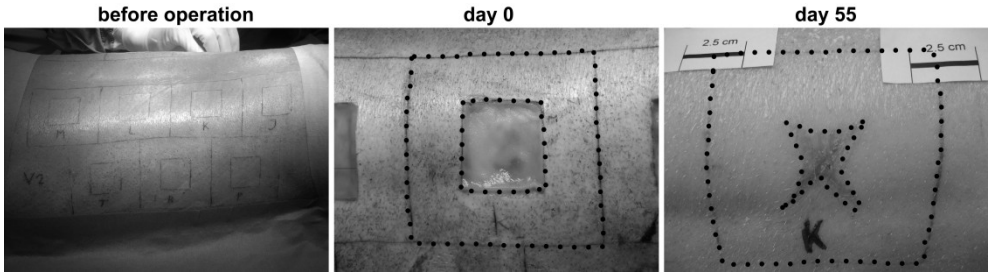

Figure 2. Tattoo method to monitor contraction in a porcine wound model. Before operation, a grid with defined dimensions was drawn on the pigs flank. At day 0, a treatment (collagen-heparin scaffold in this example) was applied. Contraction was monitored with pictures and to correct for the growth of the animal during the experiment, wound area (inner lines) was calculated as a percentage of the large, unaffected square (outer lines). Tattoo ink is highlighted with black dots for clarity at day 0 and 55.

Comparable methods were used to determine reepithelialisation [134,148], e.g. by tracing the epidermal edges on transparent papers as described in Price *et al.* [205]. However, these macroscopic methods can only be applied on wounds lacking a crust that covers the newly-forming epithelium. Since the reepithelialisation rate is dependent on the total wound area, it is important to correct for contraction when this rate is calculated.

Histological evaluation with conventional staining techniques

Depending on the structures of interest that have to be visualised, different histological staining methods can be used. However, the most important issues for a reliable histological evaluation are correct sampling and processing of these samples. Since in most cases the skin regeneration process moves from the wound edges to the centre, comparable sampling positions are important when comparing different wounds.

Almost all studies reviewed used H&E staining to evaluate different aspects of the wound healing process (Fig. 3A). These aspects include the presence and thickness of granulation tissue, degradation of the biomaterial, extracellular matrix arrangement, vascularisation, (extent of) reepithelialisation or epithelial gap, epithelial thickness and differentiation, and the presence of normal skin structures like rete ridges, papillary plexus and appendages. H&E staining is also extremely useful in the identification and localisation of different cell types involved in the wound healing process, like macrophages, granulocytes (polymorphonuclear leukocytes), lymphocytes, (foreign body multinuclear) giant cells, and fibroblasts.

Alternative dyes were used to further distinguish between different tissue/biomaterial components. Richters *et al.* used an Elastic-van Gieson (EVG, also named Verhoeff-Van Gieson) staining to visualise elastic fibres and collagen [162]. Bannasch *et al.* used an Elastic-van Gieson staining to show Alloderm degradation (containing elastin fibres) and Trichrome-Goldner staining to analyse dermal collagen structures and epithelial morphology

[151,152]. Li *et al.* used Mallory's trichrome staining to distinguish scaffold polymer (white), tissue (red), and collagen deposition (green) [136], and Myers *et al.* used it to visualise collagen organisation and blood vessels, but also the general appearance of the dermis and epidermis [157]. Several studies used Masson's Trichrome staining to visualise scaffold remnants and to present a more general histological picture (inflammatory cells, blood vessels) [143,153,154,161,167,170,179,181,187]. Lamme *et al.* used Herovici picropolychrome staining to distinguish scaffold collagen (highly crosslinked, red/purple) from newly-formed collagen (blue) [189]. After four weeks, also the newly-formed collagen started to stain red/purple.

Polarised light microscopy on Sirius red-stained sections was used to analyse the organisation and orientation of collagen fibres in the wound bed, and provide clear details on the working mechanism of this technique [154,161]. Comparable methods including phase contrast (PH) microscopy were used on H&E-stained sections to assess collagen fibre maturation and/or orientation [169,177,180,198] and Lee *et al.* used it to localise collagen and subsequently measured the staining intensity to quantify collagen deposition [163]. Windsor *et al.* used orcein to stain (scaffold) collagen and a periodic acid-Schiff (glycogen) staining to visualise basement membrane formation (Fig. 3B&C) [146]. Alternatively, collagen orientation can be assessed without staining by small-angle light scattering measurements, which is also based on scattering of polarised light and was used by Yannas *et al.* [199].

Quantification of histological data has been technically challenging for a long time and was therefore hardly performed in studies. Lamme *et al.* used a semi-quantitative 1-5 scale to score for inflammation severity [177]. Other studies quantified the total area of granulation tissue [178] or the area of remaining polymer and newly-formed tissue [136] on images of tissue sections. Baynosa *et al.* simply counted blood vessels in tissue sections [145]. Pandit *et al.* used the IBAS image processing system (formerly sold by Kontron, Eching/München, Germany) to quantify contraction, epithelialisation, volume fractions of different cell types and blood vessels on H&E-stained sections [179,183,185,187,188]. This is also possible by using pixel intensities to quantify tissue and fibroblast ingrowth [200], which can be performed using freely-available software like ImageJ (http://rsbweb.nih.gov/ij/).

In conclusion, histological evaluation is generally used, but not systematically. Since most studies use H&E staining, we would recommend to introduce a standard checklist identifying the presence or absence of key players in wound healing, like keratinocytes, fibroblasts, macrophages, giant cells, and blood vessels. Currently, it often remains unclear whether cell types that are not mentioned, were studies at all. In addition, it would be worthwhile to quantify the area occupied by certain cells/structures, or total number of cells, but this remains technically challenging.

3.4 Protein expression levels and location

Protein expression is also an important read-out parameter in the evaluation of tissue-engineered constructs in animal models. Specific protein expression was analysed in most studies by use of immunohistochemistry (Table 4, Figs. 4 and 5). This method provides information on the specific location of the proteins assessed. Often one or more antibodies

were used to visualise proliferation and differentiation of the epidermis, components of the dermal-epidermal basement membrane and/or blood vessels, proteins specific for dermal structures and cells, and general markers for cell migration and differentiation.

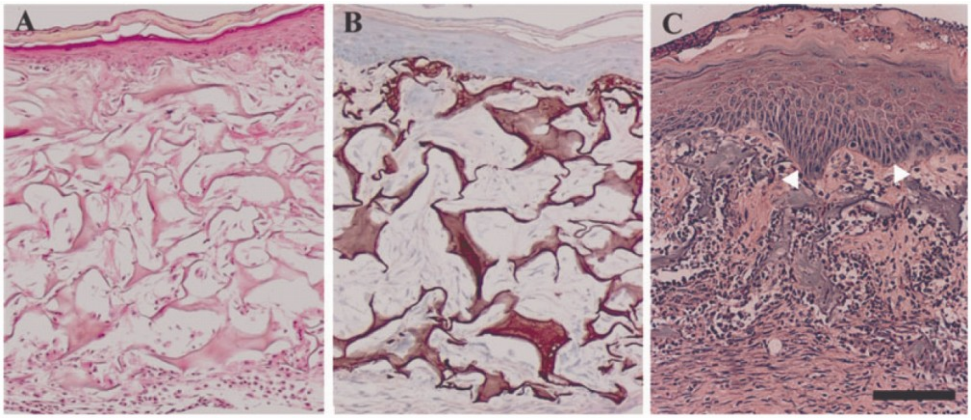

Figure 3. Examples of histological methods to evaluate wound healing, 14 days after grafting of a collagen-based construct containing human fibroblasts and keratinocytes on mice. (A) Epidermal architecture and dermal cellularity were evaluated with H&E staining. (B) An orcein staining was performed to visualise construct collagen. (C) A periodic acid-Schiff staining for glycogen visualises basement membrane formation (arrowheads). Bar is 100 µm. Copyright (2009) Wiley. Used with permission from Windsor ML *et al.* A novel model of wound healing in the SCID mouse using a cultured human skin substitute. Australas.J Dermatol 50, 29 [146].

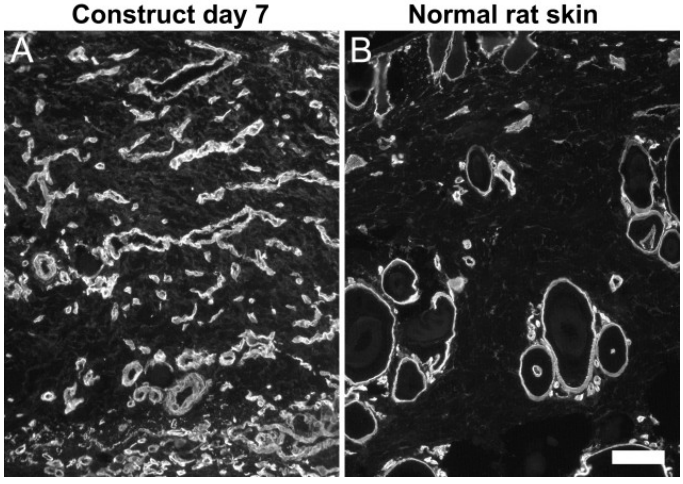

Figure 4. Immunohistological staining for type IV collagen on (A) a collagen-based construct, 7 days after implantation, visualising the basement membrane of blood vessels. (B) In normal rat skin less blood vessels are present, and mainly the basement membranes of appendages like hair follicles and sebaceous glands are visualised. Bar is 100 µm. Reprinted from Biomaterials, 31, Lammers *et al.*, High density gene expression microarrays and gene ontology analysis for identifying processes in implanted tissue engineering constructs, 8299, Copyright (2010), with permission from Elsevier [126].

Table 4 shows that many studies have used immunohistochemistry as a read-out parameter. However, there has been a huge variation in target antigens used to study epidermal and dermal components, basement membranes and blood vessels. To facilitate inter-study comparison, it is recommended to choose a standard panel of antibodies covering the most important structural aspects of skin. We suggest a panel of e.g. keratin 14 (basal keratinocytes), involucrin (cornified envelope keratinocytes), α-smooth muscle actin (myofibroblasts and mature blood vessels), type IV collagen (blood vessel and epidermal basement membrane), and CD31 (blood vessel endothelium).

As for conventional histology, quantification would be valuable, but was not often performed on immunohistologically stained sections. Lamme *et al.* used Leica Qwin image analysis software (Wetzlar, Germany) to quantify positively stained area [180] and Breen *et al.* used histological pictures and a grid to quantify cell numbers and the number of intersections with a cycloid line to quantify positively-stained blood vessels [143,161].

When human cells were transplanted to a (immunedeficient) mouse model, survival and location of the human cells were often determined by staining for human-specific HLA [131,133,139,146,150,152,153,166,173,184]. In other studies, cells were labelled before transplantation with PKH26 red fluorescent cell linker, green fluorescent protein (GFP), β-galactosidase, or DiI cell label, and the label was used to visualise these cells after explantation [130,135,142,143,147,156,163,189]. In addition, protein production after co-implantation of a gene expression vector was determined for e.g. platelet-derived growth factor (PDGF), vascular endothelial growth factor (VEGF), or endothelial nitric oxide synthase (eNOS) [161,170,174,178,182].

The presence and relative levels of proteins in a tissue sample can also be assessed by alternative methods. Perng *et al.* used SDS-PAGE followed by Western blotting to analyse the changes in protein expression levels in time after transplantation of human bone marrow-derived stem cells in a mouse wound model. They investigated the transformation in expression from the human bone marrow stem cells markers CD13 and CD105 to the epithelial cells specific E-cadherin and pancytokeratin [160]. Lamme *et al.* pre-labelled fibroblasts with PKH-26 before implantation and later used flow cytometry on a wound-derived single cell suspension to identify the presence of this label in different cell populations [189].

Gene expression levels and mRNA location

Construct-assisted wound healing in animal models can also be analysed by monitoring changes on the gene expression level. Scherer *et al.* used RT-qPCR to analyse the RNA expression levels in explanted mouse skin of the pro-angiogenic vasculature endothelial growth factor, the urokinase plasminogen activator receptor involved in cell migration, the inflammatory cytokine interleukin 1β, and matrix metalloproteinases 3 and 9 involved in extracellular matrix remodelling [134]. Other studies used real-time RT-PCR to determine gene expression levels of transplanted cells to assess the viability and contribution of these cells to the wound healing process. For example, expression of human vs. mouse housekeeping genes was analysed after transplantation of human cells in a mouse model [135], or

Y-chromosome specific gene expression after transplantation of male cells in female wounds [171].

Table 4. Overview of immunohistochemical staining used to evaluate tissue-engineered skin constructs *in vivo*.

	Antigen	Tissue/cells	Reference(s)
Epidermal	P63	Migrating keratinocytes	[134]
	(Pan)cytokeratin	Keratinocytes	[146,166,191]
	Keratin 6	Hyperproliferative keratinocytes	[171,176]
	Keratin 5	Basal keratinocytes	[172]
	Keratin 14	Basal keratinocytes	[140,163,176,191]
	Keratin 15	Basal keratinocytes	[131]
	Keratin 1	Suprabasal keratinocytes	[138,191,195]
	Keratin 10	Suprabasal keratinocytes	[140,168,172]
	Keratin 2	Cornified envelope keratinocytes	[131]
	Involucrin	Cornified envelope keratinocytes	[138,172,191,197]
	Loricrin	Cornified envelope keratinocytes	[131,172]
	Fillaggrin	Granular keratinocytes	[140]
	A6β4 integrin	Attaching keratinocytes	[190,191]
	Blood group antigens	Maturating epidermis	[146]
	HLA-DR	Langerhans cells	[146]
	Cartilage intermediate layer protein	Epidermis	[131]
	Osteoglycin	Epidermis	[131]
Dermal	α-smooth muscle actin (α-SMA)	Myofibroblasts & mature blood vessels	[138,142,152,155,162,163,173,177,180,195]
	Type I collagen	(Newly-formed) dermis	[128,166]
	Type III collagen	(Newly-formed) dermis	[128,154]
	Elastin	Elastic fibres	[155,168,180,193]
	Fibrillin-1	Microfibrils (elastic fibre formation)	[168]
	Fibronectin	Wounded dermis	[138,193]
	Periostin	Dermis	[131]
	Tenascin-C	Wounded dermis/DEJ	[138,168]
	Tenascin-X	Extracellular matrix	[168]
	Vimentin	Fibroblasts	[127,146,168,169,189,195]
	Heat-shock protein 47 (hsp47)	Fibroblasts	[142]
	F4/80	Macrophages	[163]
	CD68	Monocytes/macrophages	[129]
	'monocytes/macrophages'	Monocytes/macrophages	[169,195]
	CD8 alpha	Immune cells	[126]
BM	Chondroitin sulfate	Dermis & basement membrane	[193]
	Type VII collagen	Basement membrane	[151,152,171,190,191]
	Type IV collagen	Blood vessels & basement membrane	[126,139,151-153,155,196]
	Laminin	Blood vessels & basement membrane	[128,139,166,172,190,191,193,197,198]
BV	CD31	Blood vessels	[129,135,148,153,161]
	Factor VIII	Blood vessels/endothelial cells	[159,191]
	PECAM-1	Blood vessels	[134,163]
	Von Willebrand factor (vWF)	Blood vessels	[142,169,173,189,193,195]

(continued on next page)

Table 4 (continued)

	Antigen	Tissue/cells	Reference(s)
Other	Desmin	Muscle cells	[126]
	Phospho-MAPK	Migrating cells	[134]
	Ki67	Proliferating cells	[134,138,169,170,191]
	TUNEL	Apoptotic cells	[126]
'Labels'	Endothelial nitric oxide synthase	*In situ* transfected cells	[161]
	Platelet-derived growth factor	*In situ* transfected cells	[170,174,178,182]
	Vascular endothelial growth factor	*In situ* transfected cells	[178]
	Human HLA	Transplanted cell 'label'	[131,133,139,146,150,152,153,166,173,184]
	β-galactosidase	Transplanted cell label	[143,163]
	DiI cell label	Transplanted cell label	[135]
	Green fluorescent protein	Transplanted cell label	[142,156]
	PKH26 red fluorescent cell linker	Transplanted cell label	[130,147,189]

BM=basement membrane; BV=blood vessel, DEJ=dermal-epidermal junction

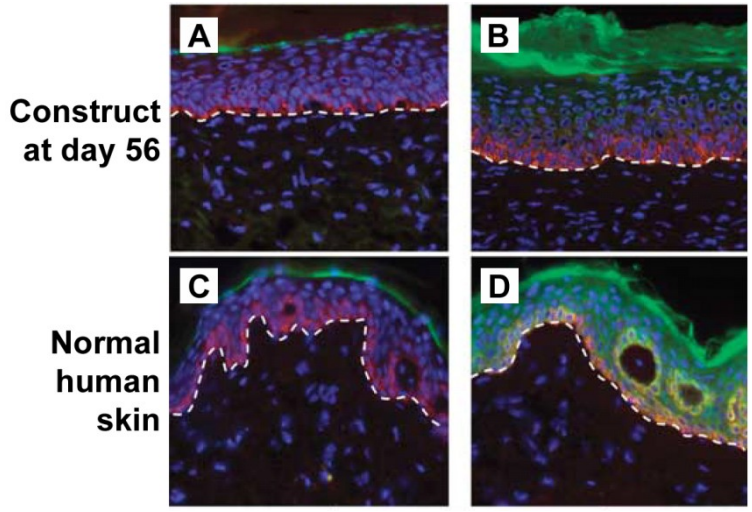

Figure 5. Immunohistological staining for keratin 15 (A-D, red) plus loricrin (A and C, green) and keratin 2 (B and D, green) 56 days after implantation of a cultured human skin construct on athymic mice (A and B), and in normal human skin (C and D). Adapted by permission from Macmillan Publishers Ltd: J. Invest Dermatol., Klingenberg *et al.*, Engineered Human Skin Substitutes Undergo Large-Scale Genomic Reprogramming and Normal Skin-Like Maturation after Transplantation to Athymic Mice, copyright (2009) [131].

A relatively novel approach is the use of gene expression microarrays. With this technique, experimental changes in gene expression levels of virtually all known genes can be assessed in a single experiment. Subsequent analysis can be performed on the level of individual genes, but the use of gene clusters also enables the identification of changes in e.g. biological processes. Klingenberg *et al.* used gene expression microarrays to evaluate changes in the gene expression profile of human cells in a cultured skin substitute after grafting onto mouse full-thickness wounds [131]. They followed up on the expression of

individual genes that had previously not been associated with skin development, and validated the presence of the proteins in their skin construct. In addition, clusters of genes with comparable expression patterns were analysed for their role in skin development. Lammers *et al.* used microarrays to analyse changes in biological processes that occurred in a collagen-based acellular skin construct after implantation in a rat full-thickness wound model (Fig. 6) [126]. By using a freely-available web-based tool, gene ontology terms for biological processes which are up- and downregulated in the construct versus normal skin were identified. Subsequently, these altered processes were validated (immuno)histochemically. Current limitations of this approach include the poor annotation of e.g. the rat genome, and the lack of tissue engineering specific gene ontology terms. However, the fast developments in this field hold promises for the future.

The location of gene expression can be visualised using *in situ* hybridisation. Although elegant in theory, this method proves to be rather specialistic in practice. It was used in only one of the reviewed studies to visualise transfected cells expressing human platelet-derived growth factor B after application to a rabbit wound model [170].

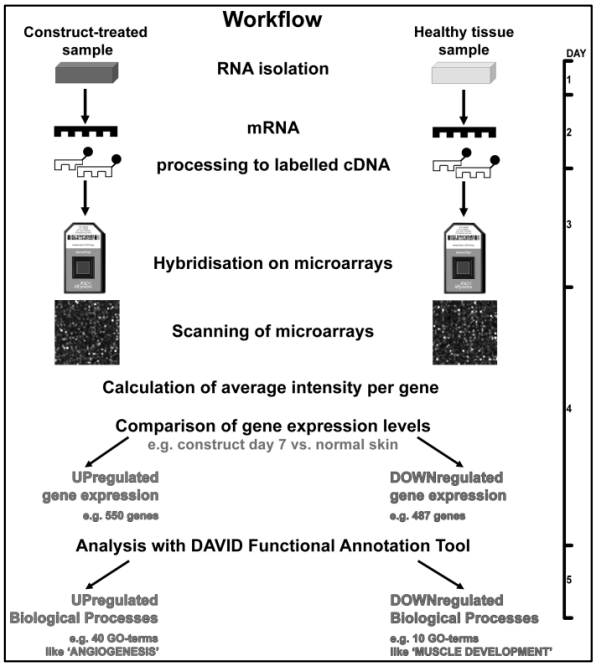

Figure 6. Schematic overview of the complete procedure for the identification of biological processes occuring *in vivo* in constructs used for tissue engineering using high-density gene expression microarrays, as proposed by Lammers *et al.* [126]. In short, mRNA was isolated from tissue samples and processed for hybridisation on rat exon arrays. The amount of hybridised RNA, reflecting the amount of specific mRNA's, was compared between groups, resulting in lists with up- and downregulated genes. Lists were uploaded in the free online DAVID functional annotation tool and the enrichment in biological process gene ontology (GO) terms was analysed. The minimal time required for each step is indicated on the right. Picture of microarray is courtesy of Affymetrix. Reprinted from Biomaterials, 31, Lammers *et al.*, High density gene expression microarrays and gene ontology analysis for identifying processes in implanted tissue engineering constructs, 8299, Copyright (2010), with permission from Elsevier [126].

Transillumination for visualisation of vascularisation

Several studies used the transillumination method developed by Egana *et al.* to visualise blood vessels in explanted nude mice skin (Fig. 7) [132,133,140,206]. Removed skin was placed over a transilluminator and digital pictures were taken to calculate vessel area and length in a semi-automated way. Altman *et al.* used a comparable method, but did not quantify the vasculature [142]. However, this method may be challenging in animals with hairs, or models like rat and pig with a thicker skin.

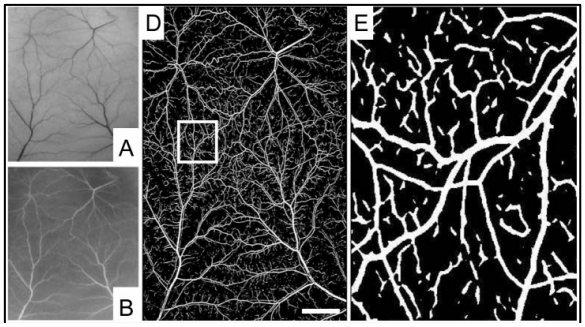

Figure 7. Transillumination technique to visualise and quantify blood vessels. Excised skin was placed over a transilluminator and a picture was taken, coverted to a greyscale (A), and inverted (B). This picture was converted to a black/white image (C) that was used for further quantification. (D) A close-up of the delineate area in (C) shows that even small blood vessels were segmented. Bar is 5 mm. Reprinted with kind permission from Springer Science+Business Media: Langenbecks Arch.Surg., Ex vivo method to visualize and quantify vascular networks in native and tissue engineered skin, 394(2):349-56, 2008. Egana *et al.* Fig. 3 [206].

In situ/in vivo imaging

Wang *et al.* compared Optical Coherence Tomography (OCT) with conventional H&E staining as a read-out tool for scaffold-assisted wound healing in mice [149] (Fig. 8). OCT uses the reflectance of an optical signal to create an image of the tissue assessed, without tissue pre-treatment. Mice were sacrificed at different time points, the regenerating wounds were imaged with OCT and then explanted and processed for H&E staining. Images to a maximum depth of 0.5 mm were obtained, thereby reaching the upper part of the subcutaneous fat layer. Removal of the highly backscattering epidermis increased the maximal imaging depth to 1.5 mm. It was possible to distinguish the epidermis, dermis, and subcutaneous fat in normal skin. During wound healing, reepithelialisation, areas of inflammatory cells and blisters could be visualised, as well as an implanted collagen scaffold and its degradation. Furthermore, the wound size determined in a lateral and vertical direction correlated highly with histology. Although these developments are promising, the resolution of obtained images is still low when compared to histology. Therefore, we would in this stage recommend the use of conventional histological methods to assess (epi)dermal characteristics.

Other studies used *in vivo* imaging to track the survival and distribution of fluorescently-labelled cells *in vivo* [135,160]. This is an elegant method, but it is dependent on fluorescent labelling and therefore difficult to apply to other cells/tissues.

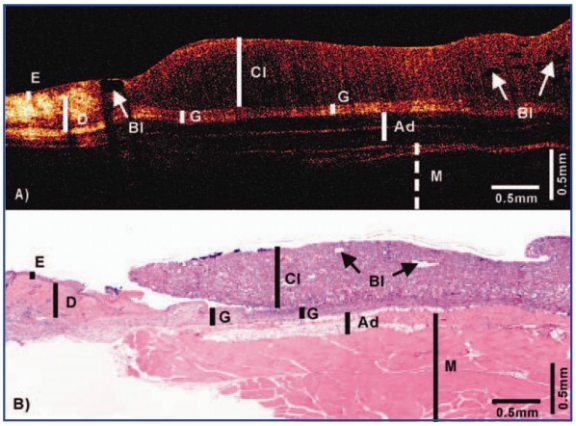

Figure 8. Images obtained by optical coherence tomography (A) and conventional histology (B) three days after implantation of a collagen construct in a mouse full-thickness wound. E=epidermis, D=dermis, Ad=adipose tissue, M=muscle layer, Cl=collagen implant, G=granular tissue, Bl=blisters. Reprinted with permission from Wang Z, *et al.* Assessment of dermal wound repair after collagen implantation with optical coherence tomography. TISSUE ENGINEERING, Part C, 2008, published by Mary Ann Liebert, Inc, New Rochelle, NY [149].

Electron microscopy

Although scanning electron microscopy is often used to characterise scaffolds before implantation, this technique is less useful as a read-out parameter. Transmission electron microscopy (TEM), on the other hand, was used by for a detailed examination of individual epidermal components and dermal elastic fibre, collagen, and fibroblast morphology [168,199]. Other studies used this technique to focus on newly-formed basement membrane components [190,196] and Lamme *et al.* used it to distinguish newly-synthesised collagen from scaffold collagen and identified myofibroblasts by visualisation of stress fibres in fibroblasts [193].

Because with TEM usually only small samples can be assessed, it is most suitable to answer specific research questions at a detailed level and is less appropriate in general wound evaluation.

Mechanical properties

Tissue strength is closely related to its functional performance and therefore it is remarkable that this important aspect of regenerated skin is often not assessed. Yannas *et al.* determined the 'peeling force' of their construct after transplantation, but the method used for this determination was not stated [202]. Pandit *et al.* tested the mechanical strength (ultimate tensile strength, stiffness, and failure strength) of explanted regenerating skin in time after treatment of rabbit wounds with a collagen scaffold with and without FGF-1 or TGF-β, and untreated wounds [179,183,185]. They used an Instron tester to evaluate 1x4 cm skin strips in uniaxial tension and calculated the ultimate tensile strength, modulus of elasticity, and strain-to-failure. Valuable information can thus be obtained, but the relatively large samples that are required may be a limiting factor.

Epidermal barrier

One of the important functions of skin is its barrier function. It is therefore striking that this function was not often assessed directly. Only few studies used a NOVA dermal phase meter to measure skin surface electrical capacitance to assess hydration and thereby barrier function after implantation of a tissue-engineered skin construct on athymic mice [184,194].

Microbiological sampling

Bacterial infection may influence the wound healing process [207] and is therefore an important aspect to monitor. Most studies did this by scoring signs of infection macro- or microscopically. For a more objective assessment of bacterial load, De Vries *et al.* took microbiological samples of wounds [198]. Quantitative microbiology of tissue samples is the only reliable method to prove tissue infection with respect to contamination or colonisation. Therefore, when facilities and expertise are available, this may be a helpful tool to obtain additional information on the condition of different wounds.

Recommendations and future outlook

A large number of tissue-engineered skin constructs has been developed and evaluated *in vivo*. Although many studies report promising results, so far only few constructs have entered the clinic. This discrepancy may in part be caused by the large variation in read-out methods used, and lack of standardisation thereof, severely hampering the systematic comparison of different studies/constructs. This variation can already be explained by the large number of different wound models used, ranging from wounds on the back of (immune-deficient) mice, rat and pigs to ear wounds in rabbits. Interstudy comparison is further hampered by the differences in description of macro- and microscopic observations and (when applicable) the large variation in antibodies used for immunohistological evaluation. We therefore propose the use of at least four standard evaluation methods (Table 5), viz: an observer scar assessment scale (OSAS), planimetry, H&E staining, and antibody staining for five key proteins in cutaneous wound healing. Using these parameters, it would be possible to calculate one over-all score for the *in vivo* performance of a tissue-engineered skin construct in an animal model. However, the importance of each single aspect may vary between studies and the reliability and validity of such a scoring system will require further investigation.

In addition, the lack of use of most of the non-invasive clinical methods (section 2) as read-out method for tissue-engineered skin constructs (section 3) is striking. Except for the measurement of wound area (planimetry), few studies describe a systematic registration of scar colour, thickness, relief, and elasticity. Most of the clinical methods listed do not interfere with subsequent invasive methods, and may therefore provide valuable additional information. Most of the methods were developed for, and validated on human skin, and this may be a reason for the lack of use in animal models, since the animal skin is different and will therefore require additional validation.

Table 5. Proposed standard assessment methods to evaluate wound healing in animal models after treatment with tissue-engineered skin constructs.

Level	Evaluation method	Scar feature
Macroscopic	Observer scar assessment scale (OSAS)	Vascularity, pigmentation, thickness, relief, and pliability
	Planimetry (direct tracing or on photographs)	Contraction
Microscopic	H&E staining	Amount of keratinocytes, fibroblasts, macrophages, giant cells, and blood vessels
	Antibody staining for keratin 14, involucrin, α-smooth muscle actin, type IV collagen, and CD31	Keratinocyte differentiation, presence of myofibroblasts and (mature) blood vessels

Another important aspect in using read-out methods is the fundamental difference between point measurements and field measurements. In general, the statistical variation is higher between point measurements (like colour measurement using a chromameter or mexameter, or skin pH measurement with an electrode) than between field measurements (like photography or scanning optical coherence tomography). Therefore, when using techniques that generate point measurements, a sound sampling plan is required to create data sets that will allow the detection of statistical differences.

Organisations like the international society for biophysics and imaging of the skin (ISBS, http://www.i-s-b-s.org/) play an important role in the development and standardisation of non-invasive methods for the assessment of skin conditions. International organisations are also working on the standardisation of skin tissue engineering. The ASTM International (previously known as the American society for testing and materials, http://www.astm.org/) and the international organization for standardization (ISO, http://www.iso.org/iso/home.htm) have developed valuable standards for the classification of therapeutic skin substitutes (ASTM F2311), characterisation and testing of biomaterial scaffolds used in tissue-engineered medical products (TEMPs, ASTM F2150), and testing for irritation and skin sensitisation of medical devices (ISO 10993-10:2010). However, to our knowledge, these do not include standards for the *in vivo* evaluation of tissue-engineered skin constructs.

Behavioural observations like scratching are of great importance since adverse effects like itching or pain are difficult to assess in animals (manuscript in preparation [208]). It is therefore recommended to closely monitor animal behaviour and report all relevant observations. Standardised methods for this evaluation are not yet available to our knowledge, but devices like the microAct (Neuroscience, Tokyo, Japan), that objectively measure scratching in mice, may be useful [209]. When possible, it is also recommended to assess gene expression. In our opinion, gene expression microarrays may provide valuable additional information on the wound healing process. With the rapid developments in the field of genomics, this technique may be replaced soon by more advanced methods like RNA-sequencing [210]. On the protein profiling level a technique such as mass-spectrometry opens new op-

portunities [211]. Also the dynamic field of imaging is rapidly developing and new techniques may be soon applicable in the field of tissue-engineering, including second harmonic imaging [212] to visualise e.g. collagen and elastic fibres in *ex vivo* skin, and multiphoton tomography [213] to visualise skin layers *in vivo* based on autofluorescence of e.g. keratinocytes, collagen and elastin.

In conclusion, a more systematic evaluation of tissue-engineered skin constructs in animal models would greatly enhance the comparison between different constructs and thereby accelerate the trajectory to application in human patients. This would be further enhanced by the embracement of clinically relevant evaluation methods. In addition, fundamental knowledge on construct-assisted wound healing may benefit by new developments in e.g gene expression analysis and non-invasive imaging.

Acknowledgements

The authors acknowledge the Dutch Program for Tissue Engineering (grants DPTE 6735 and 6739) for funding.

References

1. Gurtner GC, Werner S, Barrandon Y, Longaker MT. Wound repair and regeneration. Nature 2008;453:314-21.
2. van Zuijlen PP, Angeles AP, Kreis RW, Bos KE, Middelkoop E. Scar assessment tools: implications for current research. Plast Reconstr Surg 2002;109:1108-22.
3. Priya SG, Jungvid H, Kumar A. Skin tissue engineering for tissue repair and regeneration. Tissue Eng Part B Rev 2008;14:105-18.
4. van der Veen V, van der Wal MB, van Leeuwen MC, Ulrich MM, Middelkoop E. Biological background of dermal substitutes. Burns 2009.
5. MacNeil S. Progress and opportunities for tissue-engineered skin. Nature 2007;445:874-80.
6. Metcalfe AD, Ferguson MW. Bioengineering skin using mechanisms of regeneration and repair. Biomaterials 2007;28:5100-13.
7. Bottcher-Haberzeth S, Biedermann T, Reichmann E. Tissue engineering of skin. Burns 2010;36:450-60.
8. Lee KH. Tissue-engineered human living skin substitutes: development and clinical application. Yonsei Med J 2000;41:774-9.
9. Metcalfe AD, Ferguson MW. Tissue engineering of replacement skin: the crossroads of biomaterials, wound healing, embryonic development, stem cells and regeneration. J R Soc Interface 2007;4:413-37.
10. Brusselaers N, Pirayesh A, Hoeksema H, Richters CD, Verbelen J, Beele H, *et al.* Skin replacement in burn wounds. J Trauma 2010;68:490-501.
11. Smith GM, Tompkins DM, Bigelow ME, Antoon AY. Burn-induced cosmetic disfigurement: can it be measured reliably? J Burn Care Rehabil 1988;9:371-5.
12. Sullivan T, Smith J, Kermode J, McIver E, Courtemanche DJ. Rating the burn scar. J Burn Care Rehabil 1990;11:256-60.
13. Baryza MJ, Baryza GA. The Vancouver Scar Scale: an administration tool and its interrater reliability. J Burn Care Rehabil 1995;16:535-8.
14. Yeong EK, Mann R, Engrav LH, Goldberg M, Cain V, Costa B, *et al.* Improved burn scar assessment with use of a new scar-rating scale. J Burn Care Rehabil 1997;18:353-5.
15. Beausang E, Floyd H, Dunn KW, Orton CI, Ferguson MW. A new quantitative scale for clinical scar assessment. Plastic and reconstructive surgery 1998;102:1954-61.
16. Crowe JM, Simpson K, Johnson W, Allen J. Reliability of photographic analysis in determining change in scar appearance. J Burn Care Rehabil 1998;19:183-6.
17. Nedelec B, Shankowsky HA, Tredget EE. Rating the resolving hypertrophic scar: comparison of the Vancouver Scar Scale and scar volume. J Burn Care Rehabil 2000;21:205-12.
18. Draaijers LJ, Tempelman FR, Botman YA, Tuinebreijer WE, Middelkoop E, Kreis RW, *et al.* The patient and observer scar assessment scale: a reliable and feasible tool for scar evaluation. Plastic and reconstructive surgery 2004;113:1960-5.
19. Masters M, McMahon M, Svens B. Reliability testing of a new scar assessment tool, Matching Assessment of Scars and Photographs (MAPS). J Burn Care Rehabil 2005;26:273-84.

20. van de Kar AL, Corion LU, Smeulders MJ, Draaijers LJ, van der Horst CM, van Zuijlen PP. Reliable and feasible evaluation of linear scars by the Patient and Observer Scar Assessment Scale. Plast Reconstr Surg 2005;116:514-22.
21. Singer AJ, Arora B, Dagum A, Valentine S, Hollander JE. Development and validation of a novel scar evaluation scale. Plastic and reconstructive surgery 2007;120:1892-7.
22. Diffey BL, Oliver RJ, Farr PM. A portable instrument for quantifying erythema induced by ultraviolet radiation. Br J Dermatol 1984;111:663-72.
23. Diffey BL, Farr PM, Oakley AM. Quantitative studies on UVA-induced erythema in human skin. Br J Dermatol 1987;117:57-66.
24. Farr PM, Diffey BL. Quantitative studies on cutaneous erythema induced by ultraviolet radiation. Br J Dermatol 1984;111:673-82.
25. Alexander H, Miller DL. Determining skin thickness with pulsed ultra sound. J Invest Dermatol 1979;72:17-9.
26. Nedelec B, Correa JA, Rachelska G, Armour A, LaSalle L. Quantitative measurement of hypertrophic scar: intrarater reliability, sensitivity, and specificity. J Burn Care Res 2008;29:489-500.
27. Tan CY, Statham B, Marks R, Payne PA. Skin thickness measurement by pulsed ultrasound: its reproducibility, validation and variability. Br J Dermatol 1982;106:657-67.
28. Nedelec B, Correa JA, Rachelska G, Armour A, LaSalle L. Quantitative measurement of hypertrophic scar: interrater reliability and concurrent validity. J Burn Care Res 2008;29:501-11.
29. Taylor B, McGrouther DA, Bayat A. Use of a non-contact 3D digitiser to measure the volume of keloid scars: a useful tool for scar assessment. J Plast Reconstr Aesthet Surg 2007;60:87-94.
30. De Paepe K, Lagarde JM, Gall Y, Roseeuw D, Rogiers V. Microrelief of the skin using a light transmission method. Archives of dermatological research 2000;292:500-10.
31. Lagarde JM, Rouvrais C, Black D, Diridollou S, Gall Y. Skin topography measurement by interference fringe projection: a technical validation. Skin Res Technol 2001;7:112-21.
32. Kautzky F, Dahm MW, Drosner M, Köhler LD. Direct profilometry of the skin: Its reproducibility and variability. J Eur Acad Dermatol Venereol 1995;5:15-23.
33. Corcuff P, De Rigal J, Leveque JL. Image analysis of the cutaneous relief. Bioeng Skin Newslett 1982;4:16.
34. Saur R, Schramm U, Steinhoff R, Wolff HH. Structure analysis of the skin surface using computer-assisted laser profilometry. New method for the quantitative assessment of roughness structure of the skin. Hautarzt 1991;42:499-506.
35. Bloemen MC, van Leeuwen MC, van Vucht NE, van Zuijlen PP, Middelkoop E. Dermal substitution in acute burns and reconstructive surgery: a 12-year follow-up. Plastic and reconstructive surgery 2010;125:1450-9.
36. Vogel HG. Mechanical measurements of skin. Acta Derm Venereol Suppl (Stockh) 1994;185:39-43.
37. Barel AO, Courage W, Clarys P. Suction method for measurement of skin mechanical properties: the Cutometer®. In: Jemec GBE, ed. Handbook of non-invasive methods and the skin. Boca Raton: CRC Press Inc., 1995:335-340.
38. Draaijers LJ, Botman YA, Tempelman FR, Kreis RW, Middelkoop E, van Zuijlen PP. Skin elasticity meter or subjective evaluation in scars: a reliability assessment. Burns 2004;30:109-14.
39. Enomoto DN, Mekkes JR, Bossuyt PM, Hoekzema R, Bos JD. Quantification of cutaneous sclerosis with a skin elasticity meter in patients with generalized scleroderma. J Am Acad Dermatol 1996;35:381-7.
40. Fong SS, Hung LK, Cheng JC. The cutometer and ultrasonography in the assessment of postburn hypertrophic scar--a preliminary study. Burns 1997;23 Suppl 1:S12-S18.
41. Pierard GE, Nikkels-Tassoudji N, Pierard-Franchimont C. Influence of the test area on the mechanical properties of skin. Dermatology (Basel, Switzerland) 1995;191:9-15.
42. Pedersen LK, Hansen B, Jemec GBE. Mechanical properties of the skin: A comparison between two suction cup methods. Skin Res Tech 2003;9:111-5.
43. Elsner P, Wilhelm D, Maibach HI. Mechanical properties of human forearm and vulvar skin. Br J Dermatol 1990;122:607-14.
44. Pedersen LK, Jemec GB. Plasticising effect of water and glycerin on human skin *in vivo*. J Dermatol Sci 1999;19:48-52.
45. Serup J, Northeved A. Skin elasticity in localized scleroderma (morphoea). Introduction of a biaxial *in vivo* method for measurement of tensile distensibility, hysteresis, and resilient distension of diseased and normal skin. J Dermatol 1985;12:52-62.
46. Serup J, Northeved A. Skin elasticity in psoriasis. *In vivo* measurement of tensile distensibility, hysteresis and resilient distension with a new method. Comparison with skin thickness as measured with high-frequency ultrasound. J Dermatol 1985;12:318-24.
47. Katz SM, Frank DH, Leopold GR, Wachtel TL. Objective measurement of hypertrophic burn scar: a preliminary study of tonometry and ultrasonography. Ann Plast Surg 1985;14:121-7.
48. Spann K, Mileski WJ, Atiles L, Purdue G, Hunt J. The 1996 Clinical Research award. Use of a pneumatonometer in burn scar assessment. J Burn Care Rehabil 1996;17:515-7.
49. Lye I, Edgar DW, Wood FM, Carroll S. Tissue tonometry is a simple, objective measure for pliability of burn scar: is it reliable? J Burn Care Res 2006;27:82-5.
50. Falanga V, Bucalo B. Use of a durometer to assess skin hardness. J Am Acad Dermatol 1993;29:47-51.

51. Kissin EY, Schiller AM, Gelbard RB, Anderson JJ, Falanga V, Simms RW, *et al.* Durometry for the assessment of skin disease in systemic sclerosis. Arthritis Rheum 2006;55:603-9.
52. LeBlanc N, Falabella A, Murata H, Hasan A, Weiss E, Falanga V. Durometer measurements of skin induration in venous disease. Dermatol Surg 1997;23:285-7.
53. Merkel PA, Silliman NP, Denton CP, Furst DE, Khanna D, Emery P, *et al.* Validity, reliability, and feasibility of durometer measurements of scleroderma skin disease in a multicenter treatment trial. Arthritis Rheum 2008;59:699-705.
54. Romanelli M, Falanga V. Use of a durometer to measure the degree of skin induration in lipodermatosclerosis. J Am Acad Dermatol 1995;32:188-91.
55. Seyger MM, van den Hoogen FH, de Boo T, de Jong EM. Reliability of two methods to assess morphea: skin scoring and the use of a durometer. J Am Acad Dermatol 1997;37:793-6.
56. Barbenel JC, Evans JH. The time-dependent mechanical properties of skin. J Invest Dermatol 1977;69:318-20.
57. Finlay B. Dynamic mechanical testing of human skin '*in vivo*'. Journal of biomechanics 1970;3:557-68.
58. Finlay B. The torsional characteristics of human skin *in vivo*. Biomed Eng 1971;6:567-73.
59. Boyce ST, Supp AP, Wickett RR, Hoath SB, Warden GD. Assessment with the dermal torque meter of skin pliability after treatment of burns with cultured skin substitutes. J Burn Care Rehabil 2000;21:55-63.
60. Bartell TH, Monafo WW, Mustoe TA. A new instrument for serial measurements of elasticity in hypertrophic scar. J Burn Care Rehabil 1988;9:657-60.
61. Stark HL. Directional variations in the extensibility of human skin. Br J Plast Surg 1977;30:105-14.
62. Bohannon RW, Pfaller BA. Documentation of wound surface area from tracings of wound perimeters. Clinical report on three techniques. Phys Ther 1983;63:1622-4.
63. Bryant RA. Acute and Chronic Wounds: Nursing Management. St. Louis: CV Mosby, 1992.
64. Ferrell BA, Artinian BM, Sessing D. The Sessing scale for assessment of pressure ulcer healing. J Am Geriatr Soc 1995;43:37-40.
65. Liskay AM, Mion LC, Davis BR. Comparison of two devices for wound measurement. Dermatol Nurs 1993;5:437-41, 434.
66. Thomas AC, Wysocki AB. The healing wound: a comparison of three clinically useful methods of measurement. Decubitus 1990;3:18-20, 24.
67. Anthony D, Barnes E. Pressure sores. One. Measuring pressure sores accurately. Nurs Times 1984;80:33-5.
68. Cutler NR, George R, Seifert RD, Brunelle R, Sramek JJ, McNeill K, *et al.* Comparison of quantitative methodologies to define chronic pressure ulcer measurements. Decubitus 1993;6:22-30.
69. Johnson M, Miller R. Measuring healing in leg ulcers: practice considerations. Appl Nurs Res 1996;9:204-8.
70. Kim NH, Wysocki AB, Bovik AC, Diller KR. A microcomputer-based vision system for area measurement. Comput Biol Med 1987;17:173-83.
71. Bulstrode CJ, Goode AW, Scott PJ. Stereophotogrammetry for measuring rates of cutaneous healing: a comparison with conventional techniques. Clin Sci (Lond) 1986;71:437-43.
72. Plassmann P, Jones TD. MAVIS: a non-invasive instrument to measure area and volume of wounds. Measurement of Area and Volume Instrument System. Med Eng Phys 1998;20:332-8.
73. Frantz RA, Johnson DA. Stereophotography and computerized image analysis: a three-dimensional method of measuring wound healing. Wounds 1992;4:58-64.
74. Caspers PJ, Lucassen GW, Carter EA, Bruining HA, Puppels GJ. *In vivo* confocal Raman microspectroscopy of the skin: noninvasive determination of molecular concentration profiles. J Invest Dermatol 2001;116:434-42.
75. Visscher M, Hoath SB, Conroy E, Wickett RR. Effect of semipermeable membranes on skin barrier repair following tape stripping. Archives of dermatological research 2001;293:491-9.
76. Eberlein-Konig B, Schafer T, Huss-Marp J, Darsow U, Mohrenschlager M, Herbert O, *et al.* Skin surface pH, stratum corneum hydration, trans-epidermal water loss and skin roughness related to atopic eczema and skin dryness in a population of primary school children. Acta dermato-venereologica 2000;80:188-91.
77. Cohen JC, Hartman DG, Garofalo MJ, Basehoar A, Raynor B, Ashbrenner E, *et al.* Comparison of closed chamber and open chamber evaporimetry. Skin Res Technol 2009;15:51-4.
78. Van den Kerckhove E, Staes F, Flour M, Stappaerts K, Boeckx W. Reproducibility of repeated measurements on healthy skin with Minolta Chromameter CR-300. Skin Res Technol 2001;7:56-9.
79. Draaijers LJ, Tempelman FR, Botman YA, Kreis RW, Middelkoop E, van Zuijlen PP. Colour evaluation in scars: tristimulus colorimeter, narrow-band simple reflectance meter or subjective evaluation? Burns 2004;30:103-7.
80. Li-Tsang CW, Lau JC, Liu SK. Validation of an objective scar pigmentation measurement by using a spectrocolorimeter. Burns 2003;29:779-84.
81. Lau JC, Li-Tsang CW, Zheng YP. Application of tissue ultrasound palpation system (TUPS) in objective scar evaluation. Burns 2005;31:445-52.
82. Corica GF, Wigger NC, Edgar DW, Wood FM, Carroll S. Objective measurement of scarring by multiple assessors: is the tissue tonometer a reliable option? J Burn Care Res 2006;27:520-3.
83. Murray BC, Wickett RR. Correlations between dermal torque meter, cutometer, and dermal phase meter measurements of human skin. Skin Res Tech 1997;3:101-6.

84. van Zuijlen PP, Angeles AP, Suijker MH, Kreis RW, Middelkoop E. Reliability and accuracy of techniques for surface area measurements of wounds and scars. Int J Low Extrem Wounds 2004;3:7-11.
85. Gethin G, Cowman S. Wound measurement comparing the use of acetate tracings and Visitrak digital planimetry. Journal of clinical nursing 2006;15:422-7.
86. Wunderlich RP, Peters EJ, Armstrong DG, Lavery LA. Reliability of digital videometry and acetate tracing in measuring the surface area of cutaneous wounds. Diabetes Res Clin Pract 2000;49:87-92.
87. Stramer BM, Mori R, Martin P. The inflammation-fibrosis link? A Jekyll and Hyde role for blood cells during wound repair. J Invest Dermatol 2007;127:1009-17.
88. Hinz B. Formation and function of the myofibroblast during tissue repair. J Invest Dermatol 2007;127:526-37.
89. Toriseva M, Kahari VM. Proteinases in cutaneous wound healing. Cell Mol Life Sci 2009;66:203-24.
90. Greco JA, III, Pollins AC, Boone BE, Levy SE, Nanney LB. A microarray analysis of temporal gene expression profiles in thermally injured human skin. Burns 2010;36:192-204.
91. Nassiri M, Woolery-Lloyd H, Ramos S, Jacob SE, Gugic D, Viciana A, *et al.* Gene expression profiling reveals alteration of caspase 6 and 14 transcripts in normal skin of keloid-prone patients. Archives of dermatological research 2009;301:183-8.
92. Morey JS, Ryan JC, Van Dolah FM. Microarray validation: factors influencing correlation between oligonucleotide microarrays and real-time PCR. Biological procedures online 2006;8:175-93.
93. Derveaux S, Vandesompele J, Hellemans J. How to do successful gene expression analysis using real-time PCR. Methods (San Diego, Calif 2010;50:227-30.
94. De Felice B, Wilson RR, Nacca M. Telomere shortening may be associated with human keloids. BMC Med Genet 2009;10:110.
95. van der Slot AJ, Zuurmond AM, Bardoel AF, Wijmenga C, Pruijs HE, Sillence DO, *et al.* Identification of PLOD2 as telopeptide lysyl hydroxylase, an important enzyme in fibrosis. J Biol Chem 2003;278:40967-72.
96. Toksoy A, Muller V, Gillitzer R, Goebeler M. Biphasic expression of stromal cell-derived factor-1 during human wound healing. Br J Dermatol 2007;157:1148-54.
97. Chen XG, Wang Z, Liu WS, Park HJ. The effect of carboxymethyl-chitosan on proliferation and collagen secretion of normal and keloid skin fibroblasts. Biomaterials 2002;23:4609-14.
98. Park HJ, Cho DH, Kim HJ, Lee JY, Cho BK, Bang SI, *et al.* Collagen synthesis is suppressed in dermal fibroblasts by the human antimicrobial peptide LL-37. J Invest Dermatol 2009;129:843-50.
99. Schrementi ME, Ferreira AM, Zender C, DiPietro LA. Site-specific production of TGF-beta in oral mucosal and cutaneous wounds. Wound Repair Regen 2008;16:80-6.
100. Trengove NJ, Stacey MC, MacAuley S, Bennett N, Gibson J, Burslem F, *et al.* Analysis of the acute and chronic wound environments: the role of proteases and their inhibitors. Wound Repair Regen 1999;7:442-52.
101. Bullen EC, Longaker MT, Updike DL, Benton R, Ladin D, Hou Z, *et al.* Tissue inhibitor of metalloproteinases-1 is decreased and activated gelatinases are increased in chronic wounds. J Invest Dermatol 1995;104:236-40.
102. Lafuma C, El Nabout RA, Crechet F, Hovnanian A, Martin M. Expression of 72-kDa gelatinase (MMP-2), collagenase (MMP-1), and tissue metalloproteinase inhibitor (TIMP) in primary pig skin fibroblast cultures derived from radiation-induced skin fibrosis. J Invest Dermatol 1994;102:945-50.
103. Wysocki AB, Kusakabe AO, Chang S, Tuan TL. Temporal expression of urokinase plasminogen activator, plasminogen activator inhibitor and gelatinase-B in chronic wound fluid switches from a chronic to acute wound profile with progression to healing. Wound Repair Regen 1999;7:154-65.
104. Higuchi K, Kajiki A, Nakamura M, Harada S, Pula PJ, Scott AL, *et al.* Proteases released in organ culture by acute dermal inflammatory lesions produced *in vivo* in rabbit skin by sulfur mustard: hydrolysis of synthetic peptide substrates for trypsin-like and chymotrypsin-like enzymes. Inflammation 1988;12:311-34.
105. Rogers AA, Burnett S, Moore JC, Shakespeare PG, Chen WY. Involvement of proteolytic enzymes--plasminogen activators and matrix metalloproteinases--in the pathophysiology of pressure ulcers. Wound Repair Regen 1995;3:273-83.
106. Salonurmi T, Parikka M, Kontusaari S, Pirila E, Munaut C, Salo T, *et al.* Overexpression of TIMP-1 under the MMP-9 promoter interferes with wound healing in transgenic mice. Cell Tissue Res 2004;315:27-37.
107. Yi CF, Gosiewska A, Burtis D, Geesin J. Incorporation of fluorescent enzyme substrates in agarose gel for in situ zymography. Analytical biochemistry 2001;291:27-33.
108. Frederiks WM, Mook OR. Metabolic mapping of proteinase activity with emphasis on in situ zymography of gelatinases: review and protocols. J Histochem Cytochem 2004;52:711-22.
109. De Felice B, Garbi C, Santoriello M, Santillo A, Wilson RR. Differential apoptosis markers in human keloids and hypertrophic scars fibroblasts. Mol Cell Biochem 2009;327:191-201.
110. Andriessen MP, Niessen FB, Van de Kerkhof PC, Schalkwijk J. Hypertrophic scarring is associated with epidermal abnormalities: an immunohistochemical study. J Pathol 1998;186:192-200.
111. Kumar I, Staton CA, Cross SS, Reed MW, Brown NJ. Angiogenesis, vascular endothelial growth factor and its receptors in human surgical wounds. Br J Surg 2009;96:1484-91.
112. Tredget EE, Yang L, Delehanty M, Shankowsky H, Scott PG. Polarized Th2 cytokine production in patients with hypertrophic scar following thermal injury. J Interferon Cytokine Res 2006;26:179-89.

113. Verhaegen PD, van Zuijlen PP, Pennings NM, van Marle J, Niessen FB, van der Horst CM, *et al.* Differences in collagen architecture between keloid, hypertrophic scar, normotrophic scar, and normal skin: An objective histopathological analysis. Wound Repair Regen 2009;17:649-56.
114. de Vries HJ, Enomoto DN, van Marle J, van Zuijlen PP, Mekkes JR, Bos JD. Dermal organization in scleroderma: the fast Fourier transform and the laser scatter method objectify fibrosis in nonlesional as well as lesional skin. Lab Invest 2000;80:1281-9.
115. van Zuijlen PP, de Vries HJ, Lamme EN, Coppens JE, van Marle J, Kreis RW, *et al.* Morphometry of dermal collagen orientation by Fourier analysis is superior to multi-observer assessment. J Pathol 2002;198:284-91.
116. Har-Shai Y, Amar M, Sabo E. Intralesional cryotherapy for enhancing the involution of hypertrophic scars and keloids. Plastic and reconstructive surgery 2003;111:1841-52.
117. Har-Shai Y, Sabo E, Rohde E, Hyams M, Assaf C, Zouboulis CC. Intralesional cryosurgery enhances the involution of recalcitrant auricular keloids: a new clinical approach supported by experimental studies. Wound Repair Regen 2006;14:18-27.
118. Ng CP, Hinz B, Swartz MA. Interstitial fluid flow induces myofibroblast differentiation and collagen alignment *in vitro*. Journal of cell science 2005;118:4731-9.
119. Singer AJ, McClain SA. Development of a porcine incisional wound model and novel scarring scales. Wound Repair Regen 2006;14:492-7.
120. van Zuijlen PP, Ruurda JJ, van Veen HA, van Marle J, van Trier AJ, Groenevelt F, *et al.* Collagen morphology in human skin and scar tissue: no adaptations in response to mechanical loading at joints. Burns 2003;29:423-31.
121. van Zuijlen PP, Lamme EN, van Galen MJ, van Marle J, Kreis RW, Middelkoop E. Long-term results of a clinical trial on dermal substitution. A light microscopy and Fourier analysis based evaluation. Burns 2002;28:151-60.
122. Dorsett-Martin WA. Rat models of skin wound healing: a review. Wound Repair Regen 2004;12:591-9.
123. Lindblad WJ. Considerations for selecting the correct animal model for dermal wound-healing studies. Journal of biomaterials science 2008;19:1087-96.
124. Middelkoop E, van den Bogaerdt AJ, Lamme EN, Hoekstra MJ, Brandsma K, Ulrich MM. Porcine wound models for skin substitution and burn treatment. Biomaterials 2004;25:1559-67.
125. Sullivan TP, Eaglstein WH, Davis SC, Mertz P. The pig as a model for human wound healing. Wound Repair Regen 2001;9:66-76.
126. Lammers G, Gilissen C, Nillesen ST, Uijtdewilligen PJ, Wismans RG, Veltman JA, *et al.* High density gene expression microarrays and gene ontology analysis for identifying processes in implanted tissue engineering constructs. Biomaterials 2010;31:8299-312.
127. Matsumoto Y, Kuroyanagi Y. Design of a matrix for cultured dermal substitute suitable for simultaneous transplantation with auto-skin graft: evaluation in animal test. Journal of biomaterials science 2010;21:83-94.
128. Steinstraesser L, Wehner M, Trust G, Sorkin M, Bao D, Hirsch T, *et al.* Laser-mediated fixation of collagen-based scaffolds to dermal wounds. Lasers Surg Med 2010;42:141-9.
129. Kurpinski KT, Stephenson JT, Janairo RR, Lee H, Li S. The effect of fiber alignment and heparin coating on cell infiltration into nanofibrous PLLA scaffolds. Biomaterials 2010;31:3536-42.
130. Wang W, Zhang M, Lu W, Zhang X, Ma D, Rong X, *et al.* Cross-linked collagen-chondroitin sulfate-hyaluronic acid imitating extracellular matrix as scaffold for dermal tissue engineering. Tissue Eng Part C Methods 2010;16:269-79.
131. Klingenberg JM, McFarland KL, Friedman AJ, Boyce ST, Aronow BJ, Supp DM. Engineered Human Skin Substitutes Undergo Large-Scale Genomic Reprogramming and Normal Skin-Like Maturation after Transplantation to Athymic Mice. J Invest Dermatol 2009.
132. Egana JT, Danner S, Kremer M, Rapoport DH, Lohmeyer JA, Dye JF, *et al.* The use of glandular-derived stem cells to improve vascularization in scaffold-mediated dermal regeneration. Biomaterials 2009;30:5918-26.
133. Egana JT, Fierro FA, Kruger S, Bornhauser M, Huss R, Lavandero S, *et al.* Use of human mesenchymal cells to improve vascularization in a mouse model for scaffold-based dermal regeneration. Tissue Eng Part A 2009;15:1191-200.
134. Scherer SS, Pietramaggiori G, Matthews J, Perry S, Assmann A, Carothers A, *et al.* Poly-N-acetyl glucosamine nanofibers: a new bioactive material to enhance diabetic wound healing by cell migration and angiogenesis. Ann Surg 2009;250:322-30.
135. Kim KL, Han DK, Park K, Song SH, Kim JY, Kim JM, *et al.* Enhanced dermal wound neovascularization by targeted delivery of endothelial progenitor cells using an RGD-g-PLLA scaffold. Biomaterials 2009;30:3742-8.
136. Li B, Davidson JM, Guelcher SA. The effect of the local delivery of platelet-derived growth factor from reactive two-component polyurethane scaffolds on the healing in rat skin excisional wounds. Biomaterials 2009.
137. Okabayashi R, Nakamura M, Okabayashi T, Tanaka Y, Nagai A, Yamashita K. Efficacy of polarized hydroxyapatite and silk fibroin composite dressing gel on epidermal recovery from full-thickness skin wounds. J Biomed Mater Res B Appl Biomater 2009;90:641-6.

138. Masuda R, Mochizuki M, Hozumi K, Takeda A, Uchinuma E, Yamashina S, *et al.* A novel cell-adhesive scaffold material for delivering keratinocytes reduces granulation tissue in dermal wounds. Wound Repair Regen 2009;17:127-35.
139. Xiao S, Zhu S, Li H, Yang J, Lv K, Xia Z. Feasibility study of composite skin reconstructed by mixing keratinocytes and acellular dermal matrix for wound repair. Swiss Med Wkly 2009;139:16-21.
140. Salem H, Ciba P, Rapoport DH, Egana JT, Reithmayer K, Kadry M, *et al.* The influence of pancreas-derived stem cells on scaffold based skin regeneration. Biomaterials 2009;30:789-96.
141. Bao L, Yang W, Mao X, Mou S, Tang S. Agar/collagen membrane as skin dressing for wounds. Biomed Mater 2008;3:44108.
142. Altman AM, Yan Y, Matthias N, Bai X, Rios C, Mathur AB, *et al.* IFATS collection: Human adipose-derived stem cells seeded on a silk fibroin-chitosan scaffold enhance wound repair in a murine soft tissue injury model. Stem Cells 2009;27:250-8.
143. Breen A, Dockery P, O'Brien T, Pandit A. Fibrin scaffold promotes adenoviral gene transfer and controlled vector delivery. J Biomed Mater Res A 2009;89:876-84.
144. Yang L, Shirakata Y, Tokumaru S, Xiuju D, Tohyama M, Hanakawa Y, *et al.* Living skin equivalents constructed using human amnions as a matrix. J Dermatol Sci 2009;56:188-95.
145. Baynosa RC, Browder LK, Jones SR, Oliver JA, Van Der Harten CA, Stephenson LL, *et al.* Evaluation of artificial dermis neovascularization in an avascular wound. J Reconstr Microsurg 2009;25:405-10.
146. Windsor ML, Eisenberg M, Gordon-Thomson C, Moore GP. A novel model of wound healing in the SCID mouse using a cultured human skin substitute. Australas J Dermatol 2009;50:29-35.
147. Zhang X, Deng Z, Wang H, Yang Z, Guo W, Li Y, *et al.* Expansion and delivery of human fibroblasts on micronized acellular dermal matrix for skin regeneration. Biomaterials 2009;30:2666-74.
148. Schneider J, Biedermann T, Widmer D, Montano I, Meuli M, Reichmann E, *et al.* Matriderm versus Integra: a comparative experimental study. Burns 2009;35:51-7.
149. Wang Z, Pan H, Yuan Z, Liu J, Chen W, Pan Y. Assessment of dermal wound repair after collagen implantation with optical coherence tomography. Tissue Eng Part C Methods 2008;14:35-45.
150. Kalyanaraman B, Supp DM, Boyce ST. Medium flow rate regulates viability and barrier function of engineered skin substitutes in perfusion culture. Tissue Eng Part A 2008;14:583-93.
151. Bannasch H, Unterberg T, Fohn M, Weyand B, Horch RE, Stark GB. Cultured keratinocytes in fibrin with decellularised dermis close porcine full-thickness wounds in a single step. Burns 2008;34:1015-21.
152. Bannasch H, Stark GB, Knam F, Horch RE, Fohn M. Decellularized dermis in combination with cultivated keratinocytes in a short- and long-term animal experimental investigation. J Eur Acad Dermatol Venereol 2008;22:41-9.
153. Powell HM, Supp DM, Boyce ST. Influence of electrospun collagen on wound contraction of engineered skin substitutes. Biomaterials 2008;29:834-43.
154. Garcia Y, Wilkins B, Collighan RJ, Griffin M, Pandit A. Towards development of a dermal rudiment for enhanced wound healing response. Biomaterials 2008;29:857-68.
155. Nillesen S, Lammers G, van den Bogaerdt A, Schalkwijk J, Daamen W, van Kuppevelt T. A Double-Layered Acellular Skin Construct; Evaluation In A Rat Full-Thickness Wound Model. Wound Repair Regen 2007;15:A114.
156. Falanga V, Iwamoto S, Chartier M, Yufit T, Butmarc J, Kouttab N, *et al.* Autologous bone marrow-derived cultured mesenchymal stem cells delivered in a fibrin spray accelerate healing in murine and human cutaneous wounds. Tissue Eng 2007;13:1299-312.
157. Myers SR, Partha VN, Soranzo C, Price RD, Navsaria HA. Hyalomatrix: a temporary epidermal barrier, hyaluronan delivery, and neodermis induction system for keratinocyte stem cell therapy. Tissue Eng 2007;13:2733-41.
158. Tanihara M, Kajiwara K, Ida K, Suzuki Y, Kamitakahara M, Ogata S. The biodegradability of poly(Pro-Hyp-Gly) synthetic polypeptide and the promotion of a dermal wound epithelialization using a poly(Pro-Hyp-Gly) sponge. J Biomed Mater Res A 2008;85:133-9.
159. Ma L, Shi Y, Chen Y, Zhao H, Gao C, Han C. *In vitro* and *in vivo* biological performance of collagen-chitosan/silicone membrane bilayer dermal equivalent. J Mater Sci Mater Med 2007;18:2185-91.
160. Perng CK, Kao CL, Yang YP, Lin HT, Lin WB, Chu YR, *et al.* Culturing adult human bone marrow stem cells on gelatin scaffold with pNIPAAm as transplanted grafts for skin regeneration. J Biomed Mater Res A 2008;84:622-30.
161. Breen AM, Dockery P, O'Brien T, Pandit AS. The use of therapeutic gene eNOS delivered via a fibrin scaffold enhances wound healing in a compromised wound model. Biomaterials 2008;29:3143-51.
162. Richters CD, Pirayesh A, Hoeksema H, Kamperdijk EW, Kreis RW, Dutrieux RP, *et al.* Development of a dermal matrix from glycerol preserved allogeneic skin. Cell Tissue Bank 2008;9:309-15.
163. Lee PY, Cobain E, Huard J, Huang L. Thermosensitive hydrogel PEG-PLGA-PEG enhances engraftment of muscle-derived stem cells and promotes healing in diabetic wound. Mol Ther 2007;15:1189-94.
164. Waldeck H, Chung AS, Kao WJ. Interpenetrating polymer networks containing gelatin modified with PEGylated RGD and soluble KGF: synthesis, characterization, and application in *in vivo* critical dermal wound. J Biomed Mater Res A 2007;82:861-71.
165. Lin H, Chen B, Sun W, Zhao W, Zhao Y, Dai J. The effect of collagen-targeting platelet-derived growth factor on cellularization and vascularization of collagen scaffolds. Biomaterials 2006;27:5708-14.

166. Ng KW, Hutmacher DW. Reduced contraction of skin equivalent engineered using cell sheets cultured in 3D matrices. Biomaterials 2006;27:4591-8.
167. Lee SB, Kim YH, Chong MS, Hong SH, Lee YM. Study of gelatin-containing artificial skin V: fabrication of gelatin scaffolds using a salt-leaching method. Biomaterials 2005;26:1961-8.
168. Zweers MC, Schalkwijk J, Van Kuppevelt TH, van Vlijmen-Willems IM, Bergers M, Lethias C, *et al.* Transplantation of reconstructed human skin on nude mice: a model system to study expression of human tenascin-X and elastic fiber components. Cell Tissue Res 2005;319:279-87.
169. Druecke D, Lamme EN, Hermann S, Pieper J, May PS, Steinau HU, *et al.* Modulation of scar tissue formation using different dermal regeneration templates in the treatment of experimental full-thickness wounds. Wound Repair Regen 2004;12:518-27.
170. Gu DL, Nguyen T, Gonzalez AM, Printz MA, Pierce GF, Sosnowski BA, *et al.* Adenovirus encoding human platelet-derived growth factor-B delivered in collagen exhibits safety, biodistribution, and immunogenicity profiles favorable for clinical use. Mol Ther 2004;9:699-711.
171. Price RD, Das-Gupta V, Harris PA, Leigh IM, Navsaria HA. The role of allogenic fibroblasts in an acute wound healing model. Plast Reconstr Surg 2004;113:1719-29.
172. Llames SG, Del RM, Larcher F, Garcia E, Garcia M, Escamez MJ, *et al.* Human plasma as a dermal scaffold for the generation of a completely autologous bioengineered skin. Transplantation 2004;77:350-5.
173. Wang HJ, Pieper J, Schotel R, van Blitterswijk CA, Lamme EN. Stimulation of skin repair is dependent on fibroblast source and presence of extracellular matrix. Tissue Eng 2004;10:1054-64.
174. Breitbart AS, Laser J, Parrett B, Porti D, Grant RT, Grande DA, *et al.* Accelerated diabetic wound healing using cultured dermal fibroblasts retrovirally transduced with the platelet-derived growth factor B gene. Ann Plast Surg 2003;51:409-14.
175. Lee SB, Jeon HW, Lee YW, Lee YM, Song KW, Park MH, *et al.* Bio-artificial skin composed of gelatin and (1-->3), (1-->6)-beta-glucan. Biomaterials 2003;24:2503-11.
176. Grant I, Warwick K, Marshall J, Green C, Martin R. The co-application of sprayed cultured autologous keratinocytes and autologous fibrin sealant in a porcine wound model. Br J Plast Surg 2002;55:219-27.
177. Lamme EN, van Leeuwen RT, Mekkes JR, Middelkoop E. Allogeneic fibroblasts in dermal substitutes induce inflammation and scar formation. Wound Repair Regen 2002;10:152-60.
178. Breitbart AS, Grande DA, Laser J, Barcia M, Porti D, Malhotra S, *et al.* Treatment of ischemic wounds using cultured dermal fibroblasts transduced retrovirally with PDGF-B and VEGF121 genes. Ann Plast Surg 2001;46:555-61.
179. Pandit AS, Wilson DJ, Feldman DS. Fibrin scaffold as an effective vehicle for the delivery of acidic fibroblast growth factor (FGF-1). J Biomater Appl 2000;14:229-42.
180. Lamme EN, van Leeuwen RT, Brandsma K, van MJ, Middelkoop E. Higher numbers of autologous fibroblasts in an artificial dermal substitute improve tissue regeneration and modulate scar tissue formation. J Pathol 2000;190:595-603.
181. Gorodetsky R, Clark RA, An J, Gailit J, Levdansky L, Vexler A, *et al.* Fibrin microbeads (FMB) as biodegradable carriers for culturing cells and for accelerating wound healing. J Invest Dermatol 1999;112:866-72.
182. Breitbart AS, Mason JM, Urmacher C, Barcia M, Grant RT, Pergolizzi RG, *et al.* Gene-enhanced tissue engineering: applications for wound healing using cultured dermal fibroblasts transduced retrovirally with the PDGF-B gene. Ann Plast Surg 1999;43:632-9.
183. Pandit A, Ashar R, Feldman D. The effect of TGF-beta delivered through a collagen scaffold on wound healing. J Invest Surg 1999;12:89-100.
184. Supp AP, Wickett RR, Swope VB, Harriger MD, Hoath SB, Boyce ST. Incubation of cultured skin substitutes in reduced humidity promotes cornification *in vitro* and stable engraftment in athymic mice. Wound Repair Regen 1999;7:226-37.
185. Pandit A, Ashar R, Feldman D, Thompson A. Investigation of acidic fibroblast growth factor delivered through a collagen scaffold for the treatment of full-thickness skin defects in a rabbit model. Plast Reconstr Surg 1998;101:766-75.
186. Fauza DO, Fishman SJ, Mehegan K, Atala A. Videofetoscopically assisted fetal tissue engineering: skin replacement. J Pediatr Surg 1998;33:357-61.
187. Pandit AS, Feldman DS, Caulfield J. *In vivo* wound healing response to a modified degradable fibrin scaffold. J Biomater Appl 1998;12:222-36.
188. Pandit AS, Feldman DS, Caulfield J, Thompson A. Stimulation of angiogenesis by FGF-1 delivered through a modified fibrin scaffold. Growth Factors 1998;15:113-23.
189. Lamme EN, van Leeuwen RT, Jonker A, van MJ, Middelkoop E. Living skin substitutes: survival and function of fibroblasts seeded in a dermal substitute in experimental wounds. J Invest Dermatol 1998;111:989-95.
190. Orgill DP, Butler C, Regan JF, Barlow MS, Yannas IV, Compton CC. Vascularized collagen-glycosaminoglycan matrix provides a dermal substrate and improves take of cultured epithelial autografts. Plastic and reconstructive surgery 1998;102:423-9.
191. Compton CC, Butler CE, Yannas IV, Warland G, Orgill DP. Organized skin structure is regenerated *in vivo* from collagen-GAG matrices seeded with autologous keratinocytes. J Invest Dermatol 1998;110:908-16.

192. Butler CE, Orgill DP, Yannas IV, Compton CC. Effect of keratinocyte seeding of collagen-glycosaminoglycan membranes on the regeneration of skin in a porcine model. Plastic and reconstructive surgery 1998;101:1572-9.
193. Lamme EN, de Vries HJ, van VH, Gabbiani G, Westerhof W, Middelkoop E. Extracellular matrix characterization during healing of full-thickness wounds treated with a collagen/elastin dermal substitute shows improved skin regeneration in pigs. J Histochem Cytochem 1996;44:1311-22.
194. Boyce ST, Supp AP, Harriger MD, Pickens WL, Wickett RR, Hoath SB. Surface electrical capacitance as a noninvasive index of epidermal barrier in cultured skin substitutes in athymic mice. J Invest Dermatol 1996;107:82-7.
195. de Vries HJ, Middelkoop E, van Heemstra-Hoen M, Wildevuur CH, Westerhof W. Stromal cells from subcutaneous adipose tissue seeded in a native collagen/elastin dermal substitute reduce wound contraction in full thickness skin defects. Lab Invest 1995;73:532-40.
196. Hafemann B, Hettich R, Ensslen S, Kowol B, Zuhlke A, Ebert R, *et al.* Treatment of skin defects using suspensions of *in vitro* cultured keratinocytes. Burns 1994;20:168-72.
197. Hansbrough JF, Morgan JL, Greenleaf GE, Bartel R. Composite grafts of human keratinocytes grown on a polyglactin mesh-cultured fibroblast dermal substitute function as a bilayer skin replacement in full-thickness wounds on athymic mice. J Burn Care Rehabil 1993;14:485-94.
198. de Vries HJ, Mekkes JR, Middelkoop E, Hinrichs WL, Wildevuur CR, Westerhof W. Dermal substitutes for full-thickness wounds in a one-stage grafting model. Wound Repair Regen 1993;1:244-52.
199. Yannas IV, Lee E, Orgill DP, Skrabut EM, Murphy GF. Synthesis and characterization of a model extracellular matrix that induces partial regeneration of adult mammalian skin. Proc Natl Acad Sci U S A 1989;86:933-7.
200. Doillon CJ, Whyne CF, Berg RA, Olson RM, Silver FH. Fibroblast-collagen sponge interactions and the spatial deposition of newly synthesized collagen fibers *in vitro* and *in vivo*. Scan Electron Microsc 1984;1313-20.
201. Bell E, Ehrlich HP, Buttle DJ, Nakatsuji T. Living tissue formed *in vitro* and accepted as skin-equivalent tissue of full thickness. Science 1981;211:1052-4.
202. Yannas IV, Burke JF, Warpehoski M, Stasikelis P, Skrabut EM, Orgill D, *et al.* Prompt, long-term functional replacement of skin. Trans Am Soc Artif Intern Organs 1981;27:19-23.
203. Chardack W, Brueske D, Santamauro A, Fazekas G. Experimental studies on synthetic substitutes for skin and their use in the treatment of burns. Ann Surg 1962;155:127-39.
204. Vercelli S, Ferriero G, Sartorio F, Stissi V, Franchignoni F. How to assess postsurgical scars: a review of outcome measures. Disabil Rehabil 2009;31:2055-63.
205. Price RD, Das-Gupta V, Frame JD, Navsaria HA. A study to evaluate primary dressings for the application of cultured keratinocytes. Br J Plast Surg 2001;54:687-96.
206. Egana JT, Condurache A, Lohmeyer JA, Kremer M, Stockelhuber BM, Lavandero S, *et al.* Ex vivo method to visualize and quantify vascular networks in native and tissue engineered skin. Langenbecks Arch Surg 2008.
207. McGuckin M, Goldman R, Bolton L, Salcido R. The clinical relevance of microbiology in acute and chronic wounds. Adv Skin Wound Care 2003;16:12-23.
208. Richters CD, Van den Brand CS, Paauw NJ, Beelen RHJ, Middelkoop E, Ulrich MME. Nerve regeneration in partial thickness scalds (porcine wound model). Burns 2009;35:S32.
209. Inagaki N, Igeta K, Shiraishi N, Kim JF, Nagao M, Nakamura N, *et al.* Evaluation and characterization of mouse scratching behavior by a new apparatus, MicroAct. Skin Pharmacol Appl Skin Physiol 2003;16:165-75.
210. Shendure J. The beginning of the end for microarrays? Nat Methods 2008;5:585-7.
211. Nanney LB, Caldwell RL, Pollins AC, Cardwell NL, Opalenik SR, Davidson JM. Novel approaches for understanding the mechanisms of wound repair. J Investig Dermatol Symp Proc 2006;11:132-9.
212. Chen G, Chen J, Zhuo S, Xiong S, Zeng H, Jiang X, *et al.* Nonlinear spectral imaging of human hypertrophic scar based on two-photon excited fluorescence and second-harmonic generation. Br J Dermatol 2009;161:48-55.
213. Schenke-Layland K, Riemann I, Damour O, Stock UA, Konig K. Two-photon microscopes and *in vivo* multiphoton tomographs--powerful diagnostic tools for tissue engineering and drug delivery. Adv Drug Deliv Rev 2006;58:878-96.

Chapter 3

A comparison of seven methods to analyse heparin in biomaterials: quantification, location and anticoagulant activity

Gerwen Lammers[1]
Els M. Van de Westerlo[1]
Elly M. Versteeg[1]
Toin H. van Kuppevelt[1]
Willeke F. Daamen[1]

[1]Department of Biochemistry, Nijmegen Centre for Molecular Life Sciences, Radboud University Nijmegen Medical Centre, Nijmegen

Tissue Engineering Part C – Methods
2011 volume 17 issue 6 pages 669-676

Abstract

Glycosaminoglycans, like heparin, are frequently incorporated in biomaterials because of their capacity to bind and store growth factors and because of their hydrating properties. Heparin is also often used in biomaterials for its anticoagulant activity. Analysis of biomaterial-bound heparin is challenging because most assays are based on heparin in solution. In this study, seven different methods were probed to analyse heparin covalently attached to collagen scaffolds. For each method the basic mechanism and the advantages and disadvantages are given. Analysis by a factor Xa assay and the Farndale assay clearly indicated that the amount of immobilised heparin cannot be determined correctly when the scaffold is intact. Scaffolds had to be proteolytically digested or acid treated in order to obtain reliable measurements. Methods used to quantify the amount of bound heparin included a hexosamine assay, an uronic acid assay, a Farndale assay, agarose gel electrophoresis, and immuno dot blot analysis. Location and semi-quantification of heparin was accomplished by immunofluorescence. Although all assays had their advantages and disadvantages, the hexosamine assay turned out to be the most robust, and is recommended as the preferred assay to quantify the amount of heparin bound to scaffolds. It is applicable to all scaffolds that are acid hydrolysable. This study may allow researchers in the field to select the most appropriate method to analyse glycosaminoglycans in biomaterials.

Introduction

Glycosaminoglycans are long, negatively charged, unbranched polysaccharides, consisting of repeating disaccharide units. Being present at the cell surface and in the extracellular matrix, they play an important role in the binding and modulation of growth factors and other effector molecules, and endow tissues with water-binding capacity [1]. Consequently, glycosaminoglycans are often incorporated in tissue-engineered constructs that are designed to mimic the natural extracellular matrix [2,3].

In tissue engineering, heparin is the most employed glycosaminoglycan for a number of reasons. It is well known for its anticoagulant activity and therefore used in vascular grafts to prevent thrombus formation [4]. Heparin is relatively cheap because it is prepared in large quantities. Immobilised heparin can be used to non-covalently bind growth factors, thus avoiding the risk of loss of growth factor activity which may occur when they are covalently bound to biomaterials [5].

Heparin consists of highly sulfated disaccharide units (Fig. 1). In intestinal mucosa, a common source of commercially available heparin, about 75% of the disaccharides consist of a 2-O-sulfated iduronic acid residue and a 6-O-sulfated, N-sulfated glucosamine residue [6].

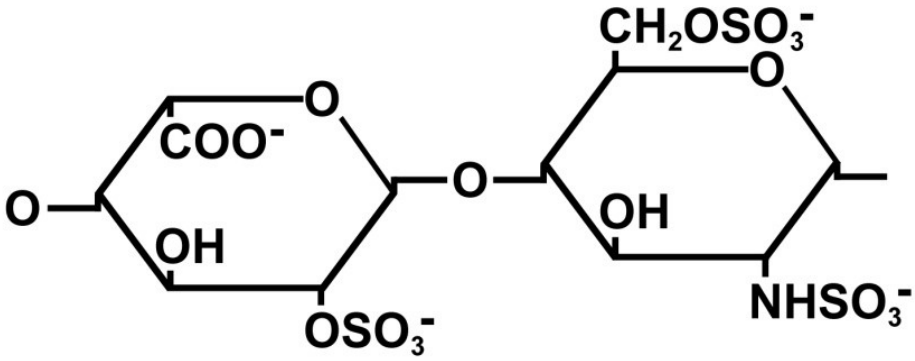

Figure 1. Frequently occurring disaccharide present in heparin from the intestinal mucosa, and consisting of a 2-O-sulfated iduronic acid (left) and a 6-O-sulfated, N-sulfated glucosamine residue (right) [6].

When immobilizing heparin to a biomaterial it is important to quantify the amount present. The analysis of heparin covalently bound to a solid substrate like a collagen scaffold, may pose a number of challenges because heparin is generally assayed in solution, and the presence of the insoluble biomaterial may interfere.

In this study, seven different methods were used to analyse the amount and location of collagen scaffold-bound heparin. Of each method, the mode of action is briefly reviewed and the advantages and disadvantages are given to enable researchers to select the most appropriate method to analyse heparin in (collagen-based) biomaterials.

Materials and methods

Materials

Insoluble type I collagen was purified from bovine Achilles tendon using extractions with aqueous acetic acid, NaCl and urea, and acetone as described [7]. Heparin sodium from porcine mucosa (187.4 units/mg) with an average molecular weight of 15 kDa (10-20 kDa), was purchased from Diosynth (Oss, The Netherlands).

Preparation of (heparinised) collagen scaffolds

Scaffolds were prepared in 24-well plates (Greiner Bio-One) by freezing 800 µl of a 0.8% type I collagen suspension in 0.25 M acetic acid per well at -20°C and subsequent lyophilisation [8].

To covalently couple heparin, scaffolds were wetted in 50 mM 2-morpholinoethane sulphonic acid buffer (MES, pH 5.0) containing 40% ethanol, and preincubated for 30 min in 400 µl of a heparin solution (0-4%) in MES buffer. Scaffolds were chemically crosslinked for 4 h by adding 400 µl 1-ethyl-3-(3-dimethyl aminopropyl) carbodiimide (EDC)/N-hydroxysuccinimide (NHS) in MES buffer, the final concentrations being 33 and 6 mM respectively, followed by washings with 0.1 M Na_2HPO_4, 1 M NaCl, 2 M NaCl and demineralised water [9]. The final contents of heparin in the crosslinking solution were 0, 0.05, 0.1, 0.2, 0.3, 0.4, 0.5, 0.75, 1 and 2%.

To ensure representative sampling, pie part-shaped pieces from the round scaffolds were assayed, unless stated otherwise.

Determination of amine group content

The amine group content of the scaffolds was estimated spectrophotometrically by using 2,4,6-trinitrobenzene sulfonic acid (TNBS) [10,11]. To calculate the amount of amine groups per mg of collagen scaffold, a correction was applied for the amount of bound heparin, using a hexosamine assay (see below).

Papain digestion of scaffolds

To digest collagen scaffolds, 1 mg was incubated in 2.5 U papain (Sigma-Aldrich, St. Louis, MO, USA) in 1 ml digestion buffer (50 mM $NaPO_4$, 2 mM cysteine, 2 mM EDTA, pH 6.5) for 16 h at 65°C.

To evaluate for the presence of large (undigested) protein fragments, 70 µl 100% trichloroacetic acid (TCA) per 400 µl sample was added and incubated on ice for 30 min, centrifuged at 10,000 g for 20 min at 4ºC. No pellet was observed, indicating that the papain treatment was sufficient to digest the collagen scaffolds to soluble protein fragments.

Seven methods used for the determination of heparin in scaffolds

Table 1 provides an overview of different aspects of the seven methods used for the determination of heparin in scaffolds.

Table 1. Overview of the mechanism, sensitivity, assay time, sample pre-treatment, and (dis)advantages of seven methods used to evaluate the amount of heparin in collagen scaffolds. *o/n = overnight.

Method	Mode of action (see also text)	Sensitivity	Assay time	Sample pre-treatment	Prime advantages	Limitations
Factor Xa assay	Antithrombin III activation => Factor Xa inactivation => less hydrolysis of chromogenic substrate (less colour)	MilliU (ng)	30 min	None or papain digestion	Functional assay (coagulation)	Detection of only anticoagulant heparin
Farndale assay	Multiple sulphate groups + dimethylmethylene blue => change in absorption maximum (metachromasia) (= colour change)	µg	2 days (2x o/n*)	Papain digestion	Specific for polysulfated molecules	Many steps required, enzymatic digestion
Hexosamine assay	Glucosamine + acetylacetone -> pyrroles. Pyrroles + p-dimethylaminobenzaldehyde => colour	µg	3 days (3x o/n)	Acid hydrolysis	Robust method	Long procedure
Uronic acid assay	Acid hydrolysis of uronic acid => carboxylated furans + m-hydroxybiphenyl => colour	µg	2 hrs	Acid hydrolysis	Fast assay	Collagen interference , hazardous chemicals (hot 80% H_2SO_4)
Agarose gel electrophoresis	Differential migration of GAGs in the presence of divalent cations containing buffer (backbone dependent) => silver staining	ng	1 day (1x o/n)	Papain digestion	Discrimination of GAG classes	Enzymatic digestion, limited number of samples per gel
Immunodot blot	Binding of GAG-protein fragment to membrane => anti-GAG antibody binding => visualisation	ng	1 day (1x o/n)	Papain digestion	Direct visual result, simple equipment	Standards for quantification not readily available, many steps required, enzymatic digestion
Immunofluorescence assay	Anti-GAG antibody binding to cryosections => visualisation	n.a.	1 day (1x o/n)	Freezing, sectioning	Topological data	Semi-quantitative

Factor Xa assay

This method is based on the conformational change of the serine proteinase inhibitor antithrombin III by heparin, resulting in factor Xa inhibition [12,13]. The capacity of scaffold-bound heparin to delay the blood coagulation cascade was assessed using a Coatest Heparin (Chromogenix, Milan, Italy) according to the manufacturer's protocol [14]. Scaffolds (0.5-1.5 mg) were incubated in 50 µl normal human plasma enriched with 2.5 mU antithrombin III

in 50 mM Tris (pH 8.4) for 5 min at 37ºC to allow antithrombin III to bind to heparin and undergo a conformational change. Heparin standards (0-100 ng) were used as controls. Then, 25 µl factor Xa was added, mixed, and incubated for 30 s at 37ºC to allow activated antithrombin III to inactivate factor Xa. A 50 µl aliquot of a 1 mM chromogenic substrate (S-2222 (Bz-IIe-Glu-(g-OR)-Gly-Arg-pNA·HCl)) was added, mixed, and incubated for 10 min at 37ºC, allowing the remaining active factor Xa to hydrolyse the substrate, thereby releasing chromophore p-nitroaniline (pNA). The reaction was stopped by the addition of 100 µl 20% acetic acid and absorbance was measured at 405 nm.

Alternatively, a factor Xa assay was performed on papain digested samples (see papain digestion section) in the presence of 25 µM antipain (Sigma-Aldrich) to prevent papain from digesting antithrombin III and factor Xa.

Farndale assay

This method is based on a shift in the maximum absorbance wavelength of the dye 1,9-dimethylmethylene blue after binding to multiple sulphate groups (metachromasia) [15]. Dry scaffold pieces were incubated in Farndale reagent (43 µM dimethylmethylene blue containing 40 mM glycine and 41 mM NaCl adjusted to pH 3.0 with 2 M HCl) and incubated at room temperature.

Alternatively, papain digested scaffold preparation after TCA precipitation was used (see papain digestion section). Glycosaminoglycans present in the supernatant (bound to small protein fragments) were analysed by precipitation with 2 ml ice cold ethanol, overnight incubation at -20ºC, and centrifugation at 17,000 g for 20 min at 4 ºC. The precipitate was dissolved in 100 µl MilliQ and 10 µl was used for analysis. Heparin standards (0-5 µg) were included and 1 ml Farndale reagent was added to the samples and the standards. The absorbance of dimethylmethylene blue after binding with the sulphate groups in heparin was measured at 525 nm [16].

Hexosamine assay

This method is based on the colourimetric determination of hexosamines, like glucosamine [17,18]. Scaffolds (0.5-4 mg dry weight) and heparin standards (0-500 µg) were hydrolysed with 500 µl 6 M HCl at 105ºC for 6 h under nitrogen gas in sealed glass tubes. HCl and water were removed by drying the hydrolysed samples in a vacuum-desiccator in the presence of NaOH pellets. Samples were dissolved in 1.25 ml MilliQ, and to 1 ml sample 1 ml 4% acetylacetone in 1.25 M Na_2CO_3 was added and incubated at 95ºC for 1 h to convert the glucosamines to pyrroles. Then, 5 ml 95% ethanol was added, followed by 1 ml Ehrlich reagent containing 2.66% p-dimethylamino-benzaldehyde in 3 M HCl and 47.5% ethanol to condense pyrroles to a coloured product. The absorbance was measured spectrophotometrically at 527 nm.

Uronic acid assay

This method is based on the conversion of uronic acids to a coloured product [19]. First, scaffolds (0.5-3 mg) were hydrolysed in 1 ml hot 83% H_2SO_4 containing 120 mM sodium

tetraborate in a 48-well plate in a water bath at 80ºC for 45 min. Heparin standards (0-150 µg) were used as controls. Uronic acids (both iduronic acid and the less frequently present glucuronic acid) were transformed to a coloured product by the addition of 200 µl 0.2% m-hydroxybiphenyl in 78.4% H_2SO_4 at room temperature for 15 min, and measured at 450 nm.

Agarose gel electrophoresis

This method is based on backbone-dependent separation of glycosaminoglycans in an agarose gel and subsequent staining with the cationic dye azure A and silver as described by Van De Lest *et al.* [20]. Papain-digested scaffold preparation (see papain digestion section) was diluted 5x in MilliQ water and 1 µl was loaded on 1% agarose gels. To enable quantification, heparin standards of 5, 10, 20 and 40 ng were included. Electrophoresis was performed in 50 mM barium acetate buffer (pH 5.0) at 60 V for 50 min. Gels were subsequently fixed and prestained in 0.1% (w/v) azure A in 50 mM sodium formate and 10 mM magnesium chloride (pH 3.5). Gels were decolourised with 10 mM sodium acetate buffer (pH 5.5, 2x 30 min) and demineralised water (30 min). After air-drying, gels were rehydrated in MilliQ water and silver-stained in 15 mM $AgNO_3$, 1.75 mM silicotungstic acid, 75 mM formaldehyde in 30 mM NH_4NO_3 and 0.24 M Na_2CO_3. Staining reaction was ceased by incubating gels in demineralised water for 2 min, 1% acetic acid for 5 min, and demineralised water for 15 min. Gels were air-dried and scanned for analysis. For quantification, the median of the pixel intensity of each band was determined with an equally-sized selection area using Adobe Photoshop (Adobe Systems, CA, USA). Values were corrected for background intensity using an adjacent area and staining differences between gels were corrected for using a 5 ng heparin standard loaded on each gel.

Immuno-dot blot

This method is based on antibody recognition of heparin, bound to a nitrocellulose membrane by virtue of small collagen fragments still attached to the heparin. Of a papain-digested scaffold preparation (see papain digestion section), 50 µl was transferred to a Hybond-ECL nitrocellulose membrane (Amersham Biosciences) using an Easy-Titer enzyme-linked immunoflow assay system (ELIFA, Pierce Biotechnology, Rockford, IL, USA). After 30 min at room temperature, non-specific binding was blocked with 1% bovine serum albumin (BSA) in phosphate-buffered saline (PBS, pH 7.2) for 16 h at 4ºC. Membrane-bound collagen peptide-heparin was detected using the phage display-derived VSV-tagged antibody HS4C3 (1:50), which recognises heparin [21], followed by mouse anti-VSV tag antibody P5D4 (1:10), and a peroxidase conjugated goat anti-mouse IgG antibody (1:20,000, Pierce), all in 1% BSA in PBS, followed by the ECL Western Blotting Detection kit (Amersham). Scanned images of exposed films were used for determination of the relative pixel intensity. Pictures were inverted, and the median of the pixel intensity of equally-sized areas containing one spot was determined using Adobe Photoshop. Values were corrected for background intensity using a spot adjacent to the spot of interest and expressed as a percentage between background intensity (0%) and complete saturation (100%).

Immunofluorescence assay

This method is based on the antibody recognition of heparin in scaffold sections. Scaffolds were carefully wetted in demineralised water, placed in TissueTek (Sakura Finetek, Alphen aan den Rijn, The Netherlands) and snap-frozen in liquid nitrogen-cooled isopentane. Cryosections of 5 µm thickness were cut, placed on SuperFrost slides (Menzel-Gläser, Braunschweig, Germany), and air-dried for 16 h at room temperature. Non-specific binding was blocked using 1% BSA in PBS for 10 min and sections were stained with anti-heparin antibody HS4C3-VSV (1:5-50), followed by mouse anti-VSV tag antibody P5D4 (1:10), and an Alexa 488-labelled goat anti-mouse IgG antibody (Molecular Probes, Eugene, OR, USA, 1:100), all in 1% BSA in PBS at room temperature. Staining was evaluated using a Leica DM6000 microscope.

Results

Porous collagen scaffolds of ~5 mm thickness were prepared in 24-well plates by lyophilisation of a frozen collagen suspension. Scaffolds were chemically crosslinked in a solution containing a fixed concentration of EDC/NHS and different amounts of heparin (0-2%), and washed extensively.

The amount of immobilised heparin was initially determined by a factor Xa assay on intact scaffolds (Fig. 2A) and on papain digested scaffolds (Fig. 2B). The shape of both curves was comparable and showed an increasing amount of incorporated heparin starting from 0.4% heparin in the crosslinking solution to a maximum at about 1%. However, a 500-fold difference was observed in the absolute values obtained (e.g. 0.022 units in intact scaffolds versus 10 units in digested scaffolds). Apparently, not all immobilised heparin can be measured in intact scaffolds, indicating the need for solubilisation of scaffolds for a reliable measurement.

This was also seen when scaffolds were assayed using the Farndale reagent. Incubation of intact scaffolds in the staining solution did result in metachromasia (i.e. a change from a blue into a purple colour, Fig. 3), thereby demonstrating the presence of heparin (the scaffolds without heparin are blue), but the intensity of the purple colour did not correspond to the amount of heparin immobilized (as assayed by a hexosamine assay, see below). Together with the factor Xa data, this clearly indicates that the amount of heparin cannot be assayed correctly when the scaffolds is intact. We did, however, notice that the blue staining intensity of the surrounding solution, negatively correlated with the amount of heparin immobilized. Therefore, this approach may be suitable for an indirect semi-quantitative determination of the amount of scaffold-bound heparin, but the development of standards will be challenging and we did not pursue this strategy.

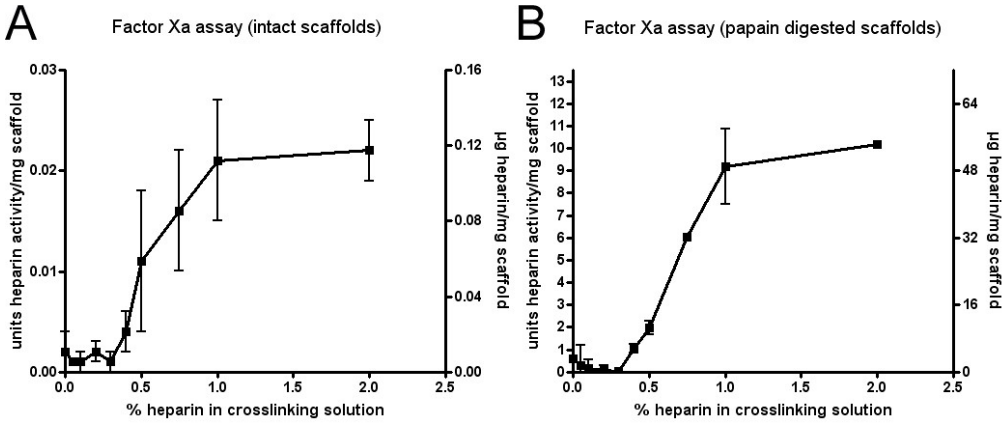

Figure 2. Analysis of immobilised heparin by the factor Xa assay. Anticoagulant activity and deduced amount of immobilised heparin after crosslinking of collagen scaffolds in the presence of 0-2% heparin in the crosslinking solution, determined for intact (A) and papain digested scaffolds (B), showing the results of a typical experiment in séxtuplo (A) and duplo (B) ± S.D.. Heparin activity is given in units on the left y-axis, and the amount of heparin is given in micrograms on the right y-axis. Note the ~500-fold difference between the values in (A) and (B).

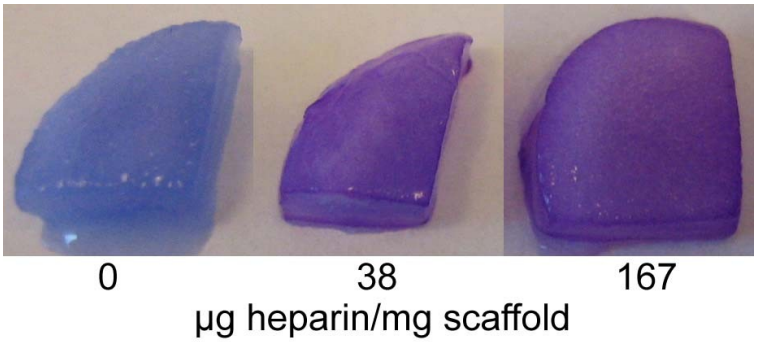

Figure 3. Analysis of immobilised heparin by the Farndale assay. Scaffolds containing 0, 38, and 167 µg heparin/mg (based on hexosamine assay results, see below) were incubated using the Farndale reagent. Scaffolds containing heparin had a different colour than scaffolds without heparin, but no difference was observed between different amounts of bound heparin.

Using papain-digested, solubilised, scaffolds, differences in the amount of heparin could be determined with the Farndale assay (Fig. 4A). The shape of the curve, however, differed from the Xa assay, with an increasing amount of incorporated heparin from 0-0.4% heparin in the crosslinking solution, to a decrease with increasing heparin content in the crosslinking solution.

Heparin was also assessed by measuring specific monosaccharides obtained after acid solubilisation of the scaffolds. The shape of the curves obtained by a hexosamine and a uronic acid assay were generally comparable to that obtained by the Farndale assay, i.e. an initial increase of the amount of heparin immobilised, followed by a decrease (Figs. 4B and C). However, a difference was observed in absolute numbers (e.g. the peak values, ranging

from 60 µg/mg (Farndale, A), 119 µg/mg (hexosamine, B) to 171 µg/mg (uronic acid assay, C; see discussion)). In the uronic acid assay, a heparin-dependent brown colour was observed in the samples containing scaffold collagen, but not in the samples containing heparin only (for the standard curve).

The hexosamine assay appeared to be the most robust assay for the quantitative determination of scaffold-bound heparin possibly because, in contrast to the other assays, no delicate precipitation steps were required and no collagen interference with the measurements was observed.

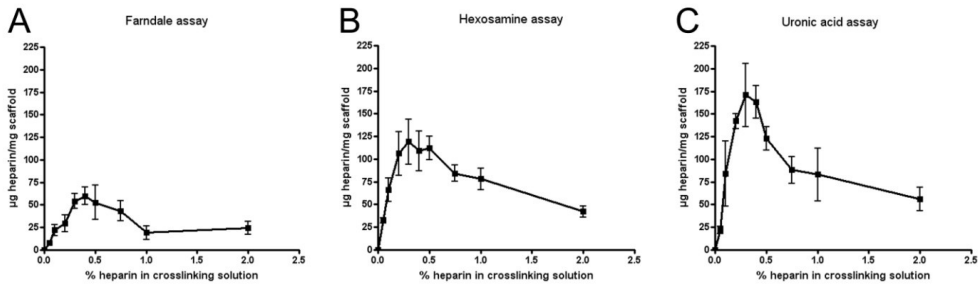

Figure 4. Analysis of immobilised heparin assayed with (A) Farndale assay, (B) hexosamine assay, and (C) uronic acid assay. Scaffolds were crosslinked in the presence of 0-2% heparin in the crosslinking solution. Results are given as n=3 ± S.E.M., in µg heparin per mg scaffold.

Agarose gel electrophoretic analysis of heparin using papain-digested scaffolds gave variable results in our hands. Staining quality varied and therefore not all gels were suitable for quantification. Results (Fig. 5) indicated a trend comparable to the Farndale, hexosamine, and uronic acid assay, i.e. an initial increase of heparin immobilised followed by a decrease. The peak value observed in the gel presented in Fig. 5 (0.3% heparin in crosslinking solution) was about 224 µg heparin/mg. Please note that since one gel contained 7-8 slots, two gels were required to load all standards and samples once, which may limit accuracy.

Immuno-dot blot analysis of papain digested samples provided comparable results (Fig. 6). In line with Kreuger *et al.* no staining was observed when free heparin was applied to the membrane [22]. As a result, no heparin standards could be applied for quantification purposes, but the relative staining intensity peaked at 0.3% heparin in the crosslinking solution.

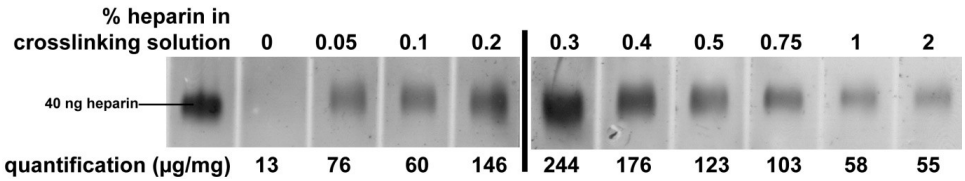

Figure 5. Analysis of immobilised heparin by agarose gel electrophoresis. Quantification (µg heparin/mg scaffold) based on heparin standards. Please note differences in background staining that may complicate quantification. This figure is a composite picture of two gels (gel 1=40 ng heparin-0.2, gel 2=0.3-2).

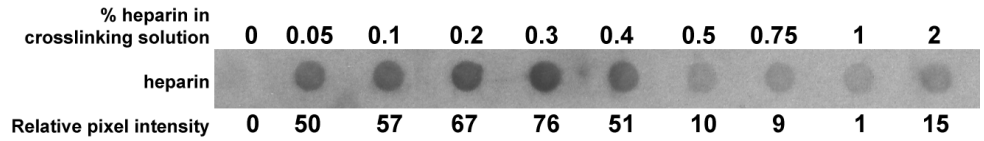

Figure 6. Analysis of immobilised heparin using an immuno-dot blot assay on papain-digested scaffolds, crosslinked with 0-2% heparin in the crosslinking solution, after incubation with anti-heparin antibody HS4C3. The relative pixel intensity of each spot was measured. No absolute amount of heparin could be calculated, since standards of free heparin do not bind to the membrane.

Finally, an immunofluorescence assay (Fig. 7) was applied to obtain additional information on the location of the immobilised heparin. Heparin was mainly localised at the scaffold surfaces for scaffolds crosslinked in the presence of 0.05% heparin. Scaffolds crosslinked in the presence of 0.4% heparin showed a more even distribution, while for scaffolds incubated in 1.0% heparin less intense staining was observed (especially at the inner side). These scaffolds contained 38, 80, and 58 µg heparin/mg, respectively (as determined with a hexosamine assay). Therefore, although semi-quantitative, results indicate the same trends as observed in figs. 4-6.

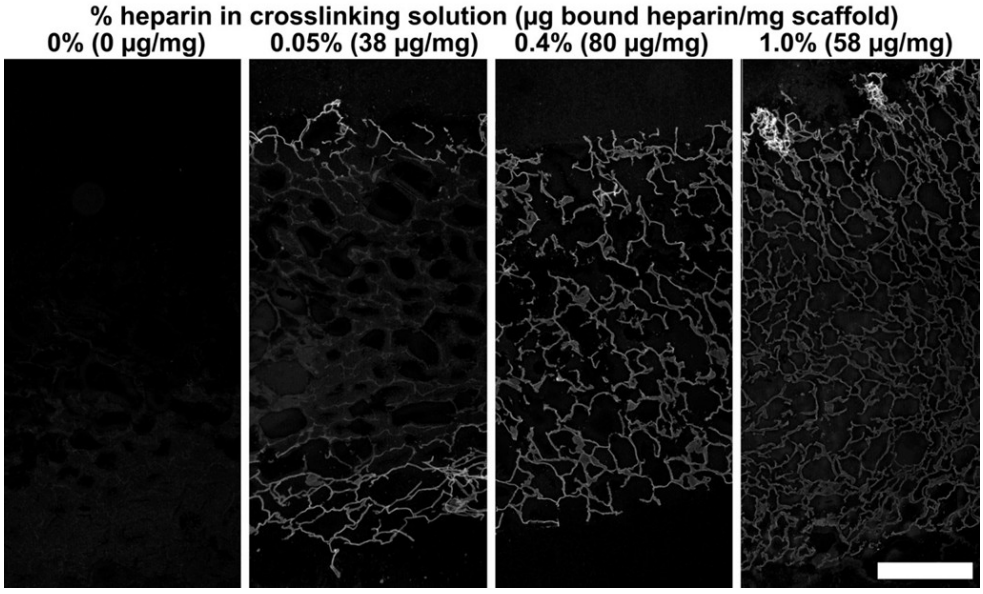

Figure 7. Analysis of immobilised heparin by an immunofluorescence assay. Scaffolds crosslinked in the presence of 0, 0.05, 0.4, and 1.0% heparin were evaluated. The amount of bound heparin as determined with a hexosamine assay on individual scaffolds is given in µg/mg scaffold. Crosslinking in the presence of 0.05% heparin resulted in staining mainly localised at the scaffold surfaces, whereas crosslinking in the presence of 0.4% heparin resulted in a more even distribution of heparin throughout the whole scaffold. Crosslinking in 1.0% heparin showed less intense staining of primarily the inner area, indicating the same trend as observed in figs. 4-6. Composite pictures, all taken with identical microscope settings. Bar is 500 µm.

To find an explanation for the shape of the curves seen in the above-mentioned assays (Figs. 2 and 4-7) we evaluated the content of free amine groups still present after the crosslinking process, with respect to the percentage of heparin present in the crosslinking solution. Non-crosslinked scaffolds contained 270 nmol amine groups per mg, and this was reduced to ~150 nmol/mg when crosslinking took place in the presence of 0-0.4% heparin. Crosslinking in the presence of higher amounts of heparin resulted in a higher number of remaining amine groups, even though the EDC concentration was constant for all crosslinking solutions. This may provide clues for the explanation of the results of the other assays (see discussion).

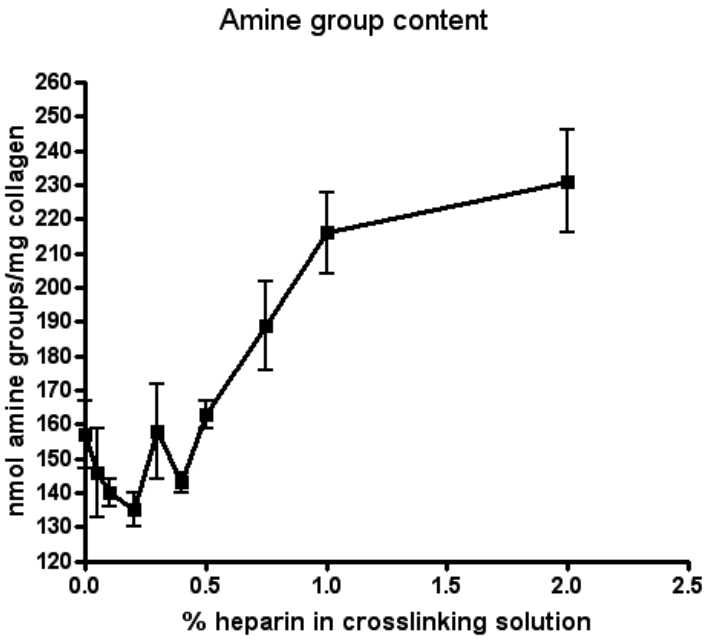

Figure 8. Amine group content of the collagen scaffolds after crosslinking in the presence of 0-2% heparin. The amine group content of non-crosslinked scaffolds was 270 nmol/mg. Results of a typical experiment in triplo ±S.D..

Discussion

In this study seven assays were evaluated for their suitability to quantify the amount of heparin immobilised to insoluble collagenous scaffolds. Both the factor Xa assay and the Farndale assay indicated that quantifying heparin when the scaffolds are intact, results to a gross underestimation of the amount of heparin present. For the factor Xa assay a ~500-fold difference was notices, when intact and papain digested scaffolds were measured, suggesting that in an intact scaffold not all heparin is accessible. Therefore, scaffolds were solubilised either using papain digestion or acid hydrolysis.

The hexosamine assay turned out to be the most robust assay and is therefore the preferred method for the quantification of immobilised heparin. It uses acid hydrolysis to digest the scaffold. It has the advantage over the uronic acid assay that it is not associated with an additional brown colouring. This additional colouring is not observed when heparin without collagen is assayed (e.g. for the standard curve), and may therefore result in an overestimation of the amount of heparin immobilized to a collagen scaffolds (an up to about 50% higher value was found using the uronic acid assay). The Farndale assay, which uses papain digestion to solubilise heparin, gave lower values compared to the assays which use acid hydrolysis. Papain digestion may result in some (solubilised) heparin which is still attached to collagen peptides, which may precipitate in the TCA protein precipitation, thereby leading to an underestimation of the amount of heparin (note that the heparin standards are not TCA precipitated). It is also possible that small heparin-bound collagen fragments interfered with the measurements, since protein (albumin) in a Farndale assay is able to reduce the readout with approximately 40% [16]. The inclusion of standards during each step of the assay and spiking experiments may elucidate the effect of the different steps.

The immuno-dot blot method, using an antibody against heparin, gave data which can be compared to each other, but does not result in absolute numbers. The reason for this is that heparin alone will not bind to a nitrocellulose membrane [22], whereas heparin with some residual amino acid residues (as is the case with papain digestion) does. As a consequence, no free heparin standards could be loaded for quantification. Agarose gel electrophoresis, on the other hand, is not dependent on the presence of peptide residues. It provides information on the backbone structure of the glycosaminoglycan under investigation and can be used quantitatively. A limiting factor is the relative small number of samples that can be assessed on a single gel and this makes high-throughput analysis challenging. Finally, the immunofluorescence assay, although at best semi-quantitative, provides information on the location of bound heparin. It was observed that at low heparin concentrations, its location was primarily at the scaffold surfaces, emphasising the importance of correct sampling.

An interesting feature of the present study is the observation that, after a binding maximum, the amount of bound heparin decreased with increasing heparin concentration in the crosslinking solution. Wissink *et al.* showed that heparin binding correlated with the ratio of EDC molecules per heparin carboxylic groups (EDC:Hep-COOH) [23]. When the ratio EDC:Hep-COOH drops (as is the case when the concentration of heparin increases in the presence of a fixed EDC concentration), a point may be reached at which heparin molecules may not be sufficiently EDC-activated to bind to collagen. This may explain the observed decrease with increasing heparin concentrations and is in line with the observed decrease in the amount of amine groups used for cross-linking (and hence the increase in free amine groups, see Fig. 8). Results of the factor Xa assay, assessing functional anti-coagulation, differed from the other assays. In this assay, the accessibility of heparin for the protein antithrombin III (and possibly factor Xa) is of crucial importance, and the way and the extent by which heparin is bound to collagen are likely important factors. It has been suggested that an increased number of covalent bonds between heparin and collagen may result in a decreased accessibility of heparin for the antithrombin III binding site and/or decreased throm-

bin binding [23]. The conditions in our study at low EDC:Hep-COOH ratio's (obtained at 1-2% heparin in the crosslinking solution) may have resulted in less binding of absolute numbers of heparin molecules, but an optimal accessibility of those heparin molecules that did bind, due to the limited number of covalent bonds between collagen and heparin. Maximal exposure of the heparin molecules to antithrombin III may have increased the functional anti-coagulation.

The precise conditions used during the crosslinking are likely critical for the amount and mode of binding. For instance, Pieper *et al.* (2000) crosslinked in the presence of 2.75% heparin and reported 129 µg bound heparin/mg scaffold using a hexosamine assay, much higher than expected from our study [9]. They also crosslinked with 33 mM EDC, but used 4 mg scaffold collagen per ml crosslinking solution instead of 8 mg, and 20 mM NHS (which forms a stable intermediate during crosslinking) instead of 6 mM, which may explain the observed differences.

Heparin shares many characteristics with other glycosaminoglycans and the methods described here are therefore broadly applicable. For immuno-dot blot and immunofluorescence analysis, additional antibodies are available that recognise specific sugar modifications present in different glycosaminoglycans [24]. All methods may be applicable to a broad range of biomaterials that can be digested by proteases (like fibrin), hydrolysed (like polylactic acid and polycaprolactone), and/or freeze-sectioned.

Conclusion

From seven methods evaluated, the hexosamine assay is the preferred method for the determination of the absolute amount of heparin bound to a scaffold. This robust method may also be applied for other acid-hydrolysable biomaterials.

Acknowledgements

This study is funded by the Dutch Program for Tissue Engineering (grant DPTE 6735) and by the EU-FP6 project EuroSTEC (soft tissue engineering for congenital birth defects in children: contract: LSHB-CT-2006-037409).

References

1. Esko JD, Kimata K, Lindahl U. Proteoglycans and Sulfated Glycosaminoglycans. 2009.
2. Bezuidenhout D, Davies N, Black M, Schmidt C, Oosthuysen A, Zilla P. Covalent surface heparinization potentiates porous polyurethane scaffold vascularization. J Biomater Appl 2010;24:401-18.
3. Geutjes PJ, Daamen WF, Buma P, Feitz WF, Faraj KA, Van Kuppevelt TH. From molecules to matrix: construction and evaluation of molecularly defined bioscaffolds. Adv Exp Med Biol 2006;585:279-95.
4. Jordan SW, Chaikof EL. Novel thromboresistant materials. J Vasc Surg 2007;45 Suppl A:A104-A115.
5. Nillesen ST, Geutjes PJ, Wismans R, Schalkwijk J, Daamen WF, Van Kuppevelt TH. Increased angiogenesis and blood vessel maturation in acellular collagen-heparin scaffolds containing both FGF2 and VEGF. Biomaterials 2007;28:1123-31.
6. Gatti G, Casu B, Hamer GK, Perlin AS. Studies on the Conformation of Heparin by 1H and 13C NMR Spectroscopy. Macromolecules 1979;12:1001-7.
7. Pieper JS, Oosterhof A, Dijkstra PJ, Veerkamp JH, Van Kuppevelt TH. Preparation and characterization of porous crosslinked collagenous matrices containing bioavailable chondroitin sulphate. Biomaterials 1999;20:847-58.

8. Faraj KA, Van Kuppevelt TH, Daamen WF. Construction of collagen scaffolds that mimic the three-dimensional architecture of specific tissues. Tissue Eng 2007;13:2387-94.
9. Pieper JS, Hafmans T, Veerkamp JH, Van Kuppevelt TH. Development of tailor-made collagen-glycosaminoglycan matrices: EDC/NHS crosslinking, and ultrastructural aspects. Biomaterials 2000;21:581-93.
10. Gilbert DL, Kim SW. Macromolecular release from collagen monolithic devices. J Biomed Mater Res 1990;24:1221-39.
11. Olde Damink LH, Dijkstra PJ, Van Luyn MJ, Van Wachem PB, Nieuwenhuis P, Feijen J. Cross-linking of dermal sheep collagen using a water-soluble carbodiimide. Biomaterials 1996;17:765-73.
12. Bjork I, Lindahl U. Mechanism of the anticoagulant action of heparin. Mol Cell Biochem 1982;48:161-82.
13. Chuang YJ, Swanson R, Raja SM, Olson ST. Heparin enhances the specificity of antithrombin for thrombin and factor Xa independent of the reactive center loop sequence. Evidence for an exosite determinant of factor Xa specificity in heparin-activated antithrombin. J Biol Chem 2001;276:14961-71.
14. Teien AN, Lie M, Abildgaard U. Assay of heparin in plasma using a chromogenic substrate for activated factor X. Thromb Res 1976;8:413-6.
15. Farndale RW, Sayers CA, Barrett AJ. A direct spectrophotometric microassay for sulfated glycosaminoglycans in cartilage cultures. Connect Tissue Res 1982;9:247-8.
16. van de Lest CH, Versteeg EM, Veerkamp JH, Van Kuppevelt TH. A spectrophotometric method for the determination of heparan sulfate. Biochim Biophys Acta 1994;1201:305-11.
17. Elson LA, Morgan WT. A colorimetric method for the determination of glucosamine and chondrosamine. Biochem J 1933;27:1824-8.
18. Yannas IV, Burke JF, Gordon PL, Huang C, Rubenstein RH. Design of an artificial skin. II. Control of chemical composition. J Biomed Mater Res 1980;14:107-32.
19. van den Hoogen BM, van Weeren PR, Lopes-Cardozo M, van Golde LM, Barneveld A, van de Lest CH. A microtiter plate assay for the determination of uronic acids. Anal Biochem 1998;257:107-11.
20. van de Lest CH, Versteeg EM, Veerkamp JH, Van Kuppevelt TH. Quantification and characterization of glycosaminoglycans at the nanogram level by a combined azure A-silver staining in agarose gels. Anal Biochem 1994;221:356-61.
21. Van Kuppevelt TH, Dennissen MA, van Venrooij WJ, Hoet RM, Veerkamp JH. Generation and application of type-specific anti-heparan sulfate antibodies using phage display technology. Further evidence for heparan sulfate heterogeneity in the kidney. J Biol Chem 1998;273:12960-6.
22. Kreuger J, Lindahl U, Jemth P. Nitrocellulose filter binding to assess binding of glycosaminoglycans to proteins. Methods Enzymol 2003;363:327-39.
23. Wissink MJ, Beernink R, Pieper JS, Poot AA, Engbers GH, Beugeling T, *et al.* Immobilization of heparin to EDC/NHS-crosslinked collagen. Characterization and *in vitro* evaluation. Biomaterials 2001;22:151-63.
24. Wijnhoven TJ, van de Westerlo EM, Smits NC, Lensen JF, Rops AL, Van D, V, *et al.* Characterization of anticoagulant heparinoids by immunoprofiling. Glycoconj J 2008;25:177-85.

Chapter 4

A molecularly defined array based on native fibrillar collagen for the assessment of skin tissue engineering biomaterials

Gerwen Lammers[1]
G. Sandra Tjabringa[2]
Joost Schalkwijk[2]
Willeke F. Daamen[1]
Toin H. van Kuppevelt[1]

[1]Department of Biochemistry, Nijmegen Centre for Molecular Life Sciences, Radboud University Nijmegen Medical Centre, Nijmegen
[2]Department of Dermatology, Nijmegen Centre for Molecular Life Sciences, Radboud University Nijmegen Medical Centre, Nijmegen

Biomaterials
2009 volume 30 issue 31 pages 6213-6220

Abstract

Large-scale *in vivo* evaluation of biomaterials is time-consuming and limited by ethical considerations. The availability of a library of biomaterials would allow a fast and rational *in vitro* selection of those biomaterials to be evaluated *in vivo*. For this reason, we developed an array of 48 different, molecularly-defined films based on native fibrillar collagen. The films differed in the type and amount of extracellular matrix components (type I/IV collagens, fibrous/solubilised elastin, glycosaminoglycans (heparin, chondroitin sulfate or dermatan sulfate), method of preparation (homogenisation) and method and extent of crosslinking (carbodiimide (EDC/NHS) or glutaraldehyde). The array was evaluated by studying morphology, proliferation and differentiation of primary human keratinocytes/fibroblasts. Major differences were observed. Only a small selection of films (especially those containing elastin fibres) specifically stimulated the proliferation of keratinocytes, but not fibroblasts. Such films may be the biomaterials of choice for *in vivo* evaluation for skin tissue engineering and regenerative medicine.

Introduction

Biomaterials are generally constructed using a basic component such as collagen or synthetic polymers, which can be further functionalised by inclusion of other components. A large variety of different biomaterials can thus be produced. In addition, other parameters like production conditions and physical/chemical treatment can be varied, resulting in an even larger multiplicity of biomaterials. *In vivo* evaluation of the functionality of these biomaterial variables in animal studies would be expensive, time consuming and ethically challenging. The availability of a large array of biomaterials, each differing from one another in only one specific aspect, would enable an economical and fast *in vitro* pre-screening, allowing a rational selection of potentially useful biomaterials for *in vivo* evaluation.

For synthetic polymers, such arrays have been developed [1-6]. The most advanced arrays are based on one basic surface with (chemically) modified spots and 2D gradients of a specific modification. However, arrays based on natural proteins require a specific approach due to the delicate nature of biomolecules. For that reason, only a few arrays have been developed that include natural extracellular matrix proteins, but the molecular composition of the basic extracellular matrix components used in these arrays has not been reported [7-10]. Therefore, there is a need for well-defined arrays based on natural extracellular matrix proteins. In this study an array of different molecularly-defined collagen-based biomaterials was constructed, and evaluated for their potential in skin tissue engineering.

Type I collagen is the most abundant extracellular matrix protein in the human body. Native, fibrillar type I collagen is therefore often used as scaffolding material for regenerative medicine. Collagen biomaterials possess many characteristics that can be modified [11], including the 3D-architecture (e.g. porous scaffold or dense film [12,13]), the type and degree of crosslinking [14], the presence of other basic components (e.g. elastin [15]), and the incorporation of additives such as glycosaminoglycans [16,17] or growth factors [18,19].

Each single modification of a biomaterial may result in a different response *in vitro* and/or *in vivo*. A number of studies have addressed this issue. For example, a decrease in pore size of a collagen-chondroitin sulfate scaffold resulted in an increase in the viability of mouse clonal osteogenic cells *in vitro* [20]. Addition of matrix proteins to basal lamina analogues enhanced attachment of keratinocytes *in vitro* [7]. Mild crosslinking with a carbodiimide resulted in an optimal balance between scaffold strength and proliferation of a keratinocyte/fibroblast co-culture [21]. Chemical crosslinking also promoted scaffold integrity and reduced antigenicity *in vivo*, and the incorporation of heparan sulfate promoted angiogenesis [22]. Addition of FGF-2 or VEGF to scaffolds increased their angiogenic potential [18,23,24]. However, large-scale bioarrays based on collagenous biomaterials and simultaneously addressing various parameters including basic components, physical pre-treatment, type and amount of additives, and nature of crosslinking have not been reported.

In this study, 48 defined collagen-based biomaterials were constructed, characterised and evaluated *in vitro* using primary human keratinocytes/fibroblasts.

Materials and Methods

Purification of fibrillar collagen, elastin fibres and soluble elastin

Insoluble type I collagen (COL) was purified from bovine achilles tendon using extractions with diluted acetic acid, aqueous NaCl and urea, and acetone as described [17]. Insoluble elastin fibres (EL_{fibre}) were purified from equine ligamentum nuchae using extractions with aqueous NaCl, organic solvents, 8% CNBr in formic acid, aqueous urea with 2-mercaptoethanol, and a trypsin digestion [25]. Solubilised elastin (EL_{sol}) was prepared from insoluble elastin fibres by oxalic acid hydrolysis [26,27].

Preparation of 48 different molecularly-defined, fibrillar collagen-based films

For an overview of all films prepared, see Table 1. Films were prepared composed of collagen only (COL), collagen + insoluble elastin fibres in an 80:20 ratio ($COL80:20EL_{fibre}$), and collagen with solubilised elastin in an 80:20 ratio ($COL80:20EL_{sol}$). A suspension of 0.8% (w/v) collagen for COL, 0.64% (w/v) collagen + 0.16% (w/v) elastin for $COL80:20EL_{fibre}$ and 0.64% (w/v) collagen for $COL80:20EL_{sol}$ was shaken overnight in 0.25 M acetic acid at 4ºC. For $COL\text{-}EL_{sol}$, 0.16% (w/v) elastin peptides was added after this incubation. The suspensions were homogenised on ice using a Potter-Elvehjem homogeniser (Louwers Glass and Ceramic Technologies, Hapert, The Netherlands) with an intervening space of 0.35 mm, until homogenisation was completed. Air-bubbles were removed from the COL and $COL\text{-}EL_{sol}$ suspensions by centrifugation at 250 g for 10 min at 4ºC, and from the $COL\text{-}EL_{fibre}$ solution by incubation in a desiccator. Twelve ml of the suspensions were poured into a petri dish (Ø 86 mm) and air-dried at room temperature.

Table 1. Overview of films prepared.

Basic film	Treatment nX	PT nX	EDC_{low}	EDC_{high}	PT EDC_{high}	GA_{low}	GA_{medium}	GA_{high}	CS_{low}	CS_{high}	DS_{low}	DS_{high}	H_{low}	H_{high}
COL	✓	✓	✓	✓	✓	✓	✓	✓	✓	✓	✓	✓	✓	✓
$COL80:20EL_{fibre}$	✓	✓	✓	✓	✓	✓	✓	✓	✓	✓	✓	✓	✓	✓
$COL80:20EL_{sol}$	✓	✓	✓	✓	✓	✓	✓	✓	✓	✓	✓	✓	✓	✓
$COL50:50EL_{fibre}$	✓			✓										
$COL20:80EL_{fibre}$	✓			✓										
$COL50:50EL_{sol}$				✓										
COL COLIV	✓													

COL=type I collagen, EL_{fibre}=elastin fibres, EL_{sol}=solubilised elastin, COLIV=type IV collagen, nX=non-crosslinked,EDC=EDC/NHS crosslinked, PT=Polytron homogenised (all other scaffolds were homogenised by Potter-Elvehjem), GA=Glutaraldehyde crosslinked, CS=chondroitin sulfate, DS=dermatan sulfate, H=heparin, $EDC/GA_{low/medium/high}$=crosslinked with a low, medium or high concentration of EDC/NHS or glutaraldehyde, $CS/DS/H_{low/high}$=crosslinked in the presence of a low or high amount of chondroitin sulfate, dermatan sulfate or heparin. For further explanation see text.

The same methodology was used to produce $COL50:50EL_{fibre}$, $COL20:80EL_{fibre}$, and $COL50:50EL_{sol}$ films. $COL20:80EL_{sol}$ films were also produced, but too weak to handle and therefore not included in this study.

To study the effect of different homogenisation procedures, additional COL, $COL80:20EL_{fibre}$ and $COL80:20EL_{sol}$ films were prepared by use of a Polytron device (PT)

(Kinematica, Luzern, Switzerland) at 2,500 rpm on ice until homogenisation was completed, rather than Potter-Elvehjem homogenisation.

To study the effect of crosslinking, films were chemically crosslinked for 4 h with 12.5 (EDC_{low}) or 33 (EDC_{high}) mM 1-ethyl-3-(3-dimethyl aminopropyl)carbodiimide (EDC) and 6 mM N-hydroxysuccinimide (NHS) in 50 mM 2-morpholinoethane sulphonic acid (MES, pH 5.0) containing 40% ethanol. This was followed by washings with 0.1 M Na_2HPO_4, 1 M NaCl, 2 M NaCl and demineralised water [28]. Alternatively, films were crosslinked in 0.025 (GA_{low}), 0.1 (GA_{medium}) or 0.5% (GA_{high}) (v/v) glutaraldehyde in 0.1 M Na-phosphate buffer (PB, pH 7.4) for 1 h at room temperature. Free aldehydes were subsequently quenched for 1 h at room temperature with respectively 2.5, 10 and 50 mM of glycine in 0.1 M PB.

To study the effect of various glycosaminoglycans, these were covalently coupled by crosslinking films using a EDC_{high} EDC/NHS solution (see above) containing: 0.075 (H_{low}) or 0.375% (H_{high}) (w/v) heparin (Diosynth, Oss, The Netherlands), 0.05 (CS_{low}) or 0.25% (CS_{high}) (w/v) chondroitin sulfate (Sigma-Aldrich, St. Louis, MO, USA), and 0.05 (DS_{low}) or 0.25% (DS_{high}) dermatan sulfate (Sigma-Aldrich).

To study the effect of an additional type of collagen, a suspension containing 20 µg/ml type IV collagen (Fluka BioChemika, Switzerland) in 0.25 M acetic acid was applied to the non-crosslinked COL films and air-dried, resulting in a coating of 10 µg type IV collagen/cm^2 film (COL COLIV).

Characterisation of the fibrillar collagen-based films

The degree of crosslinking of the films was estimated spectrophotometrically by determining the amine group content using 2,4,6-trinitrobenzene sulfonic acid [29,30].

The glycosaminoglycan content of the films was determined applying a hexosamine assay using p-dimethylamino-benzaldehyde, taking heparin as a standard [31,32].

Type IV collagen was visualised by immunofluorescence on cryosections using a goat anti-human type IV collagen antibody (1:200, Southern Biotech, USA) and donkey anti-goat Alexa Fluor 488 secondary antibody (1:200, Molecular Probes, Eugene, OR, USA).

For scanning electron microscopy, films were mounted on stubs, sputtered with an ultrathin layer of gold in a Polaron E5100 coating system and visualised with a JEOL JSM-6310 scanning electron microscope (Tokyo, Japan) operating at 15 kV. To visualise the banding pattern of the collagen fibrils, films were mounted on stubs, sputtered with an ultrathin layer of gold/palladium in a Cressington 208HR coating system (Redding, CA, USA) and visualised with a JEOL JSM-6300 scanning electron microscope operating at 3 kV.

Cell source and submerged cell culture

Keratinocytes with some residual fibroblasts were obtained from human abdominal skin derived from donors who underwent surgery for abdominal wall correction, as described [33].

To culture cells, Ø 20 mm punches of films were taken and placed in Ø 10 mm Cell-Crown24 inserts (ScaffDex, Tampere, Finland), disinfected with 70% ethanol (3x1h and once o/n), washed with sterile phosphate-buffered saline (pH 7.2, 5x1h and once o/n),

placed on the bottom of a 6-wells plate (Greiner Bio-One) and pre-incubated for 16 h in medium containing 5% calf serum (Hyclone), consisting of 2 parts DMEM (Gibco) and 1 part Ham's F12 medium (Gibco), L-glutamine (4 mM; Gibco), penicillin/streptomycin (50 IU/ml; Gibco), adenine (24.3 µg/ml; Calbiochem), ascorbic acid (50 µg/ml; Sigma), insulin (0.2 µM; Sigma), hydrocortisone (1 µM; Merck), triiodothyronine (1.36 ng/ml; Sigma) and cholera toxin (10^{-10} M; Sigma) at 37ºC. Cells were seeded at a density of 75,000 cells/insert and incubated in 2 ml medium per well at 37ºC under 8% CO_2. At day three of the culture, medium was refreshed. Cells were cultured on the films for six days.

Cell proliferation assay

Medium was replaced with 1.5 ml medium containing 10% water-soluble tetrazolium salt-1 cell proliferation reagent (WST-1, Roche, Basel, Switzerland) and cells were incubated for 1 h at 37ºC. Then, 100 µl of the supernatant was transferred to an empty plate and the absorbance was measured at 450 nm. The absorbance of the supernatant taken from cells grown on Thermanox coverslips was set at 1 and used to calculate the relative absorbance.

Morphological evaluation

Films were rinsed with 0.1 M PB (pH 7.4) and fixed with 4% paraformaldehyde in 0.1 M PB for 30 min at room temperature, washed with 0.1 M PB and divided into parts.

Cells were visualised by standard haematoxylin-eosin (H&E) staining. For scanning electron microscopy, films were critical point dried using CO_2 with a Polaron E3000 critical point drying apparatus (Watford, UK) and processed and visualised with a JEOL JSM-6310 as described above.

Immunofluorescence was performed using antibodies against cytokeratins (rabbit polyclonal pKer, 1:200; Euro Diagnostics, and mouse anti-pancytokeratin clones AE1/AE3, 1:100; Dako, Glostrup, Denmark), and vimentin (1:200, Sigma). Respectively, goat anti-rabbit Alexa Fluor 594, goat anti-mouse Alexa Fluor 594 and goat anti-mouse Alexa Fluor 488 (1:200, Molecular Probes) were used as a secondary antibody. Nuclei were visualised with DAPI (1:1000, Molecular Probes).

To calculate the film area occupied by keratinocytes, at least 2 pictures per film (stained for cytokeratins) were taken with a Leica DM6000 microscope (Solms, Germany) at 50x magnification. The surface area of fluorescently labelled cells was calculated as a percentage of the total film surface area on the pictures using ImagePro software (Media Cybernetics Inc., Bethesda, MD, USA).

Results

Characterisation of the array films

Collagen-based films were prepared without elastin (COL) and with different ratios of elastin fibres (COL80:20$EL_{fibre,}$ COL50:50EL_{fibre}, and COL20:80EL_{fibre}) or solubilised elastin (COL80:20EL_{sol} and COL50:50EL_{sol}). The incorporation of an increasing amount of elastin

fibres resulted in brittle films, which, when wetted, were relatively weak and difficult to handle. The incorporation of solubilised elastin resulted in opaque and weak films (in a dry as well as in a wet state) and COL20:80EL_{sol} films were too weak to handle and therefore discarded from this array. SEM analysis of films showed the characteristic banding pattern of the individual collagen fibrils, indicating that the spatial orientation of the collagen molecules was preserved after the purification and production process (fig. 1A). All films had a closed surface and were approximately 10 µm thick (fig. 1A and D).

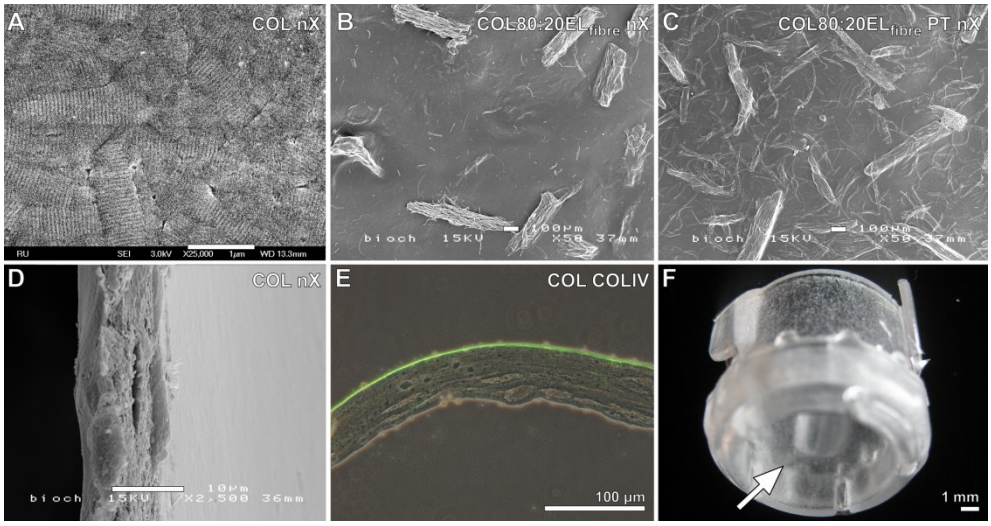

Figure 1. Morphological characteristics of the films used. A: scanning electron micrograph (SEM) of the top surface of a non-crosslinked collagen film (COL nX) illustrating the intact banding pattern of the collagen fibrils, and the closed surface of the films. B, C: SEM of the top surface of a Potter-Elvehjem (B, COL80:20ELfibre nX) and Polytron-homogenised (C, COL80:20ELfibre PT nX) elastin fibre containing film visualising the embedded elastin fibres (note the difference in fibre dispersion). D: SEM of a cross-section of a non-crosslinked collagen film (COL nX) indicating its thickness. E: immunofluoresent-phase contrast image of a composite type I/type IV collagen film (COL COLIV) with type IV collagen (green) on top. F: a transparent film (arrow) in a CellCrown insert. Scale bars are 1 µm (A), 100 µm (B, C and E), 10 µm (D), and 1 mm (F). For other abbreviations, see Table 1.

To obtain films with variable degrees and nature of crosslinking, crosslinking was performed with different concentrations of EDC/NHS (EDC) and glutaraldehyde (GA). These differences in crosslinking procedure resulted in clear differences in the amount of free amine groups, an indication of the degree of crosslinking (Table 2A). Glutaraldehyde crosslinking resulted in a larger reduction of amine groups compared to EDC-crosslinking, and even the lowest concentration of glutaraldehyde used (0.025% ≈ 2.5 mM) resulted in fewer remaining amine groups compared to the highest concentration of EDC used (33 mM) (compare EDC_{high} and GA_{low} in Table 2A). Glutaraldehyde crosslinked films were more brittle (in a dry state) and had a brownish appearance compared to the EDC-crosslinked films. Films with elastin fibres possessed less amine groups than films of collagen only, because elastin fibres contain fewer amine groups [15].

Table 2. Amount of amine groups (A) and glycosaminoglycans (B) in the biomaterial array.

A. Amount of amine groups

	nX	PT nX	EDC_{low}	EDC_{high}	PT EDC_{high}	GA_{low}	GA_{medium}	GA_{high}
COL	100	103±1	80±2	69±5	59±4	62±4	45±5	29±4
$COL80:20EL_{fibre}$	96±3	84±1	79±1	63±2	49±2	56±4	31±8	25±3
$COL80:20EL_{sol}$	112±5	100±4	88±5	72±5	52±6	62±13	46±7	26±4

	nX	EDC_{high}
$COL50:50EL_{fibre}$	60±3	30±1
$COL20:80EL_{fibre}$	37±9	16±6
$COL50:50EL_{sol}$		44±5
COL COLIV	96±3	

B. Amount of glycosaminoglycans

	DS_{low}	CS_{low}	H_{low}	DS_{high}	CS_{high}	H_{high}
COL	24±5	42±10	86±6	55±9	64±7	139±13
$COL80:20EL_{fibre}$	38±2	39±5	87±12	91±17	113±16	119±6
$COL80:20EL_{sol}$	35±8	40±9	98±1	74±18	106±27	141±12

relative amount of NH_2 groups as % of COL nX

≥90%	70-90%	50-70%	30-50%	0-30%

µg glycosaminoglycan/mg film

0-50	50-100	≥100

Relative amount of amine groups as percentage of COL nX (A) and amount of incorporated glycosaminoglycans as µg/mg film (B). Results are given as n=3 ± S.E.M. See Table 1 for abbreviations.

To obtain films prepared by different homogenisation methods, Potter-Elvehjem and Polytron homogenisation were compared. Polytron homogenisation resulted in films which were more difficult to hydrate in water and were more transparent when wetted. SEM analysis indicated that elastin fibres were more fragmented and more equally dispersed in the Polytron homogenised films compared to films derived from a pottered suspension (compare figs. 1B and 1C). In addition, the degree of crosslinking was increased in films prepared by Polytron homogenisation (compare EDC_{high} and PT EDC_{high} in Table 2A). This is likely due to increase in fibre surface.

To obtain films with different amounts and types of glycosaminoglycans, films were EDC-crosslinked in the presence of different amounts of heparin, chondroitin sulfate and dermatan sulfate. Table 2B shows that it was possible to bind low and high amounts of these three glycosaminoglycans to collagen-based films. It was possible to incorporate up to 140 µg heparin per mg film, whereas the maximum amount of bound CS and DS was lower, about 110 µg/mg and 80 µg/mg respectively. The maximum binding capacity for CS and DS was lower for the COL films than for the $COL80:20EL_{fibre}$ and $COL80:20EL_{sol}$ films. The degree of crosslinking of all glycosaminoglycan-containing films was comparable (57±6% (42-67%) reduction of amine groups).

To obtain a composite, layered film with two types of collagens, type IV collagen was coated on top of the fibrillar type I collagen film. Such a construct resembles the extracellular matrix of skin which consists of (dermal) type I collagen fibrils and (epidermal) basement membrane associated type IV collagen. Type IV collagen coating resulted in a highly confined layer on top of the type I collagen film (fig. 1E). Addition of type IV collagen did not significantly alter the amount of amine groups.

Cell proliferation

Films were placed in CellCrown inserts (fig. 1F) and primary human keratinocytes, containing a small number of residual fibroblasts, were seeded on top of 48 different films. After six days of culture, cell proliferation was measured with a WST-1 assay (Table 3).

Table 3. Cell proliferation on the biomaterial array.

Cell proliferation

	nX	PT nX	EDC_{low}	EDC_{high}	PT EDC_{high}	GA_{low}	GA_{medium}	GA_{high}
COL	7.8±2.7	8.0±1.7	7.6±1.0	7.6±0.9	6.7±0.7	1.4±0.5	0.4±0.3	0.5±0.1
COL80:20EL_{fibre}	8.3±3.2	7.9±5.7	10.0±1.0	8.3±2.4	6.9±1.6	2.3±0.9	0.5±0.1	0.7±0.1
COL80:20EL_{sol}	5.3±0.8	7.0±1.7	10.9±2.6	7.0±4.2	6.1±2.7	3.5±2.2	0.9±0.3	0.9±0.1

relative absorbance: ≥10 | 7-10 | 4-7 | 1-4 | 0-1

	DS_{low}	CS_{low}	H_{low}	DS_{high}	CS_{high}	H_{high}
COL	1.0±0.4	2.9±1.7	4.9±0.5	0.7±0.5	4.2±1.3	3.6±1.0
COL80:20EL_{fibre}	0.6±0.5	3.2±0.5	4.5±0.6	0.8±0.4	2.7±0.7	2.5±1.1
COL80:20EL_{sol}	2.5±1.1	3.9±1.4	4.6±0.2	2.3±2.6	4.0±1.5	2.7±1.4

	nX	EDC_{high}
COL50:50EL_{fibre}	8.3±5.6	4.8±3.9
COL20:80EL_{fibre}	9.4±2.7	8.4±5.2
COL50:50EL_{sol}		4.8±1.5
COL COLIV	11.6±1.6	

Cell proliferation relative to cells cultured on plastic, which was taken as 1.0. Results are given as n=3, ± S.E.M. See Table 1 for abbreviations.

Most films promoted cell proliferation compared to cells cultured on cell culture plastic. In general EDC crosslinking did not alter cell proliferation compared to non-crosslinked films. Amongst the most proliferation promoting films were the COL80:20EL_{fibre} and COL80:20EL_{sol} films both crosslinked with a low amount of EDC. Glutaraldehyde crosslinking resulted in a large reduction in cell proliferation, with low proliferation on the films crosslinked in a low concentration of glutaraldehyde and almost no proliferation on the films crosslinked in medium or high concentrations of glutaraldehyde. Addition of glycosaminoglycans resulted in lower cell proliferation than their counterparts without glycosaminoglycans, i.e. the basic EDC_{high} films. The presence of a low amount of heparin resulted in a minor reduction in cell proliferation, but films with a high amount of incorporated heparin showed a larger reduction. A comparable negative effect on cell proliferation was observed for chondroitin sulfate, but without a clear dose-response relationship. Of the three glycosaminoglycans evaluated, the incorporation of dermatan sulfate resulted in the largest reduction in cell proliferation. This negative effect appeared to be less dramatic for the films with 20% solubilised elastin, but there was a large variation between individual experiments. Interestingly, the film which promoted cell proliferation to the largest extent (about 11-fold) was the type IV collagen coated film.

Cell morphology

Films with cultured cells were processed for SEM analysis. The observed cell numbers correlated with the values found in the cell proliferation assay. An example of a film with hardly any cells (COL GA_{low}), an intermediate number of cells (COL CS_{high}), and two films with a high number of cells (COL nX and COL50:50EL_{fibre} nX), is shown in Figure 2.

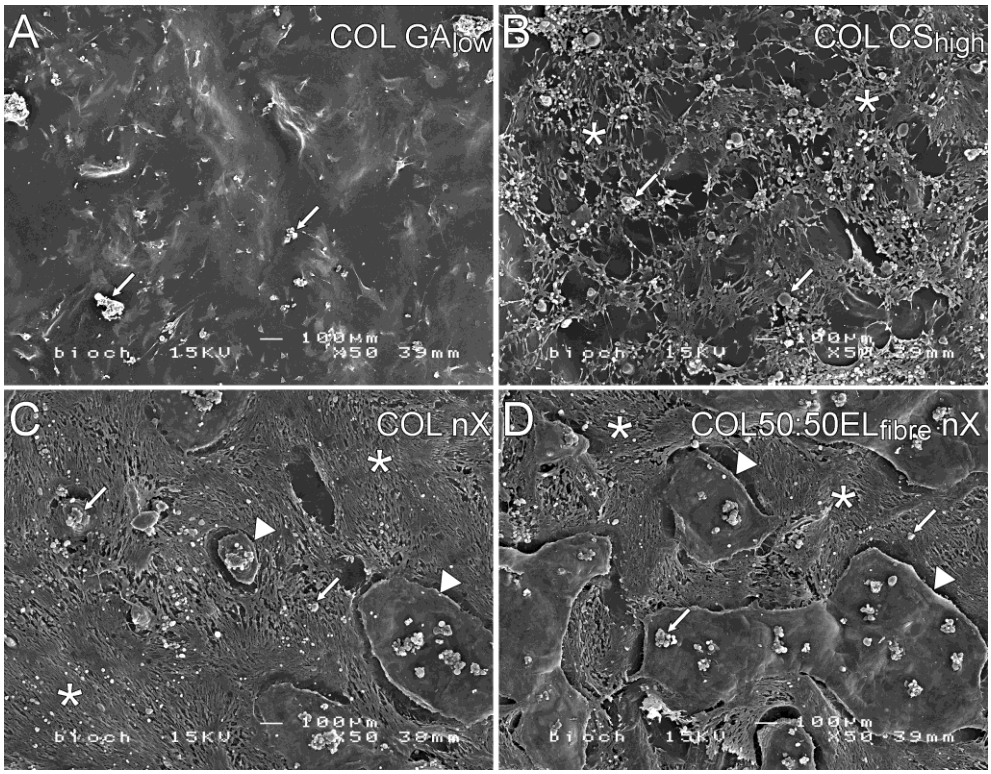

Figure 2. Scanning electron micrographs of the cells cultured on various films. A: a glutaraldehyde-fixed collagen film (COL GA_{low}) representing a film with a very low proliferative index (see Table 3). B: an EDC/NHS-fixed collagen film containing chondroitin sulfate (COL CS_{high}) representing a film with intermediate proliferative index. C, D: a non-crosslinked collagen film (COL nX; C) and a non-crosslinked collagen/elastin fibre film (COL50:50EL_{fibre} nX, D), representing films with a high proliferative index. Arrows indicate single rounded cells and cell clumps; asterisks indicate spindle-shaped fibroblast-like cells; arrowheads indicate keratinocyte colonies. Scale bars are 100 µm. For other abbreviations, see text/Table 1.

On the glutaraldehyde crosslinked films and the DS containing films, only some single round-shaped cells were visible (fig. 2A). The heparin and CS containing films showed interconnected fields of spindle-shaped cells (fig. 2B). All the other films had an almost confluent layer of spindle-shaped cells, containing islets of cobblestone-shaped flattened cells (fig. 2C and 2D). These islets represent keratinocyte colonies (see section 3.4), where the spindle-shaped cells are fibroblasts, derived from a subpopulation that was present in the isolated primary cells. Large differences in the size of the keratinocyte colonies were observed between films with comparable cell proliferation values, as illustrated in fig. 2C and 2D.

H&E staining of these films confirmed these findings, but observation of the cell morphology was hampered by staining of the underlying collagen (data not shown).

Immunostaining for cytokeratins and vimentin

To distinguish between keratinocytes and fibroblast-like cells, films were immunostained for cytokeratins ('keratinocytes') and vimentin ('fibroblasts'). Nuclei were visualised with DAPI.

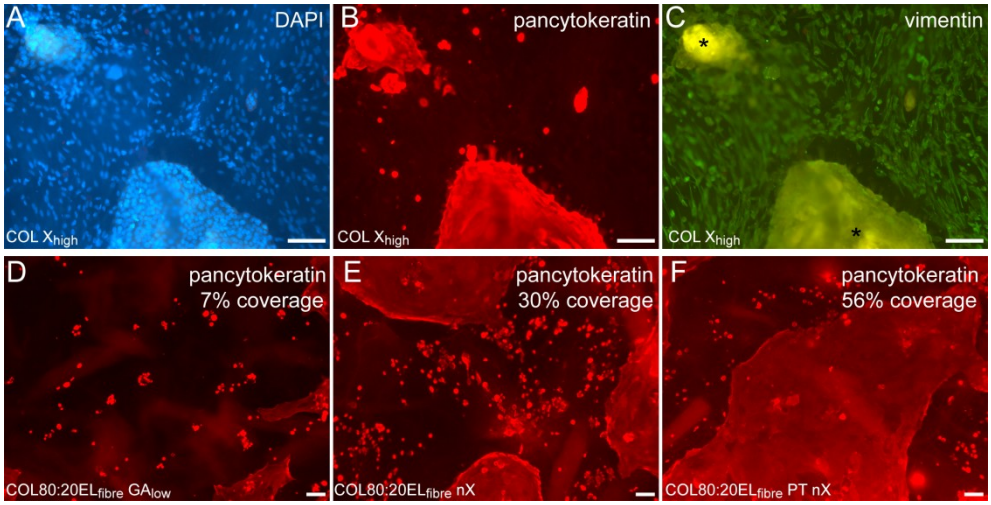

Figure 3. Immunocytochemistry of keratinocytes/fibroblasts cultured on various films. A-C: Cells cultured on an EDC/NHS-fixed collagen film (COL X_{high}) simultaneously visualised for nuclei (A, DAPI staining), for keratinocytes (B, pancytokeratin), and for fibroblasts (C, vimentin). Note the nuclei-dense keratinocyte fields. The yellow autofluoresence is derived from the keratinocytes (asterisks). D-F: Cells cultured on three different films (D, COL80:20EL_{fibre} GA_{low}; E, COL80:20EL_{fibre} nX; F, COL80:20EL_{fibre} PT nX) and stained for keratinocytes. Indicated is the percentage of coverage of the surface by immunopositive cells. Scale bars are 100 µm.

The large islets showed pancytokeratin-positive staining, indicating that these are indeed keratinocyte colonies (fig. 3B). Some other large, rounded cells also showed pancytokeratin-positive staining (fig. 3B). The remaining spindle-shaped cells all stained positive for vimentin (fig. 3C), but negative for cytokeratins.

To analyse the potential of the different films to specifically stimulate keratinocyte (and not fibroblast) proliferation, the surface percentage of pancytokeratin positive cells (coverage) was calculated (Table 4, figs. 3D-F).

When the cell proliferation index, reflecting proliferation of both keratinocytes and fibroblasts (Table 3) was compared to the film surface covered with keratinocytes (Table 4), it was noted that not all films with a high index contained many keratinocytes. This suggests that specific films differentially support either proliferation of keratinocyte or fibroblasts. Of the three films with the highest cell proliferation index (COL80:20EL_{fibre} EDC_{low}, COL80:20EL_{sol} EDC_{low}, and COL COLIV nX), only the film with elastin fibres was covered with a large area of keratinocytes (36%), whereas the other two films apparently did not specifically stimulate keratinocyte proliferation (18 and 19%, respectively).

Table 4. Surface area of the biomaterial array films covered with keratinocytes (pancytokeratin-positive cells)..

Percentage of surface covered with keratinocytes

	nX	PT nX	EDC_{low}	EDC_{high}	PT EDC_{high}	GA_{low}	GA_{medium}	GA_{high}
COL	17±5	19±10	13±7	9±3	9±3	1±0	1±1	1±0
$COL80:20EL_{fibre}$	24±16	52±12	36±10	19±9	19±5	6±4	1±1	0±0
$COL80:20EL_{sol}$	8±3	8±1	18±7	14±5	12±5	9±2	1±0	0±0

surface % covered: ≥30% | 20-30% | 10-20% | 5-10% | 0-5%

	DS_{low}	CS_{low}	H_{low}	DS_{high}	CS_{high}	H_{high}
COL	3±1	2±1	5±2	1±1	5±0	12±3
$COL80:20EL_{fibre}$	1±0	3±1	6±1	1±1	4±2	8±2
$COL80:20EL_{sol}$	4±0	4±0	8±2	3±2	4±0	17±11

	nX	EDC_{high}
$COL50:50EL_{fibre}$	32±13	25±5
$COL20:80EL_{fibre}$	26±10	24±9
$COL50:50EL_{sol}$		8±4
COL COLIV	19±6	

Film surface area covered with pancytokeratin positive cells as a percentage of the total film surface area. Results are given as n=3 ± S.E.M. See Table 1 for abbreviations.

A large surface area covered with keratinocytes was also found for all non-crosslinked films containing elastin fibres and the EDC-crosslinked films with 50 or 80% elastin fibres, with a remarkable high value for the Polytron-homogenised non-crosslinked variant (52%). These results suggest that elastin fibres specifically stimulate keratinocyte proliferation, especially when these fibres are more fragmented and equally dispersed as in the Polytron-homogenised film. A negative effect of EDC-crosslinking on keratinocyte proliferation was observed for the COL and $COL80:20EL_{fibre}$ films. For the $COL80:20EL_{sol}$ films this effect was less clear, possibly due to wash-out of solubilised elastin from the non-crosslinked films. All the glutaraldehyde-crosslinked and glycosaminoglycan-containing films possessed a relatively small surface area covered with keratinocytes, corresponding with the observed low cell proliferation values. Only the size of the keratinocyte covered area on the H_{high} films was remarkably larger than what could be expected from their proliferation value. This suggests that, although the high amount of incorporated heparin had a negative effect on overall cell proliferation, it stimulated the proliferation of keratinocytes.

Discussion

The goal of this study was to construct an array of molecularly-defined biomaterials based on native fibrillar type I collagen to enable the fast *in vitro* pre-screening of these materials for any desired application. Collagen films consisting of different basic components were produced and it was possible to control the amount of amine groups present by crosslinking the films with different concentrations of EDC/NHS or glutaraldehyde. The latter resulted in less remaining amine groups because glutaraldehyde can react with virtually any primary amine group of the collagen molecule [34], whereas EDC-crosslinking needs an amine group in close proximity to a carboxylic group [35]. It was also possible to bind different glycosaminoglycans in different amounts with EDC/NHS crosslinking by adjusting the glycosaminoglycan-concentration in the crosslinking solution. In total, a set of 48 different

molecularly-defined films was produced and characterised. The array can be easily extended by the introduction of growth factors and other effector molecules.

Biomaterial arrays have been developed for the screening of synthetic polymers [1,4-6]. Arrays that include natural proteins have also been described, generally based on soluble, rather than insoluble extracellular matrix proteins. For example, the effect of combinations of (soluble) collagens type I, III and IV, laminin and fibronectin has been evaluated on rat hepatocytes/mouse embryonic stem cells, the latter also in combination with growth factors, and another study evaluated three cell lines on different (solubilised) extracellular matrix proteins [8-10]. In the human body, however, extracellular matrix proteins like collagen and elastin are arranged in an insoluble, fibrillar and crosslinked configuration. Membranes containing insoluble collagen have been evaluated in e.g. cytotoxicity or cell-material interaction studies, but these were performed on a much smaller scale (max. 5 different membranes) than the array described in this paper [36-39]. Bush *et al.* evaluated keratinocyte attachment on an insoluble type I collagen-chondroitin sulfate membrane, coated with four different concentrations of soluble type I and IV collagen, laminin and fibronectin [7]. It is, however, not certain whether the type I collagen in the membrane represents its natural extracellular matrix form, because it was dehydrothermally crosslinked (105°C in a vacuum for 24 h). The array presented in this report is based on highly-purified and thoroughly characterised native fibrillar type I collagen and elastin [17,25]. It is also unique in the combination of the different basic proteins used and the types of modification applied, and the detailed characterisation of the films. The molecularly-defined character of the array allows a systematic analysis of parameters involved in specific cellular behaviour.

We used cultures of primary keratinocytes to evaluate the biological effects of different array parameters. Keratinocyte cultures were obtained by the Rheinwald-Green method and usually contain a small amount of fibroblasts. In previous studies from our lab we have used these cells in model systems and culture media that are selective for keratinocytes, and outgrowth of fibroblasts was not observed when cultured on plastic or in 3-D reconstructed skin [33,40]. Here, these cells were seeded on the films and cultured in DMEM/F12 with 5% foetal calf serum which is not selective for keratinocytes and allows fibroblast outgrowth. This enables the evaluation of proliferation of two relevant skin cell populations simultaneously, and indeed significant differences were observed between the behaviour of keratinocytes and fibroblasts, depending on the composition of the film. On most of the films (38/48), cell proliferation was higher than on standard cell culture plastic. Two crosslinking agents were compared and it was noticed that EDC was superior to glutaraldehyde. This is in line with literature data which indicate that glutaraldehyde has a detrimental effect on cell proliferation [41,42]. The proliferation of specifically keratinocytes (and not fibroblasts) was stimulated to the largest extent by the presence of elastic fibres, especially when these fibres were equally dispersed throughout the film. The mechanisms behind this stimulation remain elusive, but it is known that the dermal-epidermal junction contains thin embranchments of the dermal elastin fibre network and cultured human keratinocytes express tropoelastin [43,44].

Debate exists in the tissue engineering/regenerative medicine community as to what extent *in vitro* experiments are able to predict *in vivo* results [45-47]. Although efforts are made to standardise *in vitro* evaluation procedures, results are dependent on e.g. the culture conditions used. In addition, *in vivo* other types of cells (e.g. immune cells) will be present, increasing the level of complexity. Based on the *in vitro* evaluation of keratinocytes on the array, and taking best proliferation and highest area coverage as the parameters, the most optimal film would be a Polytron-homogenised type I collagen film containing 20% elastin fibres and without additional modifications like crosslinking or the incorporation of glycosaminoglycans. However, when crosslinking would be necessary, e.g. in order to strengthen a tissue-engineered construct, mild EDC/NHS crosslinking is the preferred method, and glutaraldehyde crosslinking has to be avoided. When glycosaminoglycans have to be incorporated, e.g. to enhance the binding of growth factors, a high heparin content is the best option.

For future applications, other cell type(s) of interest may be evaluated with this array, or the array itself might be extended by the incorporation of additional modifications. It would, for example, be interesting to study the effect of growth factors combined with different glycosaminoglycans. Also the combination of elastin fibres with type IV collagen coating would be worthwhile to investigate, as would be a Polytron homogenised film containing more than 20% elastin fibres.

Conclusion

We developed an extracellular matrix array, consisting of 48 different, fully characterised films based on native fibrillar collagen and differing from each other in amount and type of matrix components, method of preparation, and amount and extent of crosslinking. The array was evaluated using cultured primary human keratinocytes/fibroblasts, and film-specific differences in morphology, proliferation and differentiation were observed. Only a small selection of films (especially those containing elastin fibres) particularly stimulated the proliferation of keratinocytes without promoting fibroblast growth. Such films may be the biomaterials of choice for *in vivo* evaluation for skin tissue engineering and regenerative medicine. The array described may be generally applicable and instrumental for selection of the appropriate set of matrix molecules for use as biomaterials for regenerative medicine.

Acknowledgements

Geert-Jan Janssen of the General Instrumentation of the Radboud University Nijmegen is acknowledged for his support with the JEOL JSM-6300 scanning electron microscope, the MIC facility of the NCMLS for the use of the JSM-6310 microscope and Werner Koopman for his advice on image quantification. This study is funded by the Dutch Program for Tissue Engineering (grant DPTE 6735).

References

1. Yliperttula M, Chung BG, Navaladi A, Manbachi A, Urtti A. High-throughput screening of cell responses to biomaterials. Eur J Pharm Sci 2008;35:151-60.
2. Meredith JC, Sormana JL, Keselowsky BG, Garcia AJ, Tona A, Karim A, *et al.* Combinatorial characterization of cell interactions with polymer surfaces. J Biomed Mater Res A 2003;66:483-90.
3. Kennedy SB, Washburn NR, Simon CG, Jr., Amis EJ. Combinatorial screen of the effect of surface energy on fibronectin-mediated osteoblast adhesion, spreading and proliferation. Biomaterials 2006;27:3817-24.
4. Ateh DD, Vadgama P, Navsaria HA. Culture of human keratinocytes on polypyrrole-based conducting polymers. Tissue Eng 2006;12:645-55.
5. Anderson DG, Levenberg S, Langer R. Nanoliter-scale synthesis of arrayed biomaterials and application to human embryonic stem cells. Nat Biotechnol 2004;22:863-6.
6. Khademhosseini A, Langer R, Borenstein J, Vacanti JP. Microscale technologies for tissue engineering and biology. Proc Natl Acad Sci U S A 2006;103:2480-7.
7. Bush KA, Downing BR, Walsh SE, Pins GD. Conjugation of extracellular matrix proteins to basal lamina analogs enhances keratinocyte attachment. J Biomed Mater Res A 2007;80:444-52.
8. Flaim CJ, Chien S, Bhatia SN. An extracellular matrix microarray for probing cellular differentiation. Nat Methods 2005;2:119-25.
9. Flaim CJ, Teng D, Chien S, Bhatia SN. Combinatorial signaling microenvironments for studying stem cell fate. Stem Cells Dev 2008;17:29-39.
10. Kuschel C, Steuer H, Maurer AN, Kanzok B, Stoop R, Angres B. Cell adhesion profiling using extracellular matrix protein microarrays. Biotechniques 2006;40:523-31.
11. Geutjes PJ, Daamen WF, Buma P, Feitz WF, Faraj KA, Van Kuppevelt TH. From molecules to matrix: construction and evaluation of molecularly defined bioscaffolds. Adv Exp Med Biol 2006;585:279-95.
12. Doillon CJ, Whyne CF, Brandwein S, Silver FH. Collagen-based wound dressings: control of the pore structure and morphology. J Biomed Mater Res 1986;20:1219-28.
13. Faraj KA, Van Kuppevelt TH, Daamen WF. Construction of collagen scaffolds that mimic the three-dimensional architecture of specific tissues. Tissue Eng 2007;13:2387-94.
14. Duan X, Sheardown H. Dendrimer crosslinked collagen as a corneal tissue engineering scaffold: mechanical properties and corneal epithelial cell interactions. Biomaterials 2006;27:4608-17.
15. Daamen WF, van Moerkerk HT, Hafmans T, Buttafoco L, Poot AA, Veerkamp JH, *et al.* Preparation and evaluation of molecularly-defined collagen-elastin-glycosaminoglycan scaffolds for tissue engineering. Biomaterials 2003;24:4001-9.
16. Ellis DL, Yannas IV. Recent advances in tissue synthesis *in vivo* by use of collagen-glycosaminoglycan copolymers. Biomaterials 1996;17:291-9.
17. Pieper JS, Oosterhof A, Dijkstra PJ, Veerkamp JH, Van Kuppevelt TH. Preparation and characterization of porous crosslinked collagenous matrices containing bioavailable chondroitin sulphate. Biomaterials 1999;20:847-58.
18. Nillesen ST, Geutjes PJ, Wismans R, Schalkwijk J, Daamen WF, Van Kuppevelt TH. Increased angiogenesis and blood vessel maturation in acellular collagen-heparin scaffolds containing both FGF2 and VEGF. Biomaterials 2007;28:1123-31.
19. Yao C, Markowicz M, Pallua N, Noah EM, Steffens G. The effect of cross-linking of collagen matrices on their angiogenic capability. Biomaterials 2008;29:66-74.
20. O'Brien FJ, Harley BA, Yannas IV, Gibson LJ. The effect of pore size on cell adhesion in collagen-GAG scaffolds. Biomaterials 2005;26:433-41.
21. Powell HM, Boyce ST. EDC cross-linking improves skin substitute strength and stability. Biomaterials 2006;27:5821-7.
22. Pieper JS, Van Wachem PB, Van Luyn MJ, Brouwer LA, Hafmans T, Veerkamp JH, *et al.* Attachment of glycosaminoglycans to collagenous matrices modulates the tissue response in rats. Biomaterials 2000;21:1689-99.
23. Pieper JS, Hafmans T, Van Wachem PB, Van Luyn MJ, Brouwer LA, Veerkamp JH, *et al.* Loading of collagen-heparan sulfate matrices with bFGF promotes angiogenesis and tissue generation in rats. J Biomed Mater Res 2002;62:185-94.
24. Yao C, Roderfeld M, Rath T, Roeb E, Bernhagen J, Steffens G. The impact of proteinase-induced matrix degradation on the release of VEGF from heparinized collagen matrices. Biomaterials 2006;27:1608-16.
25. Daamen WF, Hafmans T, Veerkamp JH, Van Kuppevelt TH. Isolation of intact elastin fibers devoid of microfibrils. Tissue Eng 2005;11:1168-76.
26. Daamen WF, Nillesen ST, Wismans RG, Reinhardt DP, Hafmans T, Veerkamp JH, *et al.* A biomaterial composed of collagen and solubilized elastin enhances angiogenesis and elastic fiber formation without calcification. Tissue Eng Part A 2008;14:349-60.
27. Partridge SM, Davis HF, Dair G.S. The chemistry of connective tissues. 2. Soluble proteins derived from partial hydrolysis of elastin. Biochem J 1955;61:11-21.

28. Pieper JS, Hafmans T, Veerkamp JH, Van Kuppevelt TH. Development of tailor-made collagen-glycosaminoglycan matrices: EDC/NHS crosslinking, and ultrastructural aspects. Biomaterials 2000;21:581-93.
29. Olde Damink LH, Dijkstra PJ, Van Luyn MJ, Van Wachem PB, Nieuwenhuis P, Feijen J. Cross-linking of dermal sheep collagen using a water-soluble carbodiimide. Biomaterials 1996;17:765-73.
30. Gilbert DL, Kim SW. Macromolecular release from collagen monolithic devices. J Biomed Mater Res 1990;24:1221-39.
31. Yannas IV, Burke JF, Gordon PL, Huang C, Rubenstein RH. Design of an artificial skin. II. Control of chemical composition. J Biomed Mater Res 1980;14:107-32.
32. Elson LA, Morgan WT. A colorimetric method for the determination of glucosamine and chondrosamine. Biochem J 1933;27:1824-8.
33. Tjabringa G, Bergers M, van RD, de BR, Lamme E, Schalkwijk J. Development and validation of human psoriatic skin equivalents. Am J Pathol 2008;173:815-23.
34. Jayakrishnan A, Jameela SR. Glutaraldehyde as a fixative in bioprostheses and drug delivery matrices. Biomaterials 1996;17:471-84.
35. Grabarek Z, Gergely J. Zero-length crosslinking procedure with the use of active esters. Anal Biochem 1990;185:131-5.
36. Lesiak-Cyganowska E, Sladowski D, Jankowska E, Komender J. *In vitro* culture of human epithelial cells on a modified xenogenic collagen support. Arch Immunol Ther Exp (Warsz) 2001;49:253-9.
37. Lesiak-Cyganowska E, Jankowska-Steifer E, Kowalewski C, Komender J. Estimation of Interaction Between Human Keratinocytes and Xenogenic Collagen *in vitro*. Cell Tissue Bank 2006;7:39-46.
38. Schor SL. Cell proliferation and migration on collagen substrata *in vitro*. J Cell Sci 1980;41:159-75.
39. Tsai SP, Hsieh CY, Hsieh CY, Wang DM, Huang LLH, Lai JY, *et al.* Preparation and cell compatibility evaluation of chitosan/collagen composite scaffolds using amino acids as crosslinking bridges. J Appl Polym Sci 2007;105:1774-85.
40. Van Ruissen F., de Jongh GJ, Zeeuwen PL, Van Erp PE, Madsen P, Schalkwijk J. Induction of normal and psoriatic phenotypes in submerged keratinocyte cultures. J Cell Physiol 1996;168:442-52.
41. Gendler E, Gendler S, Nimni ME. Toxic reactions evoked by glutaraldehyde-fixed pericardium and cardiac valve tissue bioprosthesis. J Biomed Mater Res 1984;18:727-36.
42. Van Luyn MJ, Van Wachem PB, Olde Damink LH, Dijkstra PJ, Feijen J, Nieuwenhuis P. Secondary cytotoxicity of cross-linked dermal sheep collagens during repeated exposure to human fibroblasts. Biomaterials 1992;13:1017-24.
43. Cotta-Pereira G, Guerra RF, Bittencourt-Sampaio S. Oxytalan, elaunin, and elastic fibers in the human skin. J Invest Dermatol 1976;66:143-8.
44. Kajiya H, Tanaka N, Inazumi T, Seyama Y, Tajima S, Ishibashi A. Cultured human keratinocytes express tropoelastin. J Invest Dermatol 1997;109:641-4.
45. Siebers MC, ter Brugge PJ, Walboomers XF, Jansen JA. Integrins as linker proteins between osteoblasts and bone replacing materials. A critical review. Biomaterials 2005;26:137-46.
46. Malda J, Rouwkema J, Leeuwenburgh SC, Dhert WJ, Kirkpatrick CJ. Crossing frontiers in biomaterials and regenerative medicine. 8th World Biomaterials Congress, 28 May - 1 June, Amsterdam, The Netherlands. Regen Med 2008;3:765-8.
47. Hanks CT, Wataha JC, Sun Z. *In vitro* models of biocompatibility: a review. Dent Mater 1996;12:186-93.

Chapter 5

Cloning, large-scale production, and purification of active dimeric rat vascular endothelial growth factor (rrVEGF-164)

Paul J. Geutjes[1*]
Suzan T.M. Nillesen[1*]
Gerwen Lammers[1]
Willeke F. Daamen[1]
Toin H. van Kuppevelt[1]

*These authors contributed equally to this work

[1]Department of Biochemistry, Nijmegen Centre for Molecular Life Sciences, Radboud University Nijmegen Medical Centre, Nijmegen

Protein Expression and Purification
2010 volume 69 issue 1 pages 76-82

Abstract

Large-scale production of recombinant rat vascular endothelial growth factor (rrVEGF-164) is desirable for angiogenic studies. In this study, biologically active recombinant rat vascular endothelial growth factor (rrVEGF-164) was cloned and expressed in the yeast *P. pastoris,* and large-scale production was performed by fer-mentation. cDNA encoding VEGF-164 was prepared from embryonic rat tissue RNA, and a recombinant pPIC9HV/rVEGF-164 plasmid, containing an AOX1 promoter, was constructed. The methy-lotrophic *P. pastoris* was used as the eukaryotic expression system. After transformation, rrVEGF-164 was produced by fermentation (~124 mg/L) and purified by heparin affinity chromatography. SDS-PAGE indicated that rrVEGF-164 was produced as a disulphide-bridged dimer of 48 kDa which was purified to near homogeneity by heparin affinity chroma-tography in a large quantity. A bioassay indicated a three to five-fold increase in endothelial cell proliferation after 3 days, due to the addition of the produced rrVEGF-164. The produced rrVEGF-164 showed a higher biological activity than a commercially available, mouse cell line-based, growth factor. In conclusion, using the *P. Pastoris* expression system we were able to produce biologically active rat VEGF-164 in high quantities and this may provide a powerful tool for basic and applied life sciences.

Introduction

Vascular endothelial growth factor (VEGF) is one of the most celebrated mediators in the process of angiogenesis. VEGF is a hypoxia-inducible protein that promotes the proliferation and survival of vascular endothelial cells [1]). At least five different rat VEGF alternatively spliced isoforms have been identified originating from a single VEGF pre-mRNA: VEGF-120, -144, -164, -188 and -205 [2-4]). These isoforms resemble the human VEGF isoforms (VEGF-121, -145, -165, -189 and -206) and differ in length from them by one amino acid. VEGF is only active in its dimeric form [5,6]). All rat VEGF isoforms are mitogenic to vascular endothelial cells and induce permeabilisation of blood vessels [7]). VEGF-164, VEGF-188 and VEGF-205 are able to bind heparin [7-9]). VEGF-164 binds to the VEGF receptor (VEGFR) present on endothelial cells, stimulating the production of matrix metalloproteinases (MMPs). MMPs degrade the basement membrane, allowing proliferation and migration of endothelial cells towards the interstitium, so-called sprouting. Subsequently, pericytes proliferate and migrate towards the newly formed sprouts and induce maturation by forming a layer around the sprout [10,11]).

Large-scale production and purification of rat VEGF-164 is desirable for angiogenic studies *in vitro* and *in vivo*, especially in rat animal models for tissue engineering in which enhanced angiogenesis is an issue. Since the source of natural (rat) growth factors is limited, attempts have been made to produce growth factors on a large-scale by recombinant DNA technology. Growth factors have been produced in *Escherichia coli* and have played an important role in basic research of rat angiogenesis [12,13]). *E. coli* is a prokaryote and its intrinsic characteristics such as protein processing, protein folding, and post translational modi-fications, differ from those of eukaryotes. In *E. coli*, dimeric growth factors such as VEGF are produced as a monomer and need to be dimerised after production. The *Pichia pastoris* yeast expression system allows correct folding of dimeric proteins in addition to efficient expression, intact secretion, large-scale production, and stable genetics [14,15]). Human VEGF has been efficiently expressed in *P. pastoris* [16]. Expression of biologically active rat VEGF in *P. pastoris*, however, has -to our knowledge- never been published.

In this study, rrVEGF-164 was inserted into the pPIC9HV expression vector and transfected into the *P. pastoris* yeast cells. RrVEGF-164 was secreted in large quantities, purified using heparin affinity chromatography, and it's biological activity was studied *in vitro* using human umbilical vein endothelial cells (HUVECs).

Materials and Methods

Materials

Unless stated otherwise, all materials were from Merck (Darmstadt, Germany). The VEGF upstream (5'-GTA GAA TTC GCA CCC ACG ACA GAA GG-3') and VEGF downstream (5'-TAT GCG GCC GCT CAC CGC CTT GGC TTG T-3') primer containing *Eco*RI and *Not*I restriction sites were synthesised by Isogen Biosciences BV (Maarssen, The Netherlands). The *P. pastoris* expression vector pPIC9 and *P. pastoris* host strain GS115 were

purchased from Invitrogen Corp. (Carlsbad, CA, USA). The commercial rrVEGF-164, produced in a mouse myeloma cell line (R&D Systems, Minneapolis, MN, USA) was used as a positive control and for reference.

LB-medium consisted per litre of; 10 g NaCl, 10 g peptone (Gibco BRL), 5 g yeast extract (Difco Laboratories, Detroit, MI, USA), containing 10 g glucose and 0.1 g ampicillin (Sigma).

Buffered Glycerol-complex Medium (BMGY) containing glycerol as the carbon source, consisted per litre of; 10 g yeast extract, 20 g peptone, 21.2 g potassium sulphate (pH 6.0), 13.4 g yeast nitrogen base (YNB) (Sigma Chemical Co., St Louis, MO, USA), 0.4 mg biotin and 10 ml glycerol.

Buffered Methanol-complex Medium (BMMY) is similar to BMGY, but with 5 ml methanol instead of glycerol.

Basal salts medium (BSM) consisted per litre of; 26.7 ml phosphoric acid, 1.18 g calcium sulphate·$2H_2O$, 18.2 g potassium sulphate, 14.9 g magnesium sulphate·$7H_2O$, 4.1 g potassium hydroxide and 40 ml glycerol.

PTM1 trace salts (Invitrogen) consisted per litre of; 5 ml sulphuric acid, 6 g cupric sulphate·$5H_2O$, 0.08 g sodium iodide, 3 g manganese sulphate·H_2O, 0.2 g sodium molybdate·$2H_2O$, 0.02 g boric acid, 0.5 g cobalt chloride, 20 g zinc chloride, 65 g ferrous sulphate·$7H_2O$, and 0.2 g biotin.

YPD-medium consisted per litre of; 10 g yeast extract, 20 g peptone, 20 g D-glucose, with 100000 U penicillin and 0.1 g streptomycin (Gibco BRL).

YNB dropout plates consisted per litre of; 6.7 g YNB, 1.92 g yeast synthetic dropout medium supplement (Sigma), 20 g glucose and 20 g agar (Gibco BRL).

TYE agar plates consisted per litre of; 8 g NaCl, 10 g peptone, 5 g yeast extract, 15 g agar (Gibco BRL), 10 g glucose and 100 g ampicillin (Sigma).

Preparation of rat VEGF-164 cDNA

Total RNA was isolated from *Rattus norvegicus* embryonic tissue (17 days post-conception) using the SV Total RNA Isolation System (Promega, Madison, WI, USA). After denaturation (10 min at 65°C) of the total RNA (~0.5 µg), cDNA (~0.4 µg) was synthesised using hexanucleotide primers. A reverse transcriptase reaction was performed for 90 min at 37°C using the following reaction mixture; 200 units reverse transcriptase (Promega) in 50 mM Tris-HCl (pH 8.3) containing 75 mM KCl, 3 mM MgCl2 [M-MLV Reversed Transcriptase buffer (Gibco BRL, Gaithersburg, MD, USA)], 1 mM deoxynucleoside triphosphates (dNTPs) and 10 mM DTT (Gibco BRL) in a total volume of 20 µl. PCR fragments of the full-length cDNA were prepared with 10 mM Tris-HCl (pH 8.3) containing 50 mM KCl, 1.5 mM MgCl2, 100 µM dNTPs, 20 µM rrVEGF-164 primers and 1 unit Taq polymerase (Promega) in a total volume of 50 µL. The PCR was performed on a Peltier Thermal Cycler (PTC-200; MJ Research and Biozym, Landgraaf, The Netherlands), with a 30 cycles program (95°C for 60s, 65°C for 60s, 72°C for 90s and extension at 72°C for 5 min). The rrVEGF-164 cDNA was isolated from a 2% (w/v) agarose gel and purified with a QIAEX II gel extraction system

(QIAGEN, Hilden, Germany). The SMART-ladder marker (Eurogentec) was used to estimate the sizes of the PCR products.

Construction of expression vector

The purified cDNA was subcloned into the vector pPIC9HV (J.M.H. Raats, Dept. of Biochemical Chemistry, Radboud University Nijmegen Medical Centre, Nijmegen, The Netherlands, unpublished data (pPIC9 expression plasmid was obtained from Invitrogen)) after digestion with *Eco*RI and *Not*I (Invitrogen) in the presence of 1x React® 3 buffer (GibcoBRL) for 1 h at 37°C. The pPIC9HV is similar to the original pPIC9 vector [17,18]), but contains a polyhistidine and VSV-tag for detection and purification. The rrVEGF-164 insert was ligated into pPIC9HV vector DNA using T4 ligase (Gibco BRL) in T4 ligase buffer (Gibco BRL) for 24 h at 16°C.

The host strain *Escherichia coli* (supE44ΔlacU169 (φ80lacZΔM15) hsdR17 recA1 endA1 gyrA96 thi-1 relA1) was transformed with the expression vector by heat-shock (45 s at 42°C). The *E. coli* cells were incubated for 1 h at 37°C in LB-medium. After 1 min of centrifugation at 14000g, the transformed *E. coli* cells were applied to a TYE agar plates and incubated for 24 h at 37°C. The rrVEGF-164 positive transformants were selected by means of ampicillin antibiotic resistance due to the presence of ampicillin resistance gene (AMP) in the *Pichia* expression vector. Ampicillin resistant *E. coli* transformants were selected and suspended in LB-medium. After 24 h incubation at 37°C at 200 rpm in an orbital shaker, the suspension was centrifuged for 1 min at 14000g. Plasmid DNA was isolated using the QIAprep spin miniprep kit (QIAGEN) according to the manufacturer's instructions, and positive transformants were identified by automated sequencing using an α-factor primer (5'-ACTACTATTGCCAGCATTGCTGCT-3') at the DNA Sequencing Facility, Dept. of Human Genetics, Radboud University Nijmegen Medical Centre, The Netherlands.

Transformation into P. pastoris yeast cells

P. pastoris GS115 cells were grown in 100 ml YPD-medium overnight at 30°C at 200 rpm in an orbital shaker, until an OD600 of 1.5 was reached, which corresponds to a cell density of approximately 109 cells/ml. Competent GS115 cells were freshly prepared before transformation by consecutive washings with ice-cold sterile MilliQ water and 1 M sorbitol according to the Invitrogen manual. The DNA was linearised by digesting 10 µg of plasmid DNA with *Sal*I. Subsequently, the linearised DNA was purified using the QIAGEN PCR cleanup kit. To clone the expression vector into the *P. pastoris* yeast cells, cells were resuspended in 1 M sorbitol on ice, and 80 µl of competent cells were electroporated by means of pulse discharges (1.5 kV, 25 µF, 400 Ohm, Bio-Rad Gene Pulser, CA, USA) for 9 ms in the presence of 10 µg linearised plasmid DNA (20 µl). After electroporation, cells were put on ice for 5 min, 10x diluted in 1 M sorbitol and incubated for 1 h at 30°C (without shaking). Cells were spread on YNB dropout plates and incubated at 30°C. The plasmid contains the *His4* gene (encoding histidinol dehydrogenase) which initiates the yeast cell to synthesise histidine (His+). Therefore, only positive transformants can grow on the histidine deficient plates (YNB dropout plates), which can be used for positive clone selection [19]). After 2

days of culturing, the positive transformants were counted, picked, and streaked on new dropout plates. After a 45 h incubation at 30°C, single colonies were picked and cultured in a baffled flask containing 25 ml BMGY-medium for an overnight period at 30°C at 200 rpm in an orbital shaker. To store the cultures, frozen stocks were prepared by adding 60% (v/v) glycerol (0.5 ml) to the *P. pastoris* recombinants in YPD-medium (0.5 ml) and freezing at -80°C.

Expression screening of rrVEGF-164

To analyse the expression levels of the constructed transformants, a small-scale expression screening was performed using a fast induction method with methanol. His+ transformants were picked and added to 15 ml BMGY-medium, and cultured in 200 ml baffled flasks overnight at 30°C, 200 rpm in an orbital shaker. To induce production of rrVEGF-164, cells were centrifuged (1500g, 4°C, for 10 min) and resuspended in BMMY-medium containing 25% (v/v) methanol as the major carbon source. Cells were incubated for 2 days at 30°C, 200 rpm in an orbital shaker. After centrifugation (1500g, 4°C, 10 min), the secreted rrVEGF-164 was concentrated from the supernatant by adding 50 µl heparin-acryl beads (Sigma Chemical Co.) to 1 ml supernatant, and incubation for 1 h at 21°C under rotating conditions. Heparin beads were concentrated by centrifugation (1500g, 4°C, 10 min) and analysed using SDS-PAGE and Western blotting analysis as described below.

Large-scale production of rrVEGF-164

For large-scale rrVEGF-164 production, a 1 L baffled flask with 200 ml YNB-medium was inoculated with 1 ml thawed *P. pastoris* host strain GS115 containing the rrVEGF-164 expression vector. An overnight culture was incubated at 30°C at 200 rpm in an orbital shaker until an OD600 of approximately 6 was reached. The Bioflo® 3000 fermentor (New Brunswick Scientific, Edison, NJ, USA), containing 2 L of basal salts medium, was sterilised by autoclaving for 45 min at 121°C. After autoclaving, 4.35 ml/L PTM1 trace salts (Sigma) were added aseptically to the initial fermentation volume. Ammonium hydroxide (28% (w/v), Sigma) was used as a nitrogen source and to increase the pH during the fermentation process. The 200 ml inoculum was transferred into the fermentor after setting the dissolved oxygen (DO) at 100%, the pH at 6.0 and the temperature at 30°C. Anti-foam solution 289 (Sigma) diluted 1:500 in MilliQ water was used to reduce foam production during fermentation. Yeast cells use oxygen for oxidative metabolism of glycerol. When glycerol is consumed the need for oxygen declines and as a consequence the DO rises. After approximately 24 h of batch culture, the glycerol was completely consumed which was indicated by a sharp rise in DO (up to 70%, see Fig. 4). The 5 h glycerol fed-batch was started by feeding 50% (v/v) glycerol con-taining 12 ml/L PTM1 trace salts with feed rate of 18.15 ml/L/h. After the glycerol was used (DO of ~100%), the methanol feed (100% (v/v) methanol (Labscan) with 12 ml/L PTM1 trace salts) was started to fully induce the AOX1 promoter of the expression system. During the methanol feed, DO decreased rapidly from ~100% to 30% and was continued at 30% for another 30 h. The culture was then harvested and centrifuged (20 min at 5000 g). The supernatant was filtered using a 0.45 µm cellulose acetate membrane filter

(Schleicher and Schuell, Dassel, Germany) and dialysed against 10 mM phosphate buffered saline (pH 7.4).

Purification and identification of rrVEGF-164

For purification of rrVEGF-164, the dialysed supernatant (300 ml) was 1:1 diluted with 10 mM phosphate buffer (PB) containing 0.2 M NaCl and adjusted to pH 7.0 with 1 M Na_2HPO_4. The solution was subjected to fast protein liquid chromatography (FPLC), using a 5 ml heparin-sepharose HiTrap™ column (Amersham Biosciences, Stockholm, Sweden). The rrVEGF-164 was eluted with 1 M NaCl in 10 mM PB (pH 7.0) for 20 min, followed by 2 M NaCl in 10 mM PB (pH 7.0) for 20 min at 2.5 ml/min for both solutions (see Fig. 5). Five fractions (2.5 ml/fraction) with highest A280 absorbance were collected, pooled and directly frozen at -80˚C. Purity and dimer formation were evaluated by sodium dodecyl sulphate poly-acrylamide gel electrophoresis (SDS-PAGE; 15% (w/v); Serva GmbH, Frankfurt, Germany) [20]). Briefly, the supernatant was diluted 1:1 with sample buffer with and without 5% (v/v) β-mercaptoethanol (with and without reducing conditions) and denatured for 5 min at 95˚C. Then 10 µl (~0.6 µg) of denatured rrVEGF-164 was loaded on the gel and was visualised by Coomassie Brilliant Blue (0.1% (w/v)) staining or further identified by Western blotting using goat anti-rat VEGF antibody (1:1000) (R&D Systems) [21]). The amount of purified rrVEGF-164 was determined by a Lowry analysis using bovine serum albumin (BSA) as a standard [22]).

Biological activity of produced rrVEGF-164

Human umbilical vein endothelial cells (HUVECs, ATCC, CRL-1730, Rockville, MD, USA) were grown in F12K medium (Gibco BRL, Carlsbad, CA, USA) with 20% (v/v) foetal calf serum (FCS), 1.5 % (w/v) calf brain extract (as a source for endothelial cell growth factor (ECGF)), 0.14 mg/ml heparin, 200 mM L-glutamine, 100 U/ml penicillin and 100 µg/ml streptomycin (Gibco BRL). After coating the 96-wells plate with 1% (v/v) gelatine, 4000 cells were seeded per well and these were left to attach overnight in the above medium without ECGF. Next, medium was replaced by F12K medium without ECGF and 0-100 ng/ml rrVEGF-164 was added. A cell proliferation assay (WST-1, Roche, Mannheim Germany), based on the reduction of a tetrazolium salt to formazan by mitochondrial dehydrogenases in viable cells, was used to determine the relative number of cells at day 1 and 3 [23]). Proliferation of cells in medium without VEGF was set to 100%. A student's t-test was used for statistical analyses and $p<0.05$ was considered statistically significant.

Results and Discussion

Preparation of rat VEGF-164 cDNA

Total RNA was isolated from embryonic *Rattus norvegicus* tissue and transcribed into cDNA using random hexanucleotide primers. After amplification with VEGF specific primers, PCR products were separated on agarose gel, and three VEGF splice variants (VEGF-188

(564bp), VEGF-164 (492bp) and VEGF-120 (360bp)) could be identified on the basis of their molecular mass (Fig. 1A). The 492bp fragment was extracted from the gel, and reamplified. This fragment and the pPIC9HV vector were cut with *Eco*RI and *Not*I and put on an agarose gel for isolation and for further ligation (Fig. 1B).

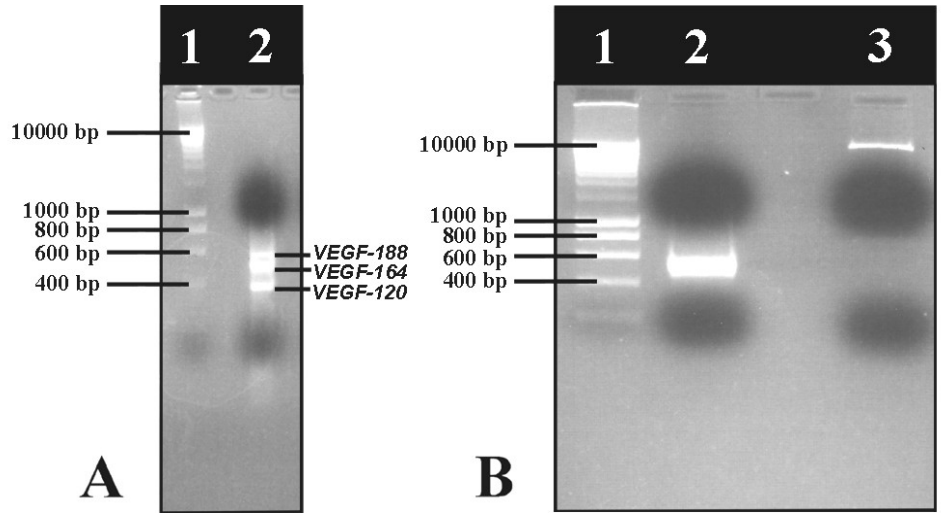

Figure 1. Agarose gel electrophoresis of PCR products. A) ethidium bromide-stained agarose gel shows in lane 1: DNA marker, lane 2: PCR products after amplification using VEGF specific primers, indicating three VEGF splice variants, VEGF-188 (564bp), VEGF-164 (492bp) and VEGF-120 (360bp). B) lane 1: DNA marker, lane 2: the rrVEGF-164 insert (492 bp) and in lane 3 the pPIC9HV vector (8580 bp).

Construction of expression vector

After *Eco*RI and *Not*I digestion, purification and ligation, the resulting pPIC9HV-rrVEGF-164 expression vector (Fig. 2) was transformed into *E. coli*. Positive clones were selected by means of ampicillin resistance. Eight of 64 colonies able to grow on ampicillin plates were sequenced. After verifying the nucleotide sequence of the insert using DNA sequencing (Fig. 3) and a subsequent BLAST search, one colony was found identical with seven rrVEGF-164 sequences published. The nucleotide sequence encoding the rrVEGF-164 (Genbank reference GQ423618) showed a 100% homology with the nucleotide sequence of rrVEGF-164 published by Conn *el al.* 1990 [24]) (Genbank reference AAA41211) and Strausberg *et al.* 2002 [25]) (Genbank reference AAI68708).

Cloning and production of rat VEGF-164

After isolation and linearisation of the plasmid DNA of the positive clone with *Sal*I, the competent *P. pastoris* GS115 cells were transformed with plasmid DNA by means of electroporation. The transformants were cultured in the absence of histidine and 6 colonies were picked and examined for rrVEGF-164 production. Western blot analyses indicated that 4 of the 6 clones produced rrVEGF-164 (data not shown).

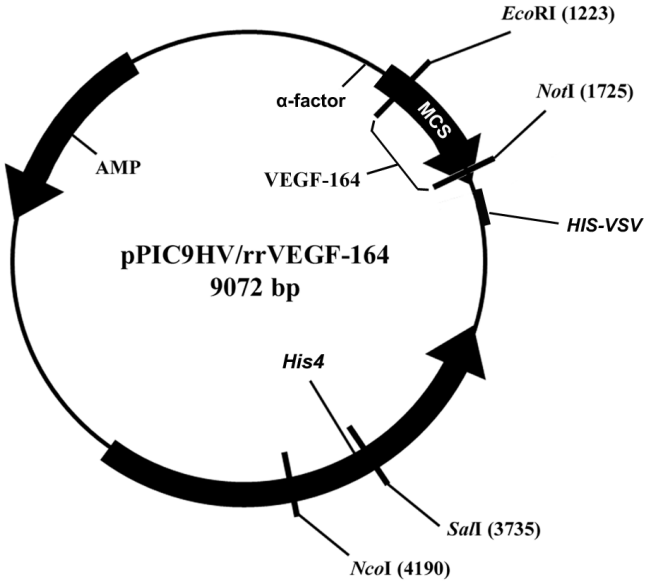

Figure 2. Map of the rrVEGF-164 expression vector based on the pPIC9HV vector. MCS: multiple cloning site. The α-factor directs VEGF to the secretory pathway. *Eco*RI and *Not*I restriction sites were used to insert rVEGF-164 into the multiple cloning site. The ampicillin resistance gene (AMP) was used for *E. coli* transformant selection. The histidine independent gene (*His4*) allows growth in the absence of histidine, and was used for *P. pastoris* transformant selection. The *Sal*I restriction site was used to inactivate the *His4* gene and only a successful ligation results in an intact *His4* gene.

Purification and identification of rrVEGF-164

From the small production screening one clone with a strong band on Western blot was selected and used for large scale production. After the fermentor run, the bulk cell mass was separated from the supernatant and the expressed rrVEGF-164 was purified from the supernatant. Because rrVEGF-164 is a heparin-binding protein, the expressed product was purified with a heparin column. The rrVEGF-164 was present in the 1 M NaCl elution peak (Fig. 5). The rrVEGF-164 content in the pooled peak fractions was ~124 mg/L as determined by Lowry protein assay [22]). Using non-reducing conditions, SDS-PAGE showed one broad band of about 48 kDa (dimer), whereas under reducing conditions a main band of about 24 kDa band (monomer) was observed (Fig. 6A). It was to be expected that on an SDS-PAGE gel dimeric and monomeric rrVEGF-164 migrate at 45 kDa and 23 kDa, respectively [26]). Western blot analysis using an anti rat VEGF-164 antibody further indicated that the protein was rat VEGF-164 (Fig.6B). Under non-reducing conditions, the expressed rrVEGF-164 existed in the biologically active form of a homodimer. Dimers of VEGF are disulphide-bridged, which is essential for the biological activity of VEGF-164 [5]). These data indicate that rrVEGF-164 is produced as a disulphide-bridged dimer which can be purified to near homogeneity by heparin affinity chromatography.

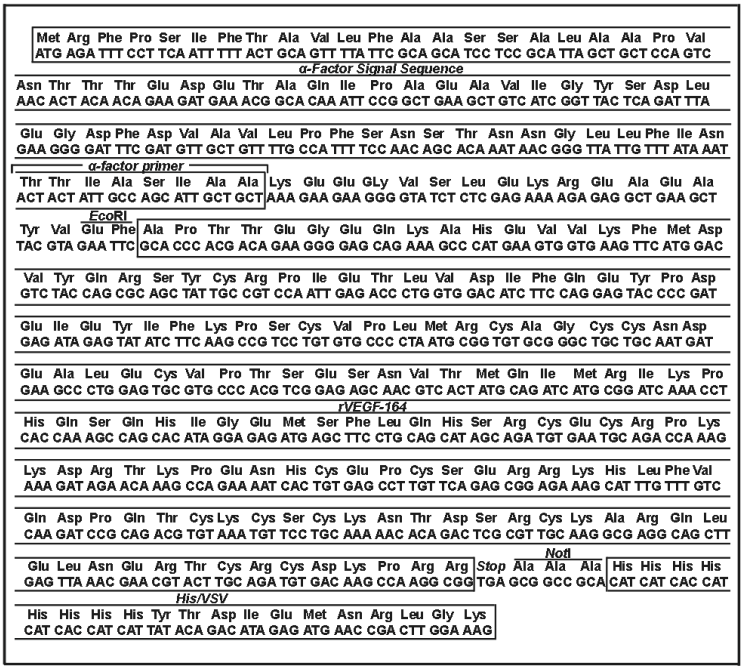

Figure 3. Nucleotide sequence and the deduced amino acid sequence of the relevant part of *P. pastoris* rrVEGF-164 expression vector, indicating α-Factor Signal Sequence, the *Eco*RI restriction site, the rVEGF-164 insert, the *Not*I restriction site and the polyhistidine-VSV tag. A stop codon was positioned between rVEGF-164 and *Not*I in order to produce VEGF without tags. The α-factor signal, the rVEGF-164, and the His/VSV tag are indicated by boxes. The α-factor primer is also indicated.

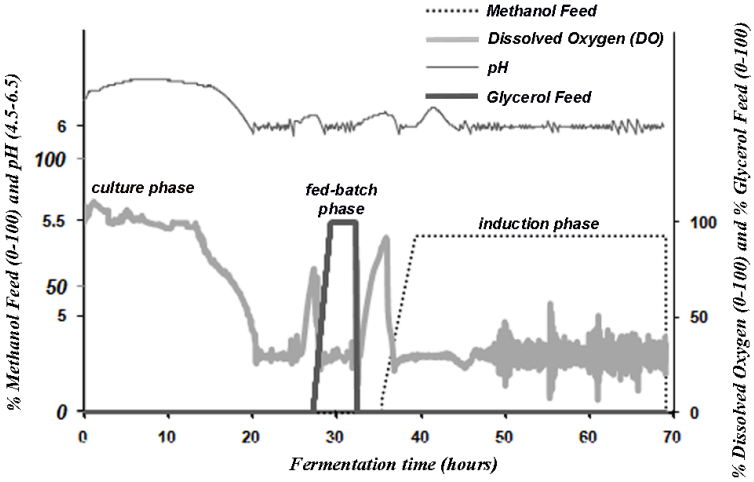

Figure 4. Profile of fermentation process describing the % methanol feed, pH, % dissolved oxygen level and % glycerol feed in time (hours). In the *culture phase* a biomass of yeast cells was formed. In the *fed-batch phase* glycerol was accumulated in the yeast cells as a major carbon source. In the *induction phase* the VEGF-164 production was induced with methanol.

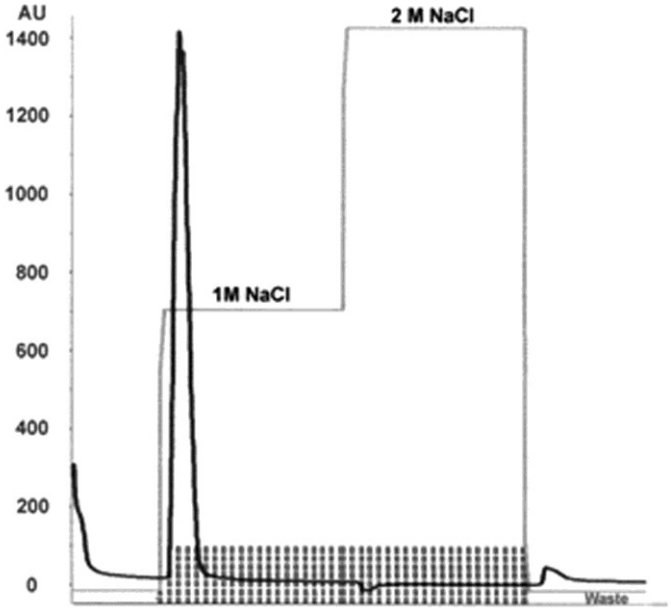

Figure 5. FPLC flow chart of the purification of rrVEGF-164 by heparin affinity chromatography. In green the elution buffers are indicated; viz. 10 mM phosphate buffer (pH 7.0) containing 1M NaCl or 2 M NaCl. The Y-axis indicates absorbance at λ =280 nm expressed in arbitrary units (AU). On the X-axis, the collected fractions (each containing 2 ml) are represented by the vertical dashed lines.

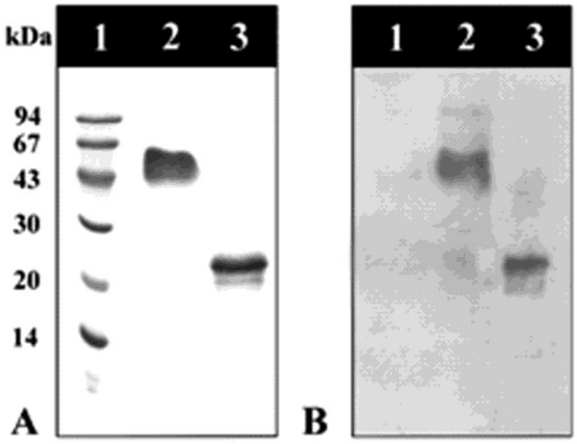

Figure 6. Analysis of produced rrVEGF-164 by SDS-PAGE and Western blot analysis. A) Coomassie Brilliant Blue staining; lane 1: markers; lane 2: rrVEGF-164 under non-reducing conditions (about 48 kDa); lane 3: rrVEGF-164 under reducing conditions (about 24 kDa). B) Western blot analysis of the produced rrVEGF-164; lane 1: markers; lane 2: rrVEGF-164 under non-reducing conditions (about 48 kDa); lane 3: rrVEGF-164 under reducing conditions (about 24 kDa). Figure A and B are both composite images of VEGF-164 monomer and dimer products, taken from separate reducing and non-reducing gels respectively.

Biological activity of produced rrVEGF-164

The biological activity of the purified rrVEGF-164 was determined by a WST-1 proliferation assay using human endothelial cells (HUVECs). HUVECs are generally used to evaluate the activity of VEGF from various species [16,27]). Already after 1 day, the 25 ng/ml content resulted in a three-fold increase in proliferation compared to medium without added VEGF (Fig 7A). After 3 days, the amount of proliferation at content of 12.5-25 ng/ml showed a three to five-fold increase (Fig 7B). We also compared our produced Pichia VEGF with commercial rrVEGF-164 which is produced in a mouse myeloma cell line. At amounts of 12.5-100 ng/ml, the produced rrVEGF-164 showed a significantly higher proliferation than the commercial batch of rrVEGF-164 ($p<0.05$; Fig. 7A and B).

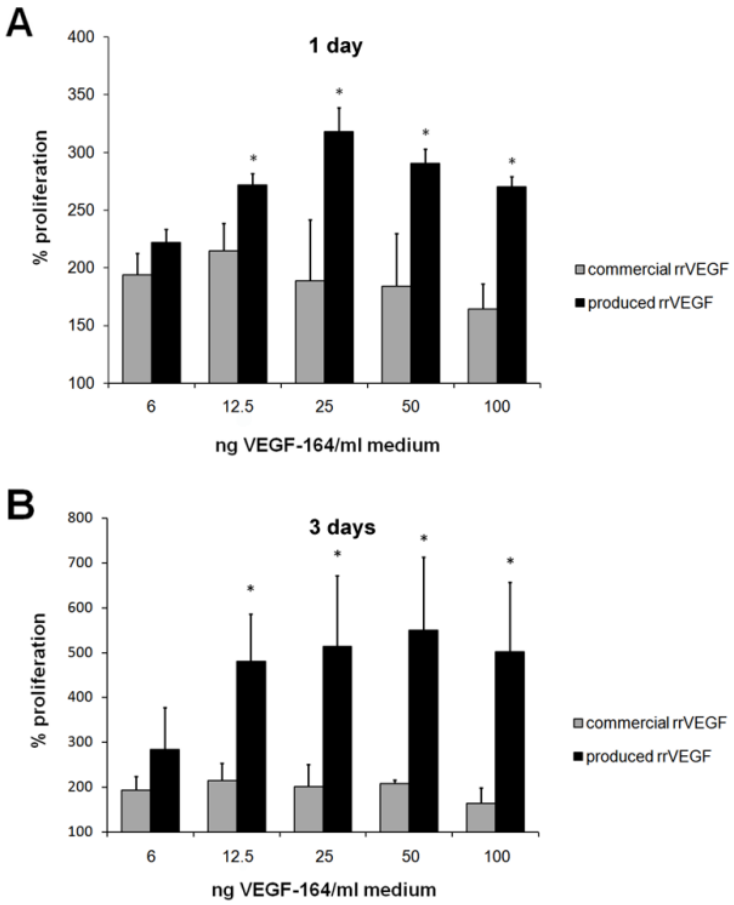

Figure 7. Biological activity of the produced rrVEGF-164 and commercially available rrVEGF-164 analysed using a WST-1 assay. A) Proliferation after 1 day of culture. B) Proliferation after 3 days of culture. The proliferation without added VEGF was set to 100%. Results are mean ± SD for 3 separate experiments. All values were significantly increased compared to the control values. * Indicates $p<0.05$ when comparing produced and commercial rrVEGF-164.

The difference in activity for the commercial VEGF and our Pichia-derived VEGF might be due to the presence of inactive forms as influenced by the production method. Until now, both mouse myeloma cell lines and *E. coli* have been used to produce rrVEGF-164 commercially. The myeloma and *E. coli* production methods can result in heterogeneity of molecules with variable biological activities [28]). Additionally, for *E. coli* the expressed product is present in inclusion bodies and in order to be active the protein must be refolded (dimerised) after purification. For rrVEGF-164 produced in *P. pastoris*, the protein has already been processed, including disulfide-linked dimers, before secretion into the cell medium. This pre-processing can result in a potentially more homogeneous, more highly active population of the product.

Conclusion

In this study, we have cloned and expressed biologically active recombinant rat vascular endothelial growth factor (rrVEGF-164) in the yeast *P. pastoris*. Recombinant rat VEGF-164 was successfully produced as an active dimer in a large quantity. The produced rrVEGF-164 had a higher biological activity than commercially available growth factor (produced in a mouse myeloma cell line). The high level expression of biologically active recombinant rat VEGF-164 provides a useful tool for basic and applied research.

Acknowledgments

This study was financially supported by the Dutch Program for Tissue Engineering (DPTE Grant No. 6735) and EMCM BV, Nijmegen, The Netherlands. We thank Dr. J.M.H. Raats (Dept. of Biochemical Chemistry, Radboud University Nijmegen Medical Centre, Nijmegen, The Netherlands) for providing the pPIC9HV expression vector, Dr. T.F.C.M. Smetsers (Future Diagnostics, Wijchen, The Netherlands) for his support and assistance, and T.J.A.M. van der Velden (Dept. of Paediatric Surgery, Radboud University Nijmegen Medical Centre, Nijmegen, The Netherlands) for providing the calf brain extract.

References

1. Ferrara N. Role of vascular endothelial growth factor in regulation of physiological angiogenesis. AJP - Cell Physiology 2001;280:C1358-C1366.
2. Burchardt T, Burchardt M, Chen MW, Buttyan R, de la TA, Shabsigh A, *et al.* Expression of VEGF splice variants 144/145 and 205/206 in adult male tissues. IUBMB Life 1999;48:405-8.
3. Hara A, Chapin CJ, Ertsey R, Kitterman JA. Changes in fetal lung distension alter expression of vascular endothelial growth factor and its isoforms in developing rat lung. Pediatr Res 2005;58:30-7.
4. Zachary I. Vascular endothelial growth factor. The International Journal of Biochemistry & Cell Biology 1998;30:1169-74.
5. Ferrara N. Molecular and biological properties of vascular endothelial growth factor. Journal of Molecular Medicine 1999;77:527-43.
6. Hoeben A, Landuyt B, Highley MS, Wildiers H, Van Oosterom AT, De Bruijn EA. Vascular Endothelial Growth Factor and Angiogenesis. Pharmacological Reviews 2004;56:549-80.
7. Houck KA, Leung DW, Rowland AM, Winer J, Ferrara N. Dual regulation of vascular endothelial growth factor bioavailability by genetic and proteolytic mechanisms. Journal of Biological Chemistry 1992;267:26031-7.

8. Park JE, Keller GA, Ferrara N. The vascular endothelial growth factor (VEGF) isoforms: differential deposition into the subepithelial extracellular matrix and bioactivity of extracellular matrix-bound VEGF. Mol Biol Cell 1993;4:1317-26.
9. Gitay-Goren H, Cohen T, Tessler S, Soker S, Gengrinovitch S, Rockwell P, *et al.* Selective binding of VEGF121 to one of the three vascular endothelial growth factor receptors of vascular endothelial cells. J Biol Chem 1996;271:5519-23.
10. Gerhardt H, Betsholtz C. Endothelial-pericyte interactions in angiogenesis. Cell and Tissue Research 2003;314:15-23.
11. Nehls V, Schuchardt E, Drenckhahn D. The Effect of Fibroblasts, Vascular Smooth Muscle Cells, and Pericytes on Sprout Formation of Endothelial Cells in a Fibrin Gel Angiogenesis System. Microvascular Research 1994;48:349-63.
12. Pieper JS, Hafmans T, van Wachem PB, van Luyn MJ, Brouwer LA, Veerkamp JH, *et al.* Loading of collagen-heparan sulfate matrices with bFGF promotes angiogenesis and tissue generation in rats. J Biomed Mater Res 2002;62:185-94.
13. Shi BM, Wang XY, Mu QL, Wu TH, Liu HJ, Yang Z. Angiogenesis effect on rat liver after administration of expression vector encoding vascular endothelial growth factor D. World J Gastroenterol 2003;9:312-5.
14. Cregg JM, Cereghino JL, Shi J, Higgins DR. Recombinant protein expression in Pichia pastoris. Mol Biotechnol 2000;16:23-52.
15. Cereghino GPL, Cereghino JL, Ilgen C, Cregg JM. Production of recombinant proteins in fermenter cultures of the yeast Pichia pastoris. Current Opinion in Biotechnology 2002;13:329-32.
16. Ma L, Wang XN, Zhang ZQ, Zhou XM, Zeng GF, Chen AJ. Expression, Purification and Biological Activity Analysis of Human Vascular Endothelial Growth Factor (VEGF(165)) in Pichia pastoris. Sheng Wu Hua Xue Yu Sheng Wu Wu Li Xue Bao (Shanghai) 2001;33:325-30.
17. Yu X, Li Z, Xia X, Fang H, Zhou C, Chen H. Expression and purification of ancrod, an anticoagulant drug, in Pichia pastoris. Protein Expression and Purification 2007;55:257-61.
18. Yan Y, Chen J, Li J. Overexpression of a small medicinal peptide from ginseng in the yeast Pichia pastoris. Protein Expression and Purification 2003;29:161-6.
19. Cregg JM, Barringer KJ, Hessler AY, Madden KR. Pichia pastoris as a host system for transformations. Mol Cell Biol 1985;5:3376-85.
20. Laemmli UK. Cleavage of Structural Proteins during the Assembly of the Head of Bacteriophage T4. Nature 1970;227:680-5.
21. Burnette WN. "Western Blotting": Electrophoretic transfer of proteins from sodium dodecyl sulfate-polyacrylamide gels to unmodified nitrocellulose and radiographic detection with antibody and radioiodinated protein A. Analytical Biochemistry 1981;112:195-203.
22. Lowry OH, Rosebrough NJ, Farr AL, Randall RJ. Protein measurement with the folin phenol reagent. Journal of Biological Chemistry 1951;193:265-75.
23. Hamasaki K, Kogure K, Ohwada K. A biological method for the quantitative measurement of tetrodotoxin (TTX): Tissue culture bioassay in combination with a water-soluble tetrazolium salt. Toxicon 1996;34:490-5.
24. Conn G, Bayne ML, Soderman DD, Kwok PW, Sullivan KA, Plisi TM, *et al.* Amino Acid and cDNA Sequences of a Vascular Endothelial Cell Mitogen that is Homologous to Platelet-Derived Growth Factor. Proceedings of the National Academy of Sciences 1990;87:2628-32.
25. Strausberg RL, Feingold EA, Grouse LH, Derge JG, Klausner RD, Collins FS, *et al.* Generation and initial analysis of more than 15,000 full-length human and mouse cDNA sequences. Proc Natl Acad Sci U S A 2002;99:16899-903.
26. Petersen W, Varoga D, Zantop T, Hassenpflug J, Mentlein R, Pufe T. Cyclic strain influences the expression of the vascular endothelial growth factor (VEGF) and the hypoxia inducible factor 1 alpha (HIF-1alpha) in tendon fibroblasts. J Orthop Res 2004;22:847-53.
27. Ono K, Hattori H, Takeshita S, Kurita A, Ishihara M. Structural features in heparin that interact with VEGF165 and modulate its biological activity. Glycobiology 1999;9:705-11.
28. Siemeister G, Schnurr B, Mohrs K, Schachtele C, Marme D, Martiny-Baron G. Expression of biologically active isoforms of the tumor angiogenesis factor VEGF in Escherichia coli. Biochem Biophys Res Commun 1996;222:249-55.

Chapter 6

Design and *in vivo* evaluation of a molecularly-defined acellular skin construct: reduction of early contraction and increase in early blood vessel formation

Gerwen Lammers[1*]
Suzan T.M. Nillesen[1*]
Ronnie G. Wismans[1]
Magda M. Ulrich[2]
Esther Middelkoop[2]
Paul H. Spauwen[3]
Kaeuis A. Faraj[1]
Joost Schalkwijk[4]
Willeke F. Daamen[1]
Toin H. van Kuppevelt[1]

*These authors contributed equally to this work

[1]Department of Biochemistry, Nijmegen Centre for Molecular Life Sciences, Radboud University Nijmegen Medical Centre, Nijmegen
[2]Association of Dutch Burn Centres, Red Cross Hospital, Beverwijk
[3]Department of Plastic Surgery, Radboud University Nijmegen Medical Centre, Nijmegen
[4]Department of Dermatology, Nijmegen Centre for Molecular Life Sciences, Radboud University Nijmegen Medical Centre, Nijmegen

Acta Biomaterialia
2011 volume 7 issue 3 pages 1063-1071

Abstract

Skin substitutes are of great benefit in the treatment of patients with full-thickness wounds, but there is a need for improvement with respect to wound closure with minimal contraction, early vascularisation, and elastin formation. In this study, we designed and developed an acellular double-layered skin construct, using matrix molecules and growth factors to target specific biological processes. The epidermal layer was prepared using type I collagen, heparin and fibroblast growth factor 7 (FGF7), whereas the porous dermal layer was prepared using type I collagen, solubilised elastin, dermatan sulfate, heparin, fibroblast growth factor 2 (FGF2) and vascular endothelial growth factor (VEGF). The construct was biochemically and morphologically characterised and evaluated *in vivo* using a rat full-thickness wound model. Results were compared with the commercial skin substitute IntegraDRT and untreated wounds. The double-layered construct was prepared according to the design specifications. The epidermal layer was about 40 μm in thickness, containing 9% heparin and 0.2 μg FGF7/mg layer, localised at the periphery. The dermal layer was 2.5 mm thick, had rounded pores, and contained 10% dermatan sulfate + heparin, and 0.7 μg FGF2 + VEGF/mg layer. The double-layered skin construct was implanted in a skin defect and on day 7, 14, 28 and 112, the (remaining) wound area was photographed, excised and (immuno)histologically evaluated. The double-layered skin construct showed more cell influx, significantly less contraction and increased blood vessel formation at early time points in comparison to IntegraDRT and/or the untreated wound. At day 14, the double-layered skin construct also had the least myofibroblasts present. At day 112, the double-layered skin construct contained more elastic fibres than IntegraDRT and the untreated wound. Structures resembling hair follicles and sebaceous glands were found in the double-layered skin construct and the untreated wound, but hardly any were found in IntegraDRT. The results provide new opportunities for the application of acellular skin constructs in the treatment of surgical wounds.

Introduction

Skin substitutes are of major importance to patients whose barrier function is compromised due to trauma, surgical wounds or ulcera. The skin is the major organ involved in thermoregulation and hydration, and acts as a barrier against infection [1]. Human full-thickness defects larger than 4 cm in diameter will not heal well without a graft [2]. Currently, autologous grafts present the most effective treatment modality, but their availability is limited, and the harvest of autologous skin creates new wounds at the donor site. Therefore, intensive research is being conducted to the development of skin substitutes which can be used for immediate wound closure, without the risk of infection, necrosis, tissue hypertrophy and contraction [3,4].

Several skin substitutes have been developed and tested *in vivo*. A number of substitutes obtained FDA approval and are available for clinical use, including Apligraf and IntegraDRT [2]. Apligraf is a cell-based construct consisting of an epidermal layer of human keratinocytes and a dermal layer composed of bovine type I collagen and human fibroblasts [5]. This construct is known to be a safe and effective graft for use in chronic wounds. The cellularity of constructs, however, makes it expensive to produce and difficult to handle [6]. IntegraDRT is an acellular construct composed of a collagen-chondroitin sulfate dermal layer and a silicon top layer. It is easy to handle with off-the-shelf availability, but requires a two stage operation, in which the dermal layer is first allowed to become vascularised [4]. In acellular constructs, angiogenesis, graft take and elastic fibre formation still need to be improved, whereas contraction needs to be reduced [1,2]. In this study, we address these issues using a molecularly-defined construct, prepared from scratch.

Using a subcutaneous implantation model, we have previously shown that a scaffold consisting of type I collagen supplemented with glycosaminoglycans and fibroblast growth factor 2 (FGF2) promotes angiogenesis [7,8]. In addition, we showed that a scaffold consisting of collagen and solubilised elastin enhances angiogenesis and elastic fibre formation [9,10], and that combined addition of two growth factors (FGF2 and vascular endothelial growth factor (VEGF)) reduced the time span to obtain vasculature from a period of 3 weeks to ~7 days [11]. Fournier et al also showed that FGF2 requires additional components like hyaluronic acid to enhance its angiogenic effect [12]. Next to its role in angiogenesis, FGF2 may also reduce wound contraction by inhibiting the phenotypic change of fibroblasts to myofibroblasts, which is likely involved in contraction [13-15]. Heparin is known to stimulate fibroblasts to produce FGF2 [16], influencing angiogenesis and myofibroblast formation. *In vitro*, TGF-β differentiates fibroblasts into myofibroblasts [15]. Lammers *et al.* showed that the extension and method of crosslinking influences the proliferation of keratinocytes [17].

Based on this knowledge, a double-layered skin construct was designed and constructed containing specific factors to stimulate important biological processes in skin regeneration (Fig. 1). The construct consisted of two layers: a collagenous epidermal layer harbouring heparin and FGF7 (which stimulates keratinocyte proliferation), and a porous dermal layer consisting of type I collagen fibrils, solubilised elastin, dermatan sulfate, heparin, FGF2 and VEGF. Both layers were chemically crosslinked using EDC/NHS. This molecularly-

defined construct was characterised and evaluated *in vivo* using a rat full-thickness wound model, suitable to evaluate skin constructs [18,19]. Results were compared with commercial IntegraDRT and untreated wounds.

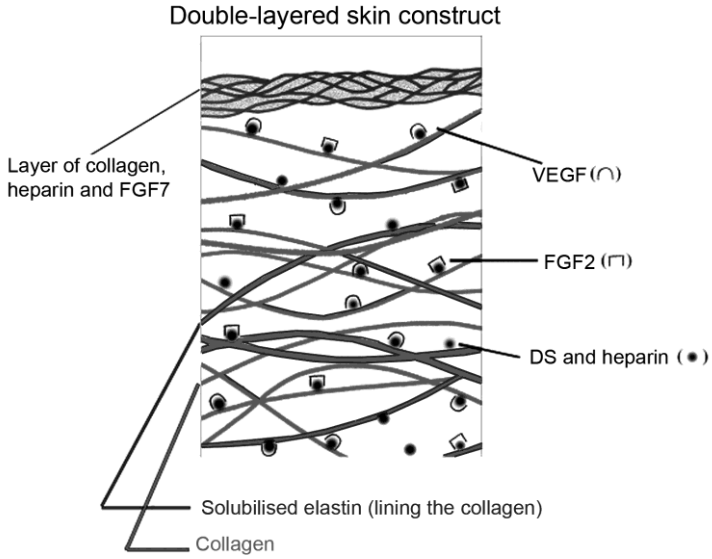

Figure 1 Design and rationale of the double-layered skin construct, consisting of an epidermal (film) layer and a dermal (porous) layer. The epidermal layer contained type I collagen, heparin and recombinant rat FGF7. The dermal layer consisted of type I collagen, solubilised elastin, dermatan sulfate (DS), heparin and the recombinant rat growth factors FGF2 and VEGF. The construct was designed to resemble the architecture of normal skin and to contain specific effector molecules. Heparin was added to the epidermal layer for hydration and growth factor binding, and FGF7 to stimulate keratinocyte migration and proliferation. Solubilised elastin was added to the dermal layer to induce elastic fibre formation, DS and heparin to provide hydration and growth factor binding, VEGF to promote angiogenesis and FGF2 to enhance fibroblast proliferation and angiogenesis, and to decrease myofibroblast formation.

Materials and methods

Materials

Unless stated otherwise, all chemicals were purchased from Merck Chemicals (Darmstadt, Germany). Type I collagen fibrils were purified from bovine achilles tendon as described [20]. Solubilised elastin was prepared from equine ligamentum nuchae as described [9]. Heparin and dermatan sulfate (DS) were purchased from Sigma Chemical Co. (St Louis, MO, USA). Recombinant rat FGF2 was produced in *E. coli* M15 PQE16 [8] and recombinant rat VEGF-164 in *P. pastoris* GS115 [21]. Recombinant rat FGF7 was purchased from QED Biosciences (San Diego, CA, USA). IntegraDRT (Integra® dermal regeneration template) was purchased from Integra Lifesciences Corporation (Plainsboro, NY, USA). Antibodies against bovine type I collagen, bovine elastin (cross-reacting with equine elastin), rat VEGF, rat elastin, rat type I collagen, rat type III collagen, bovine FGF2, human type IV collagen and α-smooth muscle actin (the last three cross-reacting with rat epitopes) were purchased and diluted as described [9,11]. Single chain variable fragment antibodies

against heparin (antibody HS4C3 [22]), DS (antibody GD3A12 [23]) and chondroitin sulfate (CS; antibody IO3H10 [24]) were prepared as described. Goat anti-human FGF7 (cross-reacting with rat FGF7) was purchased from R&D Systems (Minneapolis, MN, USA).

Preparation of the double-layered skin construct

The double-layered skin construct consisted of a dermal and epidermal layer. The dermal layer was prepared by freezing a suspension containing 0.64% (w/v) type I collagen and 0.16% (w/v) solubilised elastin in 0.25 M acetic acid at -20°C [9,25], followed by lyophilising using a Zirbus lyophiliser (Bad Grund, Germany). The resulting scaffold was chemically crosslinked with 33 mM 1-ethyl-3-dimethyl aminopropyl carbodiimide (EDC) and 6 mM N-hydroxysuccinimide (NHS) in the presence of 0.375% (w/v) DS and 0.125% (w/v) heparin for 4 h in 50 mM 2-morpholinoethane sulphonic acid (pH 5.0) containing 40% ethanol, and washed with 0.1 M Na_2HPO_4, 1 M NaCl, 2 M NaCl, and demineralised water [9]. Growth factors were bound to the dermal layer by incubation (1 ml per 8 mg scaffold) in 3.5 µg FGF2/ml and 3.5 µg VEGF/ml phosphate buffered saline (PBS) pH 7.4 for 60 min, followed by 5x15 min washings with PBS.

The epidermal layer was produced by air-drying a 0.8% type I collagen suspension in 0.25 M acetic acid [17], followed by EDC/NHS crosslinking in the presence of 0.5% heparin as described above. The epidermal layer (1 ml solution per 20 mg scaffold) was incubated in 0.5 µg FGF7/ml PBS, followed by 5x15 min washings with PBS.

The wet dermal and epidermal layer were glued to each other using a 0.5% collagen suspension in 0.25 M acetic acid. The total construct was quickly frozen at -80°C and lyophilised.

Characterisation of construct

A number of morphological and biochemical techniques was applied to characterise the double-layered skin construct and commercial IntegraDRT.

The ultrastructure of the constructs was analysed using scanning electron microscopy (SEM) [11].

The extent of crosslinking was estimated by determination of the amount of amine groups, which was analysed using 2,4,6-trinitrobenzene sulphonic acid [26].

The glycosaminoglycan content (dermatan sulfate, chondroitin sulfate and heparin) of the epidermal layer, dermal layer and IntegraDRT, was determined by a hexosamine assay using p-dimethyl-aminobenzoaldehyde [20]. Because the standard curves of heparin and chondroitin sulfate /dermatan sulfate had different slopes, two calibration curves were used. The total glycosaminoglycan content of the dermal layer was calculated by adding the numbers obtained for dermatan sulfate and heparin (in a 3:1 ratio).

The amount of growth factor bound to the epidermal and dermal layer was determined by Western blotting [27] using antibodies against FGF2 (1:2000), VEGF (1:1000) and FGF7 (1:400). Bound antibodies were visualized using peroxidase-conjugated secondary antibodies and a chemiluminescent detection kit (ECL; Amersham Biosciences) and analysed with

Gene Tools software (Syngene, Cambridge, UK). The calibration curves ranged from 0-100 ng growth factor. Scaffolds without growth factors were taken as controls.

The distribution of type I collagen, elastin, dermatan sulfate, chondroitin sulfate, heparin, FGF7, FGF2 and VEGF was determined by an immunofluorescence assay using specific antibodies as described [9,11]. For DS and CS, the secondary antibody was mouse anti-VSV tag (1:5) [22] and the tertiary antibody goat anti-mouse IgG Alexa488 (1:200). For FGF7, the secondary antibody was rabbit anti-goat IgG Alexa488 (1:200). Omission of the primary antibody was taken as a negative control.

Implantation of construct

NIH guidelines for the care and use of laboratory animals (NIH publication 85-23 Rev. 1985) were observed. The study was approved by the Ethics Committee of the Radboud University Nijmegen. Wistar rats (male, 3 months) were purchased from Harlan (Horst, The Netherlands). The rats were housed separately, fed pelleted diet (RMH-B 10 mm) and water *ad libitum*. The rats were anaesthetized with isoflurane.

7 days prior to the operation, the wound area was marked intradermally with 8 dots of tattoo ink (Hauptner, Germany).

Before surgery, analgesia (injection with midazolam, morphine and carprofen) was given. Also postoperative analgesia was given (injections with carprofen for two days, twice a day). Constructs (1.5x1.5 cm) were disinfected in 70% ethanol (3x30 min and one overnight incubation) and washed with sterile PBS (6x60 min). Two full-thickness wounds of 1.5x1.5 cm, including the panniculus carnosus, were made on each side of the back of the rat and the constructs were placed in the wounds. The wounds were treated either with the double-layered skin construct, IntegraDRT or left untreated. The double-layered skin construct and IntegraDRT were placed in the wound in such a way that they fitted exactly and touched the wound edge, without overlap with the wound edge. The constructs were kept in place by 4 resorbable sutures (5-0 Vicryl). The wounds were dressed with a gauze, Tensoplast and Leukoplast. The bandage was applied for 14 days. Each individual rat received two different treatments (double-layered skin construct and/or IntegraDRT and/or no treatment). Per time point, each treatment was applied four times, resulting in a total of 6 rats per time point. After 14 days, the silicon layer of IntegraDRT was removed. At day 7, 14, 28 and 112, the rats were sacrificed and the implants and surrounding tissues were removed. The explants were divided in several parts and processed for conventional histology and immunohistochemistry.

Analysis of contraction

At day 7, 14, 28 and 112, wound contraction was evaluated by determination of the remaining wound area using photographs and a ruler at each time point (n=4). Day 0 was taken as 100% (no wound contraction). Results were represented as mean ± SD. The effect of the different treatments on the size of the wound area was analysed by factorial analysis of variance (ANOVA) followed by a post-hoc test (Duncan's multiple range test) using the Statistica software package (StatSoft, Tulsa, OK, USA).

Processing of explants

Histology: Paraffin sections were cut and stained with haematoxylin-eosin (HE), Elastin von Gieson (EVG) [28] and a Elastic Masson's stain [29]. Phase contrast microscopy was used to study the location and direction of newly-formed collagen fibres. Histology of the explants was evaluated independently by at least two experienced investigators. Sections were scored using a - (not present) to +++ (abundant) scale.

Immunostaining: To study construct degradation, extracellular matrix formation, presence of blood vessels and amount of myofibroblasts, cryosections were stained with specific antibodies. Antibodies against bovine type I collagen, bovine elastin, heparin, dermatan sulfate and chondroitin sulfate were used to evaluate the (remains of) the construct. No major cross-reactivity was found between bovine and rat collagen, and between bovine and rat elastin, and in combination with the size and the position of the collagen fibres and elastin material, the difference between the two species could easily be distinguished. Antibodies against rat type I and type III collagen were used to analyse the presence of rat collagen, an antibody against rat elastin to visualise elastin formation, and an antibody against dermatan sulfate to evaluate glycosaminoglycan production. An anti-type IV collagen antibody was used to visualise blood vessels, and an anti-smooth muscle actin (SMA) antibody to analyse the presence of myofibroblasts and the maturity of blood vessels. Sections were scored using a scale ranging from - (not present) to +++ (abundant).

Results

Characterisation of the constructs

Double-layered skin construct The morphology of the construct was analysed using SEM (Fig. 2A-D). The epidermal top layer was a thin non-porous collagen layer with a thickness of ± 40 µm (Fig. 2A and C, Table 1). The dermal layer was approximately 2.5 mm thick with rounded pores of generally 75-125 µm (Fig. 2A and D, Table 1). The glue layer of collagen had a thickness of 25-30 µm and contained pores of ± 10 µm (Fig. 2B).

Table 1. Pore size and biochemical properties of the implanted constructs.

	Pore size [µm]	Amine group content [nmol/mg scaffold]	Glycosaminoglycan content [µg/mg scaffold]	Growth factor content [µg/mg scaffold]
Epidermal layer	<1	132 ± 16 (56%)	94 ± 10 (hep)	0.2 ± 0.07 (FGF7)
Dermal layer	75-125	154 ± 11 (48%)	103 ± 18 (DS/hep)	0.7 ± 0.3 (FGF2/VEGF)
IntegraDRT #	50-100	164 ± 35	24 ± 4 (CS)	-

measured without the silicon layer

Pore size and biochemical analysis of the epidermal layer, dermal layer and IntegraDRT. The amine group content was determined using 2,4,6-trinitrobenzene sulphonic acid [22], the percentage crosslinking in comparison to non crosslinked scaffold is displayed between brackets. The glycosaminoglycan (heparin, DS and CS) content was determined using p-dimethyl-aminobenzoaldehyde [15]. Non-crosslinked collagen contained 298 ± 57 nmol amine groups/mg scaffold Results are the mean ± SD of 3 independent experiments. Please note that no controls could be taken for the IntegraDRT construct.

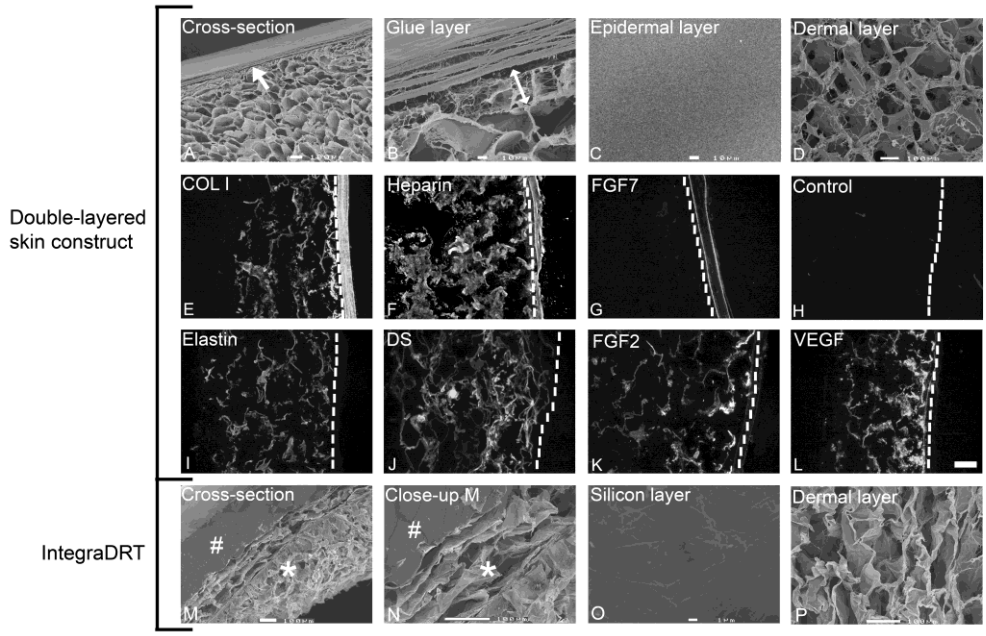

Figure 2 Electron microscopical and immunological evaluation of the double-layered skin construct and IntegraDRT. A-D: Scanning electron micrographs of the double-layered skin construct: (A) cross-section, the arrow indicates the epidermal layer, (B) glue layer, indicated by a double-headed arrow, (C) top of epidermal layer, and (D) dermal layer. E-L: Immunolocalisation of (E) type I collagen, (F) heparin, (G) FGF7, (H) negative control, (I) elastin, (J) dermatan sulfate, (K) FGF2 and (L) VEGF. The epidermal (top) layer is indicated by a dashed line. M-P: Scanning electron micrographs of IntegraDRT: (M) cross-section, (N) close-up of M, (O) top of (silicon) layer and (P) top of dermal layer. In M and N, # indicates the silicon layer and * the dermal collagen layer. Bar is 100 µm in A, D, E-N and P; 10 µm in B and C, and 1 µm in O.

The layers were individually crosslinked with EDC/NHS to covalently bind the glycosaminoglycans (94 µg heparin/mg epidermal layer, 103 µg dermatan sulfate + heparin/mg dermal layer) (Table 1). In the crosslinking process about 50% of the free amine groups were used (Table 1). The amount of growth factor bound to each layer (0.2 µg FGF7/mg epidermal layer and 0.7 µg FGF2 + VEGF/mg dermal layer) was determined by Western Blotting and Gene Tools (Table 1).

The distribution of all components in the construct was visualised using immunostaining (Fig. 2E-L), and was in accordance with the original design (Fig. 1). Both the epidermal and dermal layer contained type I collagen, whereas solubilised elastin was only present in the dermal layer. Heparin was distributed throughout the whole construct, with more intense staining of heparin in the epidermal layer. Dermatan sulfate, FGF2 and VEGF were found distributed throughout the dermal layer, the growth factors showing a more intense staining at the epidermal side. FGF7 was only present at the periphery of the epidermal layer.

IntegraDRT SEM indicated that in commercial IntegraDRT the collagen part was ~750 µm thick with 50-100 µm pores, and that the silicon layer was ~300 µm thick (Fig. 2M-P, Table 1). IntegraDRT is dehydrothermally crosslinked [30]. The analysis of the collagen layer indicated that 1 mg contained about 164 nmol amine groups and about 24 µg chondroitin sulphate (Table 1, note that a control without crosslinking or without chondroitin sulfate was not available). Immunostaining was used to analyse the distribution of type I collagen and CS and both were equally distributed throughout the collagen layer (data not shown).

Evaluation of constructs in full thickness wounds

No infections or illnesses were observed in the rats and they stayed healthy without considerable weight loss. Rats scratched more on IntegraDRT-covered wounds with the silicon layer present. Some rats even removed the layer, indicating that the silicon layer caused irritation. The tattoo ink was used to mark the wound area, but the dots were generally too large and too unequal in size to use for an accurate determination of the remaining wound area.

The double-layered skin construct was constructed from two layers, an epidermal film layer and a porous dermal layer. The two layers were attached to each other by a thin collagen “glue” layer, which firmly attached both layers in such a way that during all procedures (e.g. disinfection and suturing) the construct stayed intact and was easy to handle. During the experiment, we noticed that at day 7 and 14 the epidermal layer was still attached to the dermal layer, but that at later time points, the layer was loosened by epidermal cells that tended to migrate between the two layers.

At day 40, the wounds of all groups were closed (data not shown).

Wound contraction At day 7, a significant difference in wound contraction was found between the double-layered skin construct versus the untreated wound ($p<0.05$). The double-layered skin construct occupied a larger area (90 ± 8% of the original wound area) in comparison to the untreated wound (65 ± 23%). IntegraDRT had 84 ± 16% of the original wound area (Fig. 3B).

At day 14, the double-layered skin construct had significantly less contraction than IntegraDRT and the untreated wound ($p<0.008$ and $p<0.002$ respectively). The double-layered skin construct (80 ± 16%) occupied a larger area than IntegraDRT (47 ± 19%) and the untreated wound (39 ± 22%) (Fig. 3A, B).

At day 28 and 112, the remaining wound areas for all treatments ranged from 12-31% and no major differences were observed between the groups.

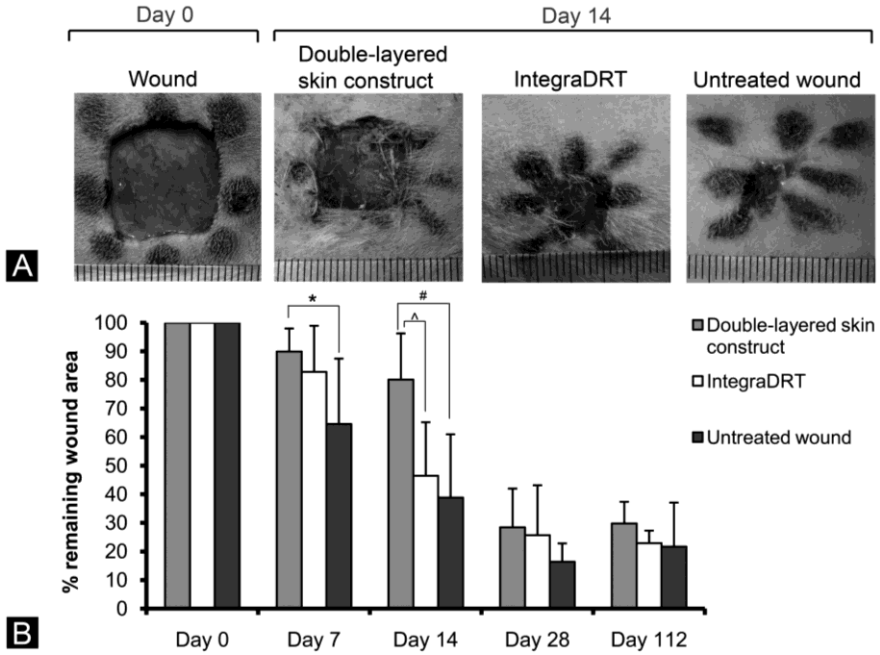

Figure 3 Degree of wound contraction as analysed by the remaining wound area. A) Macroscopical images of the wound area at day 0 and day 14. B) Quantitative data of remaining wound area. Values are mean ± SD (n=4). At day 7, a significant difference was found between the untreated wound versus the double-layered skin construct ($p < 0.05$*). At day 14, the double layered skin construct was found to have significantly less contraction than IntegraDRT and the untreated wound ($p<0.008$^ and $p<0.002$#, respectively).

Table 2. Cellular response in wound area after treatment, compared to normal skin.

	Days after implantation	Granulocytes	Phagocytic cells *	Fibroblasts	Myofibroblasts#
Double-layered skin construct	7	+++	++	++	+[2]
	14	++	++	++	+[1]
	28	+	++	++	++[2]
	112	-	+	++	-
IntegraDRT	7	++	++	++	+[1]
	14	+++	++	++	++[2]
	28	+	++	++	++[1]
	112	-	+	++	-
Untreated wound	7	+	++	++	+[1]
	14	++	++	++	++[2]
	28	+/-	+	++	+
	112	-	+	++	-
Normal skin		-	+/-	++	-

The cells were scored from absent (-) to abundantly present (+++). The absolute numbers of granulocytes are much lower than for phagocytic cells. * Phagocytic cells include macrophages and giant cells. # The myofibroblasts were visualised using an antibody against smooth muscle actin. More myofibroblasts were found at the wound edges, indicated as [1]moderate or [2]abundant.

Microscopical evaluation

Cellular response Table 2 presents a semi-quantitative analysis of cells present in the wound area.

At day 7, little epidermis had been formed in all three groups (data not shown). The double-layered skin construct had the largest number of granulocytes. The numbers of phagocytic cells and fibroblasts were equal for all three groups.

At day 14, partial coverage by epidermal tissue was observed in all three groups. The double-layered skin construct and the untreated wound showed some granulocytes, whereas larger numbers were observed in IntegraDRT. No differences were observed with respect to macrophages and fibroblasts.

At day 28, all groups showed a further coverage, but complete wound closure was not yet seen. Keratinocytes had generally migrated under the epidermal layer of the double layered skin construct, resulting in the release of the dense layer of the construct (as a scab). The double-layered skin construct and IntegraDRT contained more granulocytes and phagocytic cells than the untreated wound. No differences in fibroblasts were found between the three groups.

At day 112, all three groups had a fully developed epidermis, but no rete ridge structures were present in the newly-formed epidermis. The thickness of the epidermis (measured as number of cell-layers) was found to be variable within each group, but no major differences were observed. Granulocytes were absent. Compared to normal skin, slightly more macrophages appeared to be present in the healed area of all three groups (Table 2 and Fig. 4A). Structures resembling hair follicles and sebaceous glands were observed in the double-layered skin construct and the untreated wound, but hardly any were found in IntegraDRT. Most of these structures were located in the vicinity of the wound edges in the newly formed matrix (Fig. 4B-C).

None of the groups showed newly-formed skeletal muscle tissue (replacing the excised panniculus carnosus) at any time point examined.

Myofibroblasts At day 7, the overall score for myofibroblasts was comparable between the treatments (Table 2). Only at the wound edges, the double-layered skin construct had more myofibroblasts present than IntegraDRT and the untreated wound. At day 14, however, the double layered skin construct overall contained less myofibroblasts than IntegraDRT and the untreated wound. At day 28, the untreated wound showed the least myofibroblasts. In general, more myofibroblasts were observed at the wound edges than in the middle of the wound area. No myofibroblasts were observed at day 112 and in normal skin.

Construct components, Collagen: Immunostaining for construct type I collagen showed that at day 7 most of the material of the double-layered skin construct and IntegraDRT was still present (Table 3). At day 14, collagen remnants were found in both the double-layered skin construct and in IntegraDRT, whereas at day 28, only few collagen remnants were observed. At day 112, no scaffold collagen could be observed.

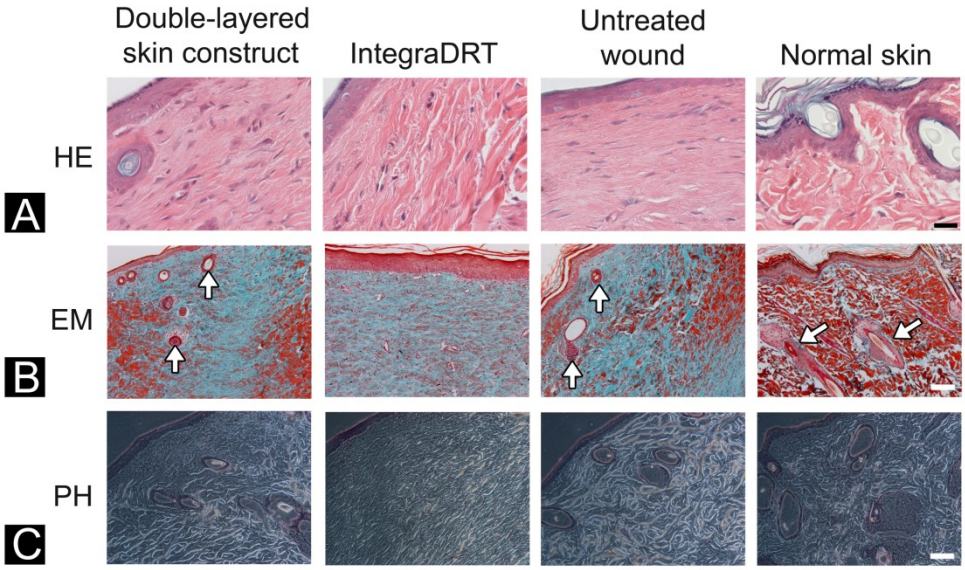

Figure 4 Histological images of the centre of the wound area at day 112. A) Haematoxylin & eosin staining (HE), B) Elastic Masson's staining (EM), C) phase-contrast (PH) of the double-layered skin construct, IntegraDRT and untreated wound compared to normal skin. A: a closed epidermis was present in all cases and no differences were found in the number of cell layers. Rete ridge structures were absent. The dermis of the double-layered skin construct, IntegraDRT and the untreated wound showed higher numbers of cells than the normal skin (nuclei of the cells are stained in blue). B) In the double-layered skin construct and the untreated wound, hair follicle-like and gland-like structures (arrows) were observed (also visible in C). Mature collagen fibres stain red, whereas the newly formed fibres are light blue. C) Phase contrast microscopy revealed that collagen fibres were more randomly oriented in the double-layered skin construct and untreated wound than in IntegraDRT. Bar in A is 25 µm, bar in B and C is 100 µm.

Table 3. Overview of immunostaining for matrix molecules in wound area after treatment, compared to normal skin.

		Construct		Newly-formed matrix components			
	Days after implantation	Type I collagen	Elastin	Type I collagen	Type III collagen	Elastin	Dermatan sulfate
Double-layered skin construct	7	++	+	+	++	+/-	++
	14	+	+	++	++	+	++
	28	+/-	-	++	++	+	+++
	112	-	-	+++	++	+++	++
IntegraDRT	7	++	-	+/-	+	-	+
	14	+	-	+	++	+/-	+
	28	+/-	-	++	++	+/-	+
	112	-	-	+++	++	++	++
Untreated wound	7	-	-	+	+	+	++
	14	-	-	++	++	+	++
	28	-	-	+++	++	++	++
	112	-	-	+++	++	++	+++
Normal skin		-	-	+++	+	++	+++

The sections were scored from absent (-) to abundantly present (+++)

Elastin: At day 7 and 14, the elastin staining of the double-layered skin construct showed small fragments, indicating degradation of the scaffold elastin. No scaffold bound elastin staining was seen at days 28 and 112.

Glycosaminoglycans: At day 7 and 14, heparin was mainly visible in the epidermal layer of the double-layered skin construct, whereas dermatan sulfate was only found on the collagen fibrils of the dermal layer (data not shown). At day 28, hardly any staining was observed of construct glycosaminoglycan remnants. IntegraDRT showed staining for chondroitin sulfate on the collagen fibrils at day 7 and 14.

Newly-formed extracellular matrix components The presence of rat extracellular matrix components is summarized in Table 3. Using immunostaining, it was shown that the normal skin contained randomly oriented type I collagen fibres, a small amount of type III collagen, a moderate amount of elastic fibres at the top of the dermal layer, and an ample amount of DS scattered throughout the dermis.

Type I collagen: The amount of rat type I collagen increased with time, being abundant for all three groups at day 112. At day 7 and 14, the double-layered skin construct and the untreated wound contained more type I collagen than IntegraDRT, whereas at day 28, the untreated wound contained most type I collagen. Phase contrast microscopy was used to analyse the location and orientation of newly-formed collagen bundles at day 112. The double-layered skin construct and the untreated wound had a more randomly oriented collagen deposition, whereas the collagen bundles in IntegraDRT were found to be more aligned (Fig. 4C). When comparing the results of the treatments with normal skin, the double-layered skin construct and the untreated wound resembled the normal skin at day 112 more closely than IntegraDRT.

Type III collagen: At day 7, the double-layered skin construct contained a moderate amount of rat type III collagen, whereas IntegraDRT and the untreated wound contained less. From day 14 on, a moderate amount was found in all three groups.

Elastin: The amount of elastic fibres increased with time, being most abundant in the double-layered skin construct at day 112 (Fig. 5). At day 7, 14 and 28, IntegraDRT contained the least elastic fibres, while the untreated wound had the same or more elastic fibres than the double-layered skin construct.

At day 7, 14 and 28, the least dermatan sulfate was found in IntegraDRT. At day 28, the double-layered skin construct contained most dermatan sulfate, whereas at day 112, the untreated wound contained most dermatan sulfate, similar to normal skin.

Blood vessels At day 7 and 14, the double-layered skin construct and the untreated wound contained more blood vessels than IntegraDRT (Fig. 6). The blood vessels already invaded the double-layered skin construct at day 7, whereas hardly any blood vessels were found inside the collagen layer of IntegraDRT. At day 28, the double-layered skin construct still had many blood vessels present, whereas the untreated wound and IntegraDRT contained a moderate amount. The blood vessels were evenly distributed throughout the wound

area. At day 112, all groups had moderate amounts of blood vessels present in the wound area. These were smaller, but more abundant than in normal skin.

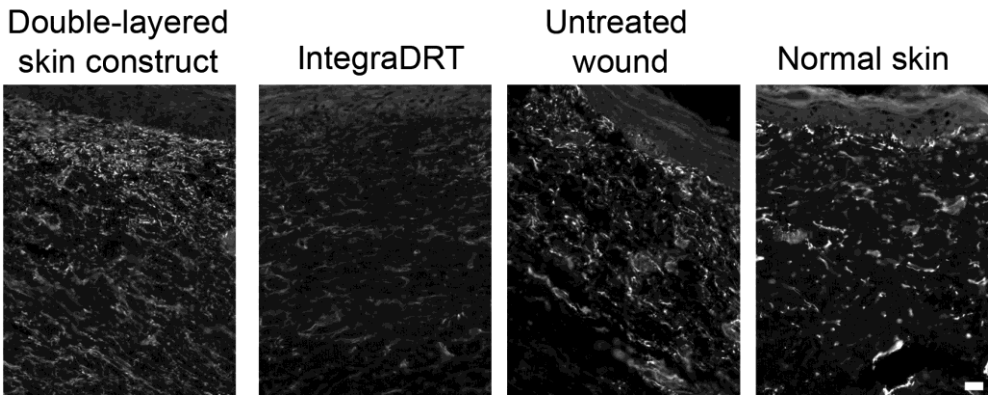

Figure 5 Immunohistochemical evaluation of newly formed elastin at day 112, analysed using an antibody for elastin. The double-layered skin construct showed elastin around blood vessels and hair follicle-like structures, and a large amount of elastic fibres throughout the upper dermis. IntegraDRT and the untreated wound contained a moderate amount of elastic fibres that were mainly located in the upper part of the dermis. The untreated wound also showed elastic fibres surrounding hair follicle-like structures. Normal skin showed elastic fibres around blood vessels and hair follicles in the dermis. Bar is 25 µm.

Discussion

In this study, an acellular double-layered skin construct was prepared from purified components, according to a pre-defined design. The biological components and their location were chosen to reflect the skin's extracellular environment. Growth factors were positioned in such a way to locally exert their activity, e.g. FGF7 at the periphery of the flat epidermal layer, and FGF2 and VEGF throughout the porous dermal layer. The double-layered skin construct was developed to accelerate and improve wound healing. In the clinic, acellular constructs may be preferred over cellular constructs for their ease of handling, transport and storage.

The performance of the double-layered skin construct was compared to IntegraDRT and to an untreated wound (no skin construct). The double-layered construct had significantly less contraction at the first two time points (day 7 and 14) compared to the untreated wound, and at day 14, compared to IntegraDRT. At later points, no significant differences were found. The number of smooth muscle actin-positive myofibroblasts, likely involved in wound contraction [14], was also the least in the double layered construct at day 14. This suggests an inhibition of the differentiation of fibroblasts to myofibroblasts by the construct. FGF2 is known to inhibit myofibroblast formation and promote a fibroblast phenotype [31]. The FGF2 present in the double-layered skin construct may have been instrumental in diminishing the amount of myofibroblasts present on day 14. The fibroblasts are involved in the production of extracellular matrix (for instance collagens, elastin), and growth factors, and play a crucial role in regulating the skin physiology [32]. Boehnke *et al.* described an equivalent consisting

of fibroblasts in a 3-D scaffold; they showed the importance of the interaction between fibroblasts and keratinocytes for the proliferation, regeneration and organogenesis of a skin equivalent [33]. The double-layered skin construct contained FGF2 to increase fibroblast proliferation in order to enhance wound repair and regeneration. However, no differences were observed in the amount of fibroblasts in the wound, suggesting that the FGF2 was more involved in angiogenesis and inhibition of myofibroblast formation.

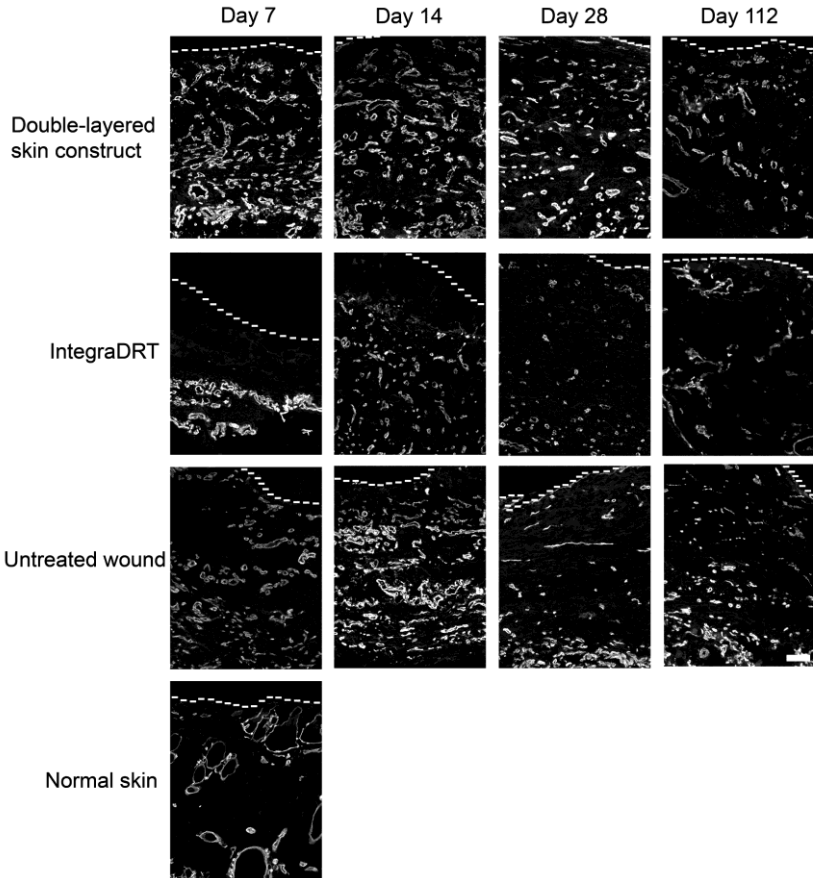

Figure 6 Presence of blood vessels in the wound area as visualised using an antibody against type IV collagen. The top of the dermis/epidermal layer is indicated by a dashed line. In the double-layered skin construct and untreated wound, more blood vessels were present on day 7 and 14, and they had penetrated more towards the epidermis in comparison to IntegraDRT. On day 28, the double-layered skin construct possessed more blood vessels than IntegraDRT and the untreated wound. On day 112, all treatments showed a similar number of blood vessels, more abundant and with a smaller diameter compared to normal skin. Bar is 100 µm.

In addition, the random orientation of the pores in the construct may have prevented the remaining myofibroblasts from contracting the wound area. When cells are randomly bound to the scaffold the sum of the contracting forces is near zero [34]. However, at day 28 more

myofibroblasts were found than at day 14 in the double-layered skin construct. FGF2 has a short life span which is increased by binding to heparin [35], but after 28 days most of the construct was degraded, and a lack of FGF2 may eventually have revoked the active inhibition of differentiation into myofibroblasts. Fournier *et al.* determined that a fibrin gel with hyaluronic acid and FGF2 gave burst release *in vivo* [12]. A more sustained release of FGF2 may reduce the degree of contraction for a longer period of time. The decrease in mechanical properties of the construct, due to degradation, may have added to this effect.

The addition of effector molecules to a scaffold generally results in an increased early infiltration of cells [8,11]. Indeed, at day 7, the double-layered skin construct showed more influx of e.g. granulocytes compared to IntegraDRT and the untreated wound (however, at day 14, IntegraDRT showed more granulocyte influx). For good and rapid wound healing, infiltration of cells is necessary in order to boost the wound healing process. Cytokines that are produced by the infiltrating cells promote angiogenesis, extracellular matrix production and remodelling [36,37]. Currently used acellular scaffolds such as IntegraDRT lack growth factors, but our study suggests that growth factors may be necessary to induce early angiogenesis and extracellular matrix production.

In commercially available acellular skin substitutes, it takes several weeks to develop a well-developed vasculature. This results in impaired wound healing, due to a lack of oxygen, nutrients and the presence of waste products [38]. Angiogenesis can be promoted by the incorporation of glycosaminoglycans or solubilised elastin to a scaffold, as we have previously shown in a subcutaneous implantation model in rat [8,9]. In addition, the combination of two growth factors (FGF2 and VEGF) in an acellular collagen-heparin scaffold induced a mature vasculature already at day 7 [11]. In the double-layered skin construct, many blood vessels were found on day 7, in contrast to IntegraDRT which did not develop a similar amount of blood vessels on any of the time-points examined. Moiemen *et al.* found that IntegraDRT was only fully vascularised after 4 weeks in humans [39]. This is in line with our findings that it took until day 28 before the newly-formed vasculature in IntegraDRT had reached the top of construct. The addition of growth factors in an acellular construct may thus greatly improve angiogenesis.

The orientation of collagen fibres in normal skin has a basket weave pattern, whereas in scars the fibres are very much aligned in a parallel way [40]. We and others have seen that the micro architecture of the original scaffold influences the orientation of newly-formed collagen fibrils [41,42]. In the double-layered skin construct, the dermal layer had large randomly oriented pores to allow random collagen deposition, which indeed occurred, as indicated by phase contrast microscopy.

An interesting feature was the presence of structures resembling hair follicles and sebaceous glands in the double-layered skin construct and untreated wound at day 112. These structures were mainly found at the outer region of the healed wound, though some were found in the centre. The group of Ito *et al.* demonstrated that in adult mice, *de novo* hair follicle formation was found after an excision of 1 cm^2 full-thickness back skin [43]. Growth factors (e.g. epidermal growth factor and FGF) are involved in hair follicle sebaceous gland development [44]. Therefore, there is a possibility that some of the hair follicles and glands

observed were generated de novo, although most of the structures are likely derived from adjacent healthy tissue. Further research will establish whether the addition of (a combination of) growth factors to an engineered skin construct can indeed induce hair follicle formation.

Conclusion

A double-layered skin construct was designed, developed and evaluated in a rat full-thickness wound model. The construct contained positioned growth factors and resulted in a reduction of contraction and an increase in angiogenesis in the early phase of skin regeneration.

Acknowledgements

Paul Jap is greatly appreciated for his valuable histological advices. The SPF unit of the Central Animal Facility is appreciated for their assistance during the animal experiment. This study was financially supported by the Dutch Program for Tissue Engineering (DPTE 6735).

References

1. Butler CE, Orgill DP. Simultaneous *in vivo* regeneration of neodermis, epidermis, and basement membrane. Adv Biochem Eng Biotechnol 2005;94:23-41.
2. MacNeil S. Progress and opportunities for tissue-engineered skin. Nature 2007;445:874-80.
3. Lee KH. Tissue-engineered human living skin substitutes: development and clinical application. Yonsei Med J 2000;41:774-9.
4. Ruszczak Z. Effect of collagen matrices on dermal wound healing. Adv Drug Deliv Rev 2003;55:1595-611.
5. Curran MP, Plosker GL. Bilayered bioengineered skin substitute (Apligraf): a review of its use in the treatment of venous leg ulcers and diabetic foot ulcers. BioDrugs 2002;16:439-55.
6. Zaulyanov L, Kirsner RS. A review of a bi-layered living cell treatment (Apligraf) in the treatment of venous leg ulcers and diabetic foot ulcers. Clin Interv Aging 2007;2:93-8.
7. Pieper JS, van Wachem PB, van Luyn MJA, Brouwer LA, Hafmans T, Veerkamp JH, *et al.* Attachment of glycosaminoglycans to collagenous matrices modulates the tissue response in rats. Biomaterials 2000;21:1689-99.
8. Pieper JS, Hafmans T, van Wachem PB, van Luyn MJ, Brouwer LA, Veerkamp JH, *et al.* Loading of collagen-heparan sulfate matrices with bFGF promotes angiogenesis and tissue generation in rats. J Biomed Mater Res 2002;62:185-94.
9. Daamen WF, Nillesen ST, Wismans RG, Reinhardt DP, Hafmans T, Veerkamp JH, *et al.* A biomaterial composed of collagen and solubilized elastin enhances angiogenesis and elastic fiber formation without calcification. Tissue Eng Part A 2008;14:349-60.
10. Daamen WF, Nillesen ST, Hafmans T, Veerkamp JH, van Luyn MJ, Van Kuppevelt TH. Tissue response of defined collagen-elastin scaffolds in young and adult rats with special attention to calcification. Biomaterials 2005;26:81-92.
11. Nillesen ST, Geutjes PJ, Wismans R, Schalkwijk J, Daamen WF, Van Kuppevelt TH. Increased angiogenesis and blood vessel maturation in acellular collagen-heparin scaffolds containing both FGF2 and VEGF. Biomaterials 2007;28:1123-31.
12. Fournier N, Doillon CJ. Biological molecule-impregnated polyester: an *in vivo* angiogenesis study. Biomaterials 1996;17:1659-65.
13. Jansen RG, Van Kuppevelt TH, Daamen WF, Kuijpers-Jagtman AM, Von den Hoff JW. FGF-2-loaded collagen scaffolds attract cells and blood vessels in rat oral mucosa. J Oral Pathol Med 2009;38:630-8.
14. Shin D, Minn KW. The effect of myofibroblast on contracture of hypertrophic scar. Plast Reconstr Surg 2004;113:633-40.
15. Khouw IM, van Wachem PB, Plantinga JA, Vujaskovic Z, Wissink MJ, de Leij LF, *et al.* TGF-beta and bFGF affect the differentiation of proliferating porcine fibroblasts into myofibroblasts *in vitro*. Biomaterials 1999;20:1815-22.
16. Carroll LA, Koch RJ. Heparin stimulates production of bFGF and TGF-beta 1 by human normal, keloid, and fetal dermal fibroblasts. Med Sci Monit 2003;9:BR97-108.

17. Lammers G, Tjabringa GS, Schalkwijk J, Daamen WF, Van Kuppevelt TH. A molecularly defined array based on native fibrillar collagen for the assessment of skin tissue engineering biomaterials. Biomaterials 2009;30:6213-20.
18. Ng KW, Hutmacher DW. Reduced contraction of skin equivalent engineered using cell sheets cultured in 3D matrices. Biomaterials 2006;27:4591-8.
19. Soejima K, Chen X, Nozaki M, Hori K, Sakurai H, Takeuchi M. Novel application method of artificial dermis: one-step grafting procedure of artificial dermis and skin, rat experimental study. Burns 2006;32:312-8.
20. Pieper JS, Oosterhof A, Dijkstra PJ, Veerkamp JH, Van Kuppevelt TH. Preparation and characterization of porous crosslinked collagenous matrices containing bioavailable chondroitin sulphate. Biomaterials 1999;20:847-58.
21. Geutjes PJ, Nillesen ST, Lammers G, Daamen WF, Van Kuppevelt TH. Cloning, large-scale production, and purification of active dimeric rat vascular endothelial growth factor (rrVEGF-164). Protein Expr Purif 2010;69:76-82.
22. Van Kuppevelt TH, Dennissen MA, van Venrooij WJ, Hoet RM, Veerkamp JH. Generation and application of type-specific anti-heparan sulfate antibodies using phage display technology. Further evidence for heparan sulfate heterogeneity in the kidney. J Biol Chem 1998;273:12960-6.
23. ten Dam GB, Yamada S, Kobayashi F, Purushothaman A, van de Westerlo EM, Bulten J, *et al.* Dermatan sulfate domains defined by the novel antibody GD3A12, in normal tissues and ovarian adenocarcinomas. Histochem Cell Biol 2009;132:117-27.
24. Smetsers TF, van de Westerlo EM, ten Dam GB, Overes IM, Schalkwijk J, van Muijen GN, *et al.* Human single-chain antibodies reactive with native chondroitin sulfate detect chondroitin sulfate alterations in melanoma and psoriasis. J Invest Dermatol 2004;122:707-16.
25. Pieper JS, Hafmans T, Veerkamp JH, Van Kuppevelt TH. Development of tailor-made collagen-glycosaminoglycan matrices: EDC/NHS crosslinking, and ultrastructural aspects. Biomaterials 2000;21:581-93.
26. Olde Damink LH, Dijkstra PJ, van Luyn MJ, van Wachem PB, Nieuwenhuis P, Feijen J. Cross-linking of dermal sheep collagen using a water-soluble carbodiimide. Biomaterials 1996;17:765-73.
27. Burnette WN. "Western blotting": electrophoretic transfer of proteins from sodium dodecyl sulfate--polyacrylamide gels to unmodified nitrocellulose and radiographic detection with antibody and radioiodinated protein A. Anal Biochem 1981;112:195-203.
28. Bancroft JD, Stoeltzing O. Theory and practice of histological techniques. Edinburgh, UK: Churchill Livingston, 1990.
29. O'Connor WN, Valle S. A combination Verhoeff's elastic and Masson's trichrome stain for routine histology. Stain Technol 1982;57:207-10.
30. Yannas IV, Burke JF, Gordon PL, Huang C, Rubenstein RH. Design of an artificial skin. II. Control of chemical composition. J Biomed Mater Res 1980;14:107-32.
31. Spyrou GE, Naylor IL. The effect of basic fibroblast growth factor on scarring. Br J Plast Surg 2002;55:275-82.
32. Lee DY, Lee JH, Yang JM, Lee ES, Park KH, Mun GH. A new dermal equivalent: the use of dermal fibroblast culture alone without exogenous materials. J Dermatol Sci 2006;43:95-104.
33. Boehnke K, Mirancea N, Pavesio A, Fusenig NE, Boukamp P, Stark HJ. Effects of fibroblasts and microenvironment on epidermal regeneration and tissue function in long-term skin equivalents. Eur J Cell Biol 2007;86:731-46.
34. Yannas IV. Similarities and differences between induced organ regeneration in adults and early foetal regeneration. J R Soc Interface 2005;2:403-17.
35. Ornitz DM, Itoh N. Fibroblast growth factors. Genome Biol 2001;2:REVIEWS3005.
36. Kibe Y, Takenaka H, Kishimoto S. Spatial and temporal expression of basic fibroblast growth factor protein during wound healing of rat skin. Br J Dermatol 2000;143:720-7.
37. Li J, Zhang YP, Kirsner RS. Angiogenesis in wound repair: angiogenic growth factors and the extracellular matrix. Microsc Res Tech 2003;60:107-14.
38. Patel ZS, Mikos AG. Angiogenesis with biomaterial-based drug- and cell-delivery systems. J Biomater Sci Polym Ed 2004;15:701-26.
39. Moiemen NS, Vlachou E, Staiano JJ, Thawy Y, Frame JD. Reconstructive surgery with Integra dermal regeneration template: histologic study, clinical evaluation, and current practice. Plast Reconstr Surg 2006;117:160S-74S.
40. Knapp TR, Daniels RJ, Kaplan EN. Pathologic scar formation. Morphologic and biochemical correlates. Am J Pathol 1977;86:47-69.
41. Faraj KA, Van Kuppevelt TH, Daamen WF. Construction of collagen scaffolds that mimic the three-dimensional architecture of specific tissues. Tissue Eng 2007;13:2387-94.
42. Wang JH, Jia F, Gilbert TW, Woo SL. Cell orientation determines the alignment of cell-produced collagenous matrix. J Biomech 2003;36:97-102.
43. Ito M, Yang Z, Andl T, Cui C, Kim N, Millar SE, *et al.* Wnt-dependent de novo hair follicle regeneration in adult mouse skin after wounding. Nature 2007;447:316-20.
44. Moore GP, du Cros DL, Isaacs K, Pisansarakit P, Wynn PC. Hair growth induction: roles of growth factors. Ann N Y Acad Sci 1991;642:308-25.

Chapter 7

High density gene expression microarrays and gene ontology analysis for identifying processes in implanted tissue engineering constructs

Gerwen Lammers[1]
Christian F.H.A. Gilissen[2]
Suzan T.M. Nillesen[1]
Peter J.E. Uijtdewilligen[1]
Ronnie G. Wismans[1]
Joris A. Veltman[2]
Willeke F. Daamen[1]
Toin H. van Kuppevelt[1]

[1]Department of Biochemistry, Nijmegen Centre for Molecular Life Sciences, Radboud University Nijmegen Medical Centre, Nijmegen
[2]Department of Human Genetics, Nijmegen Centre for Molecular Life Sciences, Radboud University Nijmegen Medical Centre, Nijmegen

Biomaterials
2010 volume 31 issue 32 pages 8299-8312

Abstract

The *in vivo* performance of tissue-engineered constructs is often based on generally accepted read-out parameters, like (immuno)histology. In this study, high-density gene expression microarrays and gene ontology (GO) analysis were used as a read-out tool to identify the biological processes occurring after implantation of an acellular collagen-based skin construct using a rat full-thickness wound model. A freely-available program (DAVID) was used to identify up/downregulated biological processes (GO-terms) and results were compared to wound healing/regeneration without a construct. The entire process from RNA isolation to biological interpretation is explained step-by-step. Conventional (immuno)histology was used to validate the biological processes identified and indicate that microarray analysis may provide a valuable, fast and unbiased tool to evaluate the *in vivo* performance of tissue-engineered constructs. However, challenges remain e.g. with regards to the development of specific GO-terms and annotation of the (rat) genome.

Introduction

The general aim of regenerative medicine is to restore organs after they have been damaged or lost. One approach to reach this goal is to implant a suitable scaffold at the site of injury, often combined with the appropriate cells [1]. Worldwide, numerous research groups and companies are developing new or improved scaffolds, that are extensively studied both *in vitro* and *in vivo* [2-4]. In most cases, *in vivo* evaluation is based on generally accepted read-out parameters, like transplant 'take', organ-specific functionality and (immuno)histology.

In order to further understand the observed process of regeneration, it is important to identify biological processes that take place in tissue-engineered constructs. The information thus obtained may provide clues for improvements e.g. in scaffold design. Currently, histological evaluation is one of the main methodologies to identify these processes. It is generally accepted, relatively easy to perform, and most laboratories have access to the required equipment. In addition, extensive histological data is available, facilitating the interpretation of novel data. However, histology comes with a number of drawbacks including the subjectivity of the scoring process, the expertise required to link histological observations to biological processes, the use of relatively small tissue samples (with the risk of missing important data), and the time-consuming nature of the process. In addition, in the case of immunohistochemistry, optimisation of the staining procedure for each individual antibody is required, and the high cost of individual antibodies (usually €200-400 per antibody of <500 µg) may limit the number of biomolecules analysed.

Gene expression microarrays may bypass some of these drawbacks. Using high density microarrays, virtually all known (and yet unknown) genes can be analysed in a single experiment. Sophisticated and user-friendly software to analyse the large amount of data is becoming available, and the knowledge on array analysis and biological interpretation is rapidly expanding, allowing objective high-throughput analysis. The technique requires no more than five days from RNA isolation to the identification of biological processes, and the computerised workflow enables an objective, unbiased analysis. Costs of the arrays (currently approximately €100-500 per array, depending on e.g. complexity) are dropping, and the same goes for the advanced equipment required to run a microarray experiment, the equipment generally being available at microarray core facilities. The genome of a growing number of species has been sequenced, and arrays have been developed for laboratory animals often used in tissue engineering research, including rat and pig [5].

In this paper we used a high-density microarray-based approach to identify biological processes up/downregulated *in vivo* in a double-layered skin construct applied in a rat full-thickness wound model studying at various time points after implantation. Results were compared to wound healing without construct, and a freely-available program (DAVID) was used for data analysis. The entire process from RNA isolation to biological interpretation is explained step-by-step and the identified processes are compared with observations using conventional immunohistology.

Materials and Methods

A schematic overview of the whole procedure from tissue sampling to the identification of biological processes is given in Fig. 1.

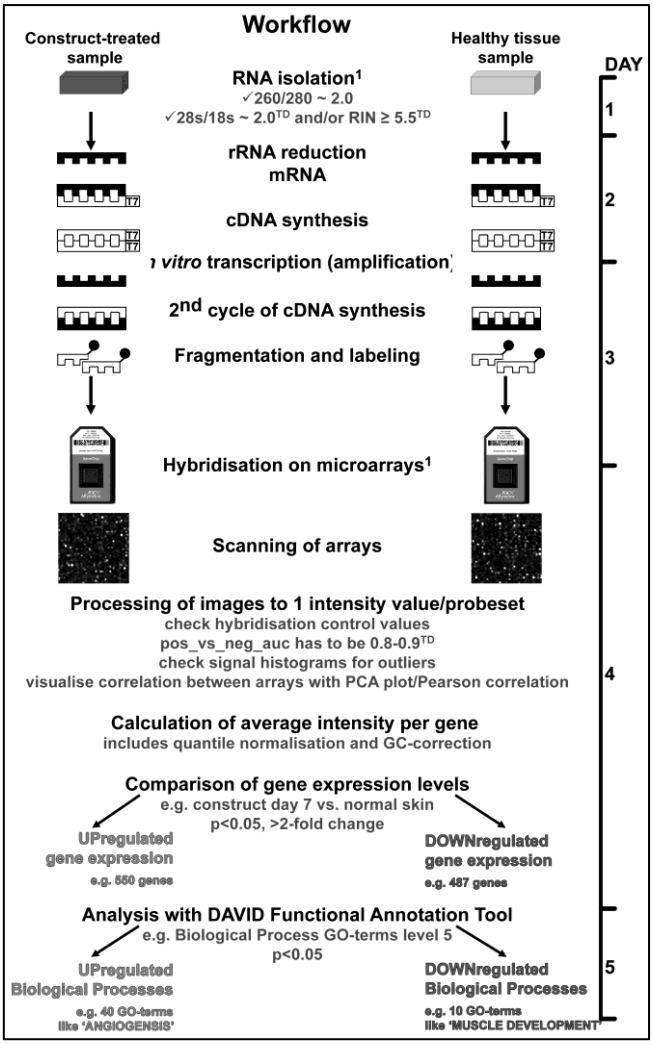

Figure 1. Schematic overview of the complete procedure for the identification of biological processes occuring *in vivo* in constructs used for tissue engineering. In short, mRNA was isolated from tissue samples and processed for hybridisation on rat exon arrays. The amount of hybridised RNA, reflecting the amount of specific mRNA's, was compared between groups, resulting in lists with up- and downregulated genes. Lists were uploaded in the DAVID functional annotation tool and the enrichment in biological process gene ontology (GO) terms was analysed. Up/down regulated biological processes were validated by conventional histology. The minimal time required for each step is indicated on the right. See text for more details. [1]Randomise/balance samples when multiple runs are necessary; [TD]Tissue-dependent; T7=T7 promoter. Picture of microarray is courtesy of Affymetrix.

High density microarrays

The Affymetrix® GeneChip® rat exon 1.0 sense target (ST) array (from here called: exon array) was used, containing 1.0 million probe sets. A probe is an antisense sequence of 25 nucleotides, of which millions of molecules are spotted on a defined physical location on the array. One probe set consists of 4 (sometimes partially overlapping) probes and covers an annotated or predicted exon. About 10% of the probe sets contain fewer than 4 probes, due to the length of the probe selection region or sequence constraints (e.g. highly repeated sequences) [6].

Because all exons of a gene are covered, gene-level analysis on exon arrays is more accurate than on e.g. GeneChip 3' expression arrays, which only covers the 3' end of the gene. In addition, it allows the evaluation of alternative splicing by analysing the correlation of the expression level of one exon with the expression levels of the whole gene.

Double-layered skin construct

The double-layered skin construct consisted of a dense film of type I collagen containing heparin and recombinant rat fibroblast growth factor 7 (rrFGF-7), and a porous scaffold of type I collagen containing solubilised elastin, dermatan sulfate, heparin, rat recombinant fibroblast growth factor 2 (rrFGF-2) and rat recombinant vascular endothelial growth factor (rrVEGF).

Animal study

This study was approved by the Ethics Committee of the Radboud University Nijmegen. Two 1.5x1.5 cm full-thickness wounds were created on both sides of the back of three-month old male Wistar rats. The wounds were treated with the construct or remained untreated. Per time point, each treatment (construct or no construct) was applied to four individual rats. The implants were removed on day 7, 14, 28 and 112 and processed for RNA isolation and histological evaluation. In case of RNA samples, surrounding skin was removed and the tissue was snap-frozen in liquid nitrogen and stored at -80ºC until RNA isolation. Samples from normal skin of 3 three-month old (called from here: day 0 normal skin) and 3 seven-month old (called from here: day 112 normal skin) rats were also collected.

RNA isolation and evaluation

Frozen tissue was pulverised with a chromium steel grinding ball in a Teflon chamber inserted in a Micro-Dismembrator (Sartorius AG, Goettingen, Germany), and dissolved in Trizol reagent (Invitrogen Ltd, Paisley, UK). Total RNA was isolated with a phenol/chloroform extraction and purified using a Qiagen RNeasy mini kit according to the manufacturer's RNA cleanup protocol, including an on-column DNase digestion.

The RNA concentration and purity were measured with a Nanodrop spectrophotometer (Thermo Scientific, Waltham, MA, USA). The 260/280 ratio was used as an indicator for

RNA purity (RNA has a maximum absorbance at 260 nm). A 260/280 ratio of ~2.0 is generally accepted as 'pure RNA' and the samples used ranged from 2.00-2.10.

RNA integrity was analysed on an Agilent Bioanalyser (Santa Clara, CA, USA), which electrophoretically separates samples based on size, applying a microfabricated chip. The resulting peak pattern is represented by the RNA integrity number (RIN), which is calculated by a built-in algorithm in the Bioanalyser software [7]. The RIN can vary between 1 (totally degraded RNA) to 10 (completely intact RNA). Alternatively, the base of the 18s and 28s ribosomal RNA peaks can be used to calculate the 28s/18s ratio. Theoretically, intact RNA has a ratio of 2.0, but this ratio is known to be tissue-dependent and often lower for tissues than e.g. for cultured cells [8]. Based on a combination of the RIN, 28s/18s ratio, and visual inspection of the peak pattern (a low baseline and no major additional peaks), the three qualitatively best samples were chosen out of the four biological replicates. The samples all had a RIN ranging from 5.5-8.0 and a 28s/18s ratio between 0.8 and 1.8.

RNA processing

From the isolated total RNA, 1 µg was further processed for microarray analysis. To reduce the ribosomal RNA (rRNA) content, the Invitrogen RiboMinus transcriptome isolation kit was applied. Removal is based on hybridisation of rRNA with biotinylated rRNA-sequence specific oligonucleotide probes, and subsequent removal of hybridised rRNA using streptavidin-coated magnetic beads.

The probes on the array are in an anti-sense configuration. Therefore, a labelled single-stranded sequence in the sense orientation has to be produced from the isolated (sense) RNA before hybridisation. This was accomplished using the GeneChip whole transcript (WT) sense target labelling assay, which produces labelled single-stranded sense DNA. This DNA results in less cross-hybridisation with the DNA probes on the array than labelled RNA, which is used for other array types [9]. First, double-stranded complementary DNA (cDNA) was synthesised from all RNA molecules. The first strand of this cDNA was synthesised by SuperScript II Reverse Transcriptase using T7 promoter-coupled random hexamer oligonucleotide sequences, the second strand using DNA polymerase I without T7-random hexamers. This cDNA was then used for *in vitro* transcription (IVT) to amplify the product, creating complementary RNA (cRNA). This cRNA was then used in a second cycle of cDNA synthesis to create single-stranded DNA in the sense orientation, using random primers and SuperScript II Reverse Transcriptase. Of this DNA, 5.5 µg was enzymatically fragmented and fluorescently labelled. Pre-labelled hybridisation controls (e.g. bacterial sequences in known amounts) were added to the mixture and this was hybridised on an exon array chip.

A total set of 30 arrays was hybridised in three separate runs. Experimental groups were randomised over the different runs, but with a few exceptions (see results section).

Data processing, quality control and statistical analysis

The arrays were scanned and converted to a processed image, which was converted to one fluorescence intensity value per probe, using Affymetrix GeneChip Operating Software

(GCOS). The values of individual probes belonging to one probe set (four probes/set in 90% of the cases) were averaged and normalised using Partek Genomics Suite 6.4 (Partek Inc., St. Louis, MO, USA, www.partek.com).

The distribution of the intensity values on the individual arrays was visualised in a signal histogram and no obvious outliers were detected. The intensity values of probe sets specific for the pre-labelled hybridization controls were analysed and they corresponded with the expected values. To check overall data quality, the array contained probe sets for exonic ("positive") and intronic ("negative") regions of reference genes (genes known to be constitutively expressed in many different samples). Their probe set intensities were used to calculate the difference between the area under the curve of the positive and negative probe sets (pos_vs_neg_auc). This value is known to be tissue-specific, but generally varies between 0.80 and 0.95 for good quality samples, and ranged from 0.81-0.94 for the 30 arrays [10].

The average fluorescence intensity of all annotated rat genes (=core dataset, 8,264 genes at the moment of analysis) was calculated using the Robust Multiarray Analysis (RMA) algorithm [11], including a quantile normalisation (all arrays are considered to have an equal intensity distribution) and using a background correction for GC-content (probes with high GC content hybridise better, corrected for with built-in probes with different known GC-contents).

Analysis of the sources of variation revealed that the hybridisation date (one of the three dates the samples were processed) was the main source of variation, a known cause of variation, indicating that despite e.g. standard protocols and solutions it is nearly impossible to control each variable that may influence RNA processing and hybridisation. Therefore, the hybridisation date was included in the subsequent statistical analysis as a covariate.

To identify differentially expressed genes between the different experimental groups, a two-way analysis of variance (ANOVA) was performed for sample group times *time point* (i.e. normal skin, untreated wound or construct-treated *day 0, 7, 14, 28* or *112*), including hybridisation date as a correction factor. The resulting p-values were corrected for multiple-testing with the Benjamini-Hochberg false discovery rate procedure [12]. To correct for possible changes in normal skin for the duration of the animal experiment, day 7, 14 and 28 untreated and construct-treated wound were compared with day 0 normal skin, whereas day 112 untreated and day 112 construct-treated wound were compared with day 112 normal skin. For each comparison between two experimental groups (e.g. construct-treated day 7 vs. normal skin day 0), the fold-change of every annotated gene, together with their corresponding p-value, was exported to Microsoft Office Excel.

Gene lists of interest (all >2-fold up/downregulated genes ($p<0.05$)) were analysed using the Database for Annotation, Visualization and Integrated Discovery functional annotation tool (DAVID, http://david.abcc.ncifcrf.gov/) with main focus on the enrichment in GO-terms of biological processes on level 5 (GOTERM_BP5 chart). Bonferroni multiple testing $p<0.05$ for enrichment p-values was used as a cut-off threshold. As reference list (dubbed the background), a list of the 8,264 annotated genes on the array was uploaded. See results section for more information.

(Immuno-)histological validation

The findings of the microarray/DAVID analysis were validated (immuno-)histochemically, under the assumption that gene expression levels generally correlate with the amount of the corresponding protein.

Samples were either fixed with 4% paraformaldehyde in 0.1 M phosphate buffer (pH 7.4) for 24 h and embedded in paraffin, or frozen in liquid nitrogen-cooled isopentane and mounted in TissueTek (Sakura Finetek, Zoeterwoude, The Netherlands).

Immunohistochemistry

Paraffin sections were deparaffinised and boiled for 10 min in 10 mM citrate buffer (pH 6.0) for antigen retrieval, and incubated with mouse anti-desmin (1:200; Biogenex, San Ramon, CA, U.S.A.) or mouse anti-rat CD8 alpha (1:400; clone OX-8) for 16 h at 4ºC. Biotin-conjugated horse anti-mouse IgG (1:400; Vector Laboratories, Burlingame, CA, USA) was used as a secondary antibody. The Vectastain Elite ABC kit (Vector Laboratories) was used for signal amplification according to the manufacturer's protocol. Bound antibody was visualised using 3,3'-diaminobenzidine (DAB) and sections were counterstained with haematoxylin. [13]

Cryosections were incubated with goat anti-human type IV collagen (Southern Biotechnology, Birmingham, AL, USA) followed by an Alexa 488-labelled donkey anti-goat IgG antibody (Molecular Probes, Eugene, OR, USA), as described [14].

TUNEL assay

Paraffin sections were incubated with terminal deoxynucleotidyl transferase-mediated deoxyuridinetriphosphate-biotin nick end labelling (TUNEL) reaction mixture (Roche, Basel, Switzerland) according to the manufacturer's labelling protocol for "difficult" tissues, which included a 1 min boiling step performed in 0.1 M citrate buffer (pH 6.0) for antigen retrieval.

Results

RNA isolation

Frozen samples were processed for RNA isolation. Normal skin and day 112 samples were difficult to pulverise in comparison with day 7, 14 and 28 samples, probably due to the larger amount of connective tissue present. The amount of total RNA isolated was 30-55 µg for day 7 and 14 untreated wounds and day 7, 14 and 28 construct-treated samples, ~20 µg for day 28 construct-treated, and 5-10 µg for day 112 untreated and construct-treated wounds and all normal skin samples. The size of the samples varied due to contraction (smaller samples at later time points), but yield differences were most likely caused by the number of cells present in the different samples (higher cell densities at early time points), since relatively large normal skin samples also gave low yields.

Correlation between biological replicates

The RNA was processed into labelled DNA fragments and each sample was hybridised on an individual exon array. Pictures from the arrays were taken and processed to one fluorescence intensity value per gene by averaging the intensity values of the probe sets belonging to one gene.

To evaluate the variation between the biological replicates in an experimental group and to compare the experimental groups with normal skin, the correlation between the arrays was examined. Pearson's correlation plots were generated, in which the fluorescence intensity of each transcript ('gene'; average intensity of all probe sets belonging to one gene) on the first array is plotted against the fluorescence intensity of the same transcript on the second array. The linear correlation of these plots was expressed with a Pearson's correlation coefficient, ranging from 1 (perfect positive correlation, meaning that there is a linear function that perfectly translates values from one array to the corresponding values on the other array) to -1 (perfect negative correlation). In this way, a Pearson's correlation coefficient was calculated for all combinations of the 30 arrays. Figure 2 shows the average correlation between the three biological replicates of each experimental group (three comparisons) and the average correlation of each group with normal skin (nine comparisons).

A high Pearson correlation reflects correlated gene expression levels. The correlation between the three biological replicates was 0.91 or higher in all cases. A tendency was observed for higher correlation when the three biological replicates were hybridised in the same microarray run (untreated wound day 7, 28 and 112). However, the least correlation was found for the day 112 normal skin replicates, which was the only group of which the biological replicates were processed in one single RNA isolation and microarray hybridisation run, indicating that other factors probably also influenced this correlation.

	day 0	day 7		day 14		day 28		day 112		
	Normal skin	Untreated	Construct	Untreated	Construct	Untreated	Construct	Untreated	Construct	Normal skin
Correlation between biological replicates	0.92±0.02	0.97±0.00	0.93±0.03	0.92±0.02	0.94±0.02	0.96±0.01	0.93±0.04	0.95±0.01	0.92±0.02	0.91±0.05
Correlation with normal skin		0.84±0.03	0.83±0.03	0.83±0.03	0.82±0.03	0.87±0.03	0.83±0.03	0.86±0.05*	0.86±0.04*	0.91±0.04

Figure 2. Average Pearson's correlation coefficient values (± S.D.) representing the correlation of three biological replicates of each experiment group and the correlation of each group with normal skin (*day 112 untreated and construct-treated wounds were compared with day 112 normal skin). Correlation between the replicates was always higher than between an experimental group and normal skin. The day 7 and 14 samples differed most from normal skin, as did the construct-treated wounds on day 28. The day 28 untreated wound was more similar to normal skin, as were all day 112 samples.

Differences in gene expression

The Pearson's correlation plots were also used to visualise the differences between the experimental groups and normal skin (Fig. 2). As expected, the arrays with untreated and construct-treated wound samples showed less correlation with normal skin (0.82-0.87) than the correlation between replicates as described before. The correlation with normal skin increased in time, likely reflecting the skin regeneration process. On day 28, the correlation

with the day 0 normal skin arrays was higher for the untreated than for the construct-treated wounds.

The differences in gene expression between the experimental groups and normal skin were analysed with an ANOVA. For every gene, the average intensity on the three arrays of an experimental group (e.g. construct-treated day 7) was compared with the average intensity on the three arrays of the normal skin (e.g. normal skin day 0).

The number of differentially expressed genes with more than 2-fold change ($p<0.05$) compared to normal skin is listed in Table 1. Lists were divided in number of down- and upregulated genes. Fold change ranged from the 2-fold cut-off to 232-fold change (*matrix metalloproteinase 12* upregulation in construct-treated day 28). Generally, the number of differentially expressed genes decreased with time (Table 1). The difference on day 28 between untreated and construct-treated wounds (numbers for untreated wound were already dropping while those for the construct-treated were still high) reflect the trends observed in the Pearson correlation values of Fig. 2.

Table 1. Number of differentially expressed genes between (A) the construct-treated wounds versus normal skin or (B) the untreated wounds versus normal skin ($p<0.05$; >2-fold change) at various time points. Upregulated means higher expression in the wounds, downregulated means higher expression in normal skin. (C) Shows the number of genes that are present in both the list of (A) the construct-treated and (B) untreated wound.

	(A) Construct-treated vs. normal skin (analysed in Table 2A)		(B) Untreated wound vs. normal skin (analysed in Table 2B)		(C) Shared between (A) construct-treated and (B) untreated wounds	
Day	upregulated	downregulated	upregulated	downregulated	upregulated	downregulated
7	550	487	514	468	420	412
14	656	545	414	408	367	352
28	600	439	272	334	174	274
112	299	408	254	360	204	317

Identification of biological processes: Gene ontology terms and DAVID

Analysis of each individual differentially expressed gene in the wound healing process is time consuming. Since the focus of this study lies on the identification of biological processes rather than individual genes, gene lists were analysed as a whole. Several (proprietary, downloadable or web-based) applications exist that enable the identification of biological processes that are under- or overrepresented in a given gene list, compared to the occurrence of these processes in a reference gene list. Most of these applications use gene ontology (GO)-terms (http://www.geneontology.org/) for analysis. A GO-term represents a certain biological process (e.g. angiogenesis), cellular component (e.g. plasma membrane), or molecular function (e.g. kinase activity) [15]. A set of genes associated with a particular biological process is labelled to a specific GO-term. GO-terms are assigned by an active consortium of database researchers, of which the rat genome database consortium (RGD,

http://rgd.mcw.edu/) is responsible for the submission of *Rattus norvegicus* annotations. GO-terms are connected with each other in a tree structure with different levels in which a specific term can have more than one (more general) parent terms. The GO-terms can be browsed in AmiGO (http://amigo.geneontology.org) to learn more about their definition, position in the tree, etc. [16]. As an example, the biological process GO-term 'skin development' (GO:0043588) is depicted in its tree format (Fig. 3).

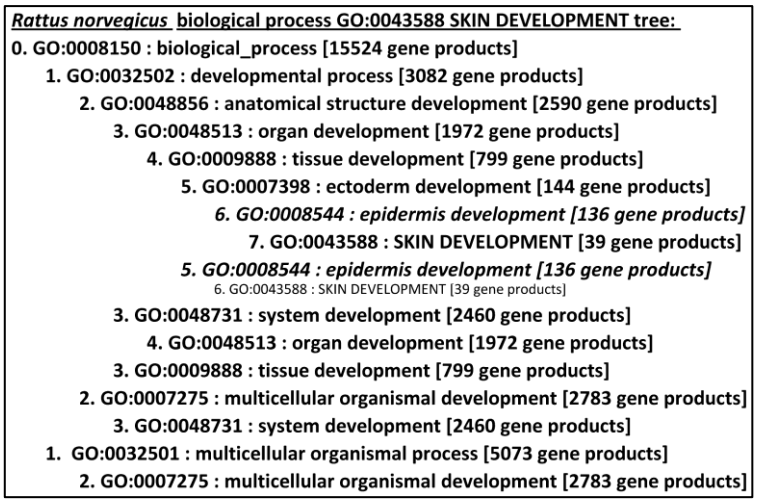

Figure 3. Compact tree view with the different levels (0-7) of the rat biological process GO-term 'skin development' (GO:0043588, in CAPITALS). When a given term is listed for the second time (e.g. *GO:0008544 epidermis development*), then the tree continues as depicted the first time (for clarity visualised in smaller text size only for *GO:0008544*). Figure based on information from the AmiGO website (http://amigo.geneontology.org) [1].

DAVID is an open web-based tool to facilitate the biological interpretation of large (microarray) datasets [17,18]. Any gene list of interest can be uploaded in DAVID's functional annotation tool, and the program compares the gene distribution in this list with the gene distribution in a list with reference genes (dubbed "background"). DAVID then calculates the GO-terms, protein domains, pathways, etc. (based on default external databases) that are overrepresented in the input list (fold enrichment plus corresponding p-value).

Because this study focuses on the biological processes occurring in the regenerating wounds, the gene lists with up- and downregulated genes were analysed for their enrichment in biological process GO-terms (and not cellular component or molecular function) on the most specific level available in DAVID (level 5). A generally accepted cut-off of $p<0.05$ after multiple testing correction and a >2-fold change was used (Table 1). This cut-off resulted in gene lists with reasonable length (several hundred genes) with respect to the length of the reference list (all 8,264 well-annotated genes on the array). Gene lists with too little or too many genes (e.g. <100 or >2,000 in this case) may result in less informative GO-terms and corresponding p-values [18]. Please note that in DAVID the gene lists consist only of gene identifiers and that the actual gene-specific fold-change and p-value is not taken into

account. This implies that e.g. both a 2- and 100-fold changed gene expression contribute equally to the enrichment in GO-terms. Table 2 gives an overview of all enriched level 5 GO-terms (Bonferroni p<0.05) after DAVID analysis for the construct-treated (Table 2A) and untreated wound (Table 2B). Also given is the associated fold enrichment score with respect to a random gene list of the same length, as calculated by the DAVID program. This fold enrichment is calculated by dividing the percentage of genes with a specific GO-term in the up/down regulated list by the percentage genes with the same GO-term in the reference list. For example a 5-fold enrichment is obtained when 10% of the genes in the upregulated list is associated with the GO-term 'angiogenesis' versus 2% of the genes in the reference list.

Table 2A. Enrichment in biological process GO-terms (level 5) of the gene lists (numbers in Table 1) with up- and downregulated expression in the construct-treated wound versus normal skin (Bonferroni p<0.05; day 7, 14 and 28 vs. day 0 normal skin, day 112 vs. day 112 normal skin). Listing is according to significance. F.E.=Fold enrichment.

UPREGULATED IN CONSTRUCT					
day 7			day 14		
Term	F.E.	Bon-ferroni	Term	F.E.	Bon-ferroni
GO:0030097~hemopoiesis	4.8	2.7E-14	GO:0048534~hemopoietic or lymphoid organ development	4.6	1.2E-17
GO:0048534~hemopoietic or lymphoid organ development	4.7	3.9E-14	GO:0030097~hemopoiesis	4.7	3.5E-17
GO:0006935~chemotaxis	6.3	4.1E-14	GO:0006935~chemotaxis	5.9	1.1E-15
GO:0030099~myeloid cell differentiation	5.6	1.7E-09	GO:0002521~leukocyte differentiation	5.8	5.5E-14
GO:0002521~leukocyte differentiation	5.5	2.4E-09	GO:0042110~T cell activation	5.7	1.5E-12
GO:0050900~leukocyte migration	8.6	3.2E-09	GO:0050900~leukocyte migration	7.5	4.4E-09
GO:0030595~leukocyte chemotaxis	9.6	3.2E-07	GO:0030099~myeloid cell differentiation	4.8	1.4E-08
GO:0042110~T cell activation	5.1	4.0E-07	GO:0030098~lymphocyte differentiation	5.8	4.1E-08
GO:0030593~neutrophil chemotaxis	11.5	4.8E-06	GO:0030595~leukocyte chemotaxis	8.5	1.8E-07
GO:0042035~regulation of cytokine biosynthetic process	7.4	5.1E-06	GO:0002449~lymphocyte mediated immunity	5.8	3.4E-07
GO:0019724~B cell mediated immunity	6.6	7.6E-06	GO:0030217~T cell differentiation	7.0	4.3E-07
GO:0002449~lymphocyte mediated immunity	5.9	1.4E-05	GO:0019724~B cell mediated immunity	6.2	1.1E-06
GO:0042108~positive regulation of cytokine biosynthetic process	9.0	2.6E-05	GO:0050776~regulation of immune response	4.0	1.7E-05
GO:0045727~positive regulation of translation	7.3	9.7E-05	GO:0030593~neutrophil chemotaxis	9.6	2.8E-05
GO:0042107~cytokine metabolic process	6.0	1.1E-04	GO:0042035~regulation of cytokine biosynthetic process	6.1	5.4E-05
GO:0019221~cytokine and chemokine mediated signaling pathway	6.5	1.4E-04	GO:0008219~cell death	1.9	6.8E-05
GO:0002573~myeloid leukocyte differentiation	7.0	1.6E-04	GO:0045727~positive regulation of translation	6.5	7.2E-05
GO:0006508~proteolysis	2.2	2.0E-04	GO:0051249~regulation of lymphocyte activation	4.9	7.6E-05
GO:0008219~cell death	2.0	2.1E-04	GO:0002684~positive regulation of immune system process	4.2	9.8E-05
GO:0050776~regulation of immune response	4.0	5.4E-04	GO:0002573~myeloid leukocyte differentiation	6.3	1.2E-04
GO:0030098~lymphocyte differentiation	5.0	5.4E-04	GO:0019221~cytokine and chemokine mediated signaling pathway	5.8	1.4E-04
GO:0030217~T cell differentiation	6.4	5.7E-04	GO:0051247~positive regulation of protein metabolic process	4.4	2.3E-04
GO:0051247~positive regulation of protein metabolic process	4.7	6.0E-04	GO:0050778~positive regulation of immune response	4.1	3.1E-04
GO:0031328~positive regulation of cellular biosynthetic process	6.0	1.2E-03	GO:0050801~ion homeostasis	2.5	4.6E-04

GO:0002526~acute inflammatory response	3.8	1.2E-03	GO:0030003~cellular cation homeostasis	2.8	5.3E-04
GO:0009891~positive regulation of biosynthetic process	4.8	2.7E-03	GO:0046651~lymphocyte proliferation	4.8	8.8E-04
GO:0006915~apoptosis	1.9	2.9E-03	GO:0042107~cytokine metabolic process	5.0	1.0E-03
GO:0048514~blood vessel morphogenesis	3.1	3.5E-03	GO:0031328~positive regulation of cellular biosynthetic process	5.4	1.2E-03
GO:0046651~lymphocyte proliferation	5.0	4.2E-03	GO:0006915~apoptosis	1.8	1.4E-03
GO:0030003~cellular cation homeostasis	2.8	5.2E-03	GO:0055082~cellular chemical homeostasis	2.5	1.5E-03
GO:0001944~vasculature development	2.9	5.4E-03	GO:0042098~T cell proliferation	5.7	1.8E-03
GO:0008285~negative regulation of cell proliferation	2.7	9.1E-03	GO:0042108~positive regulation of cytokine biosynthetic process	6.9	2.2E-03
GO:0006897~endocytosis	3.1	1.1E-02	GO:0051251~positive regulation of lymphocyte activation	5.5	2.7E-03
GO:0050801~ion homeostasis	2.5	1.3E-02	GO:0002253~activation of immune response	4.0	4.1E-03
GO:0001568~blood vessel development	2.8	1.4E-02	GO:0002526~acute inflammatory response	3.4	4.7E-03
GO:0042098~T cell proliferation	5.8	2.0E-02	GO:0050863~regulation of T cell activation	4.7	7.1E-03
GO:0055082~cellular chemical homeostasis	2.5	2.0E-02	GO:0006508~proteolysis	1.9	1.0E-02
GO:0006417~regulation of translation	3.6	3.0E-02	GO:0006417~regulation of translation	3.3	1.9E-02
GO:0006909~phagocytosis	7.1	3.4E-02	GO:0050864~regulation of B cell activation	6.2	2.3E-02
GO:0001525~angiogenesis	3.1	4.9E-02	GO:0009891~positive regulation of biosynthetic process	4.0	2.3E-02
			GO:0046968~peptide antigen transport	8.1	3.6E-02

day 28			day 112		
Term	**F.E.**	**Bonferroni**	**Term**	**F.E.**	**Bonferroni**
GO:0048534~hemopoietic or lymphoid organ development	5.0	4.1E-19	GO:0001501~skeletal development	3.5	5.8E-03
GO:0042110~T cell activation	7.0	8.3E-18	GO:0008361~regulation of cell size	3.6	3.4E-02
GO:0030097~hemopoiesis	5.0	1.1E-17			
GO:0006935~chemotaxis	6.2	9.5E-16			
GO:0002521~leukocyte differentiation	5.7	6.2E-12			
GO:0002449~lymphocyte mediated immunity	6.9	7.4E-10			
GO:0051249~regulation of lymphocyte activation	6.5	3.6E-09			
GO:0030098~lymphocyte differentiation	6.2	9.4E-09			
GO:0030217~T cell differentiation	7.9	9.5E-09			
GO:0019724~B cell mediated immunity	7.1	2.7E-08			
GO:0050863~regulation of T cell activation	6.9	4.8E-08			
GO:0046651~lymphocyte proliferation	6.4	5.6E-08			
GO:0051251~positive regulation of lymphocyte activation	7.3	1.0E-06			
GO:0030099~myeloid cell differentiation	4.4	5.6E-06			
GO:0050776~regulation of immune response	4.2	2.2E-05			
GO:0050900~leukocyte migration	6.4	3.3E-05			
GO:0046968~peptide antigen transport	10.9	5.0E-05			
GO:0019886~antigen processing and presentation of exogenous peptide antigen via MHC class II	14.1	1.4E-04			
GO:0002684~positive regulation of immune system process	4.3	1.6E-04			
GO:0008219~cell death	1.9	4.3E-04			
GO:0019221~cytokine and chemokine mediated signaling pathway	5.8	4.8E-04			
GO:0050778~positive regulation of im-	4.2	5.2E-04			

mune response					
GO:0042098~T cell proliferation	6.1	7.9E-04			
GO:0042113~B cell activation	5.2	2.2E-03			
GO:0030595~leukocyte chemotaxis	6.8	3.1E-03			
GO:0030003~cellular cation homeostasis	2.7	3.8E-03			
GO:0006915~apoptosis	1.8	4.5E-03			
GO:0045576~mast cell activation	8.5	5.3E-03			
GO:0043067~regulation of programmed cell death	1.9	5.8E-03			
GO:0042981~regulation of apoptosis	1.9	7.6E-03			
GO:0002253~activation of immune response	4.1	8.2E-03			
GO:0006508~proteolysis	1.9	1.2E-02			
GO:0043065~positive regulation of apoptosis	2.5	1.3E-02			
GO:0051247~positive regulation of protein metabolic process	4.0	1.3E-02			
GO:0043068~positive regulation of programmed cell death	2.4	1.4E-02			
GO:0016310~phosphorylation	1.9	1.6E-02			
GO:0006897~endocytosis	2.9	1.6E-02			
GO:0006664~glycolipid metabolic process	7.5	1.8E-02			
GO:0050670~regulation of lymphocyte proliferation	5.4	3.6E-02			
GO:0032944~regulation of mononuclear cell proliferation	5.4	3.6E-02			
GO:0002768~immune response-regulating cell surface receptor signaling pathway	8.1	4.0E-02			
GO:0002757~immune response-activating signal transduction	8.1	4.0E-02			
GO:0050851~antigen receptor-mediated signaling pathway	8.1	4.0E-02			
GO:0045619~regulation of lymphocyte differentiation	6.7	4.8E-02			
DOWNREGULATED IN CONSTRUCT					
day 7			**day 14**		
Term	**F.E.**	**Bonferroni**	**Term**	**F.E.**	**Bonferroni**
GO:0006941~striated muscle contraction	11.3	3.7E-09	GO:0006941~striated muscle contraction	11.1	4.5E-10
GO:0032787~monocarboxylic acid metabolic process	3.5	8.0E-09	GO:0032787~monocarboxylic acid metabolic process	3.4	1.6E-09
GO:0006631~fatty acid metabolic process	3.5	1.9E-05	GO:0019318~hexose metabolic process	3.7	6.6E-06
GO:0016126~sterol biosynthetic process	8.1	3.1E-05	GO:0005996~monosaccharide metabolic process	3.7	8.1E-06
GO:0008610~lipid biosynthetic process	3.1	6.6E-05	GO:0006631~fatty acid metabolic process	3.3	3.0E-05
GO:0019318~hexose metabolic process	3.6	1.1E-04	GO:0007517~muscle development	3.7	6.7E-05
GO:0005996~monosaccharide metabolic process	3.6	1.3E-04	GO:0016126~sterol biosynthetic process	7.4	8.0E-05
GO:0007517~muscle development	3.7	2.9E-04	GO:0014706~striated muscle development	4.1	1.9E-03
GO:0006084~acetyl-CoA metabolic process	6.7	1.3E-03	GO:0046365~monosaccharide catabolic process	4.7	1.0E-02
GO:0014706~striated muscle development	4.0	1.6E-02	GO:0008610~lipid biosynthetic process	2.5	1.5E-02
			GO:0006084~acetyl-CoA metabolic process	5.7	2.4E-02
day 28			**day 112**		
Term	**F.E.**	**Bonferroni**	**Term**	**F.E.**	**Bonferroni**
GO:0006941~striated muscle contraction	13.1	3.8E-11	GO:0006941~striated muscle contraction	11.6	2.6E-07
GO:0007517~muscle development	4.7	7.1E-08	GO:0046365~monosaccharide catabolic	6.4	7.3E-05

			process		
GO:0014706~striated muscle development	5.4	3.9E-06	GO:0019318~hexose metabolic process	3.9	1.1E-04
GO:0019318~hexose metabolic process	3.9	2.3E-05	GO:0005996~monosaccharide metabolic process	3.9	1.3E-04
GO:0005996~monosaccharide metabolic process	3.9	2.8E-05	GO:0007517~muscle development	4.0	3.8E-04
GO:0046365~monosaccharide catabolic process	5.5	1.6E-03	GO:0044275~cellular carbohydrate catabolic process	5.2	4.6E-04
GO:0006084~acetyl-CoA metabolic process	6.7	5.4E-03	GO:0006099~tricarboxylic acid cycle	10.9	1.0E-03
GO:0044275~cellular carbohydrate catabolic process	4.5	7.9E-03	GO:0009109~coenzyme catabolic process	10.3	1.8E-03
GO:0032787~monocarboxylic acid metabolic process	2.6	2.1E-02	GO:0006084~acetyl-CoA metabolic process	7.3	2.5E-03
			GO:0009060~aerobic respiration	9.2	4.7E-03
			GO:0014706~striated muscle development	4.4	1.1E-02
			GO:0032787~monocarboxylic acid metabolic process	2.7	1.3E-02

Table 2B. Enrichment in biological process GO-terms (level 5) of the gene lists (numbers in Table 1) with up- and downregulated expression in the untreated wound versus normal skin (Bonferroni p<0.05; day 7, 14 and 28 vs. day 0 normal skin, day 112 vs. day 112 normal skin). Listing is according to significance. F.E.=Fold enrichment.

UPREGULATED IN UNTREATED WOUND					
day 7			day 14		
Term	F.E.	Bonferroni	Term	F.E.	Bonferroni
GO:0042110~T cell activation	5.6	6.6E-08	GO:0006935~chemotaxis	6.7	4.0E-11
GO:0030097~hemopoiesis	4.0	1.3E-07	GO:0030097~hemopoiesis	4.6	8.3E-09
GO:0048514~blood vessel morphogenesis	4.1	3.0E-07	GO:0048534~hemopoietic or lymphoid organ development	4.4	3.9E-08
GO:0048534~hemopoietic or lymphoid organ development	3.8	5.9E-07	GO:0042110~T cell activation	6.1	1.5E-07
GO:0001944~vasculature development	3.8	7.1E-07	GO:0050900~leukocyte migration	9.3	2.4E-07
GO:0006935~chemotaxis	4.9	8.9E-07	GO:0030595~leukocyte chemotaxis	11.6	2.6E-07
GO:0002521~leukocyte differentiation	5.1	1.2E-06	GO:0002521~leukocyte differentiation	5.8	3.5E-07
GO:0019724~B cell mediated immunity	7.2	2.1E-06	GO:0030593~neutrophil chemotaxis	13.7	1.2E-05
GO:0001568~blood vessel development	3.7	2.3E-06	GO:0030098~lymphocyte differentiation	6.2	1.3E-04
GO:0002449~lymphocyte mediated immunity	6.5	3.6E-06	GO:0002449~lymphocyte mediated immunity	6.4	2.6E-04
GO:0050776~regulation of immune response	4.6	2.2E-05	GO:0019724~B cell mediated immunity	7.0	2.7E-04
GO:0001525~angiogenesis	4.2	3.0E-05	GO:0050776~regulation of immune response	4.7	2.8E-04
GO:0009887~organ morphogenesis	2.6	1.3E-04	GO:0030217~T cell differentiation	7.7	3.4E-04
GO:0042035~regulation of cytokine biosynthetic process	7.0	2.1E-04	GO:0042035~regulation of cytokine biosynthetic process	7.7	3.4E-04
GO:0002526~acute inflammatory response	4.2	3.0E-04	GO:0030099~myeloid cell differentiation	4.8	6.1E-04
GO:0050900~leukocyte migration	6.8	3.1E-04	GO:0042107~cytokine metabolic process	6.3	3.3E-03
GO:0019221~cytokine and chemokine mediated signaling pathway	6.6	4.6E-04	GO:0006909~phagocytosis	9.2	4.7E-03
GO:0030098~lymphocyte differentiation	5.2	1.2E-03	GO:0019221~cytokine and chemokine mediated signaling pathway	6.6	6.5E-03
GO:0030099~myeloid cell differentiation	4.2	1.3E-03	GO:0042108~positive regulation of cytokine biosynthetic process	8.8	7.3E-03
GO:0002684~positive regulation of immune system process	4.4	1.5E-03	GO:0002684~positive regulation of immune system process	4.4	2.8E-02
GO:0030217~T cell differentiation	6.5	2.0E-03	GO:0044254~multicellular organismal protein catabolic process	15.4	2.8E-02
GO:0042108~positive regulation of cyto-	8.2	2.3E-03	GO:0030574~collagen catabolic process	15.4	2.8E-02

kine biosynthetic process					
GO:0042107~cytokine metabolic process	5.7	2.5E-03	GO:0051247~positive regulation of protein metabolic process	4.7	3.0E-02
GO:0050778~positive regulation of immune response	4.3	5.4E-03	GO:0008361~regulation of cell size	3.2	3.1E-02
GO:0030595~leukocyte chemotaxis	7.5	5.8E-03	GO:0048514~blood vessel morphogenesis	3.2	4.0E-02
GO:0006508~proteolysis	2.1	7.6E-03			
GO:0006958~complement activation, classical pathway	9.2	2.0E-02			
GO:0030593~neutrophil chemotaxis	9.2	2.0E-02			
GO:0002253~activation of immune response	4.4	2.3E-02			
GO:0051247~positive regulation of protein metabolic process	4.2	3.5E-02			
GO:0030003~cellular cation homeostasis	2.7	3.5E-02			
GO:0006897~endocytosis	3.1	3.6E-02			
GO:0045727~positive regulation of translation	6.1	3.8E-02			

day 28			day 112		
Term	**F.E.**	**Bonferroni**	**Term**	**F.E.**	**Bonferroni**
GO:0000902~cell morphogenesis	2.7	7.8E-03	GO:0001501~skeletal development	4.0	1.7E-03
GO:0001501~skeletal development	3.6	1.7E-02	GO:0000902~cell morphogenesis	2.8	2.6E-03
GO:0001944~vasculature development	3.7	2.2E-02	GO:0001944~vasculature development	3.7	4.6E-02

DOWNREGULATED IN UNTREATED WOUND

day 7			day 14		
Term	**F.E.**	**Bonferroni**	**Term**	**F.E.**	**Bonferroni**
GO:0032787~monocarboxylic acid metabolic process	5.2	4.4E-14	GO:0006941~striated muscle contraction	14.3	1.0E-11
GO:0006941~striated muscle contraction	14.2	1.1E-09	GO:0032787~monocarboxylic acid metabolic process	3.9	7.6E-10
GO:0006631~fatty acid metabolic process	5.1	3.0E-08	GO:0006084~acetyl-CoA metabolic process	10.0	8.1E-08
GO:0016126~sterol biosynthetic process	13.5	1.3E-07	GO:0019318~hexose metabolic process	4.6	1.2E-07
GO:0006084~acetyl-CoA metabolic process	11.3	2.6E-07	GO:0005996~monosaccharide metabolic process	4.6	1.5E-07
GO:0008610~lipid biosynthetic process	4.0	3.3E-07	GO:0007517~muscle development	4.4	1.4E-05
GO:0019318~hexose metabolic process	4.6	4.4E-07	GO:0006099~tricarboxylic acid cycle	12.1	5.0E-05
GO:0005996~monosaccharide metabolic process	4.5	6.2E-07	GO:0009109~coenzyme catabolic process	11.4	9.6E-05
GO:0007517~muscle development	4.6	1.1E-05	GO:0009060~aerobic respiration	10.3	3.0E-04
GO:0006694~steroid biosynthetic process	6.4	1.7E-04	GO:0014706~striated muscle development	5.0	3.2E-04
GO:0014706~striated muscle development	5.4	5.5E-04	GO:0044275~cellular carbohydrate catabolic process	5.2	4.4E-04
GO:0016125~sterol metabolic process	5.8	1.7E-03	GO:0046365~monosaccharide catabolic process	6.0	5.8E-04
GO:0046365~monosaccharide catabolic process	4.7	6.9E-03	GO:0006631~fatty acid metabolic process	3.3	3.2E-03
GO:0006099~tricarboxylic acid cycle	10.8	1.4E-02			
GO:0008203~cholesterol metabolic process	5.4	2.8E-02			
GO:0044275~cellular carbohydrate catabolic process	3.9	3.0E-02			
GO:0009109~coenzyme catabolic process	9.2	4.1E-02			

day 28			day 112		
Term	**F.E.**	**Bonferroni**	**Term**	**F.E.**	**Bonferroni**
GO:0006941~striated muscle contraction	15.0	1.0E-09	GO:0006941~striated muscle contraction	15.6	4.5E-11
GO:0046365~monosaccharide catabolic process	8.7	5.1E-08	GO:0007517~muscle development	4.6	3.0E-05
GO:0006084~acetyl-CoA metabolic	11.1	1.4E-07	GO:0019318~hexose metabolic process	4.2	1.9E-04

process					
GO:0006099~tricarboxylic acid cycle	15.9	3.3E-07	GO:0005996~monosaccharide metabolic process	4.1	2.2E-04
GO:0044275~cellular carbohydrate catabolic process	7.0	5.3E-07	GO:0046365~monosaccharide catabolic process	6.5	8.8E-04
GO:0019318~hexose metabolic process	4.9	6.2E-07	GO:0014706~striated muscle development	5.1	1.8E-03
GO:0009109~coenzyme catabolic process	15.0	7.3E-07	GO:0044275~cellular carbohydrate catabolic process	5.3	3.1E-03
GO:0005996~monosaccharide metabolic process	4.9	7.4E-07			
GO:0009060~aerobic respiration	13.5	2.9E-06			
GO:0007517~muscle development	5.0	2.9E-06			
GO:0014706~striated muscle development	5.6	1.9E-04			
GO:0042775~organelle ATP synthesis coupled electron transport	17.2	1.7E-03			
GO:0032787~monocarboxylic acid metabolic process	3.0	5.3E-03			
GO:0006100~tricarboxylic acid cycle intermediate metabolic process	11.5	3.3E-02			

To facilitate the interpretation of the lists with enriched GO-terms, the individual terms can be divided into a number of user (self)-defined major categories. For example, the enriched GO-terms in the construct-treated wounds at day 7 could be grouped into three major categories: inflammation, apoptosis and angiogenesis (Table 2A). The majority of the GO-terms is related to inflammation. For example, terms like 'T cell activation', 'B cell mediated immunity' and 'acute inflammatory response' are clearly inflammation-related. Please note that also terms like 'hemopoiesis' and 'hemopoietic and lymphoid organ development' describe processes that include the maturation and activation of e.g. macrophages and granulocytes. The second category comprises the closely-related terms 'cell death', 'apoptosis' and 'negative regulation of cell proliferation'. The third major category consists of GO-terms related to blood vessel formation viz.: 'blood vessel morphogenesis', 'vasculature development', 'blood vessel development', and 'angiogenesis'. At day 14 and 28, the terms for the construct-treated wounds still contained inflammation- and apoptosis-related terms, but lacked those for angiogenesis. At day 112, 'skeletal development' and 'regulation of cell size' were the two remaining terms. The untreated wound at day 7 and 14 also contained inflammation- and angiogenesis-related terms, but lacked those related to apoptosis (Table 2B). At day 28 and 112, 'cell morphogenesis', 'skeletal development', and 'vasculature development' were the three remaining terms.

The lists with downregulated genes for both construct-treated and untreated wounds were enriched for the muscle-related terms 'striated muscle contraction' (GO:0006941) and '(striated) muscle development' (GO:0007517/GO:0014706) on all time points examined (Table 2A and 2B). The remaining terms are closely linked to cellular metabolism, highly active in muscle cells, and lipid production.

(Immuno)histological validation

To validate the results of the microarray-DAVID approach, a number of the up or down-regulated biological processes were evaluated (immuno)histologically.

The downregulated GO terms “muscle development”, “striated muscle development” and “striated muscle contractions” observed in both construct-treated and untreated tissue hint to a lack of skeletal muscles. Desmin staining was used for evaluation, since this is a muscle-specific protein and one of the genes associated with the GO-term ‘muscle development’ (GO:0007517), (Fig. 4). Indeed, tissue sections of day 112 untreated and construct-treated wounds (which had the longest time to potentially develop new muscle tissue) were negative in contrast to the strong staining of the subcutaneous *panniculus carnosus* muscle layer present in normal rat skin.

Similar observations were made for the subcutaneous fat layer that did not regenerate in time after wounding, likely explaining the downregulated GO-terms related to lipid production.

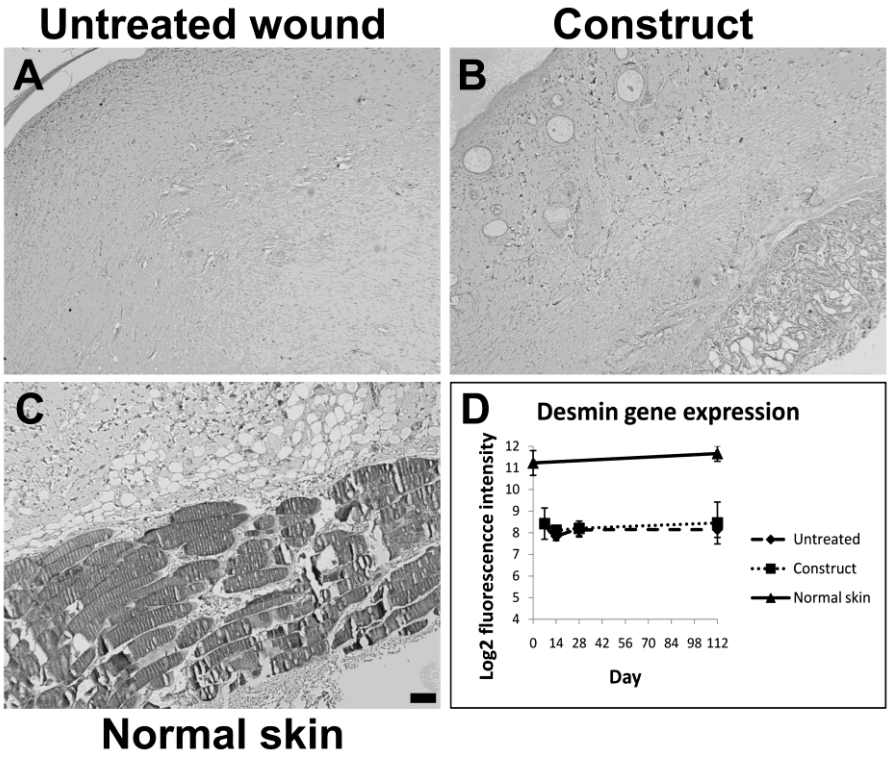

Figure 4. Immunostaining for muscle-specific desmin (A-C) and its gene expression indicated as microarray fluorescence intensities (D). In day 112 untreated (A) and construct-treated (B) wounds, no staining was visible, while a clear brown-stained muscle layer (the *panniculus carnosis*) was visible in normal skin (C). Bar is 100 µm. Desmin gene expression (in log2 fluorescence intensity) showed lower expression in construct-treated and untreated wounds than normal skin on all time-points examined (D).

Cluster of differentiation 8 alpha (CD8 alpha) is one of the genes associated with immune response related GO-terms like 'T cell activation' (GO:0042110). CD8 alpha is the subunit of the T-cell receptor co-receptor and an established marker for immune reaction in tissues. Therefore, it was used to validate the enrichment for immune response-related terms in the upregulated gene lists of the early untreated and construct-treated wounds (Fig. 5). Staining for CD8 alpha showed many positive cells on early time points and few at day 112 and in normal skin, confirming the microarray/DAVID analysis.

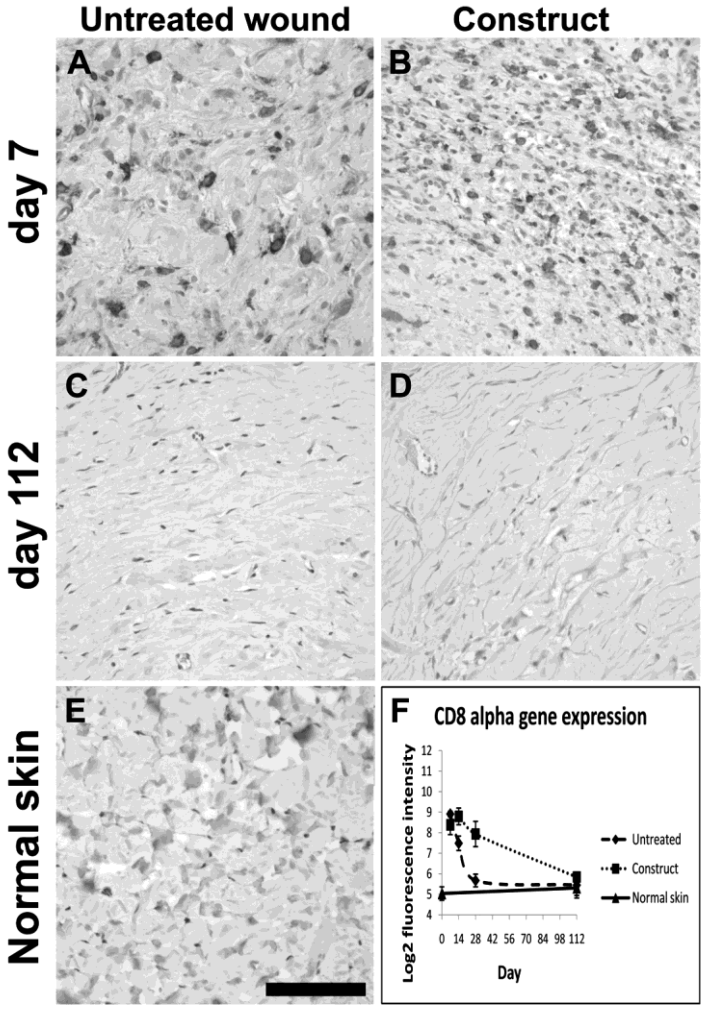

Figure 5. Immunostaining of tissue sections using an anti-CD8 alpha antibody to visualise the presence of immune cells (A-E), and its gene expression given as microarray fluorescence intensity (F). At day 7, both the untreated and construct-treated wounds contained numerous CD8 positive cells (A-B). Fewer CD8 positive cells were found at day 112 (C-D). Normal skin also showed some CD8 positive cells (E). Bar is 100 µm.

The presence of apoptosis-related terms in the upregultated gene lists of the early construct-treated wounds (and not the untreated) was validated using a TUNEL assay, which visualises fragmented DNA. Indeed, at day 7, staining was more abundant in the construct-treated wounds directly under the crust (Fig. 6). This staining corresponded with the areas where granulocytes were most abundant. At day 112 and in normal skin considerable less staining was found.

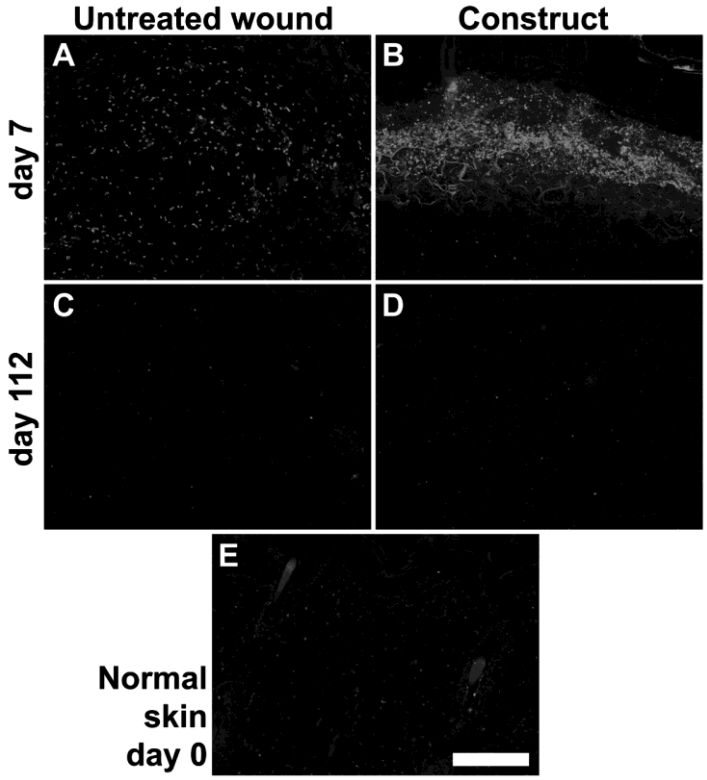

Figure 6. Tissue sections stained using the TUNEL assay to detect fragmented DNA as a marker for apoptosis. At day 7, the area directly under the crust of the construct-treated wounds stained heavily, while staining in the untreated wounds was less and more dispersed. At day 112 and in normal skin, staining was also dispersed and less abundant.

Type IV collagen is one of the proteins present in the basement membranes in skin, including that of blood vessels. Therefore, staining for type IV collagen was used as a method to visualise angiogenesis in the regenerating wounds (Fig. 7). At day 7 and 14, a large number of blood vessels was observed in both the untreated and construct-treated wounds. At later time points, this diminished to normal skin levels, except for the construct-treated wounds at day 28, which still had a large number of blood vessels. The microarray/DAVID analysis of upregulated gene lists, shows enrichment of angiogenesis- and blood vessel-related GO-terms for the untreated wounds on all time points examined, while for the con-

struct-treated wounds these terms were only present at day 7. This apparent discrepancy may be explained by accelerated blood vessel maturation using growth factor- containing scaffolds, as observed earlier [19], and indicating that the processes of blood vessel formation/development are diminished at an earlier time point compared to untreated wounds. Type IV collagen staining visualises both newly formed blood vessels as well as those already fully developed.

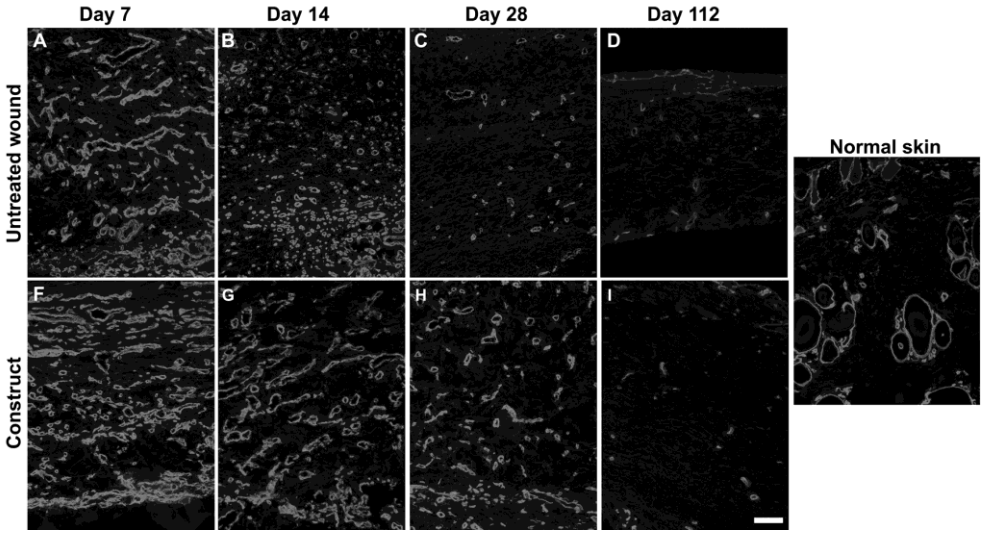

Figure 7. Tissue sections stained with an anti-type IV collagen antibody to visualise blood vessels (A-I) At day 7 and 14, blood vessels were abundantly present in the untreated and construct-treated wounds (A-B and F-G). This diminished to normal skin levels at later time-points (C-D and I), except for the construct-treated wounds at day 28 (H), which still contained many blood vessels. In normal skin, the basal lamina of appendages stained intensely and few blood vessels were present (E). Epidermal side on top, bar is 100 µm.

Discussion

Using gene expression microarrays, we identified biological processes occurring in rat full-thickness wounds treated with a collagen-based construct, or left untreated. Lists of genes differentially expressed in comparison to normal skin were analysed in the context of biological process GO-terms. By using relatively stringent thresholds ($p<0.05$, >2-fold change for gene lists and Bonferroni $p<0.05$ for enriched terms), the most significantly up/down regulated biological processes compared to normal skin were identified viz.: increase in inflammatory response and angiogenesis, lack of skeletal muscle and adipocyte (formation), and an increase in apoptosis in the construct-treated wounds at early time-points. Processes were validated by immunohistochemistry, indicating the usefulness of microarrays.

We focussed on general processes rather than individual genes, although the latter enables the identification of novel players involved in wound healing and may provide a wealth

of information with regard to specific pathways. The use of microarrays/GO analysis allows automation and high-throughput analysis of tissue engineered constructs. A number of steps involved (Fig.1) can be automated including the hybridisation and scanning of the microarrays, and the computational analysis. As costs for microarrays are dropping, it becomes appealing to evaluate the complex processes associated with the body's response to tissue engineered constructs using comprehensive microarrays and GO terms. An alternative approach to analyse processes at the mRNA level is by quantitative real-time PCR (qRT-PCR). This technique has been rapidly adopted by the field of tissue engineering to evaluate *in vitro* and *in vivo* experiments [20,21]. It is a reliable method to study gene expression, but only a small number of genes can be analysed. Methods are being developed to perform qRT-PCR on a more high-throughput scale, but evaluation is still limited to a subset of genes of interest [22].

Although analysis of the performance of tissue engineered constructs by microarrays and gene ontology software is appealing, the technology is still in its infancy, and a number of cautionary notes should be given. In this study we used rat, an organism widely used in tissue engineering. For rat, however, the number of genes assessed in the microarray core dataset is relatively small in comparison to human and mouse. Only 8,264 of the total number of ~21,000 predicted rat genes are included [23]. This in contrast to e.g. the human exon arrays, where ~18,000 of max. 25,000 predicted genes are available in the core dataset [24]. Therefore, in case of rat, the DAVID analysis is not optimal, and will become better when gene annotation and addition to the core dataset proceeds. For instance, and focussing on epidermal regeneration, important genes involved in epidermal maintenance (e.g. filaggrin, loricrin, some of the late cornified envelope genes, and transglutaminase 3) were not present on the exon array core dataset and could therefore not contribute to GO-enrichment of epidermis-related terms. However, probesets for these genes are present on the full array, so when annotation of these genes proceeds, inclusion in the core dataset will be possible.

A number of GO terms are not yet well defined, and there is a need for firm assignment of a set of genes associated with processes in the context of specific organs. For instance, using the microarray/DAVID approach the GO term 'skeletal development' (GO:0001501) was indicated as an enriched biological process in the late untreated and construct-treated wounds. Skeletal development is not a likely process in regenerating skin and a Von Kossa staining for calcification was negative in day 112 skin samples (data not shown). 'Skeletal development' has 302 associated genes and most of them are known to play a role in skin development and/or remodeling (e.g. types I and III collagen, fibronectin-1, fibrillin-1, fibroblast growth factor receptor 1 [25], and cathepsin K [26]). Obviously, the upregulation of the expression of genes associated with 'skeletal development' have a different meaning in the context of skin versus e.g. the context of bone. In general, a large number of proteins involved in skin development are also present in bone development and homeostasis [27]. For instance, Klingenberg *et al.* addressing gene expression profiles of *in vitro* cultured human skin substitutes in athymic mice, found gene expression previously known to be associated with cartilage and bone (cartilage intermediate layer protein, periostin, and osteoglycin) in their microarray analysis of cultured skin substitutes, and proved immunohistochemically

that they were actually present in (engineered) skin [28]. As more gene expression data becomes available on skin development, the GO-terms will become more suitable for organ specific analysis. In this respect, skin researchers may actively update GO-terms and their gene association, as did e.g. the muscle research community when (re)defining their GO-terms of interest [29].

The microarray approach should be regarded as complementary to other methodologies like histology. Regenerating skin is a highly heterogeneous tissue containing different cell types and structures, depending on the stage of regeneration. For instance, immune responses are major processes occurring shortly after implantation. Processes may go unnoticed if upregulation in one area of the specimen compensates for the downregulation of the same process in another area.

Since GO-terms are still in development, some terms do not yet contain all genes that are known to be involved in that specific process. For example, the GO-term 'elastic fiber assembly' (GO:0048251) contains only four genes, viz: elastin, lysyl oxidase, Cu++ transporting ATPase alpha polypeptide, and smooth muscle myosin heavy chain 11. A review of Kielty *et al.* lists 31 additional genes that code for structural and associated molecules of microfibrils and elastic fibres [30]. When we used this list to search for rat orthologs, 14 were found to be present in the analysed microarray core dataset, i.e. were well-annotated (Table 3). To calculate a fold enrichment, the number of these elastin-related genes in the >2-fold upregulated ($p<0.05$) lists was divided by the number of genes that was expected when a random gene list of the same length would have been analysed. This approach, with more elastin-related genes analysed, did not per se change the absolute fold enrichment values, e.g. at day 112 still approximately half of the genes assessed is present (elastin and lysyl oxidase of the four genes in the original GO-term and 9/17 genes in the updated term), but the increase in the number of genes in this GO-term would in this case result in a decrease in associated p-value. In that case, it would be an increase in probability that the GO-term 'elastic fiber assembly' was identified as an upregulated biological process with the microarray/DAVID approach.

In this respect it is encouraged that the tissue engineering/regenerative medicine society actively participates in the development and update of relevant GO-terms like angiogenesis, inflammatory and foreign body response, etc.. Each individual organ will require its own unique GO-terms, but once established the microarray/DAVID approach may be broadly applied to analyse the *in vivo* outcome and effectiveness of tissue-engineered constructs.

The future availability of more sophisticated options in analysis programs, the evolution of gene annotation and GO-terms, and other (new) techniques like RNA-sequencing may further improve the bioinformatics approach to analyse biological processes in tissue-engineered constructs [31]. This may also contribute to a better understanding of the effect of specific scaffold modifications on the tissue regeneration process. Eventually, these insights may help us to improve tissue-engineered constructs for optimal performance in regenerative medicine.

Table 3. Elastic-fibre associated rat genes, based on Kielty *et al.* [2], and fold enrichment for this group of genes calculated based on their presence (✓) in the (>2-fold) upregulated gene lists (p<0.05) vs. normal skin. See Discussion for more information.
U=Untreated wound, C=Construct.

	day 7		day 14		day 28		day 112	
	U	**C**	**U**	**C**	**U**	**C**	**U**	**C**
amyloid beta (A4) precursor protein								
ATPase, Cu++ transporting, alpha polypeptide								
decorin								
latent transforming growth factor beta binding protein 2								
microfibrillar-associated protein 3								
microfibrillar-associated protein 3-like								
vitronectin								
latent transforming growth factor beta binding protein 1	✓							
fibulin 5	✓				✓		✓	✓
collagen, type XVI, alpha 1	✓		✓	✓	✓	✓	✓	✓
biglycan	✓	✓	✓	✓	✓	✓	✓	✓
tenascin C	✓	✓	✓	✓	✓	✓	✓	✓
versican	✓	✓	✓	✓	✓	✓	✓	✓
lysyl oxidase-like 1	✓	✓	✓	✓	✓	✓	✓	✓
elastin			✓		✓		✓	✓
fibrillin 1					✓		✓	✓
lysyl oxidase					✓		✓	✓
Total # of genes in >2-fold upregulated list (p<0.05)	514	550	414	656	272	600	254	299
Expected # of hits with random gene distribution [E]	1.1	1.1	0.9	1.4	0.6	1.2	0.5	0.6
Actual # of elastin-related genes present in list [P]	7	4	6	5	9	5	9	9
Fold enrichment ([P]/[E])	**6.6**	**3.5**	**7.0**	**3.7**	**16.1**	**4.0**	**17.2**	**14.6**

Conclusion

Gene expression microarrays and gene ontology analysis were used to identify biological processes occurring *in vivo* after implanting of an acellular skin construct. Identified processes were confirmed with conventional (immuno)histology. Microarrays provide fast and unbiased tools to evaluate the performance of tissue-engineered constructs, and holds promise for automated high throughput analysis. However, a number of challenges remain, especially with respect to the development of specific GO-terms and annotation of the rat genome.

Acknowledgements

Simon van Reijmersdal, Petra de Vries and Suzanne Keijzers-Vloet of the Microarray Facility Nijmegen (Dept. of Human Genetics, RUNMC) are acknowledged for their technical assistance and Joost Schalkwijk (Dept. of Dermatology, RUNMC) is acknowledged for his expertise on skin biology. This study is funded by the Dutch Program for Tissue Engineering (grant DPTE 6735).

References

1. Griffith LG, Naughton G. Tissue engineering--current challenges and expanding opportunities. Science 2002;295:1009-14.
2. MacNeil S. Progress and opportunities for tissue-engineered skin. Nature 2007;445:874-80.
3. Supp DM, Boyce ST. Engineered skin substitutes: practices and potentials. Clin Dermatol 2005;23:403-12.

4. Clark RA, Ghosh K, Tonnesen MG. Tissue engineering for cutaneous wounds. J Invest Dermatol 2007;127:1018-29.
5. Zou X, Zou L, Foldager C, Bendtsen M, Feng W, Bunger CE. Different mechanisms of spinal fusion using equine bone protein extract, rhBMP-2 and autograft during the process of anterior lumbar interbody fusion. Biomaterials 2009;30:991-1004.
6. Affymetrix Datasheet. GeneChip Exon Array System for Human, Mouse, and Rat. http://www.affymetrix.com/support/technical/datasheets/exon_arraydesign_datasheet.pdf: 2009.
7. Schroeder A, Mueller O, Stocker S, Salowsky R, Leiber M, Gassmann M, *et al.* The RIN: an RNA integrity number for assigning integrity values to RNA measurements. BMC Mol Biol 2006;7:3.
8. Palmer, M and Prediger, E. Ambion Technote: Assessing RNA quality. http://www.ambion.com/techlib/tn/111/8.html: 2010.
9. Eklund AC, Turner LR, Chen P, Jensen RV, deFeo G, Kopf-Sill AR, *et al.* Replacing cRNA targets with cDNA reduces microarray cross-hybridization. Nat Biotechnol 2006;24:1071-3.
10. Affymetrix Whitepaper. Quality Assessment of Exon and Gene Arrays. http://www.affymetrix.com/support/technical/whitepapers/exon_gene_arrays_qa_whitepaper.pdf: 2007.
11. Irizarry RA, Hobbs B, Collin F, Beazer-Barclay YD, Antonellis KJ, Scherf U, *et al.* Exploration, normalization, and summaries of high density oligonucleotide array probe level data. Biostatistics 2003;4:249-64.
12. Benjamini Y, Hochberg Y. Controlling the False Discovery Rate: A Practical and Powerful Approach to Multiple Testing. J R Statist Soc 1995;57:289-300.
13. Smits NC, Robbesom AA, Versteeg EM, van de Westerlo EM, Dekhuijzen PN, Van Kuppevelt TH. Heterogeneity of heparan sulfates in human lung. Am J Respir Cell Mol Biol 2004;30:166-73.
14. Daamen WF, Nillesen ST, Hafmans T, Veerkamp JH, Van Luyn MJ, Van Kuppevelt TH. Tissue response of defined collagen-elastin scaffolds in young and adult rats with special attention to calcification. Biomaterials 2005;26:81-92.
15. Ashburner M, Ball CA, Blake JA, Botstein D, Butler H, Cherry JM, *et al.* Gene ontology: tool for the unification of biology. The Gene Ontology Consortium. Nat Genet 2000;25:25-9.
16. Carbon S, Ireland A, Mungall CJ, Shu S, Marshall B, Lewis S. AmiGO: online access to ontology and annotation data. Bioinformatics 2009;25:288-9.
17. Dennis G, Jr., Sherman BT, Hosack DA, Yang J, Gao W, Lane HC, *et al.* DAVID: Database for Annotation, Visualization, and Integrated Discovery. Genome Biol 2003;4:3.
18. Huang dW, Sherman BT, Lempicki RA. Systematic and integrative analysis of large gene lists using DAVID bioinformatics resources. Nat Protoc 2009;4:44-57.
19. Nillesen ST, Geutjes PJ, Wismans R, Schalkwijk J, Daamen WF, Van Kuppevelt TH. Increased angiogenesis and blood vessel maturation in acellular collagen-heparin scaffolds containing both FGF2 and VEGF. Biomaterials 2007;28:1123-31.
20. Brown BN, Valentin JE, Stewart-Akers AM, McCabe GP, Badylak SF. Macrophage phenotype and remodeling outcomes in response to biologic scaffolds with and without a cellular component. Biomaterials 2009;30:1482-91.
21. Valarmathi MT, Yost MJ, Goodwin RL, Potts JD. The influence of proepicardial cells on the osteogenic potential of marrow stromal cells in a three-dimensional tubular scaffold. Biomaterials 2008;29:2203-16.
22. Mees ST, Schleicher C, Mardin WA, Senninger N, Colombo-Benkmann M, Haier J. Analyzing miRNAs in Ductal Adenocarcinomas of the Pancreas. J Surg Res 2009.
23. Gibbs RA, Weinstock GM, Metzker ML, Muzny DM, Sodergren EJ, Scherer S, *et al.* Genome sequence of the Brown Norway rat yields insights into mammalian evolution. Nature 2004;428:493-521.
24. International Human Genome Sequencing Consortium. Finishing the euchromatic sequence of the human genome. Nature 2004;431:931-45.
25. Takenaka H, Kishimoto S, Tooyama I, Kimura H, Yasuno H. Protein expression of fibroblast growth factor receptor-1 in keratinocytes during wound healing in rat skin. J Invest Dermatol 1997;109:108-12.
26. Runger TM, Quintanilla-Dieck MJ, Bhawan J. Role of cathepsin K in the turnover of the dermal extracellular matrix during scar formation. J Invest Dermatol 2007;127:293-7.
27. Ross FP, Christiano AM. Nothing but skin and bone. J Clin Invest 2006;116:1140-9.
28. Klingenberg JM, McFarland KL, Friedman AJ, Boyce ST, Aronow BJ, Supp DM. Engineered Human Skin Substitutes Undergo Large-Scale Genomic Reprogramming and Normal Skin-Like Maturation after Transplantation to Athymic Mice. J Invest Dermatol 2009.
29. Feltrin E, Campanaro S, Diehl AD, Ehler E, Faulkner G, Fordham J, *et al.* Muscle Research and Gene Ontology: New standards for improved data integration. BMC Med Genomics 2009;2:6.
30. Kielty CM. Elastic fibres in health and disease. Expert Rev Mol Med 2006;8:1-23.
31. Shendure J. The beginning of the end for microarrays? Nat Methods 2008;5:585-7.

Chapter 8

Construction of a microstructured collagen membrane mimicking the papillary dermis architecture and guiding keratinocyte morphology and gene expression

Gerwen Lammers[1]
Günter Roth[2,3,4]
Matthias Heck[3]
Roland Zengerle[2,3,4]
G. Sandra Tjabringa[5]
Elly M. Versteeg[1]
Theo Hafmans[1]
Ronnie G. Wismans[1]
Dieter P. Reinhardt[6]
Eugène T.P. Verwiel[7]
Patrick L.J.M. Zeeuwen[5]
Joost Schalkwijk[5]
Roland Brock[1]
Willeke F. Daamen[1]
Toin H. van Kuppevelt[1]

[1]Department of Biochemistry, Nijmegen Centre for Molecular Life Sciences, Radboud University Nijmegen Medical Centre, Nijmegen; [2]HSG-IMIT, Villingen-Schwenningen, Germany; [3]Laboratory for MEMS Applications, Department of Microsystems Engineering (IMTEK), University of Freiburg, Freiburg, Germany; [4]BIOSS Centre for Biological Signalling Studies, Albert-Ludwigs-Universität Freiburg, Germany; [5]Department of Dermatology, Nijmegen Centre for Molecular Life Sciences, Radboud University Nijmegen Medical Centre, Nijmegen; [6]Department of Anatomy and Cell Biology, McGill University, Montreal, Canada; [7]Department of Human Genetics, Nijmegen Centre for Molecular Life Sciences, Radboud University Nijmegen Medical Centre, Nijmegen

Macromolecular Bioscience (provisionally accepted)

Abstract

Tissue-engineered constructs are used to stimulate skin regeneration after wounding, but improvements are warranted in epithelialisation and dermis formation. At the boundary of epidermis and dermis, a specific rete-ridge/dermal papillae structure is present, which is generally lacking in regenerated skin. Dermal papillae supply the epidermis with oxygen and nutrients, tighten the dermal-epidermal junction and may form specific cellular niches. In this study we constructed and evaluated a papillary-structured collagen fibril membrane mimicking the 3D-architecture of the human papillary dermis, thus templating rete-ridge architecture. A polydimethylsiloxane mould containing cone-shaped structures with a depth of 100 µm and a diameter of 175 µm was fabricated, and papillary-structured collagen membranes were prepared using a suspension of type I collagen fibrils. The effect of the papillar structures on cellular behaviour was evaluated by comparison of primary human keratinocytes cultured to confluency on papillary membranes and on flat membranes. Microscopical evaluation revealed the presence of morphologically distinct keratinocytes at the base of the papillar structures, not observed on flat membranes. Gene expression microarrays and RT-qPCR indicated that these cells were in a more proliferative/migrational state in comparison to keratinocytes cultured on flat membranes which had a more differentiated gene expression profile. Immunohistochemical stainings confirmed these results, and also indicated that keratinocytes on the top of the papillary structures expressed fibrillin 2. In conclusion, specific collagen architecture can direct keratinocyte behaviour, and this may be used to further improve skin regeneration.

Introduction

The healing of large full-thickness wounds and deep burns often results in contraction and scar tissue formation [1]. To guide and improve the wound healing process, tissue-engineered skin constructs based on natural and synthetic biomaterials have been developed [2,3]. Results of treatment with these constructs are promising, but not optimal and there is still space for improvement. For example, regeneration of the characteristic rete ridge morphology of the dermal-epidermal-junction may result in better skin regeneration (Fig. 1).

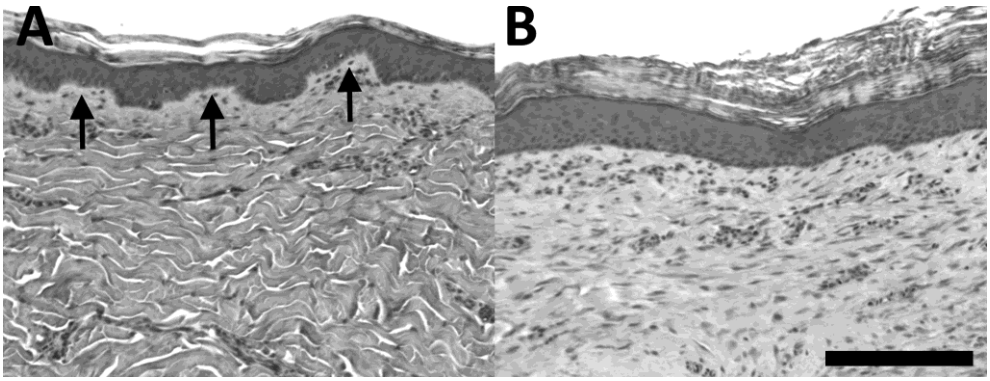

Figure 1. (A) The dermal-epidermal junction of normal porcine skin showing rete ridges and dermal papillae (arrows) on microscopic sections. (B) These structures are not observed in regenerated skin (in this example 55 days after treatment with a porous collagen scaffold). Bar is 100 µm.

Rete ridges are thickenings of the epidermis that extend downwards between the dermal papillae. The papillae provide epidermal cells with oxygen and nutrients, and reinforce the attachment of the epidermis to the dermis. In addition, several studies have indicated that defined locations in rete ridges serve as potential niches for epidermal stem cells [4,5]. These locations may provide a specific microenvironment that is required for stem cell survival. However, the proposed relationship between rete ridge location and cellular 'stemness' remains controversial [6-8].

Microstructured biomaterials may be used to stimulate the formation of epidermal rete ridges and dermal papillae. In addition, the availability of papillary-structured membranes may facilitate fundamental research to the relationship between keratinocyte niche and function. Cells including keratinocytes have been evaluated on three-dimensional microstructured surfaces, including grooved membranes composed of natural collagen and glycosaminoglycans [9,10]. However, the latter study used parallel grooves, which are technically less complex to produce than more natural rounded structures. In one study, polydimethylsiloxane pillars were coated with fibronectin and it was found that the interspace distance determined keratin 1 expression in cultured keratinocytes [11].

In this study, a microstructured collagen membrane was constructed and evaluated, mimicking the natural 3D-architecture of the papillary dermis of human skin [12]. The *in vitro*

response of primary human keratinocytes to this papillary-structured membrane was studied using high density gene expression microarrays, quantitative PCR, electron micro-scopy and (immuno)cytochemistry. This study is unique in its use of a combination of natural materials and dimensions, and the comprehensive analysis of the biological effects.

Materials and Methods

Design and construction of the papillary-structured mould

A papillary-structured mould was designed, implementing dimensions extracted from a published *in vivo* analysis of human skin using near-infrared confocal microscopy (Fig. 2) [12]. Dimensions of the inner forearm dermal papilla were deduced from histological pictures and quantitative data presented in this publication and a mould was designed to produce collagen membranes containing cones (microstructures) of 100 µm height and 175 µm width at the base, and an intercone distance of ~165 µm.

The collagen mould is made from a polydimethylsiloxane (PDMS) structure. The generation of PDMS masters as moulds of a microstructured polycarbonate master is a typical work flow in the manufacturing of microfluidic systems or microstructured foils and thin films [13]. For master fabrication, a Ø 115 mm and 4 mm thick polycarbonate disk was machined using a Minitech Mini-Mill 3PRO 3-Axis CNC milling machine (Norcross, GA, USA) and a 15° V-shaped engraving bit with 100 µm tip width to remove all material except the intended cones. A spindle turning speed of 50,000 rpm and a feed rate of 600 mm/min was applied. Vertical and horizontal milling paths were constructed in a defined pattern using Autodesk AutoCAD 2007.

The PDMS moulding was realised as casted resin by moulding an addition-curing two component PDMS (Elastosil RT 607, Wacker, Munich, Germany) from the polycarbonate master in a brass form of an hot embossing machine (Schmidt Technology, Cranberry Twp., PA, USA). Elastosil components A and B were mixed at a 9:1 ratio (w/w) at room temperature. The mixture was degassed in a desiccator and then poured onto the polycarbonate master in the brass form. The form was put into the hot embossing machine and pressed for 30 min under vacuum at 80°C to solidify. After demoulding, the PDMS was washed with 100% ethanol. The final template for the construction of papillary-structured collagen membranes was thus a 12 mm x 12 mm PDMS mould containing slightly sloped, cone shaped holes of 175 µm width and 100 µm depth, with an in between distance of 165 µm (fig. 2 C and D).

Production of papillary-structured and flat collagen membranes

Type I collagen fibrils were purified from bovine Achilles tendon using extractions with diluted acetic acid, aqueous NaCl and urea, and acetone [14]. A suspension of 0.8% (w/v) collagen fibrils in 0.25 M acetic acid was shaken overnight at 4ºC and homogenised on ice using a Potter-Elvehjem homogeniser (Louwers Glass and Ceramic Technologies, Hapert, The Netherlands) with an intervening space of 0.35 mm until homogenisation was completed. Air-bubbles were removed by centrifugation at 250 g for 10 min at 4ºC. To obtain a

container, a Ø 35 mm Petri dish (Greiner Bio-One) with the bottom removed was fixed on the papillary-structured PDMS cast and filled with 2 ml of collagen suspension. Air entrapped in the indentations was removed by placing the cast with collagen suspension in a vacuum desiccator for 3x1 min. The suspension was air-dried at room temperature. As a control, flat collagen membranes were produced on an adjacent surface of non-structured PDMS cast, using the same procedure.

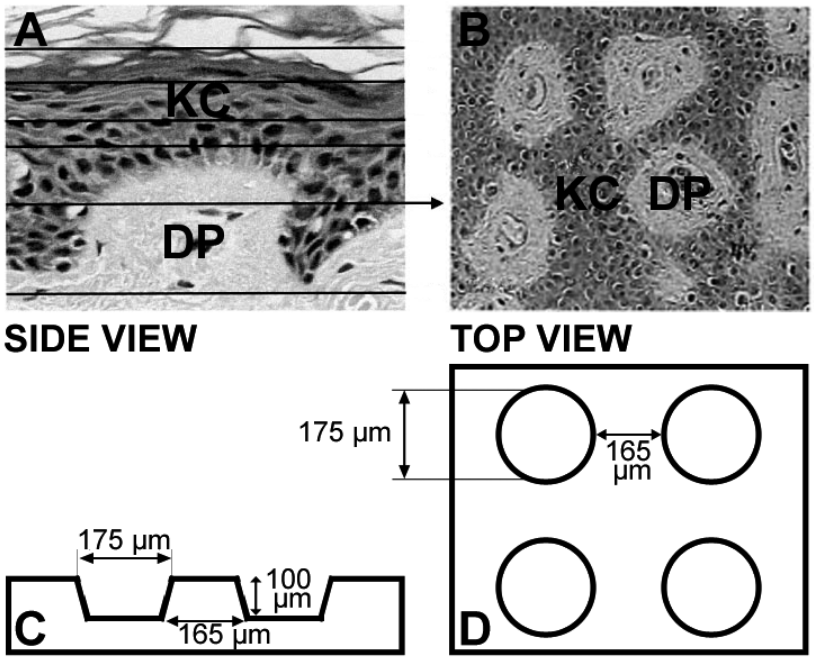

Figure 2. Design of the polydimethylsiloxane (PDMS) mould based on the architecture of the human papillary dermis. (A) Cross-section of normal human skin (inner forearm) showing the rete ridge architecture with keratinocytes (KC) and a dermal papilla (DP). (B) Top view of a longitudinal (en face) section at the height of the arrow in (A) showing the organisation of the dermal papillae (DP). Dimensions were obtained from *in vivo* reflectance confocal microscopy measurements taken from [12] A-B adapted with permission from Macmillan Publishers Ltd: The journal of Investigative Dermatology, copyright (2001) [12]. (C) Side view and (D) top view of the PDMS casting mould design that was produced from a micromilled polycarbonate master.

For morphological analysis, the papillary-structured and flat membranes were mounted on stubs, sputtered with an ultrathin layer of gold in a Polaron E5100 coating system and visualised with a JEOL JSM-6310 scanning electron microscope (Tokyo, Japan) operating at 15 kV.

Production of a papillary-structured double-layered construct

To demonstrate the feasibility of preparing a composite dermal substitute composed of a papillary dermal and a reticular dermal component, the papillary-structured papillary membrane was combined with a porous (dermal) scaffold. A collagen fibril suspension was

poured on the papillary-structured PDMS cast (see production section), and air-dried for 8 h resulting in near dry membranes. This layer was covered with 2 ml collagen suspension (resulting in a 1-2 mm layer), directly frozen at -20 ºC, and lyophilised.

This double-layered construct was analysed by scanning electron microscopy (see production section).

Culture of primary human keratinocytes on papillary-structured membranes

Keratinocytes were obtained from human abdominal skin derived from donors who underwent surgery for abdominal wall correction [15]. Three papillary-structured and three flat membranes were evaluated. To ensure that seeded cells remained on top of the membranes, films were placed in Ø 10 mm CellCrown24 inserts (ScaffDex, Tampere, Finland), disinfected with 70% ethanol (3x 1 h and 1x 16 h), washed with sterile phosphate buffered saline (pH 7.2, 5x 1 h, and 1x 16

h), placed on the bottom of a 6-well plate (Greiner Bio-One) and pre-incubated for 16 h in keratinocyte growth medium (KGM) [16]. Cells were seeded at a density of 100,000 cells/insert and incubated in 2 ml medium per well at 37ºC and 5% CO2. Cells were cultured to confluency on the membranes for ten days and medium was refreshed on day three and six. Membranes + cells were removed from the inserts, divided in two and processed for microscopical evaluation and RNA analysis.

Microscopical evaluation

One half of the membranes with cultured keratinocytes was rinsed with 0.1 M phosphate buffer (PB, pH 7.4), fixed with 4% paraformaldehyde in 0.1 M PB for 30 min at room temperature, washed with 0.1 M PB and divided in three pieces for (electron) microscopical evaluation and (immuno)cytochemistry.

For scanning electron microscopy, one piece was dehydrated in an ascending graded series of ethanol up to 100% ethanol, critical point dried using CO2 with a Polaron E3000 critical point drying apparatus (Watford, UK), processed and visualised with a JEOL JSM-6310.

For light and transmission microscopy, one piece was further fixed in 2% glutaraldehyde in 0.1 M phosphate buffer (pH 7.4), post-fixed with 1% osmium tetroxide, dehydrated in an ascending series of ethanol, and embedded in Epon 812. To obtain a general overview by light microscopy, 1 µm sections were stained with toluidine blue and basic fuchsin. For a more detailed analysis, ultrathin sections (60 nm) were cut and picked up on Formvar-coated grids, post-stained with lead citrate and uranyl acetate, and examined in a JEOL 1010 electron microscope.

For immunocytochemical evaluation, a third piece of the fixed membrane part was placed in TissueTek (Sakura Finetek, Zoeterwoude, The Netherlands), frozen in liquid nitrogen-cooled isopentane and sectioned. Cryosections were incubated in rabbit anti-human fibrillin 2 (1:200) [17], rabbit anti-human loricrin (1:500, Berkeley Antibody Company (BAbCO), Richmond, CA, USA), and rabbit anti-human cystatin M/E (1:200 [18]), followed

by an Alexa 488-labelled goat anti-rabbit IgG antibody (Molecular Probes, Eugene, OR, USA) [19].

RNA isolation

The other unprocessed half of the membrane with cultured keratinocytes was placed directly in 350 µl Qiagen lysis buffer RLT for RNA isolation, vortexed for 1 min, and processed according to the Qiagen RNeasy mini kit protocol for the purification of total RNA from animal cells using spin technology (Qiagen, Hilden, Germany), including an on-column DNase digestion. The RNA concentration and purity was measured with a Nanodrop spectrophotometer (Thermo Scientific, Waltham, MA, USA) and RNA integrity was analysed on an Agilent Bioanalyser (Santa Clara, CA, USA). Per half of a membrane, 1.5-8 µg RNA was isolated with an RNA integrity number (RIN) between 8.7 and 9.6, indicating excellent RNA quality.

High-density gene expression microarray analysis

A comprehensive gene expression analysis was performed of keratinocytes cultured on papillary-structured and on flat membranes using high density gene expression microarrays. Microarray analysis was performed as described before, with minor modifications [20]. From the isolated total RNA, 100 ng was further processed according to the Affymetrix GeneChip whole transcript sense target labelling assay manual (Affymetrix, Santa Clara, CA, USA). First, the ribosomal RNA content was reduced using the Invitrogen RiboMinus transcriptome isolation kit. Then, double-stranded complementary DNA (cDNA) was synthesised from RNA, which was used for *in vitro* transcription, creating complementary RNA. This RNA was then used to create fluorescently-labelled single-stranded DNA fragments in the sense orientation, which was hybridised on Affymetrix GeneChip human exon 1.0 sense target (ST) microarrays. These microarrays contain defined spots of oligonucleotide probes targeting a specific nucleotide sequence. Four spots with different probes form (in 90% of the cases) a probe set, covering every known and putative exon of the human genome. Using current annotation data, the 1.4 million probe sets (exons) on this array can be combined to analyse the expression of 17,859 individual genes.

The arrays were scanned and converted to a processed image, which was converted to one fluorescence intensity value per probe, using Affymetrix GeneChip Operating Software (GCOS). The values of individual probes belonging to one probe set were averaged using Partek Genomics Suite 6.4 (Partek Inc., St. Louis, MO, USA, www.partek.com). The average fluorescence intensity of all 17,859 genes on the microarrays was calculated using the Robust Multiarray Analysis (RMA) algorithm [21], including a quantile normalisation and background correction for GC-content. Human genome version HG18 was used for annotation [22].

To identify differentially expressed genes, a one-way analysis of variance (ANOVA) was performed for gene expression in keratinocytes cultured on papillary-structured versus flat membranes. Gene lists of interest were analysed for known direct interactions between their gene products using Pathway studio 7.1 software (Ariadne, Rockville, MD, USA).

RT-qPCR validation

Microarray data were validated by reverse transcriptase quantitative polymerase chain reactions (RT-qPCR) on skin-related genes [18,23-26]. For this 170 ng RNA was converted to cDNA using an Invitrogen SuperScript III first-strand synthesis system kit for RT-PCR by incubation at 65 ºC for 5 min in the presence of 50 ng random hexamers and 1 mM deoxynucleotide triphosphate (dNTP) mix. After incubation on ice, the reaction mix was diluted 1:1 to a total volume of 20 µl containing 5 mM $MgCl_2$, 0.01 M dithiothreitol (DTT), 40 U RNaseOUT, and 200 U SuperScript II Reverse Transcriptase in 20 mM Tris-HCl (pH 8.4) and 50 mM KCl. This mixture was incubated for 10 min at 25 ºC, and cDNA was synthesised for 50 min at 50 ºC. Reaction was terminated at 85 ºC for 5 min, placed on ice, and samples were stored at -20 ºC.

In a 20 µl reaction, 1 ng cDNA was mixed with 10 µl SYBR green 2x supermix (Bio-Rad), 12 pmol forward and 12 pmol reverse primer (Table 1). RT-qPCR was performed in a Bio-Rad (Hercules, CA, USA) C1000 thermal cycler with a CFX96 real-time PCR detection system using a hot start at 50 ºC for 2 min and 95 ºC for 10 min, followed by 40 cycles of 95 ºC for 15 s, 60 ºC for 1 min, including a plate read after every cycle, followed by 95 ºC for 15 s, and a melt curve from 60 ºC to 95 ºC, incrementing 0.5 ºC every 5 s accompanied by a plate read.

The cycle in which the fluorescence intensity passed a threshold (Ct) was determined using Bio-Rad CFX manager. The ΔCt of a sample was then calculated by subtraction of the Ct value of the reference gene large ribosomal protein P0 (RPLP0) from the Ct value of the gene of interest. To calculate the ΔΔCt, the average ΔCt of keratinocytes cultured on flat membranes was subtracted from the average ΔCt of keratinocytes cultured on papillary-structured membranes. The fold change was calculated as $2^{-\Delta\Delta Ct}$. RT-qPCR products were checked on agarose gel and were of expected size. To identify statistically significant changes in gene expression, an unpaired t-test was performed on the $2^{-\Delta Ct}$ values of the individual genes assessed on papillary-structured versus flat membranes, and $p<0.05$ was considered significant.

Table 1. Primer sequences and amplicon size of the genes assessed by RT-qPCR.

Primer name	Gene symbol	Forward primer (5'-3')	Reverse primer (5'-3')	Amplicon size (bp)
Dickkopf homolog 1 (Xenopus laevis)	DKK1	atcatagcaccttggatgggtatt	cttcttgtcctttggtgtgatacattt	75
Interleukin 6 (interferon, beta 2)	IL6	agccctgagaaaggagacatgta	ggcaagtctcctcattgaatcc	140
Vanin 1 [27]	VNN1	gaacccagtatgtctttcct	catacaacctcccaaacaga	147
Lumican	LUM	cttcaatcagatagccagactgc	agccagttcgttgtgagataaac	151
Late cornified envelope 2B [23]	LCE2B	ggttgactaaactctgccagg	cactggggcaggcattta	128
Defensin, beta 1 [25]	DEFB1	atggcctcaggtggtaactttc	cacttggccttccctctgtaac	146
Cystatin E/M [24]	CST6	tccgagacacgcacatcatc	ccatctccatcgtcaggaagtac	75
Ribosomal protein, large, P0 *(reference gene)* [24,27]	RPLP0	caccattgaaatcctgagtgatgt	tgaccagcccaaaggagaag	116

Results

Construction of microstructured collagen membranes mimicking the papillary dermis

A polycarbonate master was constructed based on literature values for dermal papillae architecture in the human inner forearm [12] (Fig. 2). The master closely matched the general architecture of the dermal papillae and could be used to produce multiple PDMS moulds. One PDMS mould (Fig. 3A) was used to produce multiple papillary-structured collagen membranes (Fig. 3B-D). It was found essential to completely fill the dips of the mould by de-aeration of the collagen suspension before air-drying. Dry membranes could easily be pealed off and it was possible to reuse the mould multiple times without complications. The architecture of the papillary-structured membranes adequately reflected the dimensions of the original design, thereby reproducing the natural morphology of dermal papillae. The potential of creating a two-layered dermal substitute with a papillary dermis architecture combined with a porous reticular dermis layer was demonstrated (Fig. 3E). For this construct, the papillary-structured membrane was prepared as described, but care was taken to prevent complete air-drying the collagen suspension on the mould. A fresh collagen suspension was poured on top of the slightly hydrated papillary-structured membrane, followed by freezing and lyophilisation. In this way, a porous construct was created mimicking the entire dermis with a papillary-structured semi-closed surface on top (Fig. 3E).

Morphological differences related to collagen film topography of keratinocytes cultured on papillary-structured collagen membranes

To investigate the effect of the papillary membrane architecture on cell growth and differentiation, primary human keratinocytes were cultured submerged on papillary-structured and flat membranes.

Scanning electron microscopical analysis showed the presence of a confluent cell layer on both the papillary-structured and flat membranes (the papillary-structured membrane is shown in Fig. 4). Cells showed the typical morphology of cultured keratinocytes and completely covered the membrane including the side and top of the papillar structures.

Staining of sections with toluidine blue and basic fuchsin showed the presence of predominantly a single layer of cells on the flat membranes and horizontal surfaces of the papillary-structured membranes (Fig. 5 A and B) . At the base of the papillar structures, multiple cell layers were observed consisting of larger and more rounded cells, especially those in the corner regions.

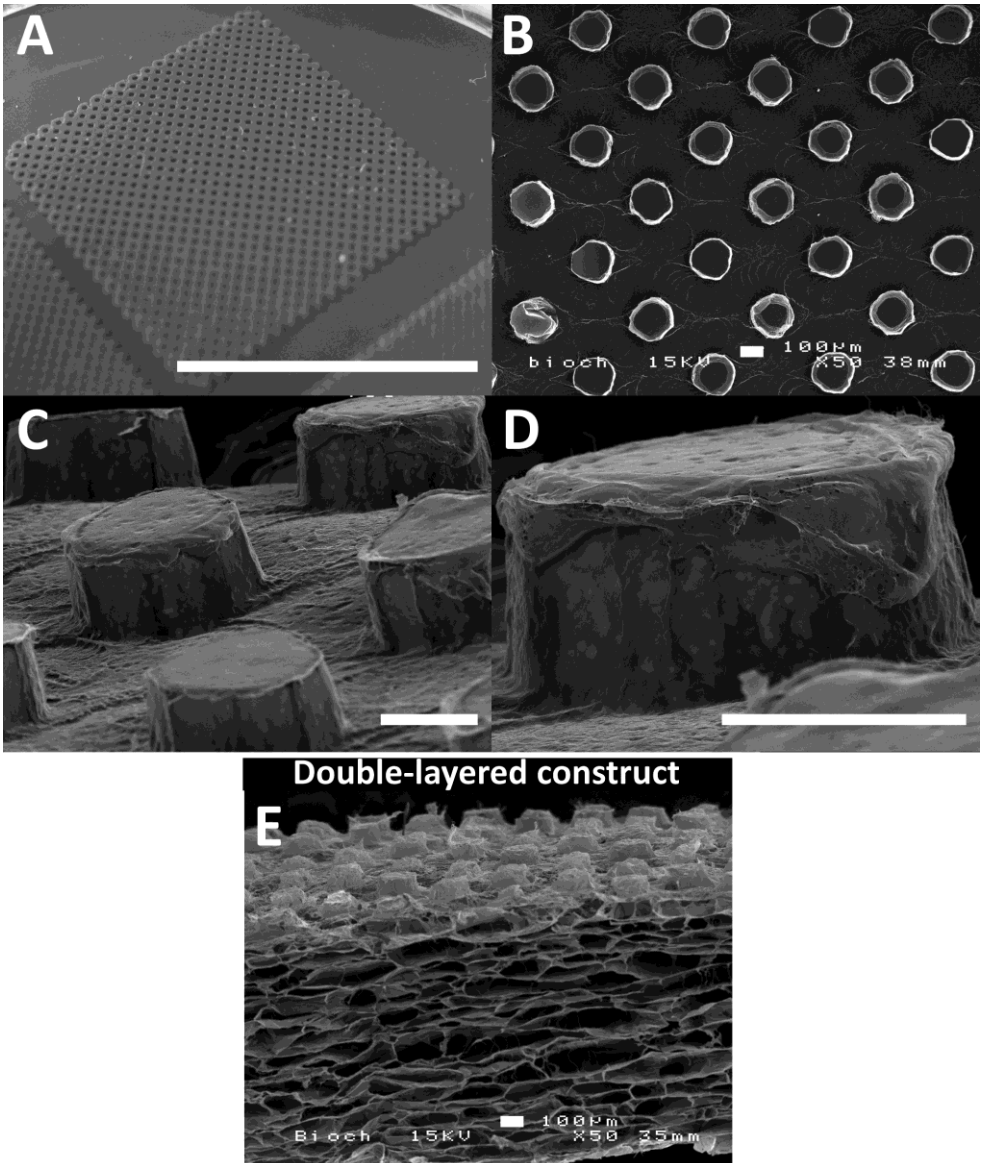

Figure 3. (A) Macroscopic picture of the microstructured PDMS mould and (B-E) scanning electron micrographs of papillary-structured collagen membranes produced with this mould. (B) Top view and (C) side view of a collagen membrane showing multiple papillar structures. (D) Close-up view of a single collagen papillar structure. (E) Double-layered collagen construct mimicking the two layers of the dermis: the papillary dermis (upper layer) and the reticular dermis (lower layer) . Bar in (A) is 1 cm, bars in (B-E) are 100 µm.

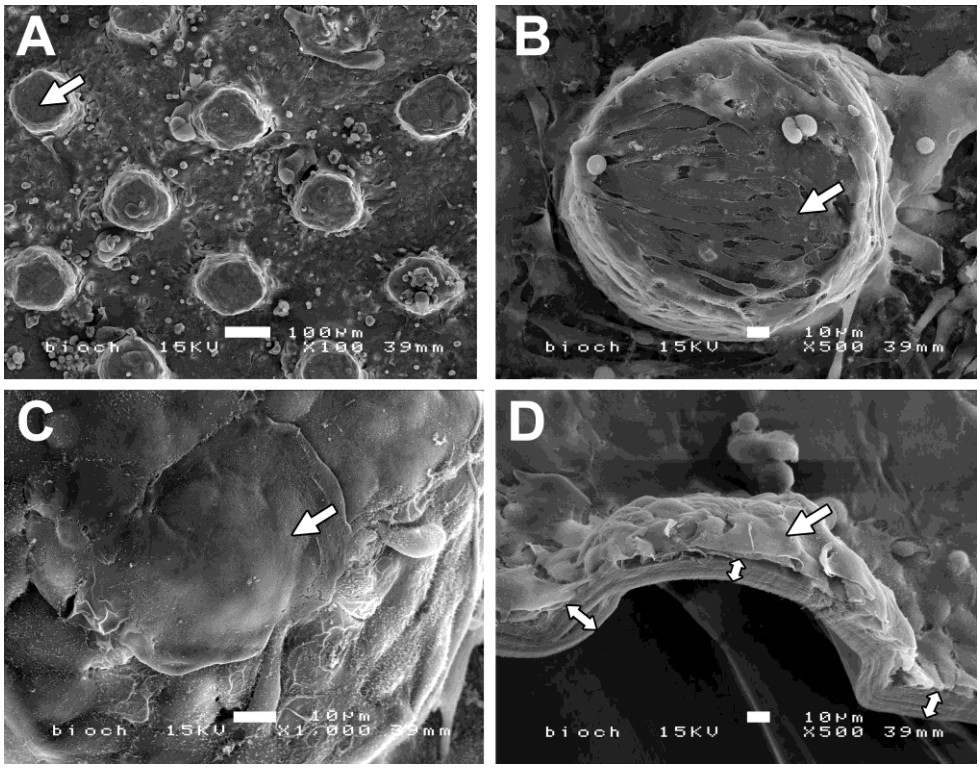

Figure 4. Scanning electron micrographs of human keratinocytes cultured on papillary-structured collagen membranes. Membranes were covered with a confluent layer of cells. (A) Top overview, (B) and (C) keratinocytes on a single papillar structure, (D) cross-sectional view of a single papillar structure. Typical cultured keratinocytes were visible (arrows). The collagen membrane in (D) is indicated with double arrow heads. Bars are (A) 100 µm and (B-D) 10 µm.

Transmission electron microscopy confirmed these morphological differences (Fig. 5 C-F). The flat membranes and the horizontal parts of the papillary-structured membranes contained a single layer of cultured keratinocytes with their typical morphology (Fig. 5C). Cells were closely attached to each other and contained intracellular keratin filaments and microvilli on top that extended into the cell culture medium. Melanin granules were visible, some subjected to autophagic fusion, which is known to occur in cultured keratinocytes. A basement membrane was observed at the interface between the cells and the collagen membrane (Fig. 5D). At the base of the papillar structures, the cultured sheet thickened up to approximately 6-7 cell layers, containing morphologically diverse cells (Fig. 5E). This included cells with the typical morphology of cultured keratinocytes, but also cells with a lobed nuclear membrane, and a mitochondria-rich and electron-light cytoplasm. Closer examination of these cells showed the presence of keratin filaments peripheral in their cytoplasm (Fig. 4F), confirming that these were also keratinocytes. Together with the observed nuclear membrane looping, which is characteristic for young cells, this demonstrated the presence of young keratinocytes at the base of the papillar structures.

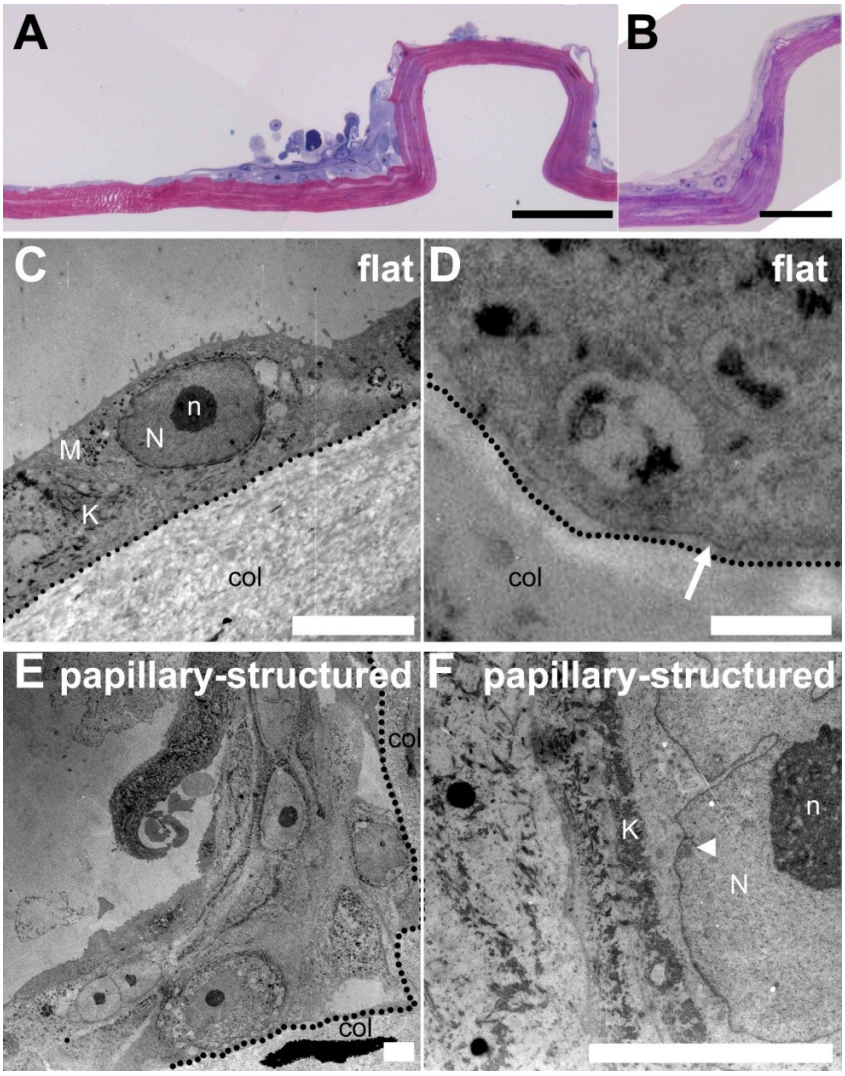

Figure 5. Morphology of keratinocytes cultured on papillary-structured and flat collagen membranes. A, B: Cross-sections of papillary-structured membranes with keratinocytes stained with toluidine blue and basic fuchsin. C-F: Electron microscopy of (C,D) flat and (E,F) papillary-structured membranes with keratinocytes. The horizontal parts of the membranes were covered with a single layer of flat keratinocytes, while at the bottom of the papillar structures multiple layers of larger, more rounded cells were visible. Please note that (B) is derived from a pilot experiment where 75,000 cells were cultured on the membrane for 7 days in another culturing medium [28]. The dotted lines in C-E indicate the border between collagen membrane and cell layer. (C) Flat membranes were covered with a single layer of keratinocytes containing melanin granules and keratin filaments. (D) Higher magnification showing the basement membrane (thin line, arrow) of the keratinocytes. (E) At the base of the papillar structures up to 6-7 cell layers were present containing morphologically different cells. (F) The presence of keratin filaments (K) inside the cytoplasm of a cell with lobed nucleus demonstrates that this was also a keratinocyte, and the looping in the nuclear membrane (arrowhead) is characteristic for young cells.
N=nucleus; n=nucleolus, M=melanin granules, K=keratin filaments, col=collagen membrane. (A) is composed of two pictures. Bars in (A) and (B) are 100 µm, bars in (C), (E) and (F) are 10 µm, and bar in (D) is 1 µm.

Gene expression profile of keratinocytes on papillary-structured collagen membranes

Gene expression microarrays provide an unbiased and comprehensive approach to gain insight into the nature of the different cells observed at different positions on the papillary-structured membrane (e.g. the morphological distinct cells observed at the base of the papillar structures vs. on flat surfaces). An attempt was made to separate cells associated with the papillar structures from cells associated with the flat surface in between the papillar structures, using laser dissection. Membranes with cultured keratinocytes were placed on crosslinked polyethylene naphthalate (PEN) membrane slides (Leica Microsystems, Wetzlar, Germany) and subjected to a Leica AS LMD microdissection system with a UV laser (Leica Microsystems). However, collagen membranes were too thick to cut out a ring at the base of the papillar structures without damaging the cultured cell layer. As an alternative, we compared RNA isolated from all the cells on the papillary-structured membranes to RNA isolated from cells on the flat membranes. Genes were ranked on their fold-change and of the 17,859 genes assessed, 88 were >1.5-fold higher expressed in keratinocytes cultured on papillary-structured membranes (Table 2A), and 168 were >1.5-fold higher expressed on flat membranes (Table 2B). It should be noted that since the papillary-structured membrane consists of both flat surfaces and papillar structures, specific gene profiles of cells of interest (e.g. those present at the base of the papillar structures) are diluted by the majority of associated flat surface. For instance, if cells at the base of papillar structures represent only 5% of the cell population, a 21 x differential gene expression in these cells will only give a 2-fold change for the entire cell population. This probably explains the small fold-changes observed and the absence of statistical significance for the differentially expressed genes. However, this analysis nevertheless provided a valuable starting point for further analyses using RT-qPCR and immunohistochemistry.

Table 2A. List of all 88 genes > 1.5x higher expressed in keratinocytes cultured on papillary-structured collagen membranes than on flat membranes.

#	Gene symbol	Gene name	Fold change
1	TSPAN7	tetraspanin 7	2.7
2	C6orf155	chromosome 6 open reading frame 155	2.7
3	IL13RA2	interleukin 13 receptor, alpha 2	2.5
4	TAS2R4	taste receptor, type 2, member 4	2.2
5	TFPI2	tissue factor pathway inhibitor 2	2.1
6	CCBE1	collagen and calcium binding EGF domains 1	2.1
7	ZNF737	zinc finger protein 737	2.0
8	TAS2R20	taste receptor, type 2, member 20	2.0
9	PTGS2	prostaglandin-endoperoxide synthase 2 (prostaglandin G/H synthase and cyclooxygenase)	2.0
10	ABI3BP	ABI family, member 3 (NESH) binding protein	2.0
11	IL24	interleukin 24	2.0
12	GSR	glutathione reductase	1.9
13	IFNE	interferon, epsilon	1.9
14	OC554202	hypothetical LOC554202	1.9
15	AMY2B	amylase, alpha 2B (pancreatic)	1.9
16	ANO1	anoctamin 1, calcium activated chloride channel	1.9
17	ABCC3	ATP-binding cassette, sub-family C (CFTR/MRP), member 3	1.8
18	NRCAM	neuronal cell adhesion molecule	1.8
19	IL1R2	interleukin 1 receptor, type II	1.8
20	LCP1	lymphocyte cytosolic protein 1 (L-plastin)	1.8
21	STEAP1	six transmembrane epithelial antigen of the prostate 1	1.8
22	RPL31	ribosomal protein L31	1.8
23	AKR1C1	aldo-keto reductase family 1, member C1 (dihydrodiol dehydrogenase 1; 20-alpha (3-alpha)-hydroxysteroid dehydrogenase)	1.8

24	CYP4F11	cytochrome P450, family 4, subfamily F, polypeptide 11	1.8
25	MRPS17	mitochondrial ribosomal protein S17	1.8
26	PTGS1	prostaglandin-endoperoxide synthase 1 (prostaglandin G/H synthase and cyclooxygenase)	1.8
27	C20orf197	chromosome 20 open reading frame 197	1.8
28	TRIM52	tripartite motif-containing 52	1.8
29	TSPAN4	tetraspanin 4	1.8
30	GUSBL2	glucuronidase, beta-like 2	1.8
31	SD17B7P2	hydroxysteroid (17-beta) dehydrogenase 7 pseudogene 2	1.7
32	TAGLN3	transgelin 3	1.7
33	MMP3	matrix metallopeptidase 3 (stromelysin 1, progelatinase)	1.7
34	DNAJB4	DnaJ (Hsp40) homolog, subfamily B, member 4	1.7
35	FBN2	fibrillin 2	1.7
36	PLA2G4A	phospholipase A2, group IVA (cytosolic, calcium-dependent)	1.7
37	CTNNAL1	catenin (cadherin-associated protein), alpha-like 1	1.7
38	ACAT2	acetyl-Coenzyme A acetyltransferase 2	1.7
39	GPR39	G protein-coupled receptor 39	1.7
40	DKK1	dickkopf homolog 1 (Xenopus laevis)	1.7
41	TFRC	transferrin receptor (p90, CD71)	1.7
42	ADAMTS6	ADAM metallopeptidase with thrombospondin type 1 motif, 6 (Affymetrix transcript cluster 1)	1.7
43	POPDC3	popeye domain containing 3	1.7
44	ANKRD36B	ankyrin repeat domain 36B	1.7
45	WNT7B	wingless-type MMTV integration site family, member 7B	1.7
46	TUBA1B	tubulin, alpha 1b	1.6
47	C6orf105	chromosome 6 open reading frame 105	1.6
48	ADAMTS6	ADAM metallopeptidase with thrombospondin type 1 motif, 6 (Affymetrix transcript cluster 2)	1.6
49	---		1.6
50	NRN1	neuritin 1	1.6
51	HSD17B2	hydroxysteroid (17-beta) dehydrogenase 2	1.6
52	QRFP	pyroglutamylated RFamide peptide	1.6
53	EVI2B	ecotropic viral integration site 2B	1.6
54	CTSK	cathepsin K	1.6
55	FGF2	fibroblast growth factor 2 (basic)	1.6
56	PXN	paxillin	1.6
57	PMS2CL	PMS2 C-terminal like pseudogene	1.6
58	GOLGA8B	golgi autoantigen, golgin subfamily a, 8B	1.6
59	---		1.6
60	CYR61	cysteine-rich, angiogenic inducer, 61	1.6
61	OCLM	oculomedin	1.6
62	LOX	lysyl oxidase	1.6
63	AXL	AXL receptor tyrosine kinase	1.6
64	PHLDB2	pleckstrin homology-like domain, family B, member 2	1.6
65	TXNRD1	thioredoxin reductase 1	1.6
66	SLIT2	slit homolog 2 (Drosophila)	1.6
67	FGF5	fibroblast growth factor 5	1.5
68	CMC1	COX assembly mitochondrial protein homolog (S. cerevisiae)	1.5
69	RAB3B	RAB3B, member RAS oncogene family	1.5
70	EID3	EP300 interacting inhibitor of differentiation 3	1.5
71	MAP9	microtubule-associated protein 9	1.5
72	CAPRIN2	caprin family member 2	1.5
73	FAM101A	family with sequence similarity 101, member A	1.5
74	SUZ12P	suppressor of zeste 12 homolog pseudogene	1.5
75	IL1RL1	interleukin 1 receptor-like 1	1.5
76	EFEMP1	EGF-containing fibulin-like extracellular matrix protein	1.5
77	NAV3	neuron navigator 3	1.5
78	---		1.5
79	TSPAN1	tetraspanin 1	1.5
80	IL6	interleukin 6 (interferon, beta 2)	1.5
81	C13orf15	chromosome 13 open reading frame 15	1.5
82	SPP1	secreted phosphoprotein 1	1.5
83	GLIS3	GLIS family zinc finger 3	1.5
84	ZNF675	zinc finger protein 675	1.5
85	RCN1	reticulocalbin 1, EF-hand calcium binding domain	1.5
86	PPP1R12B	protein phosphatase 1, regulatory (inhibitor) subunit 1	1.5
87	MME	membrane metallo-endopeptidase	1.5
88	BMS1P5	BMS1 pseudogene 5	1.5

Table 2B. List of all 168 genes > 1.5x higher expressed in keratinocytes cultured on flat membranes than on papillary-structured collagen membranes.

#	Gene symbol	Gene name	Fold change
1	SPINK1	serine peptidase inhibitor, Kazal type 1	-3.8
2	---		-2.8
3	MPRSS11E	transmembrane protease, serine 11E	-2.5
4	DCT	dopachrome tautomerase (dopachrome delta-isomerase, tyrosine-related protein 2)	-2.3
5	PSG6	pregnancy specific beta-1-glycoprotein 6	-2.3
6	FAM70A	family with sequence similarity 70, member A	-2.3
7	BPIL2	bactericidal/permeability-increasing protein-like 2	-2.3
8	ELMOD1	ELMO/CED-12 domain containing 1	-2.2
9	XKRX	XK, Kell blood group complex subunit-related, X-linked	-2.2
10	CYP1A1	cytochrome P450, family 1, subfamily A, polypeptide 1	-2.2
11	SERPINA3	serpin peptidase inhibitor, clade A (alpha-1 antiproteinase, antitrypsin), member 3	-2.2
12	C12orf36	chromosome 12 open reading frame 36	-2.1
13	ACPP	acid phosphatase, prostate	-2.1
14	MLANA	melan-A	-2.1
15	STEAP4	STEAP family member 4	-2.1
16	IFIT1	interferon-induced protein with tetratricopeptide repeats 1	-2.1
17	OR10A3	olfactory receptor, family 10, subfamily A, member 3	-2.1
18	SEPT3	septin 3	-2.1
19	TPPP3	tubulin polymerization-promoting protein family member 3	-2.1
20	TYRP1	tyrosinase-related protein 1	-2.0
21	NEBL	nebulette	-2.0
22	ATP12A	ATPase, H+/K+ transporting, nongastric, alpha polypeptide	-2.0
23	SILV	silver homolog (mouse)	-2.0
24	SPINK6	serine peptidase inhibitor, Kazal type 6	-2.0
25	KRT4	keratin 4	-2.0
26	MUC15	mucin 15, cell surface associated	-2.0
27	LIPH	lipase, member H	-2.0
28	ANKRD22	ankyrin repeat domain 22	-1.9
29	HSPB8	heat shock 22kDa protein 8	-1.9
30	LCE1D	late cornified envelope 1D	-1.9
31	SERPINB4	serpin peptidase inhibitor, clade B (ovalbumin), member 4	-1.9
32	PSG4	pregnancy specific beta-1-glycoprotein 4	-1.9
33	LCE2B	late cornified envelope 2B	-1.9
34	DEFB1	defensin, beta 1	-1.9
35	CST6	cystatin E/M	-1.9
36	AZGP1	alpha-2-glycoprotein 1, zinc-binding	-1.9
37	SMPD3	sphingomyelin phosphodiesterase 3, neutral membrane (neutral sphingomyelinase II)	-1.9
38	CALB1	calbindin 1, 28kDa	-1.9
39	ZNF750	zinc finger protein 750	-1.9
40	AQP9	aquaporin 9	-1.9
41	MX1	myxovirus (influenza virus) resistance 1, interferon-inducible protein p78 (mouse)	-1.9
42	IFI44L	interferon-induced protein 44-like	-1.9
43	ALDH3B2	aldehyde dehydrogenase 3 family, member B2	-1.9
44	TAS2R39	taste receptor, type 2, member 39	-1.9
45	EPHX3	epoxide hydrolase 3	-1.8
46	TYR	tyrosinase (oculocutaneous albinism IA)	-1.8
47	FOXN1	forkhead box N1	-1.8
48	CDRT1	CMT1A duplicated region transcript 1	-1.8
49	PSG9	pregnancy specific beta-1-glycoprotein 9	-1.8
50	SLC5A1	solute carrier family 5 (sodium/glucose cotransporter), member 1	-1.8
51	DSG4	desmoglein 4	-1.8
52	PDIA6	protein disulfide isomerase family A, member 6	-1.8
53	TTC39A	tetratricopeptide repeat domain 39A	-1.8
54	CLDN17	claudin 17	-1.8
55	GDA	guanine deaminase	-1.8
56	SCNN1B	sodium channel, nonvoltage-gated 1, beta	-1.8
57	USP2	ubiquitin specific peptidase 2	-1.8
58	KLK13	kallikrein-related peptidase 13	-1.8
59	TMEM86A	transmembrane protein 86A	-1.8
60	LCN2	lipocalin 2	-1.8
61	SLC39A2	solute carrier family 39 (zinc transporter), member 2	-1.8
62	PLA2G4E	phospholipase A2, group IVE	-1.7
63	CPA4	carboxypeptidase A4	-1.7
64	TMPRSS4	transmembrane protease, serine 4	-1.7
65	RSAD2	radical S-adenosyl methionine domain containing 2	-1.7
66	KLK14	kallikrein-related peptidase 14	-1.7
67	FAM83C	family with sequence similarity 83, member C	-1.7
68	MPRSS11F	transmembrane protease, serine 11F	-1.7
69	LCE2D	late cornified envelope 2D	-1.7

70	RDH12	retinol dehydrogenase 12 (all-trans/9-cis/11-cis)	-1.7
71	PLA2G7	phospholipase A2, group VII (platelet-activating factor acetylhydrolase, plasma)	-1.7
72	SLC6A14	solute carrier family 6 (amino acid transporter), member 14	-1.7
73	UQCRFS1	ubiquinol-cytochrome c reductase, Rieske iron-sulfur polypeptide 1	-1.7
74	TNFSF10	tumor necrosis factor (ligand) superfamily, member 10	-1.7
75	LY6G6C	lymphocyte antigen 6 complex, locus G6C	-1.7
76	TXNIP	thioredoxin interacting protein	-1.7
77	RAET1L	retinoic acid early transcript 1L	-1.7
78	SPINK7	serine peptidase inhibitor, Kazal type 7 (putative)	-1.7
79	TRIM48	tripartite motif-containing 48	-1.7
80	CXCL14	chemokine (C-X-C motif) ligand 14	-1.7
81	BMP6	bone morphogenetic protein 6	-1.7
82	RGS2	regulator of G-protein signaling 2, 24kDa	-1.7
83	IFI27	interferon, alpha-inducible protein 27	-1.7
84	MT1G	metallothionein 1G	-1.7
85	KRT78	keratin 78	-1.7
86	BBOX1	butyrobetaine (gamma), 2-oxoglutarate dioxygenase (gamma-butyrobetaine hydroxylase) 1	-1.7
87	CYP4B1	cytochrome P450, family 4, subfamily B, polypeptide 1	-1.7
88	NDUFA4L2	NADH dehydrogenase (ubiquinone) 1 alpha subcomplex, 4-like 2	-1.7
89	PI15	peptidase inhibitor 15	-1.7
90	HIST1H4H	histone cluster 1, H4h	-1.7
91	GRHL1	grainyhead-like 1 (Drosophila)	-1.7
92	CCL22	chemokine (C-C motif) ligand 22	-1.6
93	EGR3	early growth response 3	-1.6
94	OCA2	oculocutaneous albinism II	-1.6
95	KRT80	keratin 80	-1.6
96	OBP2B	odorant binding protein 2B	-1.6
97	PDZK1IP1	PDZK1 interacting protein 1	-1.6
98	TMPRSS13	transmembrane protease, serine 13	-1.6
99	SCNN1A	sodium channel, nonvoltage-gated 1 alpha	-1.6
100	GSTTP1	glutathione S-transferase theta pseudogene 1	-1.6
101	CYP1B1	cytochrome P450, family 1, subfamily B, polypeptide 1	-1.6
102	EDNRB	endothelin receptor type B	-1.6
103	PVRL4	poliovirus receptor-related 4	-1.6
104	RPL23AP32	ribosomal protein L23a pseudogene 32	-1.6
105	IFIT3	interferon-induced protein with tetratricopeptide repeats 3	-1.6
106	OPN4	opsin 4	-1.6
107	NOV	nephroblastoma overexpressed gene	-1.6
108	OAS1	2',5'-oligoadenylate synthetase 1, 40 /46kDa	-1.6
109	CLIC3	chloride intracellular channel 3	-1.6
110	PGLYRP3	peptidoglycan recognition protein 3	-1.6
111	ATG9B	ATG9 autophagy related 9 homolog B (S. cerevisiae)	-1.6
112	OAS2	2'-5'-oligoadenylate synthetase 2, 69/71kDa	-1.6
113	CAMK1D	calcium/calmodulin-dependent protein kinase ID	-1.6
114	RAB27B	RAB27B, member RAS oncogene family	-1.6
115	CCNA1	cyclin A1	-1.6
116	MUCL1	mucin-like 1	-1.6
117	FLVCR2	feline leukemia virus subgroup C cellular receptor family, member 2	-1.6
118	CXCL11	chemokine (C-X-C motif) ligand 11	-1.6
119	TMEM45B	transmembrane protein 45B	-1.6
120	SPRR2C	small proline-rich protein 2C (pseudogene)	-1.6
121	CLDN7	claudin 7	-1.6
122	POF1B	premature ovarian failure, 1B	-1.6
123	SCEL	sciellin	-1.6
124	OVOL1	ovo-like 1(Drosophila)	-1.6
125	TRIM16	tripartite motif-containing 16	-1.6
126	SAMD9	sterile alpha motif domain containing 9	-1.6
127	ABCG1	ATP-binding cassette, sub-family G (WHITE), member 1	-1.6
128	MPZL3	myelin protein zero-like 3	-1.6
129	HIST1H2BK	histone cluster 1, H2bk	-1.6
130	SLC24A5	solute carrier family 24, member 5	-1.6
131	KLK6	kallikrein-related peptidase 6	-1.6
132	TRIM2	tripartite motif-containing 2	-1.6
133	POTEE	POTE ankyrin domain family, member E	-1.6
134	GGT6	gamma-glutamyltransferase 6	-1.6
135	TCP11L2	t-complex 11 (mouse)-like 2	-1.6
136	GPR110	G protein-coupled receptor 110	-1.6
137	KRT23	keratin 23 (histone deacetylase inducible)	-1.6
138	SULT2B1	sulfotransferase family, cytosolic, 2B, member 1	-1.6
139	PSG8	pregnancy specific beta-1-glycoprotein 8	-1.6
140	GRHL3	grainyhead-like 3 (Drosophila)	-1.6
141	ERBB3	v-erb-b2 erythroblastic leukemia viral oncogene homolog 3	-1.6
142	IGFBP5	insulin-like growth factor binding protein 5	-1.6
143	CLIC5	chloride intracellular channel 5	-1.6
144	FKBP9	FK506 binding protein 9, 63 kDa	-1.6
145	PGLYRP4	peptidoglycan recognition protein 4	-1.6

146	C6orf35	chromosome 6 open reading frame 35	-1.5
147	PLEKHA7	pleckstrin homology domain containing, family A member 7	-1.5
148	CA9	carbonic anhydrase IX	-1.5
149	BMP4	bone morphogenetic protein 4	-1.5
150	ATP10B	ATPase, class V, type 10B	-1.5
151	GALNT5	UDP-N-acetyl-alpha-D-galactosamine:polypeptide N-acetylgalactosaminyltransferase 5 (GalNAc-T5)	-1.5
152	CRABP2	cellular retinoic acid binding protein 2	-1.5
153	LCE2A	late cornified envelope 2A	-1.5
154	DGAT2	diacylglycerol O-acyltransferase homolog 2 (mouse)	-1.5
155	MAFB	v-maf musculoaponeurotic fibrosarcoma oncogene homolog B (avian)	-1.5
156	GMPR	guanosine monophosphate reductase	-1.5
157	SBSN	suprabasin	-1.5
158	CYP2F1	cytochrome P450, family 2, subfamily F, polypeptide 1	-1.5
159	KRT13	keratin 13	-1.5
160	TGM1	transglutaminase 1 (K polypeptide epidermal type I, protein-glutamine-gamma-glutamyltransferase)	-1.5
161	TIAM1	T-cell lymphoma invasion and metastasis 1	-1.5
162	CCBP2	chemokine binding protein 2	-1.5
163	CEBPA	CCAAT/enhancer binding protein (C/EBP), alpha	-1.5
164	FLJ13744	hypothetical FLJ13744	-1.5
165	BNIPL	BCL2/adenovirus E1B 19kD interacting protein like	-1.5
166	AADACL2	arylacetamide deacetylase-like 2	-1.5
167	RHCG	Rh family, C glycoprotein	-1.5
168	RAB11FIP1	RAB11 family interacting protein 1 (class I)	-1.5

Gross examination of the gene lists provided a first indication of the nature of the differences between the cells on the two membranes. For example, the list of genes with higher expression on the papillary-structured membranes (Table 2A) contained three transmembrane tetraspanins, three interleukin (IL) receptors and two interleukins, molecules generally associated with proliferation, which were all absent from the list of genes with higher expression on the flat membranes (Table 2B). The papillar list also contained development-related genes like fibroblast growth factor 2 (basic) (FGF2), wingless-type MMTV integration site family, member 7B (WNT7B), and dickkopf homolog 1 (Xenopus laevis) (DKK1). In addition, fibrillin 2 (FBN2) was present, which is known to be expressed by keratinocytes and is probably involved in the development and maintenance of the elastic dermal-epidermal network [29]. The list of genes with higher expression on the flat membranes (Table 2B), on the other hand, was more related to keratinocyte differentiation. It contained five keratins, four late cornified envelope (LCE) genes, beta 1 defensin (DEFB1) and cystatin E/M (CST6).

RT-qPCR validation of microarray results

To validate the microarray results, RT-qPCR was performed on seven >1.3-fold differentially expressed genes selected for their reported association with skin biology [18,23-26] (Fig. 6), including four upregulated genes (#40: dickkopf homolog 1 (Xenopus laevis) (DKK1); #80: interleukin 6 (interferon, beta 2) (IL6); #97: vanin 1 (VNN1); and #306: lumican (LUM)), and three downregulated genes (#33: late cornified envelope 2B (LCE2B); #34: defensin, beta 1 (DEFB1); and #35: cystatin E/M (CST6)). All genes evaluated showed an up/downregulation as indicated by the microarray results. Upregulation of DKK1 and downregulation of LCE2B and CST6 were statistically significant using this approach. These results indicate that despite the heterogeneity of the cell populations, the microarray findings reflect real changes in gene expression.

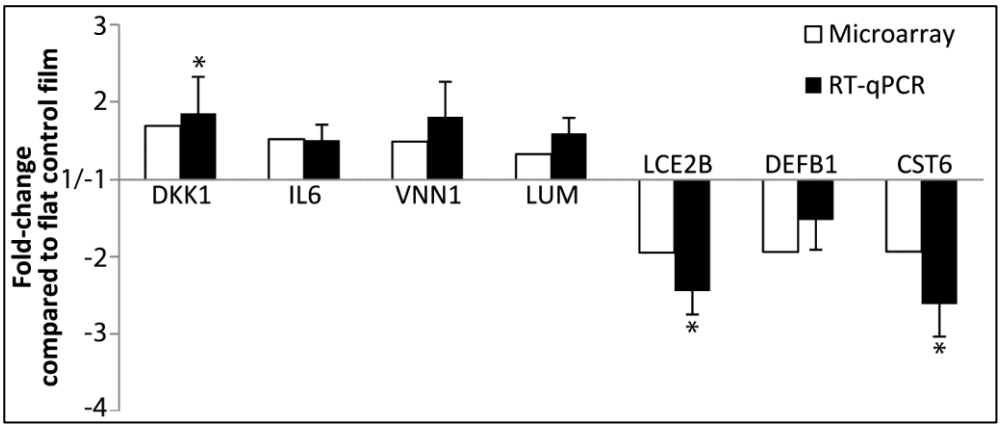

Figure 6. RT-qPCR validation of differentially expressed genes in keratinocytes on papillary-structured membranes compared to flat membranes. Depicted are the fold-changes identified with the gene expression microarrays (open bars) and their validation using RT-qPCR (filled bars) ±S.E.M.. An asterisk (*) indicates statistically significant changes on papillary-structured versus flat membranes ($p<0.05$).

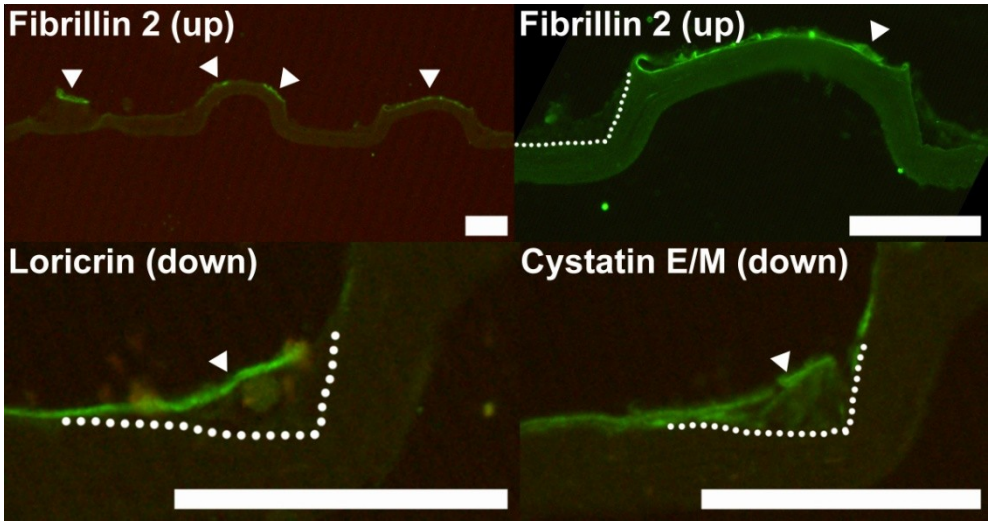

Figure 7. Visualisation of proteins (bright green, arrowheads) from differentially expressed genes on papillary-structured membranes with keratinocytes. Staining for fibrillin 2 (upregulated on papillary-structured membranes), and loricrin and cystatin E/M (both downregulated on papillary-structured membranes). The dotted line indicates a part of the border between the collagen membrane and cultured cell layer. Bars are 50 µm.

Localisation of differentially expressed gene products on papillary-structured membranes

To investigate whether the observed changes in gene expression are related to the location of the cell on the collagenous membranes, the protein product of three >1.3-fold differ-

entially expressed genes was visualised by immunohistochemical staining on cryosections of papillary-structured membranes (Fig. 7).

Antibody staining for fibrillin 2 (upregulated #35) showed the presence of this protein on top of the papillar structures, while less staining was observed in the single cell layer on the flat part of the membrane between the papillar structures. In line with the microarray results, there was a link with the papillar structures, but apparently this was not related to the morphologically distinct cells at the base of the structures, but at their top. Loricrin (downregulated #236) and cystatin E/M (downregulated #35) staining was found in almost all cells, but at the base of the papillar-structures where multiple cell layers were present, staining was less intense for the more basal cells in the corner. This difference in staining intensity supports the microarray data.

Pathway analysis of differentially expressed genes

To obtain more insights in the biological meaning of the microarray data, the differentially expressed genes (Tables 2A and B) were analysed for known direct interactions between their protein products (Figs. 8A and B).

Of the 88 genes upregulated in keratinocytes on papillary-structured membranes, 27 had a known direct interaction with each other (Fig. 8A). These proteins are mainly located at the plasma membrane or in the extracellular space. Key proteins in this network appear to be fibroblast growth factor 2 (FGF2), interleukin 6 (IL6), group IV A phospholipase A2 (PLA2G4A), and prostaglandin-endoperoxide synthase 2 (PTGS2).

Of the 168 genes upregulated in keratinocytes on flat membranes, 32 directly interacted with each other (Fig. 8B). Key player in this network is the transcription factor CCAAT/enhancer binding protein alpha (CEBPA) involved in differentiation and in mitotic growth arrest, whereas tyrosinase (oculocutaneous albinism IA) (TYR) acts as a central player in another part of the network.

Discussion

A collagen membrane matching the natural architecture of the human skin's basement membrane was constructed, by mimicking the topology of dermal papillae. Cultured keratinocytes were able to establish a confluent layer. In contrast to the single layered keratinocytes on the flat part of the membrane, multiple layers were present at the base of the papillary structures, containing morphologically distinct cells including young keratinocytes. This provided a first indication that the membrane architecture could result in a direct biological effect on the cultured cells. Microarray analysis was used as an unbiased and comprehensive tool to obtain insight in the differences between keratinocytes on papillary-structured and flat membranes. The gene expression profiles obtained hinted to specific cell behaviour, and expression levels were validated by RT-qPCR, indicating that the observed differences in gene expression reflects real changes. This was confirmed by antibody staining for a number of proteins encoded by the differentially expressed genes. Thus, despite the initial concerns that differences could be diluted out, significant differences were found.

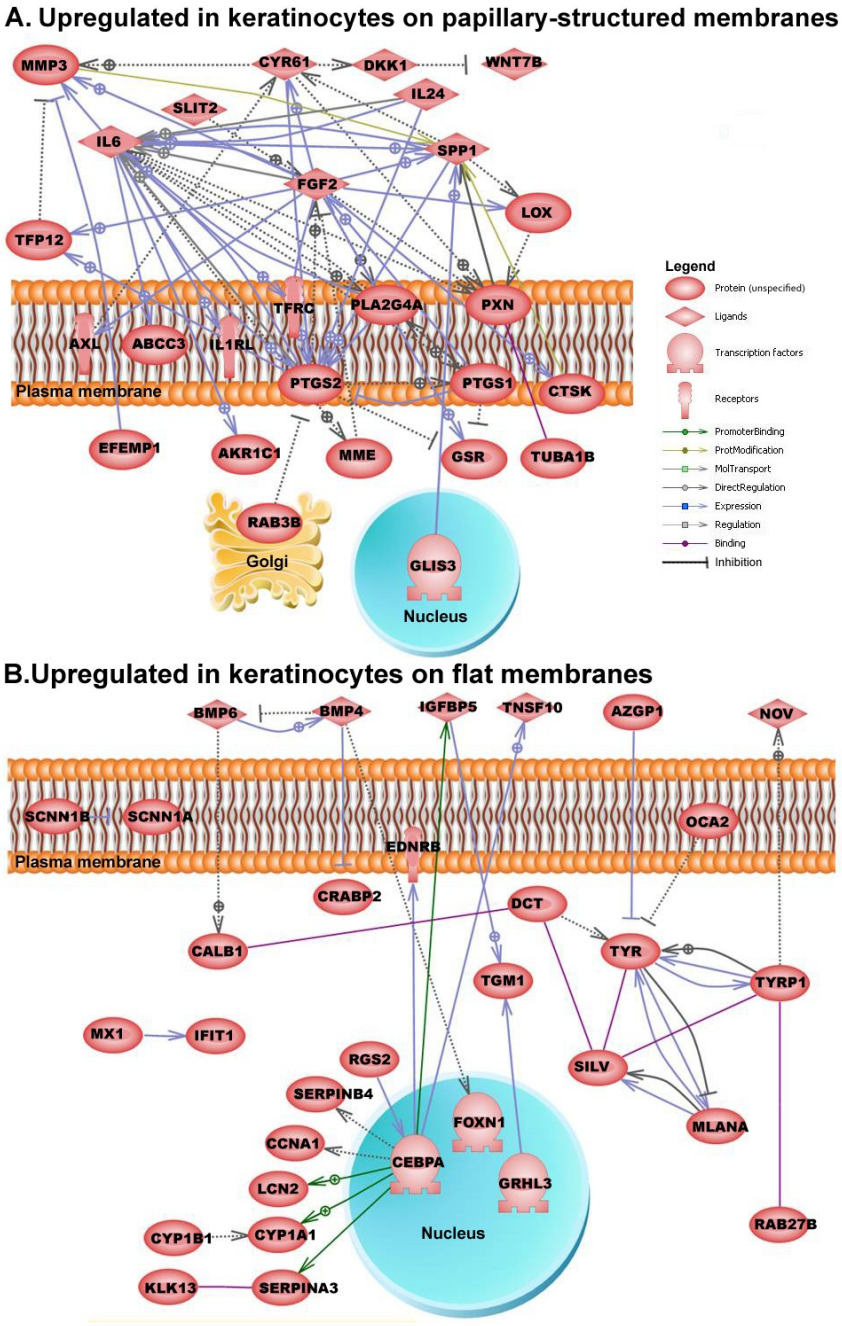

Figure 8. Pathway analysis of (A) the genes upregulated in keratinocytes on papillary-structured membranes and (B) upregulated in keratinocytes on flat membranes.

The list of upregulated genes on papillary-structured membranes contained genes known to be involved in cell signalling, development and proliferation. Pathway analysis provided more insight in the biological nature of the differences in gene expression. The protein products of genes upregulated on papillary-structured membranes were mainly situated on the plasma membrane and in the extracellular space. The key proteins in this network have been reported to be involved in keratinocyte proliferation and migration. Fibroblast growth factor 2 (FGF2), for example, stimulates keratinocyte proliferation [30]. Interleukin 6 (IL6) can indirectly induce keratinocyte migration [26]. In addition, group IV A phospholipase A2 (PLA2G4A) and prostaglandin-endoperoxide synthase 2 (PTGS2, also known as cyclooxygenase 2 (COX-2)) are both required for the conversion of cell membrane phospholipids into prostaglandins that are involved in keratinocyte migration and proliferation [31]. Fibrillins form microfibrils that act as a scaffold for elastin, and in skin fibrillin 2 is mainly found at the dermal-epidermal junction [32,33]. In our study, fibrillin 2 was found on top of the papillary structures resembling the top of dermal papillae. Since the protein was not found at the horizontal surfaces between the structures, it is possible that these cells on top experienced a distinct tension (stress) that stimulated fibrillin deposition. Very clearly, the cells sense their local microenvironment. The interplay of topological cues and intercellular communication will be subject of more detailed future studies.

The list of genes upregulated on flat membranes contained a remarkable number of genes related to keratinocyte differentiation. Pathway analysis showed a more intracellular localisation of the gene products. The central transcription factor of one part of the network, C/EBPalpha is known for its role in keratinocyte terminal differentiation [34]. Proteins of the other part of the network, including tyrosinase (TYR), dopachrome tautomerase (DCP) and tyrosinase-related protein 1 (TYRP1), are known to be involved in the process of melanogenesis [35].

In this study, only type I collagen was used as a matrix for cell growth. To mimic the natural basement membrane, present between keratinocytes and the dermis, the papillary membrane may also be covered with basement membrane components such as type IV collagen and glycosaminoglycans. In addition, elastin may be included in the dermal structure, since it has been shown to stimulate keratinocyte proliferation [28]. Future research may also include the evaluation of keratinocytes cultured at the air-liquid interface, better representing the natural environmental conditions of keratinocytes. These additional experiments will probably lead to a better understanding of the direct effect of membrane architecture on keratinocyte behaviour.

Conclusion

A collagen membrane representing the natural architecture of the dermal papillae in human skin was constructed. Cellular morphology, gene expression signatures and protein expression of keratinocytes cultured on these membranes were different when compared to flat membranes. This indicates that cellular characteristics can be directed by physical modi-

fication of biomaterials, which may form specific cellular niches. This knowledge may be used for the construction of improved tissue-engineered skin constructs.

Acknowledgements

We like to thank Dr. Magda Ulrich and Prof. dr. Esther Middelkoop of the Association of Dutch Burn Centres for their help with the porcine wound model (Fig. 1). The MIC facility of the NCMLS is acknowledged for the use of the scanning electron microscope and cryostat, and we would like to express our gratitude to Paul Jap for the interpretation of TEM micrographs. We would like to thank Marcel Nelen and Suzanne Keijzers-Vloet of the Microarray Facility (Dept. of Human Genetics) for their assistance, and Henry Dijkman (Dept. of Pathology) and Peter Uijtdewilligen (Dept. of Biochemistry) for the use and their assistance in the laser microdissection pilot, respectively. This study is funded by the Dutch Program for Tissue Engineering (grant DPTE 6735 and 6739) and by the EU-FP6 project EuroSTEC (soft tissue engineering for congenital birth defects in children: contract: LSHB-CT-2006-037409).

References

1. Gurtner GC, Werner S, Barrandon Y, Longaker MT. Wound repair and regeneration. Nature 2008;453:314-21.
2. MacNeil S. Progress and opportunities for tissue-engineered skin. Nature 2007;445:874-80.
3. Metcalfe AD, Ferguson MW. Bioengineering skin using mechanisms of regeneration and repair. Biomaterials 2007;28:5100-13.
4. Jensen UB, Lowell S, Watt FM. The spatial relationship between stem cells and their progeny in the basal layer of human epidermis: a new view based on whole-mount labelling and lineage analysis. Development 1999;126:2409-18.
5. Lavker RM, Sun TT. Heterogeneity in epidermal basal keratinocytes: morphological and functional correlations. Science 1982;215:1239-41.
6. Ghazizadeh S, Taichman LB. Organization of stem cells and their progeny in human epidermis. J Invest Dermatol 2005;124:367-72.
7. Muffler S, Stark HJ, Amoros M, Falkowska-Hansen B, Boehnke K, Buhring HJ, et al. A stable niche supports long-term maintenance of human epidermal stem cells in organotypic cultures. Stem Cells 2008;26:2506-15.
8. Pincelli C, Marconi A. Keratinocyte stem cells: friends and foes. J Cell Physiol 2010;225:310-5.
9. Pins GD, Toner M, Morgan JR. Microfabrication of an analog of the basal lamina: biocompatible membranes with complex topographies. FASEB J 2000;14:593-602.
10. Flemming RG, Murphy CJ, Abrams GA, Goodman SL, Nealey PF. Effects of synthetic micro- and nano-structured surfaces on cell behavior. Biomaterials 1999;20:573-88.
11. Steinberg T, Schulz S, Spatz JP, Grabe N, Mussig E, Kohl A, et al. Early keratinocyte differentiation on micropillar interfaces. Nano Lett 2007;7:287-94.
12. Huzaira M, Rius F, Rajadhyaksha M, Anderson RR, Gonzalez S. Topographic variations in normal skin, as viewed by in vivo reflectance confocal microscopy. J Invest Dermatol 2001;116:846-52.
13. Focke M, Kosse D, Muller C, Reinecke H, Zengerle R, von SF. Lab-on-a-Foil: microfluidics on thin and flexible films. Lab Chip 2010;10:1365-86.
14. Pieper JS, Oosterhof A, Dijkstra PJ, Veerkamp JH, Van Kuppevelt TH. Preparation and characterization of porous crosslinked collagenous matrices containing bioavailable chondroitin sulphate. Biomaterials 1999;20:847-58.
15. Tjabringa G, Bergers M, van RD, de BR, Lamme E, Schalkwijk J. Development and validation of human psoriatic skin equivalents. Am J Pathol 2008;173:815-23.

16. Van Ruissen F., Van Erp PE, de Jongh GJ, Boezeman JB, van de Kerkhof PC, Schalkwijk J. Cell kinetic characterization of growth arrest in cultured human keratinocytes. J Cell Sci 1994;107 (Pt 8):2219-28.
17. Lin G, Tiedemann K, Vollbrandt T, Peters H, Batge B, Brinckmann J, et al. Homo- and heterotypic fibrillin-1 and -2 interactions constitute the basis for the assembly of microfibrils. J Biol Chem 2002;277:50795-804.
18. Zeeuwen PL, van Vlijmen-Willems IM, Jansen BJ, Sotiropoulou G, Curfs JH, Meis JF, et al. Cystatin M/E expression is restricted to differentiated epidermal keratinocytes and sweat glands: a new skin-specific proteinase inhibitor that is a target for cross-linking by transglutaminase. J Invest Dermatol 2001;116:693-701.
19. Daamen WF, Nillesen ST, Hafmans T, Veerkamp JH, Van Luyn MJ, Van Kuppevelt TH. Tissue response of defined collagen-elastin scaffolds in young and adult rats with special attention to calcification. Biomaterials 2005;26:81-92.
20. Lammers G, Gilissen C, Nillesen ST, Uijtdewilligen PJ, Wismans RG, Veltman JA, et al. High density gene expression microarrays and gene ontology analysis for identifying processes in implanted tissue engineering constructs. Biomaterials 2010;31:8299-312.
21. Irizarry RA, Hobbs B, Collin F, Beazer-Barclay YD, Antonellis KJ, Scherf U, et al. Exploration, normalization, and summaries of high density oligonucleotide array probe level data. Biostatistics 2003;4:249-64.
22. Lander ES, Linton LM, Birren B, Nusbaum C, Zody MC, Baldwin J, et al. Initial sequencing and analysis of the human genome. Nature 2001;409:860-921.
23. Bergboer JG, Tjabringa GS, Kamsteeg M, van Vlijmen-Willems IM, Rodijk-Olthuis D, Jansen PA, et al. Psoriasis Risk Genes of the Late Cornified Envelope-3 Group Are Distinctly Expressed Compared with Genes of Other LCE Groups. Am J Pathol 2011;178:1470-7.
24. Cheng T, Tjabringa GS, van Vlijmen-Willems IM, Hitomi K, Van Erp PE, Schalkwijk J, et al. The cystatin M/E-controlled pathway of skin barrier formation: expression of its key components in psoriasis and atopic dermatitis. Br J Dermatol 2009;161:253-64.
25. de Jongh GJ, Zeeuwen PL, Kucharekova M, Pfundt R, Van D, V, Blokx W, et al. High expression levels of keratinocyte antimicrobial proteins in psoriasis compared with atopic dermatitis. J Invest Dermatol 2005;125:1163-73.
26. Gallucci RM, Sloan DK, Heck JM, Murray AR, O'Dell SJ. Interleukin 6 indirectly induces keratinocyte migration. J Invest Dermatol 2004;122:764-72.
27. Jansen PA, Kamsteeg M, Rodijk-Olthuis D, van Vlijmen-Willems IM, de Jongh GJ, Bergers M, et al. Expression of the Vanin Gene Family in Normal and Inflamed Human Skin: Induction by Proinflammatory Cytokines. J Invest Dermatol 2009;129:2167-74.
28. Lammers G, Tjabringa GS, Schalkwijk J, Daamen WF, Van Kuppevelt TH. A molecularly defined array based on native fibrillar collagen for the assessment of skin tissue engineering biomaterials. Biomaterials 2009;30:6213-20.
29. Haynes SL, Shuttleworth CA, Kielty CM. Keratinocytes express fibrillin and assemble microfibrils: implications for dermal matrix organization. Br J Dermatol 1997;137:17-23.
30. O'Keefe EJ, Chiu ML, Payne RE, Jr. Stimulation of growth of keratinocytes by basic fibroblast growth factor. J Invest Dermatol 1988;90:767-9.
31. Rys-Sikora KE, Konger RL, Schoggins JW, Malaviya R, Pentland AP. Coordinate expression of secretory phospholipase A(2) and cyclooxygenase-2 in activated human keratinocytes. Am J Physiol Cell Physiol 2000;278:C822-C833.
32. Brinckmann J, Hunzelmann N, Kahle B, Rohwedel J, Kramer J, Gibson MA, et al. Enhanced fibrillin-2 expression is a general feature of wound healing and sclerosis: potential alteration of cell attachment and storage of TGF-beta. Lab Invest 2010;90:739-52.
33. Cotta-Pereira G, Guerra RF, Bittencourt-Sampaio S. Oxytalan, elaunin, and elastic fibers in the human skin. J Invest Dermatol 1976;66:143-8.
34. Lopez RG, Garcia-Silva S, Moore SJ, Bereshchenko O, Martinez-Cruz AB, Ermakova O, et al. C/EBPalpha and beta couple interfollicular keratinocyte proliferation arrest to commitment and terminal differentiation. Nat Cell Biol 2009;11:1181-90.
35. Scherer D, Kumar R. Genetics of pigmentation in skin cancer--a review. Mutat Res 2010;705:141-53.

Chapter 9

Summary and future directions
Nederlandse samenvatting en toekomstvisie

Summary

This thesis started with a general introduction in **chapter 1**, which described that the skin is the largest organ of the body and plays an important role in the defence against pathogens, regulation of body temperature, and the prevention from dehydration. When the skin is wounded, its original structure and functions have to be restored as quickly as possible. Tissue-engineered constructs are being developed to guide this skin regeneration process and reduce the formation of scar tissue.

Chapter 2 provided an overview of methods that are used for the evaluation of tissue-engineered skin constructs in animal models. The large variation in evaluation methods, animal models, and wound models is remarkable and hampers a systematic comparison between different studies. Therefore, the standard use of four evaluation methods is recommended: viz. an observer scar assessment scale, planimetry, H&E staining, and antibody staining for five key proteins in cutaneous wound healing.

The following chapters described different aspects of the development of advanced tissue-engineered constructs.

Chapter 3 described how glycosaminoglycans like heparin can be incorporated in such a construct, and showed that scaffold pre-treatment and the type of analysis method may result in different estimations of the amount and activity of bound heparin. It is therefore important that assays are always adapted and validated for accurate measurements in the presence of a biomaterial. Additionally, this study underlined the importance to control crosslinking conditions on, in this case, the final amount and anticoagulant activity of bound heparin. Therefore, a detailed knowledge of the crosslinking process is essential to prepare a construct with desired properties.

Chapter 4 described how this type of knowledge can be used for the preparation of an array of 48 different collagen membranes with defined characteristics. It was demonstrated that the array could be used to identify materials that specifically stimulated the proliferation of keratinocytes. The availability of robust *in vitro* arrays will allow a pre-selection of the most promising biomaterials for further evaluation in animal models and may thereby reduce the number of required laboratory animal.

The formation of new blood vessels (angiogenesis) is often a time-consuming process in wounds treated with a tissue-engineered construct, and may thereby delay wound healing. Vascular endothelial growth factor (VEGF) stimulates angiogenesis and the cloning, large-scale production, and purification of this protein was described in **chapter 5**. It was demonstrated that this VEGF was biologically active, and this heparin-binding growth factor can be incorporated in tissue-engineered constructs that are designed to accelerate angiogenesis.

The design, construction, and evaluation of a molecularly-defined acellular skin construct was described in **chapter 6**. This collagen-based double-layered construct was designed to mimic the skins architecture and contained effector molecules to modulate specific processes. Compared with a commercially available construct (Integra) and an untreated wound in a rat full-thickness wound model, the double-layered skin construct resulted at early time

points in the formation of more blood vessels, less contraction, and a higher cell influx. At a later time point, the presence of more elastic fibres was observed. Although the long-term differences were limited, these results indicated that the double-layered skin construct was able to guide the wound healing process.

The next chapters described the development and use of a new method to evaluate the wound healing process, and the construction of an innovative biomaterial.

Chapter 7 introduced gene expression microarrays as a novel read-out tool, and this was used to evaluate the construct of chapter 6. Using a freely-available online tool (DAVID), it was possible to identify biological processes that were up- or downregulated in construct-treated wounds. The presence or absence of these processes was validated by classical (immuno)histochemistry, confirming that this fast and unbiased approach can be used as an alternative read-out method.

Finally, **chapter 8** dealt with the production of a novel collagen membrane that mimics the 3D-architecture of the natural dermal papillae. The morphology and gene expression profile of keratinocytes cultured on these microstructured membranes was studied and demonstrated that cellular growth and differentiation can be guided by modulation of their 3D-environment.

In conclusion, this thesis described both the construction of innovative collagen-based biomaterials for skin tissue engineering applications and novel methods that can be used for the *in vitro* and *in vivo* evaluation of these materials.

Future directions

For future studies, the *in vitro* biomaterial array described in chapter 4 may be extended by the use of new combinations of modifications (e.g. the promising combination of type IV collagen and elastic fibres), the incorporation of new components (like growth factors, as produced in chapter 5), inclusion of other types of scaffold (e.g. porous scaffolds or the microstructured membranes of chapter 8), and evaluation of other cell types. Future experiments with keratinocytes will also have to assess air-exposed culturing, since this better resembles the natural environment of these cells. In addition, it will be interesting to use alternative read-out methods like gene expression microarrays to characterise the cellular response to different biomaterials with defined modifications.

An improved double-layered skin construct may be produced by using the papillar-structured membranes of chapter 8 as a top layer. This epidermal layer may be supplemented with elastic fibres, since these stimulated keratinocyte growth in the biomaterial array (chapter 4). *In vivo* evaluation of these modified constructs will obviously include the recommended methods of chapter 2. In addition, methods for the objective quantification of e.g. histological observations will continuously be monitored and adopted when feasible. Combined with the standardisation of animal and wound models, this will allow a better comparison of different constructs and lead to an acceleration of the pre-clinical research and developmental phase.

Gene expression microarrays will probably soon be used as a fast and unbiased approach for the evaluation of other tissue-engineered constructs and/or organs. Interpretation of our study in chapter 7 was limited by a combination of the incompleteness of the underlying gene ontology (GO) terms and relatively poor annotation of the rat genome. Therefore, future development of these terms and annotations, in combination with the availability of new analysis tools will improve the interpretation of microarray results. In addition, new techniques will allow faster, cheaper and more in-depth analysis. For example, next generation sequencing holds promises for even more reliable RNA expression level analysis, and may soon replace microarrays.

A better understanding of the regenerative process may lead to the identification of novel important players in wound healing. Like VEGF in chapter 5, additional effector molecules that are interesting for tissue engineering applications can be cloned and produced for further evaluation. In addition, the availability of the VEGF expression vector opens opportunities for molecular fusion of the protein to tracking molecules like green fluorescent protein (GFP) to investigate e.g. its *in vitro* and *in vivo* distribution.

In the end, this research will hopefully result in a future where a patient with burns, acute wounds, or a non-healing ulcer enters the hospital, the surgeon takes an affordable construct from the shelf, cuts it in the right dimensions, and places it on the wounded area where this construct will immediately fulfil the skin's protective function and guides the regeneration process to a quick restoration of the original skin.

Nederlandse samenvatting

De huid is het grootste orgaan van het menselijk lichaam en speelt een belangrijke rol in de afweer tegen ziekteverwekkers, de regulatie van de lichaamstemperatuur en het voorkomen van uitdroging. Indien de huid beschadigd raakt is het zaak deze functies zo snel mogelijk te herstellen. In het geval van grote (brand)wonden gaat dit meestal gepaard met contractie en littekenvorming. Dit is ongewenst, aangezien littekens vaak afwijken van de omringende gezonde huid wat betreft kleur en functie en ze rondom gewrichten de mobiliteit kunnen beperken. Een mogelijke oplossing van dit probleem is het gebruik van *tissue engineering*/regeneratieve geneeskunde.

Tissue engineering is een interdisciplinair vakgebied dat de principes van levenswetenschappen en technologie aanwendt om biologische substituten te ontwikkelen die de functie van weefsels repareert, behoudt of verbetert. Kort samengevat is *tissue engineering* dus het "bouwen van weefsels". Onze aanpak om beschadigde huid te genezen is door middel van het implanteren van een construct (zonder cellen) dat de natuurlijke huid zo veel mogelijk nabootst. Als basismateriaal hiervoor wordt het belangrijkste structurele eiwit van de huid gebruikt, collageen type I. Dit kan worden gecombineerd met bijvoorbeeld elastine en biologisch actieve suikers (glycosaminoglycanen) en groeifactoren, die elk hun specifieke rol spelen in de biologie van de huid. Het construct wordt vaak verstevigd door middel van een crosslink methode die tegelijkertijd het koppelen van glycosaminoglycanen mogelijk maakt.

Na een algemene introductie (**hoofdstuk 1**) begint dit proefschrift in **hoofdstuk 2** met een overzicht van methoden die momenteel in de kliniek gebruikt worden om littekenweefsel te evalueren. Dit wordt gevolgd door een uitgebreid overzicht van methoden die in de literatuur beschreven zijn om *tissue-engineered* huidconstructen in diermodellen te evalueren. Opvallend is dat hiervoor een groot aantal verschillende evaluatiemethoden, dier- en wondmodellen gebruikt worden. Standaardisatie is noodzakelijk om een goede vergelijking tussen verschillende studies mogelijk te maken.

Hierna volgt een aantal hoofdstukken waarin verschillende aspecten worden belicht die nodig zijn om tot de ontwikkeling van een huidconstruct te komen.

Het glycosaminoglycaan heparine wordt vaak in *tissue-engineered* constructen ingebouwd. **Hoofdstuk 3** beschrijft zeven verschillende methoden die gebruikt kunnen worden om de hoeveelheid en activiteit van dit ingebouwde heparine te analyseren. De resultaten maken duidelijk dat de gekozen methode en de voorbehandeling van het biomateriaal van groot belang zijn voor een goede analyse. Ook wordt bevestigd dat het belangrijk is om de crosslinkcondities te controleren, aangezien dit een groot effect kan hebben op de hoeveelheid gebonden heparine en de activiteit hiervan.

In **hoofdstuk 4** wordt de ontwikkeling beschreven van een celkweekopzet om in één keer een groot aantal variaties van een biomateriaal te kunnen testen. Als voorbeeld wordt de groei geëvalueerd van opperhuidcellen (keratinocyten) op 48 verschillende moleculair gedefinieerde collageenmembranen. Deze modificaties laten een duidelijk effect op de celgroei zien en bijvoorbeeld de toevoeging van elastine vezels blijkt de groei van keratinocy-

ten te stimuleren. Door nieuw ontwikkelde materialen eerst in een dergelijk celkweeksysteem te screenen kunnen vervolgens enkel de meest veelbelovende in diermodellen worden geëvalueerd. Deze aanpak kan het aantal gebruikte proefdieren verminderen.

Het wondgenezingsproces kan vertraagd worden door de langzame vorming van nieuwe bloedvaten waardoor het weefsel te weinig zuurstof en voeding krijgt. Vasculair endotheel groeifactor (VEGF) is een eiwit dat kan worden gebruikt om deze bloedvatvorming te stimuleren. In **hoofdstuk 5** wordt het kloneren, de productie en zuivering van actief rat VEGF beschreven. Dit gezuiverde eiwit kan vervolgens in huidconstructen worden geïncorporeerd.

In **hoofdstuk 6** wordt de ontwikkeling van een geavanceerd dubbellaags huidconstruct beschreven, bestaande uit moleculair gedefinieerde componenten als collageen type I, elastine, glycosaminoglycanen en groeifactoren. Tevens wordt beschreven hoe dit construct in een rat wondmodel is geïmplanteerd en wordt het vergeleken met een commercieel verkrijgbaar huidconstruct (Integra) en onbehandelde wond. Op vroege tijdstippen leidt de toepassing van dit dubbellaags construct tot minder wondcontractie, de vorming van meer bloedvaten en een hogere infiltratie van cellen. Op de lange termijn blijkt er meer vorming van elastinevezels plaats te vinden. Toepassing van dit construct leidt dus tot (tijdelijke) verbetering van verschillende aspecten van het wondgenezingsproces.

In de daarop volgende hoofdstukken ligt de focus op de ontwikkeling van een nieuwe methode om wondgenezing te evalueren en op de constructie van een innovatief biomateriaal.

In **hoofdstuk 7** wordt de wondgenezing na toepassing van het dubbellaags construct uit hoofdstuk 6 geëvalueerd met behulp van genexpressie microarrays. Het achterliggende idee is dat ieder gen codeert voor een eiwit met een specifieke biologische functie en dat het expressieniveau van ieder gen correleert met de hoeveelheid geproduceerd eiwit. Door gelijktijdig de expressieniveaus voor alle bekende genen (tijdens deze studie ~8.000 voor de rat) te analyseren wordt getracht inzicht te verkrijgen in de rol van verschillende biologische processen tijdens wondgenezing. Lijsten van genen met veranderde expressie worden geanalyseerd en biologische processen worden geïdentificeerd die verhoogd of juist verminderd plaats vinden in de regenererende huid. Bevestiging van deze observaties met (immuno)histologische technieken toont aan dat deze snelle en objectieve aanpak geschikt is als alternatieve evaluatiemethode.

Tot slot wordt in **hoofdstuk 8** de productie beschreven van een membraan dat de driedimensionale structuur van de papillaire dermis in de huid nabootst. Het is mogelijk keratinocyten te kweken op deze membranen. Rondom de basis van de microstructuren op deze membranen zijn cellen met een afwijkende morfologie te zien. Het gaat hier waarschijnlijk om jonge, minder gedifferentieerde keratinocyten. Genexpressieanalyse met behulp van microarrays wijst op de gestructureerde membranen in de richting van processen als migratie en proliferatie, terwijl op vlakke membranen meer differentiatie optreedt. Door de driedimensionale omgeving aan te passen is het dus mogelijk om cellen in een bepaalde richting te sturen.

Concluderend beschrijft dit proefschrift zowel de constructie van vernieuwende collagene biomaterialen voor toepassing in huid *tissue engineering* alsmede nieuwe methoden om de *in vitro* en *in vivo* respons op deze materialen te evalueren.

Toekomstvisie

Voor toekomstige studies kan de *in vitro* celkweektest uit hoofdstuk 4 worden uitgebreid door toevoegingen te combineren (zoals de veelbelovende combinatie van collageen type IV en elastine vezels), nieuwe componenten toe te voegen (bijvoorbeeld groeifactoren, zoals geproduceerd in hoofdstuk 5), andere typen scaffold te gebruiken (bijvoorbeeld poreuze scaffolds of het gestructureerde membraan uit hoofdstuk 8) en andere celtypen te evalueren. Keratinocyten zullen tijdens de kweek ook aan de lucht blootgesteld worden, aangezien dit de natuurlijke situatie beter benadert. Ook is het interessant om alternatieve uitleesmethoden zoals genexpressie microarrays te gebruiken om de cellulaire reactie op verschillende moleculair gedefinieerde biomaterialen te analyseren.

Door de gestructureerde membraan van hoofdstuk 8 als toplaag voor een construct te gebruiken kan deze mogelijk worden verbeterd. Aan deze epidermale laag kunnen elastinevezels worden toegevoegd, aangezien in hoofdstuk 4 werd aangetoond dat deze keratinocytgroei stimuleren. Uiteraard zullen bij *in vivo* evaluatie van deze vernieuwde constructen de aanbevelingen van hoofdstuk 2 in acht worden genomen. Daarnaast zullen de ontwikkelingen op het gebied van histologische quantificatie nauwlettend worden gevolgd en, indien geschikt, worden geïmplementeerd. In combinatie met de standaardisatie van dier- en wondmodellen zal dit een betere vergelijking tussen constructen mogelijk maken en leiden tot een kortere preklinische onderzoeks- en ontwikkelingsfase.

Genexpressie microarrays zullen spoedig gebruikt worden als snelle en onbevooroordeelde methode om andere *tissue-engineered* huidconstructen en/of organen te analyseren. De interpretatie van onze resultaten in hoofdstuk 7 werd belemmerd door een combinatie van de onvolledigheid van de onderliggende genontologie (GO) termen en relatief beperkte annotatie van het rattengenoom. Verdere ontwikkeling van deze termen en annotaties zullen daarom, in combinatie met de beschikbaarheid van nieuwe analysemethoden, de interpretatie van microarrayresultaten verbeteren. Daarnaast zullen nieuwe technieken een snellere, goedkopere en meer grondige analyse mogelijk maken. *Next generation sequencing* is bijvoorbeeld veelbelovend om RNA expressieniveaus nog betrouwbaarder te detecteren.

Een beter begrip van het herstelproces zal leiden tot de identificatie van nieuwe belangrijke spelers in wondgenezing. Net zoals VEGF in hoofdstuk 5 kunnen andere interessante biologisch actieve moleculen worden gekloond en geproduceerd voor verdere evaluatie. Daarnaast maakt de beschikbaarheid van de VEGF expressievector het mogelijk om dit eiwit moleculair te verbinden aan signaalmoleculen zoals *green fluorescent protein* (GFP) om op deze manier bijvoorbeeld de *in vitro* en *in vivo* distributie van het eiwit te onderzoeken.

Uiteindelijk zal deze aanpak hopelijk resulteren in een toekomst waarin een patiënt met brandwonden, acute wonden of een moeilijk helende zweer het ziekenhuis binnen komt, de

chirurg een betaalbaar construct van de plank pakt, het in de juiste vorm knipt en op het wondgebied legt, waarna het construct direct de beschermende rol van de huid vervult en het regeneratieproces dirigeert naar een spoedig herstel van de originele huid.

Chapter 10

Curriculum Vitae
List of publications
Dankwoord

Curriculum Vitae (Nederlands)

Gerwen Lammers werd geboren op 25 oktober 1980 te Doetinchem. In 1999 behaalde hij zijn VWO diploma aan het Christelijk College Schaersvoorde in Aalten. Aansluitend is hij biologie gaan studeren aan de Universiteit Utrecht. Onderdeel van deze studie vormde een stage bij het Hubrecht laboratorium voor ontwikkelingsbiologie in de groep van dr. Freek van Eeden. Deze stage omvatte de analyse van het zebravis 'bazooka' gen en karakterisatie van een proliferatie mutant. Vervolgens nam hij deel aan de cursus *Fundamentals of Business and Economics* (business voor bèta's), waarvan een theoretische stage bij een bedrijf een onderdeel vormde. Tijdens deze stage bij Bioceros B.V. in Utrecht voerde hij onder supervisie van dr. Joost van Neerven een marktonderzoek uit naar de commerciële mogelijkheid van een nieuw therapeutisch antilichaam. Dit werd vervolgd met een praktische stage bij hetzelfde bedrijf onder supervisie van dr. Marcel den Hartog en resulteerde in de moleculaire fusie van een kameelantilichaam met een toxine en de productie hiervan.

In november 2004 behaalde Gerwen zijn doctoraal examen en in april 2005 startte hij zijn promotieonderzoek bij het UMC St. Radboud, Nijmegen Centre for Molecular Life Sciences (NCMLS) op de afdeling Biochemie onder begeleiding van dr. Toin van Kuppevelt en dr. Willeke Daamen. Dit proefschrift is het resultaat van het verrichte onderzoekswerk. Tijdens deze periode was hij betrokken bij verschillende practica voor bachelor en master studenten en heeft hij stagiaires begeleid van het middelbaar laboratorium onderwijs (MLO) en masteropleiding medische biologie (bèta faculteit RU). Hij heeft zijn resultaten op verschillende nationale en internationale wetenschappelijke congressen gepresenteerd. In 2009 heeft hij de presentatieprijs van de Nederlandse vereniging voor biomaterialen en tissue engineering (NBTE) in ontvangst mogen nemen.

Sinds 1 januari 2011 is Gerwen werkzaam als post-doctoraal onderzoeker bij de afdeling Fysiologie van het UMC St. Radboud, waar hij in de groep van prof. dr. Maria Hopman onderzoek doet naar de moleculair-biologische mechanismen die verantwoordelijk zijn voor de schadelijke gevolgen van fysieke inactiviteit en de gezonde effecten van lichaamsbeweging.

Curriculum Vitae (English)

Gerwen Lammers was born on 25 October 1980 in Doetinchem. In 1999 he obtained his VWO at the Christelijk College Schaersvoorde in Aalten. Afterwards he studied Biology at the Utrecht University. Part of this education was an internship at the Hubrecht laboratory for Developmental Biology in the group of Dr. Freek van Eeden, and consisted of the analysis of the zebrafish 'bazooka' gene and characterisation of a proliferation mutant. Thereafter, he followed the course 'Fundamentals of Business and Economics', which partially consisted of a theoretical internship at a company. During this internship at Bioceros B.V. in Utrecht he performed a market research for the commercial potential of a novel therapeutic antibody, under supervision of Dr. Joost van Neerven. This was continued by a practical internship at the same company under supervision of Dr. Marcel den Hartog, and resulted in the molecular fusion of a camelid antibody to a toxin, and the production of this construct.

In November 2004 Gerwen graduated, and in April 2005 he started with his Ph.D. research project at the Radboud University Nijmegen Medical Centre, Nijmegen Centre for Molecular Life Sciences (NCMLS) at the Department of Biochemistry under supervision of Dr. Toin van Kuppevelt and Dr. Willeke Daamen. This Ph.D. thesis is the result of this research project. During this period, he was involved in several practical workgroups for Bachelor and Master students and he supervised students from the *middelbaar laboratorium onderwijs* (MLO) and Master Medical Biology (RU). He presented his results on several national and international scientific conferences. In 2009 he received the presentation prize of the Netherlands Society for Biomaterials and Tissue Engineering (NBTE).

From January 1st 2011, Gerwen is working as a post-doctoral researcher at the Department of Physiology of the Radboud University Nijmegen Medical Centre. In the group of Prof. Dr. Maria Hopman, he studies the molecular-biological mechanisms that are responsible for the detrimental effects of physical inactivity and the healthy effects of exercise.

List of publications

Lammers G, Tjabringa GS, Schalkwijk J, Daamen WF, Van Kuppevelt TH.
A molecularly defined array based on native fibrillar collagen for the assessment of skin tissue engineering biomaterials.
Biomaterials. 2009 Oct;30(31):6213-6220.

Geutjes PJ*, Nillesen ST*, **Lammers G**, Daamen WF, Van Kuppevelt TH.
Cloning, large-scale production, and purification of active dimeric rat vascular endothelial growth factor (rrVEGF-164).
Protein Expr Purif. 2010 Jan;69(1):76-82. *Authors contributed equally.

Lammers G, Gilissen CFHA, Nillesen STM, Uijtdewilligen PJE, Wismans RG, Veltman JA, Daamen WF, Van Kuppevelt TH.
High density gene expression microarrays and gene ontology analysis for identifying processes in implanted tissue engineering constructs.
Biomaterials. 2010 Nov;31(32):8299-312.

Lammers G, Verhaegen PDHM, Ulrich MM, Schalkwijk J, Middelkoop E, Weiland D, Nillesen STM, van Kuppevelt TH, Daamen WF.
An overview of methods for the *in vivo* evaluation of tissue-engineered skin constructs.
Tissue Engineering part B – Reviews 2011 Feb;17(1):33-55.

Lammers G*, Nillesen STM*, Wismans, RG, Ulrich MM, Middelkoop E, Spauwen PH, Faraj KA, Schalkwijk J, Daamen WF, Van Kuppevelt TH.
Design and *in vivo* evaluation of a molecularly-defined acellular skin construct: reduction of early contraction and increase in early blood vessel formation.
Acta Biomaterialia 2011 Mar;7(3):1063-71. *Authors contributed equally.

Lammers G, Van de Westerlo EM, Versteeg EM, Van Kuppevelt TH, Daamen WF.
A comparison of seven different methods to analyse the amount of heparin bound to collagen scaffolds.
Tissue Engineering Part C - Methods 2011 Jun;17(6):669-76.

Brouwer KM, Daamen WF, Reijnen D, Verstegen RH, **Lammers G**, Hafmans TG, Wismans RG, Van Kuppevelt TH, Wijnen RM.
Repair of surgically created diaphragmatic defect in rat with use of a crosslinked porous collagen scaffold.
Journal of Tissue Engineering and Regenerative Medicine In press.

Lammers G, Roth G, Heck M, Zengerle R, Tjabringa S, Versteeg E, Hafmans T, Wismans R, Reinhardt DP, Verwiel E, Zeeuwen PLJM, Schalkwijk J, Brock R, Daamen WF, Van Kuppevelt TH.
Construction of a microstructured collagen membrane mimicking the papillary dermis architecture and guiding keratinocyte morphology and gene expression.
Macromolecular Bioscience Provisionally accepted.

Daamen WF, Faraj KA, Koens MJW, **Lammers G**, Brouwer KM, Uijtdewilligen PJE, Nillesen STM, Roelofs LA, Nuininga JE, Geutjes PJ, Feitz WFJ, Van Kuppevelt TH.
Extracellular-matrix based scaffolds from scratch (chapter 21).
Handbook of intelligent scaffold for regenerative medicine. Expected: December 2011.

Dankwoord

Onderzoeken doe je samen. Daarom wil ik een heleboel mensen bedanken voor hun bijdrage, hulp en interesse, met name de volgende personen:

Prof. dr. Brock, beste Roland, bedankt voor de goede aansturing van de afdeling Biochemie, het vertrouwen in mijn onderzoek en je rol als mijn promotor. Dr. van Kuppevelt, beste Toin, bedankt voor het binnenhalen van de DPTE subsidie waarop ik mocht gaan promoveren. De dwarsverbanden die jij tussen verschillende vakgebieden weet te leggen, monden vaak uit in unieke onderzoeksprojecten en door jouw originele visie kwam ik regelmatig tot nieuwe inzichten, waardoor ik veel heb geleerd. Dr. Daamen, beste Willeke, hartelijk bedankt voor alle begeleiding, het meedenken over het opzetten van onderzoeken, de interpretatie van data en het grondig nakijken van mijn manuscripten. Ook de leden van de manuscriptcommissie, Prof. dr. John Jansen, Prof. dr. Esther Middelkoop en Dr. Patrick Zeeuwen wil ik hierbij hartelijk bedanken voor de snelle beoordeling van het manuscript.

Suzan en Paul, *tissue* voorgangers op het lab, jullie hebben mij snel wegwijs gemaakt en stonden altijd klaar om te helpen. Af en toe met jullie bijkletsen blijft nog steeds een gezellige bezigheid! Ook de overige AiO's van het eerste uur: Nicole, Joost, Tessa en Mieke bedankt voor alle hulp en leuke paasbrunches, kerstdiners en AiO-retraites. Die werden later moeiteloos overgenomen door de 'nieuwe' lichting onderzoekers: Martin, Peter, Xander, Katrien, Etienne, Myrtille en Henk, bedankt voor de leuke tijd en heel veel succes met (het afronden van) jullie eigen onderzoeken! Zonder analytische ondersteuning zou dit proefschrift een aantal belangrijke resultaten en figuren missen. Hierbij denk ik vooral aan de kleuringen van Ronnie, GAG-gelen en stollingsassays van Els, GAG én *tissue* kennis van Elly, labwijsheden van Herman en celkweekervaring van Arie, waarvoor dank! Kaeuis, ik heb je altijd gewaardeerd als goede collega met verrassende humor en Gerdy bedankt voor alle theoretische en praktische hulp. En niet te vergeten de longziekten afvaardiging bij ons op het lab: Cindy, Marijke en Marianne, jullie waren perfect geïntegreerd!

Het medische faculteitscafé de Aesculaaf kan in dit dankwoord natuurlijk niet onvermeld blijven. In combinatie met de onderhoudende avonden bij Guido thuis, diverse pizzeria's en de Perfectaria, heeft deze voor de nodige ontspanning gezorgd. Theo, als stabiele factor in dit geheel wil ik je hartelijk bedanken voor alle morele en ook praktische immunohistologische en (electronen)microscopische hulp. Datzelfde geldt ook voor histologische vraagbaak Paul Jap, die ik zelfs op latere leeftijd nog heb mogen leren hakken! Ook de inmiddels alweer mature AiO Xander wil ik op deze plek graag alsnog acknowledgen voor het gebruik van de labtafel en opoe wenst je heel veel succes in Xan Diego! En natuurlijk mede *tissue twin* en broertje Martin, samen in dienst geweest van 1 april tot 1 april, maar ook daarbuiten de nodige avonturen beleefd en gesprekken gevoerd. Als paranimf was jouw promotie een zeer geslaagde generale repetitie en het is mij dan ook een hele eer dat Dr. Koens nu mij als paranimf terzijde wil staan!

Ka Wai en Daniela, hopelijk hebben jullie tijdens jullie stage net zo veel van mij geleerd als ik van jullie. Het is mij nooit gelukt om een ijklijn zo strak te pipetteren als Ka Wai op het

MLO had geleerd. En Daniela, co-auteur op het review omdat ik jouw scriptie als basis kon gebruiken, heel veel succes nog met je eigen promotieonderzoek in Köln!

Binnen het DPTE project liep er al snel een goede samenwerking met de afdeling Dermatologie van het UMC St. Radboud. Joost Schalkwijk, Sandra, Mieke en Diana, bedankt voor jullie keratinocytexpertise en –kweekvaardigheden waaruit een aantal gezamenlijke publicaties zijn voortgekomen. Dit geldt ook voor de onderzoekers van het brandwondencentrum Beverwijk: Esther, Magda, Pauline, Vincent, Bouke en Neeltje, bedankt voor de goede samenwerking en gezelligheid tijdens congressen en experimenten. Ook Sue Gibbs hartelijk bedankt voor de waardevolle inbreng tijdens de diverse DPTE bij- eenkomsten.

Daarnaast wil ik de medewerkers van het Centraal Dierenlaboratorium Nijmegen en het grote dierenlab van het VUmc bedanken voor al hun hulp. Ook de microarray studies waren anders verlopen zonder de afdeling Antropogenetica: Christian, Eugène, Suzanne, Petra, Simon, Marcel en Joris, hartelijk dank voor alle hulp hiermee. Ik heb jullie, en Terry en Jayne onder anderen ook via GeNeYouS, leren kennen als een stel gezellige personen! Dear Günter, thank you very much for the nice and productive collaboration that, together with Matthias and Prof. Zengerle, resulted in the production of a microstructured mould that we successfully used for the production of innovative collagen membranes. Ook Huib en Jack van de MIC faciliteit van het NCMLS hartelijk bedankt voor al jullie hulp en geduld bij bijvoorbeeld problemen met de scanning electronenmicroscoop.

Ook een woord van dank aan mijn nieuwe collega's van de afdeling Fysiologie, waar ik in de integratieve fysiologie groep van Prof. dr. Maria Hopman de kans krijg om mijzelf verder te ontwikkelen door mijn moleculair-biologische kennis te gebruiken om de fysiologische effecten van fysieke (in)activiteit te onderzoeken. Het is een stimulerende, sociale en erg prettige afdeling om werkzaam te zijn!

De bioloogjes uit Utrecht: Marlies & Harold, Richard & Alien, Gerold en Quint, heel erg bedankt voor alle momenten van ontspanning en bezinning tijdens high-tea's, 90's parties, dancefeesten, weekendjes Antwerpen, Aachen, Amsterdam, Utrecht, Berlijn en Sardinië. Uit dezelfde periode stamt ook het nog steeds voortdurende contact met al die leuke oudhuisgenootjes van IBB 109-3, waarvan een deel zelf inmiddels al is gepromoveerd.

Cindy, Gido, Henkjan, Jacqueline, Jan, Jenneken, Jeroen, Jurgen, Jurjen, Maartje, Margriet, Marieke, Remco, Robert, Robert, Wendy en Willeke: Ieder weekend (Rad)Staken verandert langzaam in bruiloften en kinderen, maar iedere Varsseveldse kermis en MKW word ik weer trots aan mijn 8erhoekse afkomst herinnerd, heel erg bedankt voor jullie eindeloze vriendschap!

Lieve oma's, ik ben erg trots dat jullie de voltooiing van mijn promotieonderzoek mee mogen maken! Lieve papa & mama, vanuit een warm nest is het goed uitvliegen. Heel erg bedankt voor jullie onvoorwaardelijke liefde en steun. En ik schep graag op over jullie smartphone-bestuurbare melkrobots! Lieve Tienke & Martin & Jody, Rinie & Daan en Jelien & Richard, geweldige zusjes, zwager, 'aanhang' en schattig nichtje, met jullie erbij is het helemaal een veelzijdige dolle boel! En Rinie, ik vind het super dat jij mijn paranimf wilt zijn!

TensLotte, netjes gewacht tot het praktische werk erop zat en mijn contract was afgelopen. Nog niet zo lang geleden mijn leven binnen komen lopen en nu al niet meer weg te denken. Meteen nóg een leuke familie erbij met Mat, Hetty, Fieke, Olaf, Lisa en Floor. Hoe kun je een wetenschappelijke dissertatie nu beter eindigen dan met een hoogstaand citaat uit een Nederlandstalige songtekst? “M’n lieve Lotte is een lotje uit de loterij / O, ik hou zo veel van jou en jij houdt ook van mij / Lieve Lotte blijf bij mij, de hoofdprijs van m’n leven dat ben jij!” De toekomst straalt ons tegemoet!

Allemaal hartelijk bedankt!

Gerwen

Publication of this thesis was financially supported by:
Radboud University Nijmegen, Nijmegen Centre for Molecular Life Sciences, Dutch Burns Foundation, the Netherlands society for Biomaterials and Tissue Engineering, Scaffdex, European Medical Contract Manufacturing, Greiner Bio-One, and Zirbus Technology Benelux.